

1994

Potential energy surface for highly energetic species: fuels for thoughts

Kiet Anh Nguyen
Iowa State University

Follow this and additional works at: <https://lib.dr.iastate.edu/rtd>

 Part of the [Physical Chemistry Commons](#)

Recommended Citation

Nguyen, Kiet Anh, "Potential energy surface for highly energetic species: fuels for thoughts " (1994). *Retrospective Theses and Dissertations*. 10632.

<https://lib.dr.iastate.edu/rtd/10632>

This Dissertation is brought to you for free and open access by the Iowa State University Capstones, Theses and Dissertations at Iowa State University Digital Repository. It has been accepted for inclusion in Retrospective Theses and Dissertations by an authorized administrator of Iowa State University Digital Repository. For more information, please contact digirep@iastate.edu.

9 4

2 4 2 4 6

U·M·I
MICROFILMED 1994

INFORMATION TO USERS

This manuscript has been reproduced from the microfilm master. UMI films the text directly from the original or copy submitted. Thus, some thesis and dissertation copies are in typewriter face, while others may be from any type of computer printer.

The quality of this reproduction is dependent upon the quality of the copy submitted. Broken or indistinct print, colored or poor quality illustrations and photographs, print bleedthrough, substandard margins, and improper alignment can adversely affect reproduction.

In the unlikely event that the author did not send UMI a complete manuscript and there are missing pages, these will be noted. Also, if unauthorized copyright material had to be removed, a note will indicate the deletion.

Oversize materials (e.g., maps, drawings, charts) are reproduced by sectioning the original, beginning at the upper left-hand corner and continuing from left to right in equal sections with small overlaps. Each original is also photographed in one exposure and is included in reduced form at the back of the book.

Photographs included in the original manuscript have been reproduced xerographically in this copy. Higher quality 6" x 9" black and white photographic prints are available for any photographs or illustrations appearing in this copy for an additional charge. Contact UMI directly to order.

U·M·I

University Microfilms International
A Bell & Howell Information Company
300 North Zeeb Road, Ann Arbor, MI 48106-1346 USA
313/761-4700 800/521-0600

Order Number 9424246

Potential energy surface for highly energetic species: Fuels for thoughts

Nguyen, Kiet Anh, Ph.D.

Iowa State University, 1994

U·M·I

**300 N. Zeeb Rd.
Ann Arbor, MI 48106**



Potential energy surface for highly energetic species: Fuels for thoughts

by

Kiet Anh Nguyen

**A Dissertation Submitted to the
Graduate Faculty in Partial Fulfillment of the
Requirements for the Degree of
DOCTOR OF PHILOSOPHY**

**Department: Chemistry
Major: Physical Chemistry**

Approved:

Members of the Committee:

Signature was redacted for privacy.

In Charge of Major Work

Signature was redacted for privacy.

For the Major Department

Signature was redacted for privacy.

For the Graduate College

Signature was redacted for privacy.

**Iowa State University
Ames, Iowa**

1994

To my wonderful mother and the memory of my father, and to Ly

TABLE OF CONTENTS

ACKNOWLEDGMENTS	vii
ABSTRACT	viii
CHAPTER 1. GENERAL INTRODUCTION	1
1.1 General Overview	1
1.2 Dissertation Organization	2
1.3 Theoretical Background	3
References	14
CHAPTER 2. THE STRUCTURE AND BONDING IN GROUP IV [1.1.1]PROPELLANES	17
Introduction	17
Computational Approach	20
Results and Discussion	22
Conclusions	34
Acknowledgment	34
References	35
CHAPTER 3. STRUCTURES AND BONDING OF GROUP IV SULFUR AND OXYGEN PROPELLANE DERIVATIVES	60
I. Introduction	60
II. Computational Approach	65
III. Results and Discussion	66
IV. Conclusions	71
Acknowledgment	71
References	72

CHAPTER 4. STRUCTURES, BONDING AND ENERGETICS OF N₂O₂ ISOMERS	84
I. Introduction	84
II. Methods of Calculation	86
III. Results and Discussion	88
IV. Summary and Conclusion	94
Acknowledgment	94
References	95
CHAPTER 5. THE INVERSION OF BICYCLOBUTANE AND BICYCLODIAZOXANE	116
I. Introduction	116
II. Methods of Calculation	119
III. Results and Discussion	121
IV. Summary and Conclusion	128
Acknowledgment	128
References	129
CHAPTER 6. THE ISOMERIZATION OF BICYCLOBUTANE TO BUTADIENE	153
Introduction	153
Methods of Calculation	156
Results and Discussion	157
Summary and Conclusions	164
Acknowledgment	164
References	165

CHAPTER 7. STABILIZATION OF β POSITIVE CHARGE BY SILICON, GERMANIUM, OR TIN	182
Introduction	182
Computational Methods	187
Results and Discussion	188
Conclusions	191
Acknowledgment	191
References	192
CHAPTER 8. MECHANISM AND ENERGETICS OF THE REACTION OF Si^+ WITH $\text{CH}_3\text{-SiH}_3$	206
Introduction	206
Computational Methods	210
Results and Discussion	211
Summary and Conclusions	224
Acknowledgment	225
References	226
CHAPTER 9. PARAMETERS FOR SCALING THE CORRELATION ENERGY OF THE BONDS Si-H, P-H, S-H, and Cl-H AND APPLICATION TO THE REACTION OF SILYL RADICAL WITH SILANE	257
Introduction	257
Theory	258
Calculations	259
Discussion	260
Acknowledgment	261
References	261

CHAPTER 10. EFFECT OF HYDRATION AND DIMERIZATION OF THE FORMAMIDINE REARRANGEMENT	266
I. Introduction	266
II. Computational Methods	269
III. Results and Discussion	270
IV. Summary and Conclusions	274
Acknowledgment	274
References	275
CHAPTER 11. CONCLUSIONS	288

ACKNOWLEDGMENTS

I would like to thank my major advisor, Professor Mark Gordon for the guidance and encouragement. I am grateful for the opportunity to learn a great deal of technical knowledge in electronic structure theory with a caring mentor, Professor Gordon. During my research I have benefited greatly from the interactions with the members of Professor Gordon's research group, especially Dr. Mike Schmidt, whose knowledge has been invaluable to me. I thank Drs. Jerry Boatz, Marshall Carroll, Joseph Lambert, Harvey Michels, John Montgomery Jr., Krishnan Raghavachari, and Donald Truhlar for the fruitful collaborations. I am especially indebted to the supports from my mother and brothers, my cousin Oanh, and my foster parents Donna and Allen Anderson. Finally, I would like to thank my fiancée for her patience and understanding, and for enriching my life.

ABSTRACT

The research in this thesis involves the development and application of electronic structure theory to obtain an understanding of the molecular electronic structure, bonding, and reaction mechanisms of main group organic and organometallic chemistry, with the emphasis on highly energetic species. Areas of research include: 1) systematic investigations of the molecular electronic structures and bonding of Group IVB [1.1.1]propellanes, and Group IVB 2,4,5-trioxa[1.1.1]propellanes and Group IVB 2,4,5-trithia[1.1.1]propellanes; 2) predicting the structures, stabilities, and dissociation barriers of metastable molecules for possible high energy density material (HEDM) applications; 3) analysis of the mechanism and potential energy surface of the $\text{Si}^+ + \text{CH}_3\text{-SiH}_3$ reaction; 5) evaluation the β effect of carbon, silicon, germanium, or tin on the carbenium ions in $\text{H}_2\text{R}'\text{MCH}_2\text{CHR}^+$ ($\text{R}' = \text{H}$; $\text{R} = \text{H}, \text{CH}_3$; $\text{M} = \text{C}, \text{Si}, \text{Ge}, \text{Sn}$); 6) developing parameters for scaling electron correlation energy; 7) study the effect of hydration and dimerization of the formamidine [1,3] sigmatropic rearrangement.

CHAPTER 1. GENERAL INTRODUCTION

1.1 General Overview

The chemistry of highly strained cyclic compounds have always been of interest to chemists due to their unusual bonding nature and their ability to store large amounts of energy. These species, therefore, have potential applications as new high energy density materials (HEDM) such as high performance fuels. Since many of these compounds are often highly reactive (or explosive), the advantage in pursuing knowledge of structures, energetics, bonding and chemical reactivities theoretically is clear. Another type of reaction of wide interest reported in this thesis is the ion-molecule reaction. In particular, gas phase studies of small silicon cluster ions with different reagents have proven valuable in understanding chemical deposition and etching. Furthermore, as the demands of silicon device fabrications grow, there is considerable advantage in understanding silicon ion-molecule reactions.

At present, most of our understanding of the structural, bonding, energetics and other properties of chemical systems is based on the *ab initio* or semi-empirical molecular orbital (MO) theory. In *ab initio* MO theory, the Schrödinger equation is approximately solved using only a small number of physical constants, i.e., Planck's constant, masses and charges of electrons and nuclei. In its simplest form, MOs describe the motion of electrons in an average electric field generated by electrons and nuclei with occupational restriction of two, one and zero for doubly occupied, singly occupied and virtual MOs. Such an approach leads to the Hartree-Fock (HF) models described below. MO theory, however, is not restricted to the HF models. When the single configurational HF models are not adequate, a set of HF trial orbitals is often used as a starting point for generating multi-configurational (MC) wave functions. MOs constructed in this way

relax the integer occupational restrictions in the HF model and introduce more flexibility and electron correlation effects into the wave function and energy, respectively. In this thesis, both single configurational and multi-configuration based methods are used.

1.2 Thesis Organization

This thesis is a collection of nine papers, five of which have been published in refereed journals. The remaining four been submitted or will be submitted to scholarly journals for review and publication. The research reported in this thesis begin with a study of group IVA [1.1.1]propellane and derivatives. Chapter 2 examines the structures, energetics and bonding of group IVA [1.1.1]propellanes in comparison with corresponding bicyclopentanes. The structural, energetic and bonding analysis of Group IVA 2,4,5-trioxo[1.1.1]metallapropellanes, group IVA 2,4,5-trithia[1.1.1]metallapropellanes and the bicyclopentane analogs are presented in Chapter 3. Besides attempting to develop a broad understanding of the structures and bonding in these compounds, an ancillary objective of Chapters 2 and 3 is to assess the ability of effective core potentials—implemented in the GAMESS quantum chemistry program—to reproduce the structure and (valence) electron densities predicted by full *ab initio* calculations.

Chapter 4 concerns structures, energetics and bonding of high energy N_2O_2 isomers. These metastable species are of interest because they are isoelectronic with bicyclobutane and due to their potential applications as new high energy density materials. Chapter 5 details the inversion processes of bicyclobutane and its isoelectronic congener bicyclodiazoxane (N_2O_2). Chapter 6 investigates the isomerization mechanism of bicyclobutane to butadiene.

The concept of stabilization of β positive charge on the carbenium ion in $H_2R'MCH_2CHR^+$ ($M = C, Si, Ge, Sn$; $R' = H$; $R = H, CH_3$) is explored in chapter 7.

focusing on the structures and relative stabilities of these ions. The relative stabilities of these carbenium ions provided by M are determined by calculating the energy change in the isodesmic reactions. In chapter 8, mechanisms of the reaction of Si⁺ with methylsilane are elucidated.

In Chapter 9, parameters for scaling the correlation energy in Møller-Plesset perturbation theory (MP-SAC) are developed. Chapter 10 applies the MP-SAC method to study different proton transfer mechanisms in formamidine, a molecule of medical and biochemical importance. Chapters 2-9 are preceded by the Theoretical Background Section where a brief overview of the theoretical methods used in the thesis is given. A general conclusion is given in Chapter 11.

1.3 Theoretical Background

The quantum chemistry literature contains a large number of theoretical methods; each has its own niche in the theoretical world. The capability of a method in delivering the desired accuracy is limited by the approximations made in its derivations. The following sections provide a brief overview of the approximations made in deriving the methodologies used in this thesis.

1.3.1 Fundamental Approximations to The Nonrelativistic Schrödinger Equation

The energy and all properties of a chemical system in a stationary state can be obtained by the solution of the Schrödinger equation (1.1).¹

$$\hat{H}\Psi = E\Psi \quad (1.1)$$

\hat{H} and Ψ are the Hamiltonian operator and wave function. Ψ is a function of Cartesian coordinates of all particles (electrons and nuclei). Analytical solutions of the Schrödinger equation can be obtained only for the simplest systems (two interacting-body). One

fundamental approximation to simplify the molecular problem is to separate the nuclear and electronic motions, the Born-Oppenheimer (adiabatic) approximation.² The Born-Oppenheimer nonrelativistic³ electronic Hamiltonian can be written as

$$\hat{H} = -1/2 \sum_i \nabla_i^2 - \sum_{i,A} Z_A r_{i,A}^{-1} + \sum_{i<j} r_{ij}^{-1} + \sum_{A<B} Z_A Z_B R_{AB}^{-1} \quad (1.2)$$

where the first term of (1.2) corresponds to the electronic kinetic energy, the second term is the electron-nuclear attraction, the third term is the electron-electron repulsion, and the fourth term is the nuclear-nuclear repulsion. The expectation value of the energy is

$$E = \frac{\langle \Psi | \hat{H} | \Psi \rangle}{\langle \Psi | \Psi \rangle} \quad (1.3)$$

We can write the wave function as

$$\Psi = \sum_i C_i \Phi_i, \quad (1.4)$$

where the Φ_i are a (basis) set of N-electron functions. If we substitute (1.4) into (1.3), and apply the variational principle to minimize the function (1.3) with respect to the parameters C_i , we obtain a set of secular equations or CI equations,

$$\sum_j (H_{ij} - ES_{ij}) C_j = 0 \quad (1.5)$$

where

$$H_{ij} = \langle \Phi_i | \hat{H} | \Phi_j \rangle \quad (1.6)$$

and

$$S_{ij} = \langle \Phi_i | \Phi_j \rangle \quad (1.7)$$

are the Hamiltonian and overlap matrix elements between the functions $\{\Phi_i\}$. These are known functions that depend on the coordinates of all N electrons in the molecule, they are called the N -electron basis. If the N -electron basis were a complete set (infinite dimension), this approach would introduce no approximation. Practical considerations require working with incomplete N -electron basis sets. The N -particle basis functions are obtained as linear combinations of products of one-electron functions, orbitals,

$$\Phi_i = \mathfrak{R} \prod_k^N \psi_{ik}(q) \quad (1.8)$$

where \mathfrak{R} is chosen to satisfy the correct spin and symmetry.⁴ The functions $\{\psi\}$ are called molecular orbitals (MOs). The MOs are typically constructed as orthonormal linear combinations of a one-electron basis (AOs⁵):

$$\psi_{ik} = \sum_{\mu} C_{\mu,ik} \phi_{\mu} \quad (1.9)$$

So the one-electron basis (AOs) determines the MOs, which in turn determine the N -electron basis. If the one-electron basis were complete (infinite dimension), it would be possible to form a complete N -electron basis and to obtain an exact wave function (complete CI) variationally. Using a truncated one-electron basis and *all* possible N -electron basis functions, one can obtain a full CI wave function. At present, full CI calculations are computationally feasible only for small systems, and the results are often used as a reference for comparisons with other methods.

1.3.2. Potential Energy Surface

The energy obtained as a function of relative nuclear coordinates R ($E(R)$) is referred to as a potential energy surface (PES). The lowest $E(R)$ from an approximate solution of the Schrödinger equation is called the ground state potential energy surface. Since potential energy surfaces are $3N-6$ ($3N-5$ for linear systems) dimensional hypersurfaces in coordinate space of N -nuclei, complete acquisition of the functions $E(R)$ are not practical for systems with N greater than 3. Therefore, we typically focus on obtaining important parts of the PES for systems of interests. Points on potential energy surfaces for which the first derivative of $E(R)$ with respect to nuclear coordinates vanishes are called *critical* or *stationary* points. The energy second derivative matrix with respect to nuclear coordinates is called the hessian. Stationary structures whose Hessians have zero and one negative eigenvalues are referred to as minima and transition states, respectively. Minima correspond to stable equilibrium structures that may be observed experimentally provided that significant barriers (relative energy between minima and transition states) for adiabatic and non-adiabatic processes leading to other minima exist. A path connecting two minima and a transition state—composed of two steepest-descent paths in the mass-weighted Cartesian coordinates that emerge from a transition state in both directions—corresponds to the minimum energy reaction path for an elementary chemical transformation.⁶

Since minima, transition states, reaction paths and the corresponding wave functions are fundamental to the description of chemical reactions, practical theoretical electronic structure methods used to obtain them are discussed in the following sections.

1.3.3. The Hartree-Fock Approximation

The HF wave function for a closed-shell system can be obtained by minimizing the energy with respect to the orbitals (ψ_i), subject to the constraint that the set ψ_i remain

orthonormal. This leads to a set of algebraic equations for $C_{\mu i}$ (Roothaan equations^{4a}).

In the AO basis the restricted Hartree-Fock (RHF) equations are

$$\sum_{\nu=1}^N (F_{\mu\nu} - \varepsilon_i S_{\mu\nu}) C_{\nu i} = 0 \quad \mu = 1, 2, \dots, N \quad (1.10)$$

where ε_i is the one-electron energy of molecular orbital ψ_i , $S_{\mu\nu}$ are elements of the overlap matrix. The Fock matrix element $F_{\mu\nu}$ is

$$F_{\mu\nu} = H_{\mu\nu}^{core} + \sum_{\lambda=1}^N \sum_{\sigma=1}^N P_{\lambda\sigma} [(\mu\nu|\lambda\sigma) - \frac{1}{2}(\mu\lambda|\nu\sigma)] \quad (1.11)$$

where $P_{\lambda\sigma}$ is the one-electron density matrix. The quantities $(\mu\nu|\lambda\sigma)$ are two-electron repulsion integrals.

$$H_{\mu\nu}^{core} = \langle \phi_\mu | \hat{H}^{core} | \phi_\nu \rangle \quad (1.12)$$

$$H^{core}(1) = -\frac{1}{2} \nabla_1^2 - \sum_{A=1}^M \frac{Z_A}{r_{1A}} \quad (1.13)$$

$$(\mu\nu|\lambda\sigma) = \int \phi_\mu^*(1) \phi_\nu(1) r_{12}^{-1} \phi_\lambda^*(2) \phi_\sigma(2) dr_1 dr_2 \quad (1.14)$$

Equation (1.10) must be solved iteratively. This procedure, called the *self-consistent-field* (SCF) method^{4a,7}, begins with a guess of the one-electron density matrix $P_{\lambda\sigma}$ to calculate the first iteration of the Hartree-Fock potential

$$E_0 = \frac{1}{2} \sum_{\mu} \sum_{\nu} P_{\mu\nu} (H_{\mu\nu}^{core} + F_{\mu\nu}) \quad (1.15)$$

This is repeated until E_0 and the density matrix no longer change. The Roothaan equations can be modified to open-shell systems in which electrons are not restricted to

occupied orbitals in pairs. This gives rise to restricted open-shell HF (ROHF^{7b}) and unrestricted open-shell HF (UHF^{7c}) SCF procedures.

1.3.4. Effective Core Potentials

Eliminating the core electrons in studying the electronic structures and properties of molecules can significantly reduce the computational costs, especially in systems with heavy elements. Since core electrons—being strongly bound to atomic nuclei—are acting largely as a shield to provide an effective field in which valence electrons move, most valence chemical properties arise from the valence electrons in molecules. Therefore *ab initio* effective core potentials are becoming widely used in quantum chemistry.

The Hartree-Fock equation can be reformulated in terms of valence electrons by incorporating the effective core potential V^{eff} into the Hamiltonian operator.⁸ This angular-momentum-dependent (l) local potential has the form

$$V^{eff} = \frac{Z_c}{r} + V_{L+1}(r) + \sum_{l=0}^L [V_l(r) - V_{L+1}] P_{lm} \quad (1.16)$$

where L is the maximum value of l in the core, and P_{lm} is the angular momentum projection operator

$$P_{lm} = |Y_{lm}(\theta, \varphi)\rangle \langle Y_{lm}(\theta, \varphi)| \quad (1.17)$$

$Y_{lm}(\theta, \varphi)$ are the spherical harmonics; the potentials V_L and V_l are Gaussian expansions of the form

$$V_l(r) = \sum_k A_{ik} r^{n_{kl}} e^{-B_{ik} r^2} \quad (1.18)$$

where n_{lk} are either 0, 1, or 2, and A_{lk} and B_{lk} are parameters obtained by atomic Hartree-Fock calculations.

Although the simple SCF methods are successfully used in many applications, there are limitations such as an inability to describe the dissociation of molecules into open-shell fragments. The next four sections discuss methods for obtaining correct descriptions of the PES and electron correlation energy, which is defined as the difference between the exact nonrelativistic energy and the Hartree-Fock energy.⁹ These methods relax the occupational restrictions imposed on the molecular orbitals (0, 1 or 2) by the HF methods.

1.3.5. The Multiconfiguration Self-Consistent Field (MCSCF)

Approximation

The MCSCF¹⁰ wave function is obtained as a truncated CI expansion (1.4)

$$\Psi_{MCSCF} = \sum_I C_I \Phi_I \quad (1.19)$$

in which both the expansion coefficients (C_I) and the orbitals contained in Φ_I are optimized. The truncation of (1.19)—defining an active space—requires chemical intuition. An active space which includes all possible configurations (constructed by distributing the electrons among the active orbitals) is referred to as the *complete active space* (CAS) or *fully optimized reaction space* (FORS).¹¹

Consider H₂ as a simple example. The CASSCF wave function for this molecule contains two closed-shell configurations

$$|\Psi_{MCSCF}\rangle = C_A |\psi_A \bar{\psi}_A\rangle + C_B |\psi_B \bar{\psi}_B\rangle \quad (1.20)$$

where ψ_A and ψ_B are the bonding and antibonding combinations of the AOs.

$$\psi_i = \sum_{\mu} C_{\mu i} \phi_{\mu} \quad i = A, B \quad (1.21)$$

The MCSCF energy is obtained by minimizing $\langle \Psi_{MCSCF} | \hat{H} | \Psi_{MCSCF} \rangle$, subject to the constraints

$$\langle \psi_A | \psi_A \rangle = \langle \psi_B | \psi_B \rangle = 1 \quad \langle \psi_A | \psi_B \rangle = 0 \quad (1.22)$$

and

$$C_A^2 + C_B^2 = 1 \quad (1.23)$$

1.3.6. The MR-CI Configuration Expansion

Correlation corrections for SCF and MCSCF wave functions can be obtained by performing configuration interaction (CI)¹² or perturbation theory (PT)¹³ calculations. Since the Hamiltonian operator does not contain more than two-electron operators, the simplest (single reference) correlated wave function, and often a very good approximation to the true wave function, can be written as

$$\Psi_{SD} = C_0 \Phi_0 + \sum_{ia} C_i^a \Phi_i^a + \sum_{ijab} C_{ij}^{ab} \Phi_{ij}^{ab} \quad (1.24)$$

where Φ_0 is the Hartree-Fock configuration and Φ_i^a and Φ_{ij}^{ab} are single and double replacements out of Φ_0 . The occupied (internal) orbitals $i, j, (k, l)$ are replaced by the unoccupied (external or virtual) orbitals $a, b, (c, d)$.

There are two fundamentally different approaches for extending the treatment of electron correlation beyond CISD for cases in which the single determinant wave function is less than adequate. These involve either the addition of triply or even quadruply excited configurations functions (CFs) to the single reference wave function

$$\Psi_{SDTQ} = \Psi_{SD} + \sum_{ijkabc} C_{ijk}^{abc} \Phi_{ijk}^{abc} + \sum_{ijklabcd} C_{ijkl}^{abcd} \Phi_{ijkl}^{abcd} \quad (1.25)$$

or the addition of reference configurations to (1.24).

$$\Psi_{MR-CI} = \sum_J \Psi_{SD}(J) \quad (1.26)$$

where the sum over J runs over all selected reference configurations. The MRCI expression above can be rewritten as

$$\Psi_{MR-CI} = \sum_I C^I \Phi_I + \sum_S \sum_a C_a^S \Phi_S^a + \sum_P \sum_{ab} C_{ab}^P \Phi_P^{ab} \quad (1.27)$$

where Φ_I , Φ_S^a , Φ_P^{ab} are internal, singly external (N-1), and doubly external (N-2) CFs.

Even for moderate size systems, the number of configurations generated by (1.27) can become extremely large ($>10^6$). A method called internally contracted CI (ICCI)¹³ alleviates this problem. In ICCI, the configurations are generated by applying one and two electron excitation operators (\hat{E}_{ri} , $\hat{E}_{ri,sj}$) to the complete reference wave function Ψ_0 .

$$\Psi_0 = |0\rangle = \sum_{\mu} C_{\mu} \Phi_{\mu} \quad (1.28)$$

$$\Psi_i^a = \hat{E}_{ai} |0\rangle = \sum_{\mu} d_{\mu} \Phi_{\mu}^a \quad (1.29)$$

$$\Psi_{ij}^{ak} = \hat{E}_{ai} \hat{E}_{kj} |0\rangle = \sum_{\mu} d_{\mu} \Phi_{\mu}^a \quad (1.30)$$

$$\Psi_{ij}^{ab} = (\hat{E}_{ia} \hat{E}_{bj} + p \hat{E}_{aj} \hat{E}_{bi}) |0\rangle = \sum_{\mu} d_{\mu} \Phi_{\mu}^{ab} \quad (1.31)$$

$$\hat{E}_{ij} = \hat{a}_{i\alpha}^+ \hat{a}_{j\alpha} + \hat{a}_{i\beta}^+ \hat{a}_{j\beta} \quad (1.32)$$

where \hat{a} and \hat{a}^+ are the annihilation and creation operators of spin orbitals (i,j) . The contraction coefficients d_μ will be linear combination of C_μ .

$$\Psi_{MR-ICCI} = C_0 \Psi_0 + \sum_{ia} C_i^a \Psi_i^a + \sum_{ijka} C_{ij}^{ak} \Psi_{ij}^{ak} + \sum_{ijab} C_{ij}^{ab} \Psi_{ij}^{ab} \quad (1.33)$$

For a single reference case the internally contracted CI method is identical to the uncontracted case, but for the multi-reference case the number of variational parameters are drastically reduced. The contraction coefficients d_μ can be obtained by operating on equation (1.31) from the left by Φ_μ^{ab} .

ICCI calculations are carried out with uncontracted (1.29) and (1.30), since in order to orthonormalize Ψ_i^a and Ψ_{ij}^{ak} , the third- and fourth-order density matrices, respectively, are needed. Furthermore, calculation of the direct CI coupling coefficients becomes very difficult if Ψ_i^a and Ψ_{ij}^{ak} are used as a basis.

1.3.7. Rayleigh-Schrödinger Perturbation Theory For Arbitrary Zero-Order Functions

In Rayleigh-Schrödinger many-body perturbation (RSMP) theory,¹³ we wish to solve the eigenvalue problem

$$\hat{H}|\Phi_i\rangle = (\hat{H}_0 + \hat{V})|\Phi_i\rangle = E_i|\Phi_i\rangle \quad (1.33)$$

where we know the eigenfunctions and eigenvalues of \hat{H}_0 ,

$$\hat{H}_0|\Psi_i^{(0)}\rangle = E_i^{(0)}|\Psi_i^{(0)}\rangle \quad \text{or} \quad \hat{H}_0|i\rangle = E_i^{(0)}|i\rangle \quad (1.34)$$

If the perturbation, V , is small, E_i and Φ_i would be close to $E_i^{(0)}$ and $|i\rangle$, respectively.

We can systematically improve the eigenfunctions and eigenvalues of \hat{H}_0 by introducing an ordering parameter λ (which will be set equal to 1)

$$\hat{H} = \hat{H}_0 + \lambda \hat{V} \quad (1.35)$$

We can then expand the exact eigenfunctions and eigenvalues in a Taylor series in λ ,

$$E_i = E_i^{(0)} + \lambda E_i^{(1)} + \lambda^2 E_i^{(2)} + \dots \quad (1.36)$$

$$|\Phi_i\rangle = |i\rangle + \lambda |\Psi_i^{(1)}\rangle + \lambda^2 |\Psi_i^{(2)}\rangle + \dots \quad (1.37)$$

Equating coefficients of λ^n , we can obtain the following expression for the n th-order energies

$$E_i^{(0)} = \langle i | \hat{H}_0 | i \rangle \quad (1.38)$$

$$E_i^{(1)} = \langle i | \hat{V} | i \rangle \quad (1.39)$$

$$E_i^{(2)} = \langle i | \hat{V} | \Psi_i^{(1)} \rangle \quad (1.40)$$

A partitioning scheme for the case in which \hat{H}_0 is the sum of the Fock operators—Møller-Plesset (MP) partition—reduces equations (1.40) to

$$E_0^{(2)} = \frac{1}{2} \sum_a \sum_b \sum_r \sum_s \frac{\langle ab | rs \rangle \langle rs | ab \rangle}{\epsilon_a + \epsilon_b - \epsilon_r - \epsilon_s} - \frac{1}{2} \sum_a \sum_b \sum_r \sum_s \frac{\langle ab | rs \rangle \langle rs | ba \rangle}{\epsilon_a + \epsilon_b - \epsilon_r - \epsilon_s} \quad (1.41)$$

where ϵ_i in the denominators are the HF orbital energies, and $\langle ab | rs \rangle$ are two-electron integrals (a, b denote occupied MOs, and r, s denote virtuals MOs).

When the reference wave function is a CASSCF, the first order wave function for a state of interest can be expanded as¹⁵

$$|\Psi^{(1)}\rangle = \sum_{j=1}^M C_j |j\rangle, \quad j \in V_{SD} \quad (7.42)$$

where $M \geq \dim V_{SD}$ (the first order interacting space, all functions in V_{SD} can be generated by excitation operators similar to ICCI) and $\{C_j, j=1, \dots, M\}$ is a solution of the system of linear equations

$$\sum_{j=1}^M C_j \langle i | \hat{H}_0 - E_0 | j \rangle = -\langle i | \hat{H} | 0 \rangle, \quad i=1, \dots, M \quad (1.43)$$

where $E_0 = \langle 0 | \hat{H} | 0 \rangle$ is the zeroth-order energy.

$$\hat{H}_0 = \hat{P}_0 \hat{F} P_0 + \hat{P}_K \hat{F} P_K + \hat{P}_{SD} \hat{F} P_{SD} + \hat{P}_{TQ} \hat{F} P_{TQ} \quad (1.44)$$

$$\hat{F} = \sum_p \varepsilon_p \hat{E}_{pp} \quad (1.46)$$

$$\varepsilon_{pq} = h_{pq} + \sum_{rs} D_{rs} \left[\langle pq | rs \rangle - \frac{1}{2} \langle pr | qs \rangle \right] \quad (1.47)$$

where P_i are projection operators, p runs over the entire orbital space, and D_{rs} are one-particle matrix elements.

References

- (1) (a) Schrödinger, E. *Ann. Physik*, **1926**, 79, 361. (b) Schrödinger, E. *Ann. Physik*, *Ann. Physik*, **1926**, 79, 489. (c) Schrödinger, E. *Ann. Physik*, **1926**, 80, 437. (d) Schrödinger, E. *Ann. Physik*, **1926**, 81, 109.
- (2) Born, M.; Oppenheimer, J. R. *Ann. Physik*, **1927**, 84, 457.
- (3) Relativistic effects on the total energy are usually small ($\sim Z^4/c^2$; Z = nuclear charge; $c = 137$ au). For discussions on relativistic effects on chemical properties see: (a) Pitzer, K. S. *Acc. Chem. Res.* **1979**, 12, 271. (b) Pyykko, P.; Desclaux, J. P. *Acc. Chem. Res.* **1979**, 12, 276.
- (4) (a) Roothan, C. C. J. *Rev. Mod. Phys.* **1951**, 23, 69. (b) Paunz, R. *Spin Eigenfunctions*, Plenum, New York, 1979.

- (5) For discussions on atomic basis set selection for molecular calculations see: (a) Davidson, E. R.; Feller, D. *Chem. Rev.* **1986**, 86, 681. (b) Wilson, S. *Proceeding of The NATO Advanced Study Institute on Methods in Computational Molecular Physics*. Bad Windsheim, West Germany, 1992.
- (6) For discussions on the PES for polyatomic systems see: a) Müller, K. *Angew. Chem. Int. Ed. Engl.* **1980**, 19, 1.
- (7) (a) A discussion of the SCF procedure and illustrative examples is given by Szabo, A.; Ostlund, N. S. in *Modern Quantum Chemistry*, First Ed. Rev., McGraw-Hill, New York, 1989; pp 108-230. (b) Guest, M. F.; Saunders, V. R. *Mol. Phys.* **1974**, 28, 819. (c) Pople, J. A.; Nesbet, R. K. *J. Chem. Phys.* **1954**, 22, 571.
- (8) For discussions on effective core potential methods see: (a) Christiansen, P. A.; Ermler, W. C.; Pitzer, K. S. *Ann. Rev. Phys. Chem.* **1985**, 36, 407. (b) Krauss, M.; Stevens, W. J. *Ann. Rev. Phys. Chem.* **1984**, 34, 357. (c) Weeks, J. D.; Hazi, A.; Rice, S. A. *Adv. Chem. Phys.* **1969**, 16, 283.
- (9) Löwdin, P.-O. *Adv. Chem. Phys.* **1959**, 2, 207.
- (10) For reviews on MCSCF methods see: (a) Roos, B. *lecture Notes in Chemistry*, **1992**, 59, 177. 1. (b) Werner, J.-H. *Adv. Chem. Phys.* **1987**, 59, 1. (c) Shepard, R. *Adv. Chem. Phys.* **1987**, 59, 63.
- (11) (a) Lengsfeld, B. H. III; *J. Chem. Phys.* **1980**, 73, 382. (b) Jarkony, D. R. *Chem. Phys. Lett.* **1981**, 77, 634. (c) Ruedenberg, K.; Schmidt, M. W.; Dombek, M. M.; Elbert, S. T. *Chem. Phys.* **1982**, 71, 41,51 65. (e) Roos, B. O.; Taylor, P. R.; Siegbahn, P. E. M. *Chem. Phys.* **1980**, 48, 157. (f) Siegbahn, P. E. M.; Heiberg, A.; Roos, B. O.; Levy, B. *Phys. Scr.* **1980**, 21, 323. (g) Siegbahn, P. E. M. Almlöf, J.; Heiberg, A.; Roos, B. O. *J. Chem. Phys.* **1981**, 74, 2384.

- (12) For discussions on CI see Siegbahn, P. E. M. *lecture Notes in Chemistry*, **1992**, 59, 255
- (13) Szabo, A.; Ostlund, N. S. in *Modern Quantum Chemistry*, First Ed. Rev., McGraw-Hill, New York, 1989; pp 320-379.
- (14) (a) Werner, H.-J.; Knowles, P. J. *J. Chem. Phys.* **1988**, 89, 5803. (b) Werner, H.-J.; Knowles, P. J. *Chem. Phys. Lett.* **1988**, 145, 514.
- (15) (a) Anderson, K. Malmqvist, P.-Å., Roos, B. O. *J. Chem. Phys.* **1992**, 96, 1218. (b) Anderson, K. Malmqvist, P.-Å., Roos, B. O. *J. Phys. Chem.* **1990**, 94, 5483.

CHAPTER 2. THE STRUCTURE AND BONDING IN GROUP IV

[1.1.1]PROPELLANES

A paper published in *Polyhedron* **1991**, 7924-7929

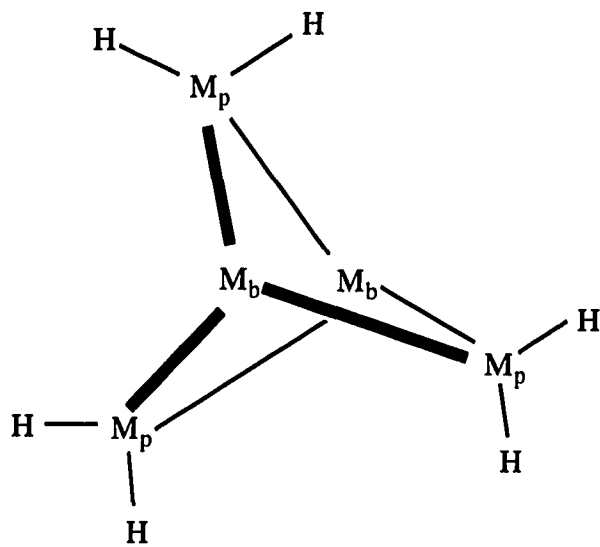
Mark S. Gordon, Kiet A. Nguyen, and Marshall T. Carroll

Abstract

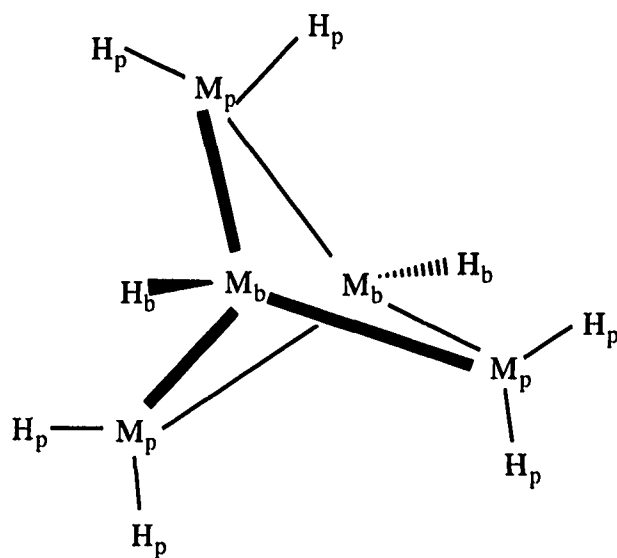
The structures of Group IV [1.1.1]propellanes are determined using *ab initio* all-electron and effective core potential methods. The bonding in these systems is examined using the theory of atoms in molecules and localized molecular orbital analysis. Singlet-triplet splittings are also calculated. Comparisons with the corresponding bicyclopentanes are made. The bonding interaction between the two bridgehead atoms decreases upon descending the group. Further, the similarities in the internuclear bridgehead region between the propellanes and bicyclopentanes increases upon descending the group.

Introduction

In a recent series of papers Sita and co-workers¹ have prepared several intriguing polycyclic tin compounds. One of these species, 2,2,4,4,5,5-hexakis(2,6-diethylphenyl)pentastanna[1.1.1]propellane (**1**) is particularly interesting, in view of the continuing discussion of the nature of bonding, especially between the bridge atoms, in propellanes.¹⁻¹¹ According to the X-ray crystal structure of **1** (M = Sn), the distance between the bridgehead (br) atoms, 3.367 Å, is much longer than that between the bridgehead and peripheral (pe) atoms, 2.841-2.871 Å. This suggests that the bond connecting the two bridgehead atoms is extremely weak, if it exists at all. Significantly, addition across the br-br bond yields a pentastannabicyclopentane (**2**, M = Sn) whose br-br distance



1



2

(3.361Å) differs only slightly from that in the parent [1.1.1]propellane **1** ($M = \text{Sn}$). This reinforces the notion that there is little or no br-br bonding in **1** ($M = \text{Sn}$).

The simplest group IV [1.1.1]propellane, with $M = \text{C}$, has received considerable attention from both experimentalists¹²⁻¹⁴ and theoreticians^{2,3,7-11,15} in recent years, in an

attempt to unravel the nature of the bonding in this compound. In contrast to the case of Sn, the br-br bond in the parent [1.1.1]propellane (1.60\AA)¹³, is only slightly longer than the br-pe bondlength in the same compound (1.52\AA) and much shorter than the corresponding br-br distance in **2** with $M = \text{C}$ (1.84\AA)¹⁶. These experimental distances suggest that there is much more likely to be a bond connecting the bridgehead atoms in the parent propellane than in its pentastanna analog.

The numerous theoretical studies of the parent [1.1.1]propellane have recently been reviewed by Wiberg.¹² A detailed analysis of the bonding in this compound has been presented by Wiberg, Bader, and Lau², using the density analysis developed by Bader and co-workers.^{15,17,18} These authors emphasize the point that it is essential in analyzing molecular structure and bonding to consider the *total* electron density and not just the contributions from a subset of orbitals. Indeed, the density analysis based on a self-consistent field (SCF) calculation with the 6-31G(d) basis set¹⁹ reveals a *bond critical point*¹⁵ (that is, a saddle point in the total electron density) connecting the bridgehead atoms. Such a point is indicative of the existence of a bond connecting these atoms and is at variance with the conclusions of earlier analyses,^{8,9} based on a subset of the occupied molecular orbitals. Further evidence for the br-br bond is the existence of three *ring critical points*, one for each three-membered ring.

The pentasila analog of [1.1.1]propellane is unknown experimentally, but has been investigated by Schleyer and Janoschek.³ Using a two-configuration (TCSCF) wave function and an effective core potential, these authors find a rather long (2.735\AA) br-br bond length and "substantial singlet diradical character". If the latter is defined as twice the square of the coefficient for the excited configuration, the percent diradical character from the TCSCF wavefunction is 12.5%. This plus a very small natural atomic orbital bond order²⁰ is taken as an indication that there is only very weak br-br bonding in this

compound. Schoeller and co-workers have also predicted a long br-br bond length in the pentasila compound.⁶ The ring strain in pentasila[1.1.1]propellane has been investigated by Nagase and Kudo^{4a} and Allen and co-workers,¹⁰ both of whom find this species to be less strained than the carbon parent. In a related paper, Nagase et al. have suggested that placement of electronegative elements in the peripheral positions should stabilize the br-br interaction in the pentasila compound^{4b} and also in the pentagerma compound.⁵ To our knowledge, no calculations have been reported to date on pentastanna[1.1.1]propellanes.

In the present paper, we present a systematic analysis of the group IV [1.1.1]propellanes **1**, with M = C, Si, Ge, Sn, in an attempt to develop a broad understanding of the structure and bonding in these compounds. An ancillary objective of this work is to assess the ability of effective core potentials^{21,22} to reproduce the structures and (valence) electron densities predicted by full *ab initio* calculations.

Computational Approach

The electronic structure calculations presented here have been carried out at several levels of theory. Species which are formally closed shell singlets have been investigated with restricted Hartree-Fock (RHF) wavefunctions, within the LCAO (linear combination of atomic orbitals) approximation. Because there is a question with regard to the existence of a br-br bond in the species **1**, with M = Si, Ge, Sn, and there is the possibility that significant diradical character exists in these compounds,³ the propellane structures were also investigated with generalized valence bond²³ wavefunctions. The corresponding triplet states, investigated to obtain a *qualitative* handle on the relative singlet-triplet splittings as a function of M, were studied with unrestricted Hartree-Fock (UHF) wavefunctions.

The fully *ab initio* calculations have been performed with the 3-21G(d) basis set,²⁴ with d orbital exponents taken from the original papers. Two different sets of effective

core potentials, due to Stevens, Basch, and Krauss²¹ (SBK) and Wadt and Hay²² (WH) have also been used to analyze the same set of compounds, using the same d orbital exponents as in the full *ab initio* calculations. Geometries were determined using the analytical gradients and algorithms contained in GAMESS.²⁵ Structures were verified as minima by verifying that the Hessians (matrices of energy second derivatives) are positive definite. These Hessians were constructed from second derivatives obtained analytically (RHF *ab initio*) or from finite differences of the analytically determined gradients.

The nature of the bonding in the compounds of interest have been investigated using the density analysis developed by Bader and co-workers.^{15,17,18} Because we have found²⁶ that spurious behavior can be obtained in this analysis when heavier elements (such as Si) are involved and standard basis sets are used, two, rather than one, sets of d functions have been used for this analysis. The d orbital exponents used for this purpose are 1.12, 0.32 (C), 0.79, 0.1975 (Si), 0.492, 0.123 (Ge), 0.366, 0.0915 (Sn) for the all electron calculations. For the ECP basis sets the same values are used except 1.6, 0.4 is used for carbon. The density analysis has been discussed in detail elsewhere^{15,17,18}, and only a few key points will be repeated here. Bond (\mathbf{r}_b), ring (\mathbf{r}_r) and cage (\mathbf{r}_c) critical points will be of interest in the following discussion. A bond critical point exists between two atoms if there is a "saddle point" in the electron density $\rho(\mathbf{r})$ between the two atoms. At such a point the Hessian of the electron density has one positive eigenvalue along the bond axis (λ_1) and two negative eigenvalues (λ_2, λ_3) along the axes orthogonal to the bond axis. The existence of a bond critical point implies the existence of a bond path (path of maximum electron density passing through \mathbf{r}_b), and the two atoms are said to be bonded. The Hessian at a ring critical point has two positive and one negative eigenvalues, with the density $\rho(\mathbf{r}_r)$ at the ring critical point being smaller than that at all of the surrounding bond critical points. The Hessian at a cage critical point has three positive

curvatures and $\rho(\mathbf{r})$ is a local minimum at this point. According to this analysis, a [1.1.1] propellane should have a bond critical point between the two bridgehead atoms if a br-br bond exists, as well as three ring critical points, one on the face of each three-membered ring. The lack of such a bond critical point is evidence that there is no "formal bond" connecting these two atoms.^{15,17,18} However, such arguments may not reflect the existence of very flat electron density surfaces.

As an additional tool, the localized molecular orbitals (LMO's) obtained using the prescription of Foster and Boys²⁷ have been calculated. These LMO's will prove to enhance the Bader analysis outlined above.

Results And Discussion

Structures

The calculated geometries for the [1.1.1]propellanes and the bicyclopentanes are listed in Tables 1 and 2, respectively. All structures have been predicted at all levels of theory using the SBK effective core potentials. The same is true for the WH ECP's, except that these are not available for carbon. The *ab initio* GVB structures for the Ge and Sn compounds and the RHF Sn₅Hg structure have been omitted in the interest of conservation of computer time. The ECP structures are generally in quite good agreement with the fully *ab initio* geometries. For C, Si, and Ge, the SBK ECP tends to over-estimate bond lengths, the worst case being the Ge_b-Ge_b bond which is over-estimated by 0.1 Å. On the other hand, the WH ECP under-estimates bond lengths to C and Si, but over-estimates those to Ge and Sn. In general, the SBK bond lengths are closer to the fully *ab initio* ones. The bond angles predicted by all three methods are quite similar.

Since the GVB wavefunction mixes anti-bonding character into the previously RHF description, it is expected that the GVB bond lengths will be longer than those obtained at the RHF level. This will be particularly true for the M_b-M_b distance, since the highest

occupied (HOMO) and lowest unoccupied (LUMO) orbitals correspond to the bonding and antibonding interactions for these atoms. This is indeed seen to be the case in Table 1. For the 3-21G(d) structures, the GVB-RHF difference in the M_b-M_b distance is 0.06 and 0.07 Å for C and Si, respectively. The corresponding differences for the SBK ECP are 0.05 and 0.06 Å, respectively, so the trend is well reproduced. In contrast, both ECP methods predict a progressively smaller change in this bond length upon going from RHF to GVB, when $M = \text{Si, Ge, and Sn}$. This suggests that as M gets heavier, the bonding interaction between the bridgehead atoms decreases. Further evidence for this conclusion is provided by comparing the predicted br-br distances in M_5H_6 with those in M_5H_8 (Table 2). For $M = \text{C}$, the RHF/3-21G(d) br-br distance in bicyclopentane is 0.27 Å longer than the GVB/3-21G(d) value for the same distance in [1.1.1]propellane. This considerable difference is expected if one is comparing a bonded to a non-bonded interaction. The SBK ECP comparison is similar. For $M = \text{Si}$, this difference decreases to 0.15 Å (3-21G(d)), 0.13 Å (SBK), 0.17 Å (WH). This suggests, as before, that the br-br bonding interaction is smaller for Si than for C. The M_5H_6 vs. M_5H_8 br-br distance is even smaller for $M = \text{Ge}$ and virtually non-existent for Sn. So, the calculated geometries suggest a successively decreasing bonding interaction between the bridgehead atoms as M moves vertically downward in group IV.

As discussed by Schleyer,³ the loss of bonding interaction between the bridgehead atoms can result in significant diradical character in the propellane species. The calculated GVB coefficients and corresponding natural orbital occupation numbers (NOON) are listed in Table 3. Taking the latter values as a measure of the percent diradical character, we do find a slight increase upon going from C to Si. (Note that the calculated value of 14% for Si is similar to the value of 12.5% found by Schleyer and Janoschek³). However, the %

diradical character calculated by this measure for $M = \text{Ge}$ and Sn is actually lower than that found for Si !

Another approach to this question of diradical character is to investigate the structures and energies of the corresponding triplets, since the triplet states are, by definition, true diradicals. The triplet propellane structures are also listed in Table 1. While the difference between the UHF triplet and GVB singlet M_b-M_b distance does decrease as M gets heavier, this difference is still greater than 0.1\AA , even for $M = \text{Sn}$. One would expect the singlet and triplet distances to be the same if the singlet were really a diradical. Similarly, one would expect the triplet to be the ground electronic state in this case. Instead, the triplet is at least 1 eV higher in energy than the singlet, even for $M = \text{Sn}$ (Table 4). Further, these splitting values actually are lower limits since the UHF level of theory describes the triplet state better than RHF describes the singlet state. As these observations suggest fairly small diradical character in the ground state [1.1.1]propellanes, it is imperative to examine in detail the characteristics of the electron distributions in these systems.

Analysis of Electron Density and Bonding

While the examination of internuclear distances allows for suggestions as to the strengths of interactions between atoms, shorter internuclear distances do not always imply stronger interactions.²⁸ A topological analysis of the charge density is a more useful tool to probe the strength and nature of the bonding in these systems.

In general, the electron densities in the valence region generated from ECP wavefunctions (RHF, GVB or UHF) are of the same topological form as the corresponding densities generated from all-electron (AE) wavefunctions (Figs. 1-4). Therefore, the two charge distributions have the same number of bond, ring and cage critical points located in approximately the same positions. What is remarkable is that the

AE and ECP values of the charge density at these points are very similar (Table 5). For example, differences in the RHF AE and ECP charge densities evaluated at cage critical points do not exceed 0.0061 au. This value is found for Ge_5H_6 in which the geometric differences between AE and ECP are also the largest. In general, valence densities generated from ECP wavefunctions are both qualitatively and quantitatively similar to the corresponding densities generated from AE wavefunctions.

The above observation is encouraging and suggests that a topological analysis of the charge density of large organic, biochemical or transition metal systems determined using ECP may well yield results which are similar to a corresponding analysis using AE. Since all electron calculations are often not feasible for these large systems, the usefulness of ECP becomes readily apparent. Charge distributions calculated from ECP wavefunctions contain the necessary topological features to determine which atoms are bonded to each other, as well as the relative strengths of the interactions.

Though in the vast majority of cases the absence of the core density in the ECP charge distributions does not affect the determination of critical points in the valence region, the bond critical point between M and H ($M = \text{Si}, \text{Ge}, \text{Sn}$) cannot be located using the ECP wavefunctions. Hydrogen withdraws electrons from M in these cases due to the relative electronegativities of M and H. Since there is no core density on M, there is no maximum at this nuclear position in the charge distribution. Therefore, instead of a saddle point in $\rho(\mathbf{r})$, $\rho(\mathbf{r})$ monotonically increases from the beginning of the valence region of M_p to H (Figs. 2-4).

The SBK density has a bond critical point between Si_b and Si_p but WH does not. The WH charge density at the beginning of the valence region is not of sufficient magnitude to cause a saddle to form between Si_b and Si_p . Instead, a non-nuclear local maximum is found and this point is purely an artifact of the WH basis set. For the Sn_bSn_p

bond in Sn_5H_8 , it is with SBK that this type of critical point is found; WH yields a bond critical point.

We now proceed to analyze bonding in the propellane systems. With the exceptions noted above, the observations made from AE densities are the same as those made from ECP densities. Where possible, we quote AE values; otherwise we use SBK values.

Relief maps of the RHF all electron total charge distributions in σ_v and σ_h planes for the M_5H_6 and M_5H_8 systems are given in Figs. 1-4. Note that the charge density is a maximum only at the nuclear positions. In the σ_v plane, containing the two M_b and one M_p atoms, there are maxima at the two M_b and one M_p nuclei (and also at the two H_b nuclei in M_5H_8). In the σ_h plane, containing the three M_p and six H atoms, there are maxima at the three M_p and six H nuclei. In the σ_v plane there is a saddle point in each charge distribution between each (M_b, M_p) pair. This saddle point has one positive curvature of r along the bond axis and two negative curvatures of ρ orthogonal to the bond axis. As noted in the Introduction, such a saddle point is termed a bond critical point. The σ_v plane affords a view of the positive curvature and one of the negative curvatures associated with a (M_b, M_p) pair. The two gradient paths of ρ that originate at the bond critical point and terminate at the M_b and M_p nuclei define the bond path between these atoms. The charge density is a maximum with respect to any lateral displacement along the bond path. For C_5H_6 , there is also a bond path between the two bridgehead carbons. The σ_v plane shows the positive and one of the negative curvatures of the $\text{C}_b\text{-C}_b$ bond while the σ_h plane shows both negative curvatures. Only for this system is there a bond critical point between the two M_b atoms. In the remaining systems, a cage critical point is found between the two M_b atoms. This kind of critical point is a local minimum and has three positive curvatures: two are displayed in the σ_v plane in M_5H_6 ($\text{M} = \text{Si}, \text{Ge}, \text{Sn}$), and the

third curvature (along with one of the positive curvatures also seen in the σ_v plane) is displayed in the σ_h plane.

There are three ring critical points in C_5H_6 , one on each three-membered ring face. The σ_v plane shows the two positive curvatures in the ring surface and the σ_h plane shows the negative curvature perpendicular to the ring surface and one of the positive curvatures. There are also three ring critical points in C_5H_8 , one associated with each four-membered ring. The arrangement of ring critical points in C_5H_8 is similar to that in the heavier M_5H_6 and M_5H_8 systems ($M = Si, Ge, Sn$).

Having identified the different types of critical points (points at which the gradient of the charge density, $\nabla\rho$, vanishes), it is now useful to discuss the values of the charge density ρ and the Laplacian of the charge density $\nabla^2\rho$ at these points to gain a better understanding of the bonding and strengths of interaction in the M_5H_6 and M_5H_8 systems. The M_b and M_p atoms are said to be bonded because a bond critical point, and hence a bond path, exists between them.^{15,17,18} For homologous series of molecules, the value of the charge density at this point has been correlated with the bond order and strength of the bond.^{2,29-31} These studies have shown that the bond order increases with increasing $\rho(r_b)$. In the hydrocarbon study, ethane, ethene and ethyne were assigned bond orders of 1, 2 and 3 respectively.^{2,29} Since the value of $\rho(r_b)$ for C_bC_p in C_5H_6 (Table 5) is very close to the analogous value for the CC bond in ethane (Table 6), the C_bC_p bond in propellane may be referred to as a single bond of approximately unit bond order. The $\rho(r_b)$ value for C_bC_p in C_5H_8 is also close to the ethane value.

The M_bM_p $\rho(r_b)$ values for M_5H_6 and M_5H_8 ($M = Si, Ge, Sn$) are slightly smaller than the corresponding M_2H_6 values but never less than 84% of the latter value. These bonds in the propellane and bicyclopentane systems can therefore be referred to as single bonds with bond orders slightly smaller than one.

An analysis of the Laplacian of the charge density $\nabla^2\rho$ determines the nature of the interaction between bonded atoms.^{32,33} If the value of $\nabla^2\rho(\mathbf{r}_b)$ is negative, then a shared or covalent interaction results. If the value is positive, then a closed-shell (e.g. ionic) interaction results. In the M_2H_6 systems, the sign of $\nabla^2\rho(\mathbf{r}_b)$ is negative, implying a covalent interaction. This value becomes less negative as the family is descended because the charge density to be shared between the heavy atoms is more diffuse and because some of this density has been removed by the more electronegative hydrogens. The M_bM_p bonds in the propellanes and bicyclopentanes have negative values for $\nabla^2\rho(\mathbf{r}_b)$ though the magnitudes are slightly smaller than those in the corresponding M_2H_6 systems. The ECP $\nabla^2\rho(\mathbf{r}_b)$ values are not in as good agreement with the corresponding AE values as are the $\rho(\mathbf{r}_b)$ values themselves.

In summary, topological analyses of the M_5H_6 and M_5H_8 charge distributions and comparison with M_2H_6 distributions and distances reveal that the M_bH_p bond is basically a covalent single bond, slightly weaker than the prototype MM bond in M_2H_6 .

Using the same analyses as above reveals that the MH bond is a single bond, slightly stronger than the prototype MH bond in M_2H_6 . The interaction is a covalent one only for the carbon compounds. In the heavier systems, where the electronegativity of H substantially exceeds that of Si, Ge and Sn, the interaction is closed-shell (ionic).

A bond path exists between the two bridgehead atoms only in C_5H_6 . The ring critical points are in close proximity to the bond critical point (0.096Å away) and the value of $\rho(\mathbf{r}_r)$ is 97% the value of $\rho(\mathbf{r}_b)$. This means there is a broad bonded maximum in ρ in the interatomic surface (Fig. 1) and a substantial accumulation of charge between the bridgehead nuclei. Wiberg et al² have referred to the C_bC_b interaction as a "fat bond" in order to reflect the flat density surface in the bonding region. The value of $\rho(\mathbf{r}_b)$ for the

C_bC_b bond in C_5C_6 is 80% of the corresponding value in C_2H_6 . The bond order of the C_bC_b bond in C_5H_6 has been calculated to be 0.73.²

A similar "fat bond" is not found for C_bC_b in C_5H_8 . In fact, a cage critical point exists in the bridgehead region, not a bond critical point. Therefore, a bond path does not connect the M_b nuclei in this (or any of the other) group IV bicyclopentanes investigated here. The value of ρ at the cage critical point is only half the value of $\rho(r_b)$ in C_bC_b of C_5H_6 . Fig. 1 displays little charge density in the C_bC_b internuclear region of C_5H_8 .

As mentioned above, there are three ring critical points in C_5H_8 , one associated with each of the three curved four membered ring surfaces. These ring critical points are in close proximity to the cage critical point (0.054 Å away) and are also very close in r values ($\rho(r_r) = 0.0999$ au; $\rho(r_c) = 0.0977$ au). Since the cage critical point is a local minimum in ρ , the ring critical points near it will always be higher in ρ value, even if the difference is very small as it is in this and the other bicyclopentanes.

It is important to recognize that the charge distribution in the bridgehead region of C_5H_8 is different in form from the corresponding region in C_5H_6 . In C_5H_8 , there is not much charge density in the shallow, flat region between the two bridgehead nuclei, and there is no bond path. In C_5H_6 , there is a significant accumulation of charge density and a bond path exists between the two bridgehead nuclei.

The value of $\rho(r_c)$ in the internuclear bridgehead region in Si_5H_6 is only 48% of the value of $\rho(r_b)$ in Si_2H_6 . This suggests that the interaction between the two silicons is weaker in Si_5H_6 than that in Si_2H_6 . The ring critical points in Si_5H_6 are only 0.021 Å from the cage critical point and $\rho(r_r)$ are only very slightly higher than $\rho(r_c)$. Thus, a shallow, flat distribution of charge exists between the bridgehead silicons in Si_5H_6 and no bond path is found.

In Si_5H_8 , the value of $\rho(\mathbf{r}_c)$ is 61% of the corresponding value in Si_5H_6 . The formation of the M_bH_b bonds upon going from M_5H_6 to M_5H_8 removes density from the bridgehead region more than from other regions of the molecule. Though the charge distributions differ quantitatively, qualitatively they have the same topological form. Thus, in the bridgehead region M_5H_6 and M_5H_8 are qualitatively identical in form for $\text{M} = \text{Si}, \text{Ge}$ and Sn (Figs. 2-4).

In Ge_5H_6 , the value of $\rho(\mathbf{r}_c)$ is 41% the value of $\rho(\mathbf{r}_b)$ in Ge_2H_6 . In Ge_5H_8 , the value of $\rho(\mathbf{r}_c)$ is 70% of the corresponding value in Ge_5H_6 . In Sn_5H_6 , the value of $\rho(\mathbf{r}_c)$ is 35% the value of $\rho(\mathbf{r}_b)$ in Sn_2H_6 . In Sn_5H_8 , the value of $\rho(\mathbf{r}_c)$ is 80% of the corresponding value in Sn_5H_6 .

These results lead to the following conclusions: (i) In as much as r at the critical point between M_bM_b is a measure of the strength of the M_bM_b interaction (the greater the value of r , the stronger the interaction), the M_bM_b interaction in M_5H_6 is weaker than that in M_2H_6 , with the interaction becoming progressively weaker as Group IV is descended. (ii) The M_bM_b interaction is weaker in M_5H_8 than in M_5H_6 . As the group is descended, the charge distribution in the bridgehead region in M_5H_6 more closely resembles that in M_5H_8 both qualitatively and quantitatively. Thus, the Sn_bSn_b interaction is the weakest of all the interactions.

It has been shown for C_5H_6 that when the C_bC_b distance is increased over the equilibrium distance, the C_bC_b bond critical point eventually coalesces with the three ring critical points and an unstable critical point (possessing one zero curvature) is formed.^{2,15} A further infinitesimal increase in the C_bC_b distance yields a cage critical point in the internuclear bridgehead region and three new ring critical points, one associated with each of the newly formed four membered rings. We have performed this procedure in reverse for the heavier systems. If we squeeze the two Si_b 's closer together by 0.20\AA in Si_5H_6

(reducing the M_bM_b distance to 2.494Å), the three ring critical points coalesce with the cage critical point. Upon a further infinitesimal compression, a bond critical point and three new ring critical points are created, one on the face of each three membered ring. Thus it takes only 0.20Å (and a corresponding energy increase of only 1.9 kcal mol⁻¹) to form a bond path between the two Si_b atoms. It should be noted that the remainder of the geometry was not reoptimized upon compression of the bridgehead distance, and so, the energy increase values are upper limits. The value of $\rho(\mathbf{r}_b)$ in the compressed geometry is 0.0590 au and this value is 0.0124 au greater than the cage value in the equilibrium geometry. Still, the value of $\rho(\mathbf{r}_b)$ is 0.0260 au less than the M_bM_p $\rho(\mathbf{r}_b)$ value of 0.0850 au, where the M_bM_p distance = 2.331Å. Therefore, the shortening of the M_bM_p distance creates a bond path between these atoms although the bond is still weak compared to a normal SiSi bond.

For a similar change in the molecular graph to occur in Ge₅H₆, the bridgehead nuclei must be squeezed together by 0.29Å. The energy increase is 11.9 kcal mol⁻¹. The value of r at the newly created bond critical point is 0.0506 au, 0.0153 au greater than that at the cage critical point in the equilibrium geometry. This newly created bond (of distance 2.593Å) is weaker than the Ge_bGe_p bond (the Ge_bGe_p distance is 2.449Å) because $\rho(\mathbf{r}_b)$ in the former is 0.0161 au smaller than the corresponding value in the latter bond.

For a similar change in the molecular graph change to occur in Sn₅H₆, the bridgehead nuclei must be squeezed together by 0.37Å and the energy increase is 13.2 kcal mol⁻¹. The value of r at the newly created bond critical point is 0.0315 au, 0.0104 au greater than the cage critical point in the equilibrium geometry. This newly created bond (of distance 3.092Å) is weaker than the Sn_bSn_p bond (of distance 2.876Å) because $\rho(\mathbf{r}_b)$ in the former is smaller than $\rho(\mathbf{r}_b)$ in the latter bond by 0.0190 au.

The ease with which a molecule can change from one structure to another is related to the weakness of the interaction of primary importance in the change.^{2,15,34} The equilibrium M_bM_b distances need to decrease by 7, 10, and 11% for the M_bM_b bond path to form ($M = \text{Si, Ge, Sn}$ respectively). The energy needed to bring about this compression increases upon descending group IV. This supplies further evidence that the Si_bSi_b interaction is stronger than the Ge_bGe_b interaction which in turn is stronger than the Sn_bSn_b interaction. The two bridgehead Si's are more predisposed to bond path formation than the other heavier systems.

Table 5, in addition to listing the RHF values, also includes the GVB (for singlets) and UHF (for triplets) values. The conclusions made above in the RHF discussion hold for GVB and UHF with one exception. No bond path is found between the C_b 's in C_5H_6 (UHF). The C_bC_b distance is much greater in UHF than RHF ($\text{UHF-RHF} = 0.28\text{\AA}$) and the UHF C_bC_b interaction is weaker.

Since the coefficient of the RHF term in the GVB wavefunction is dominant, (Table 3) it is useful to inspect localized orbitals.²⁷ The M_bM_b Boys localized orbital densities are displayed in Fig. 5. The all electron and effective core potential densities are similar in the valence regions. This observation is further evidence of the success with which ECP's describe valence density. There are two electrons in each of the localized molecular orbitals, and there is a critical point (a maximum) in the orbital density at the M_bM_b midpoint. The values of r at this point are 0.1899, 0.0411, 0.0288 and 0.0174 au for $M = \text{C, Si, Ge, Sn}$ respectively. These values are 93, 88, 82, and 82% of the *total* density at the same point for the respective propellanes. Thus, the localization procedure works well to localize the bonding electrons in the bridgehead bonding orbital.

From the above ρ values and from the contour maps, one sees that there is less density in the M_bM_b bonding region as the family is descended. The amount of density in

the localized bridgehead orbital is smallest for Sn_5H_6 owing to the fact that the M_bM_b distance is largest for this system and the effective orbital overlap is smallest.

Though there exists a localized M_bM_b bond orbital in each of the propellane systems, a bond path in the total density exists only in the C_5H_6 case. This is because inclusion of the remaining occupied orbital densities to form the total density creates ring critical points of smaller ρ value than the M_bM_b bond critical point in C_5H_6 . However, in the remaining systems, the M_bM_b critical point becomes a cage critical point as the surrounding ring critical points are slightly higher in ρ value. Thus, the existence or lack of a bond critical point and associated bond path as a function of M , especially upon going from C to Si, arises from a subtle difference in the role played by the other LMO's in the M_bM_b region.

Figure 6 displays maps of the singlet RHF minus triplet UHF densities at the RHF geometries for the σ_h plane of the M_5H_6 systems. Going from the triplet to the singlet, the greatest buildup of charge is in the bridgehead bonding region in the vicinity of the M_bM_b critical point. The density differences become increasingly smaller as the group is descended and the M_bM_b bonding interaction decreases. Indeed the difference in the value of $\rho(\mathbf{r}_c)$ between RHF and UHF is smallest in Sn_5H_6 , and Sn_5H_6 has the smallest magnitude for the singlet-triplet splitting. In the carbon case, enough density flows into the singlet system for a bond critical point to form between the bridgehead atoms. In the heavier systems, this is not the case. Note that the same conclusions are reached using either the all electron or ECP basis set.

Conclusions

The structures and bonding in [1.1.1]propellanes have been studied in this work. The following points are emphasized:

(i) The bonding interaction between the two bridgehead atoms decreases on descending group IV so that for Sn, there is little difference between Sn_5H_6 and Sn_5H_8 in the M_bM_b region, in agreement with the experimental observations of Sita and co-workers.¹ This statement is supported by geometry comparisons to the corresponding bicyclopentanes and ethanes, by a topological examination of the charge density, by GVB-PP calculations, by singlet - triplet energy and density differences and by localized orbital density analyses.

(ii) Valence electron densities generated from effective core potential basis sets are similar to the corresponding densities generated from all electron basis sets. Since these densities are alike, so will be the second derivative density field (the Laplacian). It has been shown that the Laplacian of the charge density field determines the sites of electrophilic and nucleophilic attack and the reactivity of the molecule.^{35,36} Therefore, the reactivity of large biochemical and transition metal systems not amenable to all electron calculations, may well be successfully determined by analyzing the Laplacian of the charge density generated from ECP basis sets.

Acknowledgements—The computations described in this work were performed on the North Dakota State University IBM 3090/120E vector computer, obtained in part with the aid of a joint study agreement between IBM and NDSU, and on the Cray Y-MP at the San Diego Supercomputer Center. This work was supported in part by a grant from the National Science Foundation (CHE-8911911). We thank Professors Richard Bader, Michael Schmidt, Larry Sita and Keith Laidig for useful discussions.

References

1. (a) L. R. Sita and R. D. Bickerstaff, *J. Am. Chem. Soc.* 1989, **111**, 6454. (b) L. R. Sita and R. D. Bickerstaff, *J. Am. Chem. Soc.* 1989, **111**, 3769; (c) L. R. Sita and I. Kinoshita, private communications (1990).
2. K. B. Wiberg, R. F. W. Bader and C. D. H. Lau, *J. Am. Chem. Soc.* 1987, **109**, 985.
3. P. v. R. Schleyer and R. Janoschek, *Angew. Chem. Int. Ed. Engl.* 1987, **26**, 1267.
4. (a) S. Nagase and T. Kudo, *Organometallics* 1987, **6**, 2456; (b) S. Nagase, T. Kudo and T. Kurakake, *J. Chem. Soc., Chem. Commun.* 1988, 1063.
5. S. Nagase and T. Kudo, *Organometallics* 1988, **7**, 2534.
6. W. W. Schoeller, T. Dabisch and T. Busch, *Inorg. Chem.* 1987, **26**, 4383.
7. W. D. Stohrer and R. Hoffmann, *J. Am. Chem. Soc.* 1972, **94**, 779.
8. M. D. Newton and J. M. Schulman, *J. Am. Chem. Soc.* 1972, **94**, 773.
9. J. E. Jackson and L. C. Allen, *J. Am. Chem. Soc.* 1984, **106**, 591.
10. D. B. Kitchen, J. E. Jackson and L. C. Allen, *J. Am. Chem. Soc.* 1990, **112**, 3408.
11. N. D. Epiotis, *J. Am. Chem. Soc.* 1984, **106**, 3170.
12. K. B. Wiberg, *Chem. Rev.* 1989, **89**, 975.
13. (a) K. B. Wiberg and F. H. Walker, *J. Am. Chem. Soc.* 1982, **104**, 5239; (b) K. B. Wiberg, W. P. Dailey, F. H. Walker, S. T. Waddell, L. S. Crocker and M. D. Newton, *J. Am. Chem. Soc.* 1985, **107**, 7247.
14. K. B. Wiberg and S. T. Waddell, *J. Am. Chem. Soc.* 1990, **112**, 2194.
15. R. F. W. Bader, T. T. Nguyen-Dang and Y. Tal, *Rep. Prog. Phys.* 1981, **44**, 893.
16. K. B. Wiberg and J. J. Wendoloski, *J. Am. Chem. Soc.* 1982, **104**, 5679.
17. R. F. W. Bader and T. T. Nguyen-Dang, *Adv. Quant. Chem.* 1981, **14**, 63.
18. R. F. W. Bader, *Acc. Chem. Res.* 1985, **18**, 9.

19. (a) P. C. Hariharan and J. A. Pople, *Theoret. Chim. Acta.* 1973, **28**, 213; (b) M. S. Gordon, *Chem. Phys. Lett.* 1980, **76**, 163.
20. (a) A. E. Reed and F. Weinhold, *J. Chem. Phys.* 1985, **83**, 1736; (b) A. E. Reed, R. B. Weinstock and F. Weinhold, *J. Chem. Phys.* 1985, **83**, 735.
21. W. J. Stevens, H. Basch and M. Krauss, *J. Chem. Phys.* 1984, **81**, 6026.
22. W. R. Wadt and P. J. Hay, *J. Chem. Phys.* 1985, **82**, 284.
23. W. A. Goddard III, T. H. Dunning, W. J. Hunt and P. J. Hay, *Acc. Chem. Res.* 1973, **6**, 368.
24. (a) J. S. Binkley, J. A. Pople and W. J. Hehre, *J. Am. Chem. Soc.* 1980, **102**, 1980; (b) M. S. Gordon, J. S. Binkley, J. A. Pople, W. J. Pietro and W. J. Hehre, *J. Chem. Phys.* 1982, **104**, 2997.
25. M. W. Schmidt, K. K. Baldrige, J. A. Boatz, J. H. Jensen, S. Koseki, M. S. Gordon, K. A. Nguyen, T. L. Windus and S. T. Elbert, *QCPE Bulletin, GAMESS, North Dakota State University* 1990, **10**, 52.
26. J. A. Boatz and M. S. Gordon, *J. Phys. Chem.* 1989, **93**, 3025.
27. J. M. Foster and S. F. Boys, *Rev. Mod. Phys.* 1963, **32**, 300.
28. M. S. Gordon, T. J. Packwood, M. T. Carroll and J. A. Boatz, *J. Phys. Chem.* 1990, submitted.
29. R. F. W. Bader, T. S. Slee, D. Cremer, and E. Kraka, *J. Am. Chem. Soc.* 1983, **105**, 5061.
30. E. Kraka, *Ph.D. Thesis, University of Köln* 1984.
31. M. T. Carroll, *Ph.D. Thesis, McMaster University* 1989.
32. R. F. W. Bader and H. Essén, *J. Chem. Phys.* 1984, **80**, 1943.
33. R. F. W. Bader, P. J. MacDougall and C. D. H. Lau, *J. Am. Chem. Soc.* 1984, **106**, 1594.

34. S. M. Bachrach, *J. Mol. Struct. (Theochem)* 1990, **204**, 131.
35. R. F. W. Bader and P. J. MacDougall, *J. Am. Chem. Soc.* 1985, **107**, 6788.
36. M. T. Carroll, J. R. Cheeseman, R. Osman and H. Weinstein, *J. Phys. Chem.* 1989, **93**, 5120.

Table 1. Geometries of M_5H_6 systems (distances in Å; angles in degrees; M_b denotes bridgehead atom and M_p denotes peripheral atom).

Systems	Wave function	Basis set	Distances			Angles		
			M_b-M_b	M_b-M_p	M_p-H	$M_b-M_b-M_p$	$M_b-M_p-M_b$	M_b-M_p-H
C_5H_6	RHF	a	1.544	1.508	1.079	59.0	62.0	117.5
		b	1.573	1.517	1.080	58.8	62.5	117.5
	GVB	a	1.611	1.518	1.080	57.9	64.2	117.3
		b	1.625	1.523	1.081	57.8	64.5	117.4
	UHF	a	1.834	1.555	1.084	53.9	72.3	116.8
		b	1.835	1.556	1.086	53.9	72.3	117.0
Si_5H_6	RHF	a	2.694	2.331	1.476	54.7	70.6	117.2
		b	2.736	2.352	1.480	54.4	71.2	117.4
		c	2.635	2.309	1.462	55.2	69.6	117.4
	GVB	a	2.759	2.340	1.479	53.9	72.3	117.2
		b	2.793	2.358	1.481	53.7	72.6	117.4
		c	2.700	2.316	1.463	54.4	71.3	117.4
	UHF	a	2.933	2.364	1.480	51.7	76.7	116.6
		b	2.952	2.382	1.484	51.7	76.6	116.8
		c	2.895	2.343	1.466	51.8	76.3	116.9
Ge_5H_6	RHF	a	2.884	2.449	1.545	53.9	72.1	116.9
		b	2.980	2.492	1.533	53.3	73.5	117.4
		c	2.974	2.503	1.540	53.6	72.9	117.5
	GVB	b	2.991	2.488	1.533	53.0	73.9	117.5
		c	2.993	2.500	1.540	53.2	73.5	117.5
	UHF	a	3.044	2.470	1.548	52.0	76.1	116.3
		b	3.097	2.504	1.553	51.8	76.4	116.7
		c	3.120	2.517	1.540	51.7	76.6	116.7
	Sn_5H_6	RHF	a	3.463	2.876	1.748	53.0	74.1
b			3.462	2.863	1.709	52.8	74.4	117.7
c			3.500	2.881	1.715	52.6	74.8	117.9
GVB		b	3.469	2.857	1.708	52.6	74.8	117.8
		c	3.497	2.875	1.715	52.5	74.9	117.9
UHF		a	3.627	2.888	1.748	51.1	77.8	117.0
		b	3.578	2.867	1.707	51.4	77.2	116.8
		c	3.605	2.884	1.715	51.3	77.4	116.9

^a3-21G(d). ^bSBK(d). ^cWH(d)

Table 2. RHF geometries of M_5H_8 systems (distances in Å; angles in degrees; M_b and H_b denote bridgehead atoms and M_p and H_p denote peripheral atoms).

System	Basis set	Distances				Angles			
		M_b-M_b	M_b-M_p	M_b-H_b	M_p-H_p	$M_b-M_b-M_p$	$M_b-M_p-M_b$	$M_p-M_p-H_b$	$M_b-M_p-H_p$
C_5H_8	a	1.879	1.552	1.084	1.087	52.8	74.5	127.2	116.6
	b	1.883	1.555	1.087	1.089	52.7	74.5	127.3	116.9
Si_5H_8	a	2.905	2.353	1.478	1.481	51.9	76.3	128.1	116.7
	b	2.925	2.368	1.480	1.484	51.9	76.3	128.1	117.0
	c	2.869	2.334	1.465	1.466	52.1	75.8	127.9	117.1
Ge_5H_8	a	3.025	2.444	1.534	1.548	51.8	76.5	128.2	116.3
	b	3.053	2.477	1.527	1.534	52.0	76.1	128.0	116.9
	c	3.076	2.494	1.535	1.540	51.9	76.2	128.1	117.0
Sn_5H_8	b	3.509	2.840	1.698	1.708	51.8	76.3	128.2	117.0
	c	3.534	2.857	1.707	1.713	51.8	76.4	128.2	117.2

^a3-21G(d). ^bSBK(d). ^cWH(d).

Table 3. GVB-PP coefficients and natural orbital occupation numbers (NOON) for M_5H_6 systems.

Systems	Basis set	GVB-PP coefficients		NOON	
		HOMO	LUMO	HOMO	LUMO
C_5H_6	a	0.975	-0.223	1.900	0.100
	b	0.975	-0.223	1.903	0.097
Si_5H_6	a	0.964	-0.265	1.860	0.140
	b	0.964	-0.265	1.860	0.140
	c	0.963	-0.269	1.854	0.146
Ge_5H_6	b	0.972	-0.233	1.891	0.109
	c	0.968	-0.252	1.873	0.127
Sn_5H_6	b	0.970	-0.241	1.883	0.117
	c	0.968	-0.250	1.875	0.125

^a3-21G(d). ^bSBK(d). ^cWH(d).

Table 4. Singlet (RHF) - triplet (UHF) splittings for M_5H_6 systems.

System	ΔE (kcal mol ⁻¹) ^a					
	3-21G(2d)	3-21G(d)	SBK(2d)	SBK(d)	WH(2d)	WH(d)
C_5H_6	65.3	63.4	63.7	64.4	—	—
Si_5H_6	32.9	29.6	30.2	29.4	28.3	27.5
Ge_5H_6	36.4	38.3	40.1	40.3	33.8	32.9
Sn_5H_6	25.3	26.4	31.9	31.9	29.9	28.9

^a Energies (triplet minus singlet) are calculated at the SCF optimized geometries where only 1d set of functions is placed on each heavy atom.

Table 5. Bond, ring and cage critical point analysis of M_5H_6 and M_5H_8 systems. M_b and H_b denote bridgehead atoms; M_p and H_p denote peripheral atoms. All values are in atomic units.

Systems	Bond A-B	Wavefunction	Basis set	$\rho(r)$	$\nabla^2\rho(r)$
C_5H_6	M_b-M_b	RHF	a	0.2046	-0.1600
			b	0.1890	0.0031
		GVB	a	0.1762	0.0424
			b	0.1660	0.1491
	M_b-M_p	RHF	a	0.2552	-0.7165
			b	0.2403	-0.4972
		GVB	a	0.2542	-0.7346
			b	0.2397	-0.5129
		UHF	a	0.2459	-0.7340
			b	0.2340	-0.5319
	M_p-H	RHF	a	0.2866	-1.0139
			b	0.2831	-1.0835
		GVB	a	0.2855	-1.0066
			b	0.2816	-1.0683
		UHF	a	0.2817	-0.9832
			b	0.2774	-1.0227
	ring [‡]	RHF	a	0.1977	0.0288
			b	0.1840	0.1273
		GVB	a	0.1747	0.1052
			b	0.1652	0.1822
cage [‡]	UHF	a	0.1020	0.4812	
		b	0.1027	0.4371	
	UHF	a	0.1005	0.4870	
		b	0.1005	0.4738	

[continued]

Table 5—continued

Systems	Bond A-B	Wavefunction	Basis set	$\rho(\mathbf{r})$	$\nabla^2\rho(\mathbf{r})$	
Si ₅ H ₆	M _b -M _p	RHF	a	0.0850	-0.1142	
			b	0.0813	-0.1024	
		GVB	a	0.0855	-0.1176	
			b	0.0821	-0.1056	
		UHF	a	0.0874	-0.1280	
			b	0.0841	-0.1144	
	M _p -H	RHF	a	0.1165	0.3106	
		GVB	a	0.1158	0.3096	
		UHF	a	0.1150	0.3128	
	ring [‡]	RHF	a	0.0467	0.0348	
			b	0.0433	0.0393	
			c	0.0494	0.0305	
		GVB	a	0.0414	0.0506	
			b	0.0391	0.0491	
			c	0.0450	0.0419	
		UHF	a	0.0307	0.0718	
			b	0.0299	0.0614	
			c	0.0313	0.0771	
		cage [‡]	RHF	a	0.0466	0.0340
				b	0.0430	0.0403
				c	0.0493	0.0297
	GVB		a	0.0409	0.0507	
			b	0.0382	0.0536	
			c	0.0448	0.0406	
UHF	a		0.0280	0.0849		
	b		0.0269	0.0793		
	c		0.0285	0.0902		

[continued]

Table 5—continued

Systems	Bond A-B	Wavefunction	Basis set	$\rho(\mathbf{r})$	$\nabla^2\rho(\mathbf{r})$	
Ge ₅ H ₆	M _b -M _p	RHF	a	0.0751	-0.0762	
			b	0.0655	-0.0633	
			c	0.0702	-0.0832	
		GVB	b	0.0658	-0.0643	
			c	0.0670	-0.0760	
			a	0.0782	-0.0992	
		UHF	b	0.0692	-0.0777	
			c	0.0701	-0.0870	
			a	0.1226	0.1597	
	M _p -H	RHF	a	0.1215	0.1654	
		UHF	a	0.0356	0.0409	
		RHF	a	0.0356	0.0409	
	ring [‡]	GVB	b	0.0300	0.0377	
			c	0.0302	0.0429	
			b	0.0301	0.0381	
			c	0.0309	0.0359	
			UHF	a	0.0255	0.0663
			b	0.0230	0.0536	
		cage [‡]	RHF	c	0.0231	0.0548
				a	0.0353	0.0398
				b	0.0292	0.0388
GVB			c	0.0302	0.0421	
			b	0.0292	0.0394	
			c	0.0303	0.0356	
UHF	a	0.0235	0.0738			
	b	0.0210	0.0633			
	c	0.0210	0.0632			

[continued]

Table 5—continued

Systems	Bond		Wavefunction	Basis set	$\rho(r)$	$\nabla^2\rho(r)$
	A-B	M _b -M _p				
Sn ₅ H ₆	M _b -M _p	RHF	a	0.0505	-0.0095	
			b	0.0451	-0.0390	
			c	0.0444	-0.0386	
	GVB	b	0.0462	-0.0424		
		c	0.0448	-0.0403		
		a	0.0532	-0.0222		
	UHF	b	0.0484	-0.0468		
		c	0.0478	-0.0467		
		a	0.0974	0.1136		
	M _p -H	RHF	a	0.0970	0.1159	
		UHF	a	0.0215	0.0230	
		RHF	a	0.0194	0.0211	
	ring [‡]	GVB	b	0.0191	0.0196	
			c	0.0188	0.0239	
			b	0.0188	0.0206	
UHF		a	0.0159	0.0334		
		b	0.0152	0.0300		
		c	0.0148	0.0301		
cage [‡]	RHF	a	0.0211	0.0237		
		b	0.0186	0.0220		
		c	0.0184	0.0198		
	GVB	b	0.0180	0.0254		
		c	0.0180	0.0210		
		a	0.0142	0.0396		
UHF	b	0.0137	0.0356			
	c	0.0132	0.0352			

[continued]

Table 5—continued

Systems	Bond A-B	Wavefunction	Basis set	$\rho(r)$	$\nabla^2\rho(r)$
C ₅ H ₈	M _b -M _p	RHF	a	0.2484	-0.7492
			b	0.2353	-0.5367
	M _b -H		a	0.2814	-0.9939
			b	0.2767	-1.0332
	M _p -H		a	0.2800	-0.9740
			b	0.2557	-1.0050
	ring [‡]		a	0.0999	0.4999
			b	0.1012	0.4435
	cage [‡]		a	0.0977	0.5126
			b	0.0986	0.4847
Si ₅ H ₈	M _b -M _p	RHF	a	0.0895	-0.1352
			b	0.0853	-0.1171
	M _b -H		a	0.1153	0.2979
	M _p -H		a	0.1146	0.3126
	ring [‡]		a	0.0313	0.0747
			b	0.0310	0.0631
			c	0.0319	0.0794
	cage [‡]		a	0.0285	0.0882
			b	0.0278	0.0837
			c	0.0291	0.0920

[continued]

Table 5—continued

Systems	Bond A-B	Wavefunction	Basis set	$\rho(\mathbf{r})$	$\nabla^2\rho(\mathbf{r})$
Ge ₅ H ₈	M _b -M _p	RHF	a	0.0818	-0.1094
			b	0.0726	-0.0876
			c	0.0731	-0.0963
	M _b -H		a	0.1241	0.1610
	M _p -H		b	0.1214	0.1684
	ring [¥]	a	0.0270	0.0707	
		b	0.0246	0.0246	
		c	0.0243	0.0592	
	cage [¥]	a	0.0249	0.0790	
		b	0.0227	0.0684	
		c	0.0224	0.0676	
	Sn ₅ H ₈	M _b -M _p	RHF	c	0.0500
ring [¥]		b	0.0162	0.0332	
		c	0.0156	0.0332	
cage [¥]		b	0.0148	0.0386	
		c	0.0143	0.0382	

^a3-21G(2d). ^bSBK(2d). ^cWH(2d). [¥]see text

Table 6. Bond distances (Å) and bond critical point (r_b) analysis (au) of M_2H_6 systems.

System	Wavefunction	Distance	M-M		Distance	M-H	
			$\rho(r_b)$	$\nabla^2\rho(r_b)$		$\rho(r_b)$	$\nabla^2\rho(r_b)$
C_2H_6	a	1.533	0.2562	-0.8481	1.089	0.2766	-0.9545
	b	1.542	0.2392	-0.5949	1.090	0.2724	-0.9764
Si_2H_6	a	2.350	0.0960	-0.1651	1.482	0.1141	0.3194
	b	2.367	0.0920	-0.1488	1.486		
Ge_2H_6	a	2.443	0.0862	-0.1327	1.550	0.1210	0.1766
	b	2.449	0.0784	-0.1446	1.536		
Sn_2H_6	a	2.845	0.0598	-0.0383	1.748	0.0972	0.1203
	b	2.812	0.0542	-0.0666	1.709		

^aRHF/3-21G(2d)//RHF/3-21G(d). ^bRHF/SBK(2d)//RHF/SBK(d).

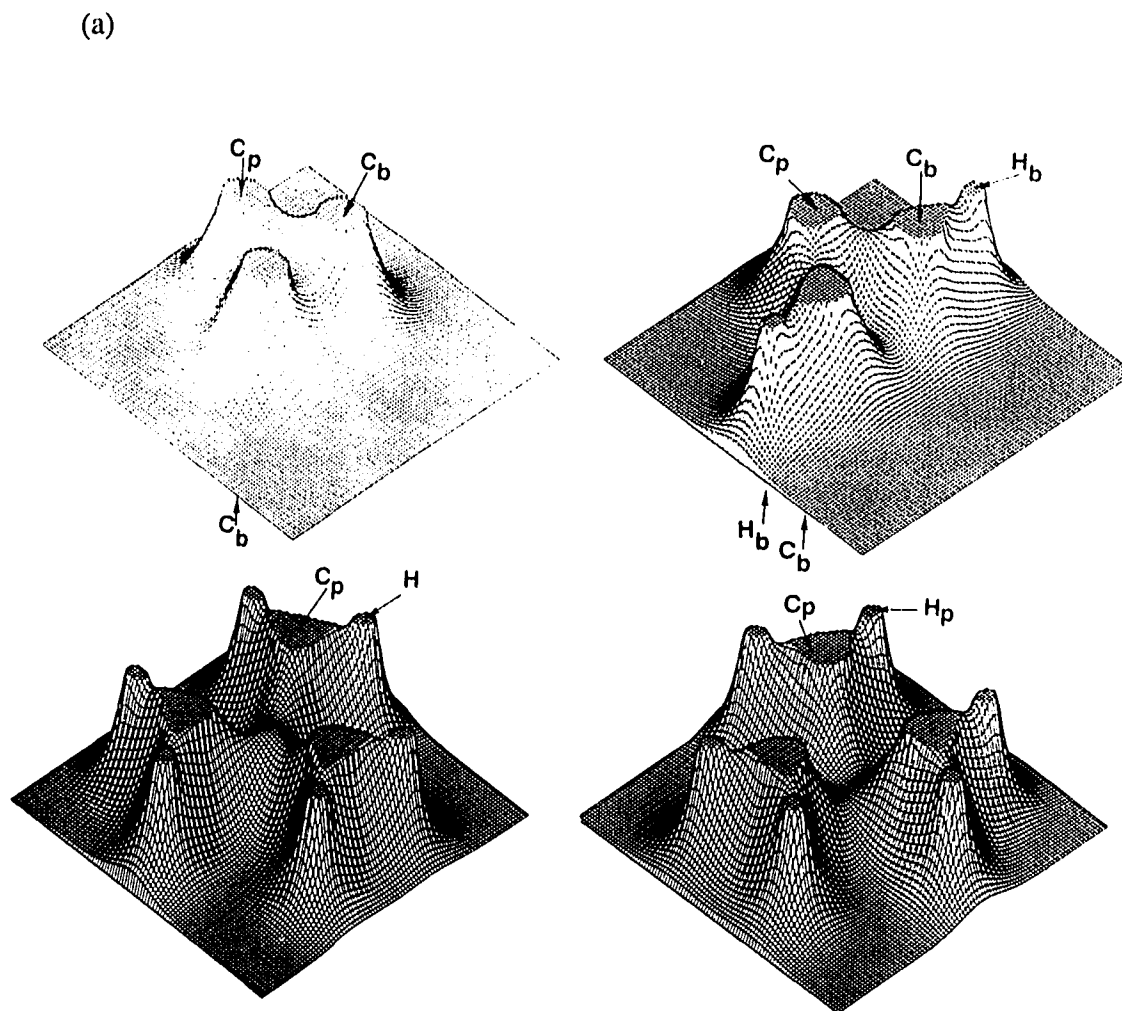


Fig. 1. (a) Relief maps of the charge distributions of C_5H_6 and C_5H_8 systems in the σ_v and σ_h planes. The σ_v maps are displayed in the top half of the figure and the σ_h planes are displayed in the bottom half of the figure. C_5H_6 maps are on the left side of the figure and C_5H_8 maps are on the right side of the figure. The charge distributions are generated from all electron RHF/3-21G(2d)//RHF/3-21G(d) wavefunctions. The charge density cutoff is 0.30 au. (b) Corresponding maps to (a) except that here the charge distributions are generated from RHF/SBK(2d)//RHF/SBK(d) wavefunctions.

(b)

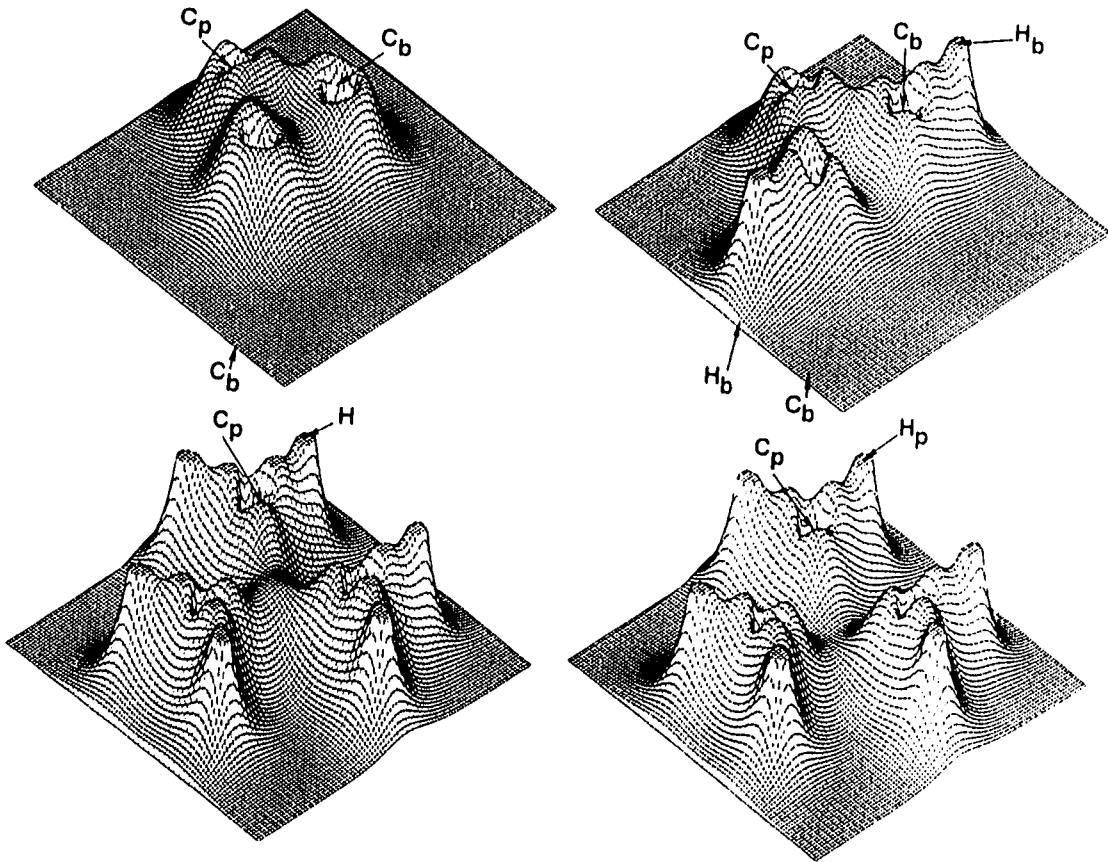


Fig. 1.—continued.

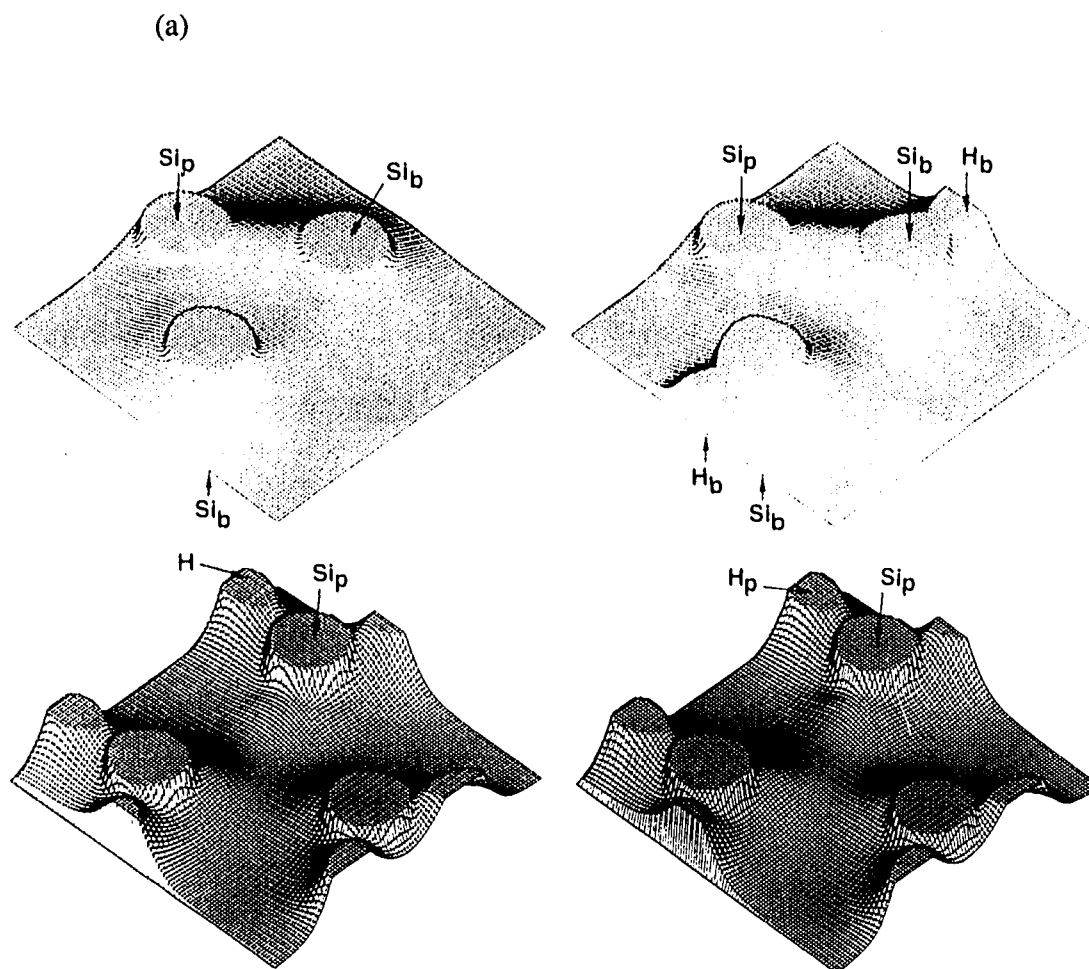


Fig. 2. (a) Relief maps of the charge distributions of Si_5H_6 and Si_5H_8 in the σ_v and σ_h planes. The σ_v maps are displayed in the top half of the figure and the σ_h planes are displayed in the bottom half of the figure. Si_5H_6 maps are on the left side of the figure and Si_5H_8 maps are on the right side of the figure. The charge distributions are generated from all electron RHF/3-21G(2d)//RHF/3-21G(d) wavefunctions. The charge density cutoff is 0.10 au in the σ_v plane and 0.13 au in the σ_h plane. (b) Corresponding maps to (a) except that here the charge distributions are generated from RHF/SBK(2d)//RHF/SBK(d) wavefunctions.

(b)

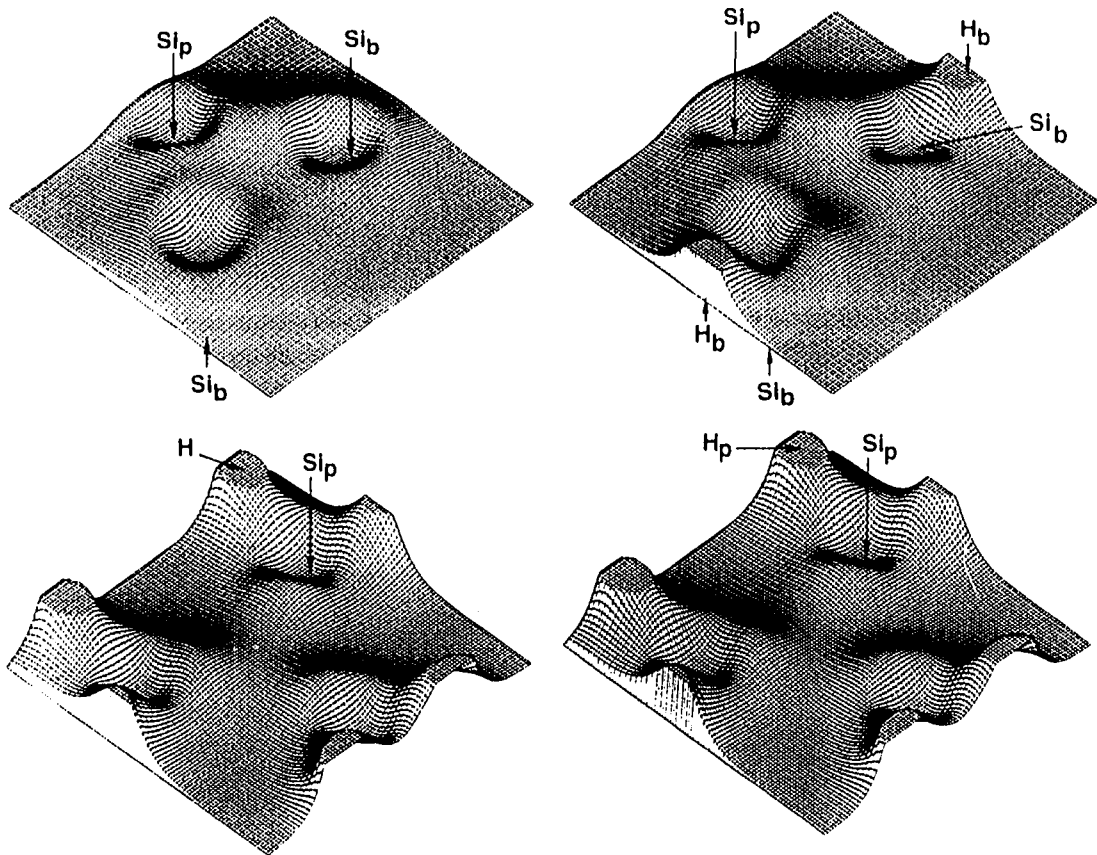


Fig. 2.—continued.

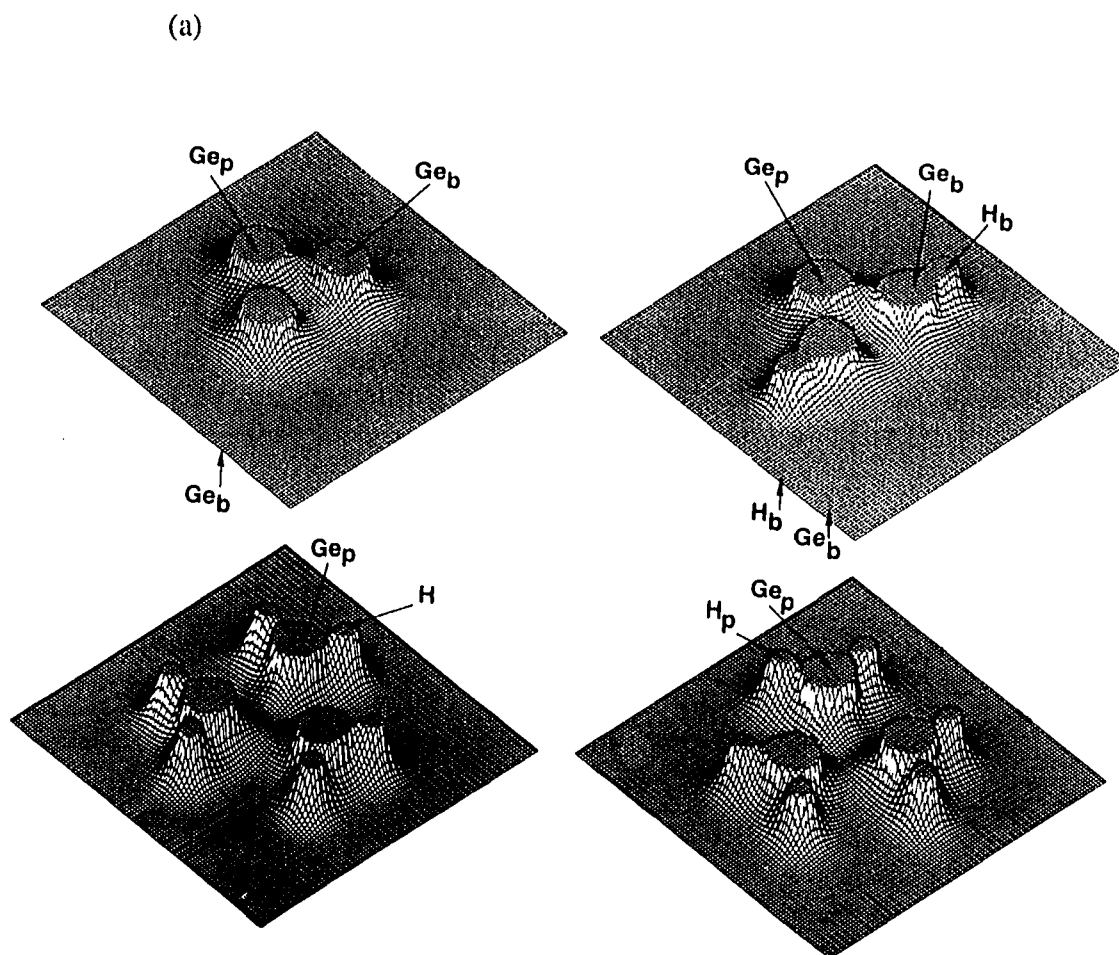


Fig. 3. (a) Relief maps of the charge distributions of Ge_5H_6 and Ge_5H_8 in the σ_v and σ_h planes. The σ_v maps are displayed in the top half of the figure and the σ_h planes are displayed in the bottom half of the figure. Ge_5H_6 maps are on the left side of the figure and Ge_5H_8 maps are on the right side of the figure. The charge distributions are generated from all electron RHF/3-21G(2d)//RHF/3-21G(d) wavefunctions. The charge density cutoff is 0.10 au in the σ_v plane and 0.13 au in the σ_h plane. These maps are scaled down by a factor of two compared to the carbon and silicon maps. (b) Corresponding maps to (a) except that here the charge distributions are generated from RHF/SBK(2d)//RHF/SBK(d) wavefunctions.

(b)

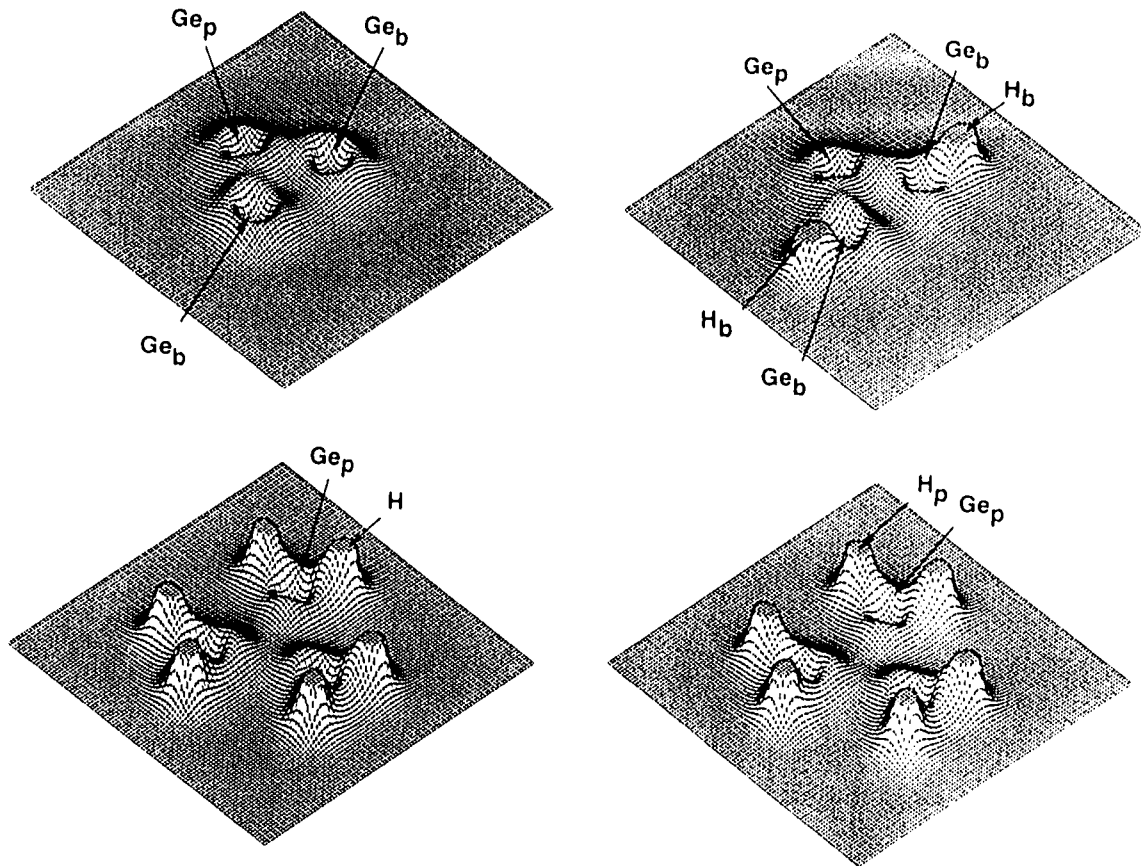


Fig. 3.—continued.

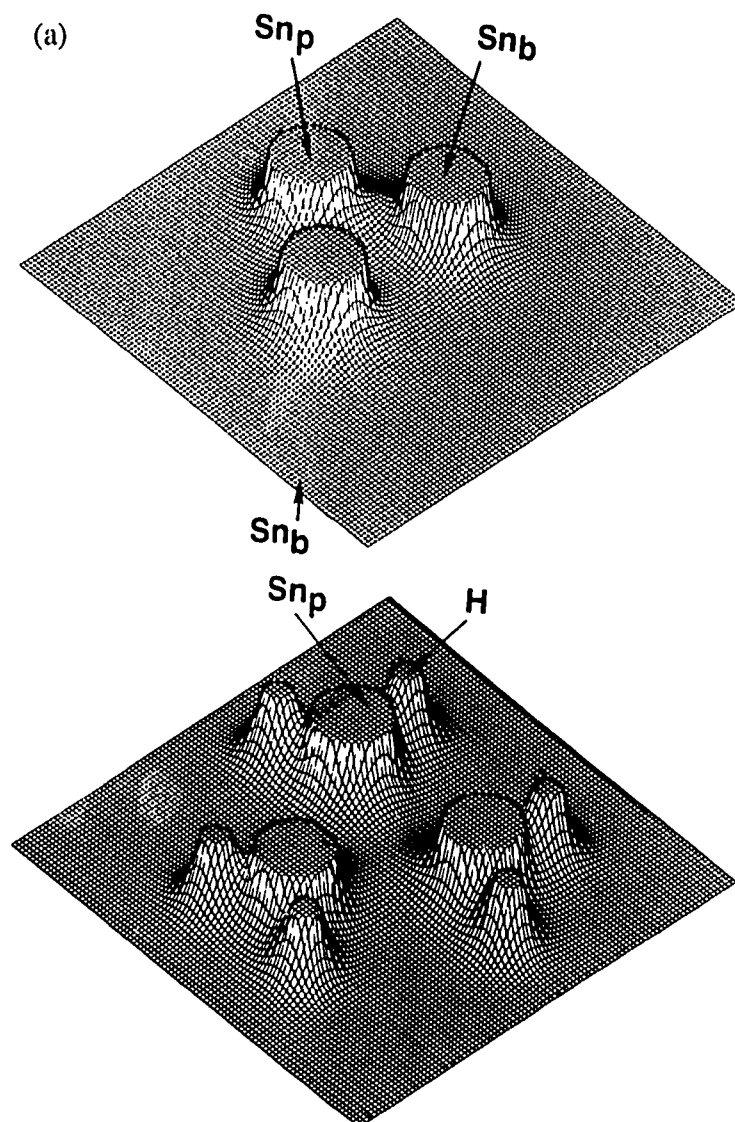


Fig. 4. (a) Relief maps of the charge distributions of Sn_5H_6 in the σ_v and σ_h planes. The σ_v map is displayed in the top half of the figure and the σ_h plane is displayed in the bottom half of the figure. The charge distributions are generated from all electron RHF/3-21G(2d)//RHF/3-21G(d) wavefunctions. The charge density cutoff is 0.10 au in the σ_v plane and 0.13 au in the σ_h plane. These maps are scaled down by a factor of two compared to the carbon and silicon maps. (b) Corresponding maps to (a) except that here the charge distributions are generated from RHF/SBK(2d)//RHF/SBK(d) wavefunctions. In addition, Sn_5H_8 maps are displayed on the right hand side of this figure.

(b)

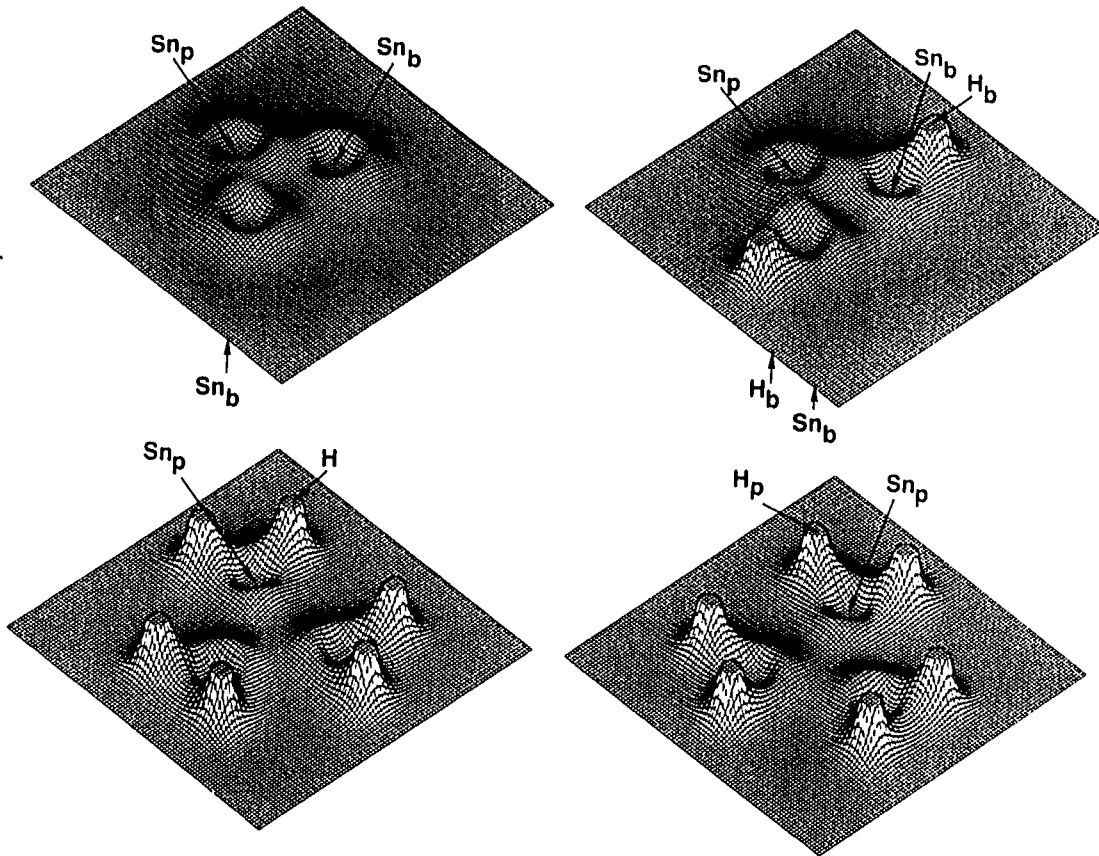


Fig. 4.—continued.

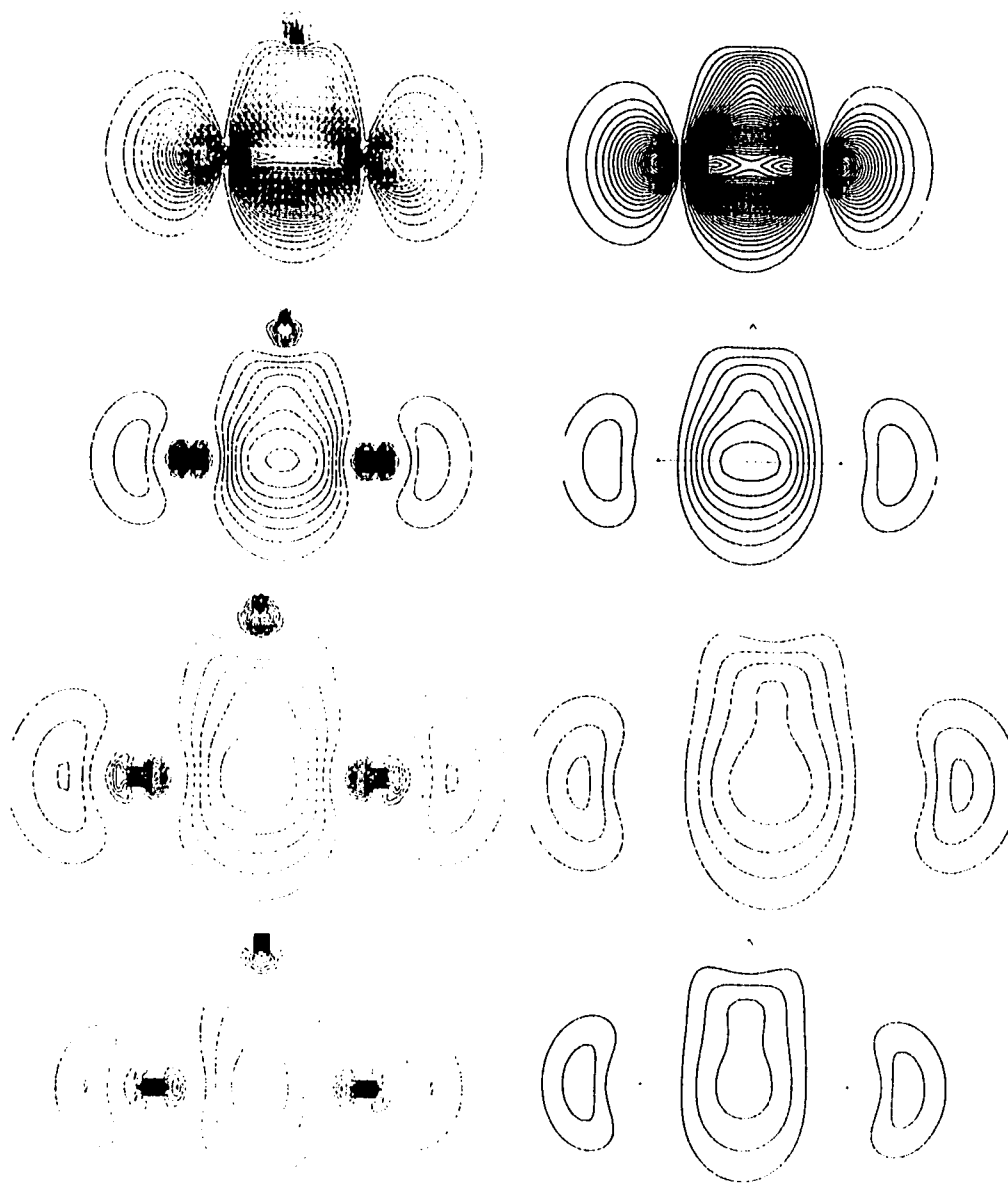


Fig. 5. Contour maps of $M_b M_b$ localized orbital densities in the σ_v plane. The charge distributions for the four maps displayed down the left-hand side of the figure (C_5H_6 , Si_5H_6 , Ge_5H_6 and Sn_5H_6) are generated from all electron RHF/3-21G(2d)//RHF/3-21G(d) wavefunctions while the charge distributions for the corresponding four maps displayed down the right-hand side of the figure are generated from RHF/SBK(2d)//RHF/SBK(d) wavefunctions.

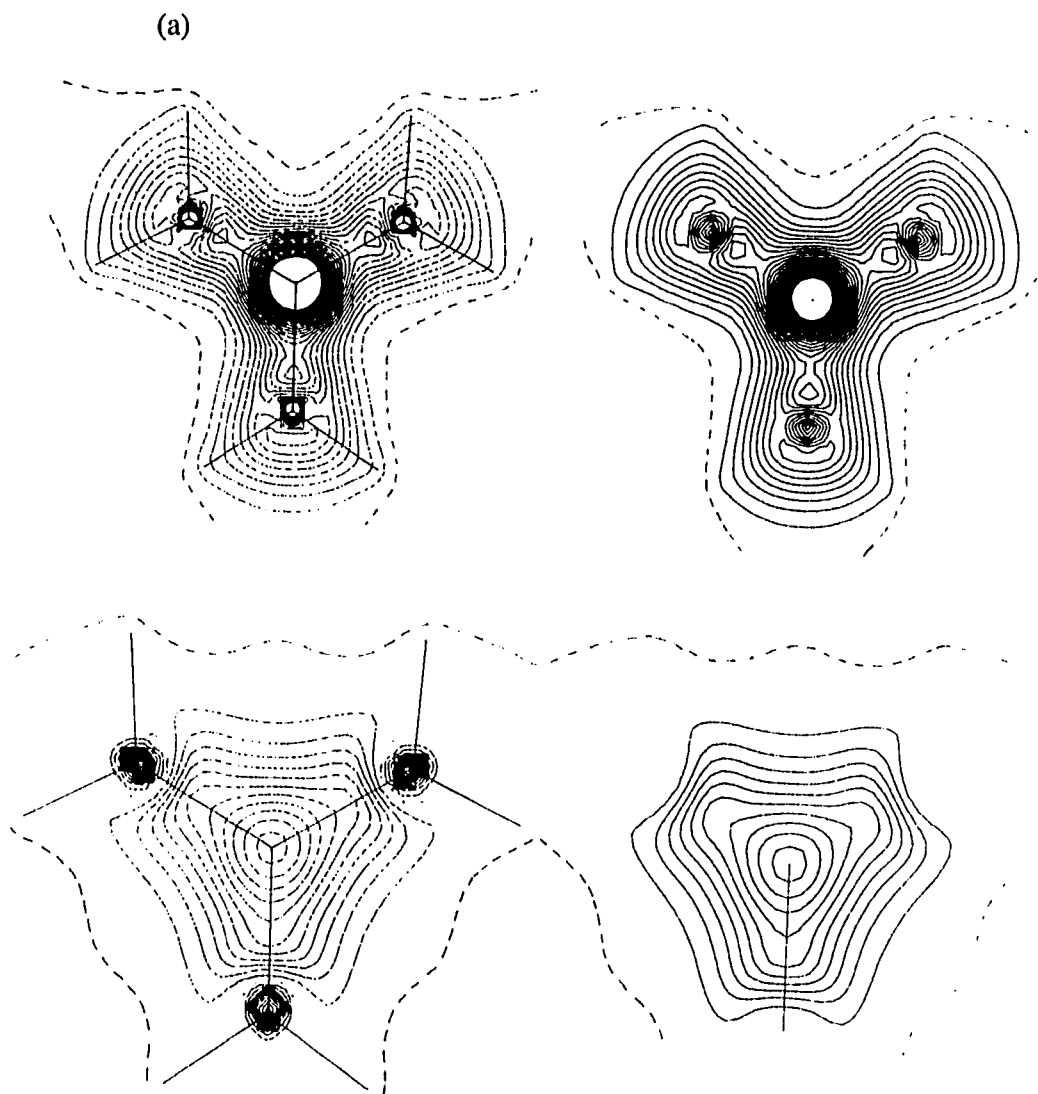


Fig. 6. Contour maps of the RHF minus UHF densities at the RHF geometries for the $M_5H_6 \sigma_h$ planes). Solid (dashed lines) are positive (negative) values. The largest magnitude contour has a value of ± 0.025 au in all cases. Left-hand side maps are determined by subtracting densities generated using the all electron 3-21G(2d) basis set while right-hand side maps use the SBK(2d) basis set. (a) Top half: C_5H_6 ; bottom half: Si_5H_6 . (b) Top half: Ge_5H_6 ; bottom half: Sn_5H_6 .

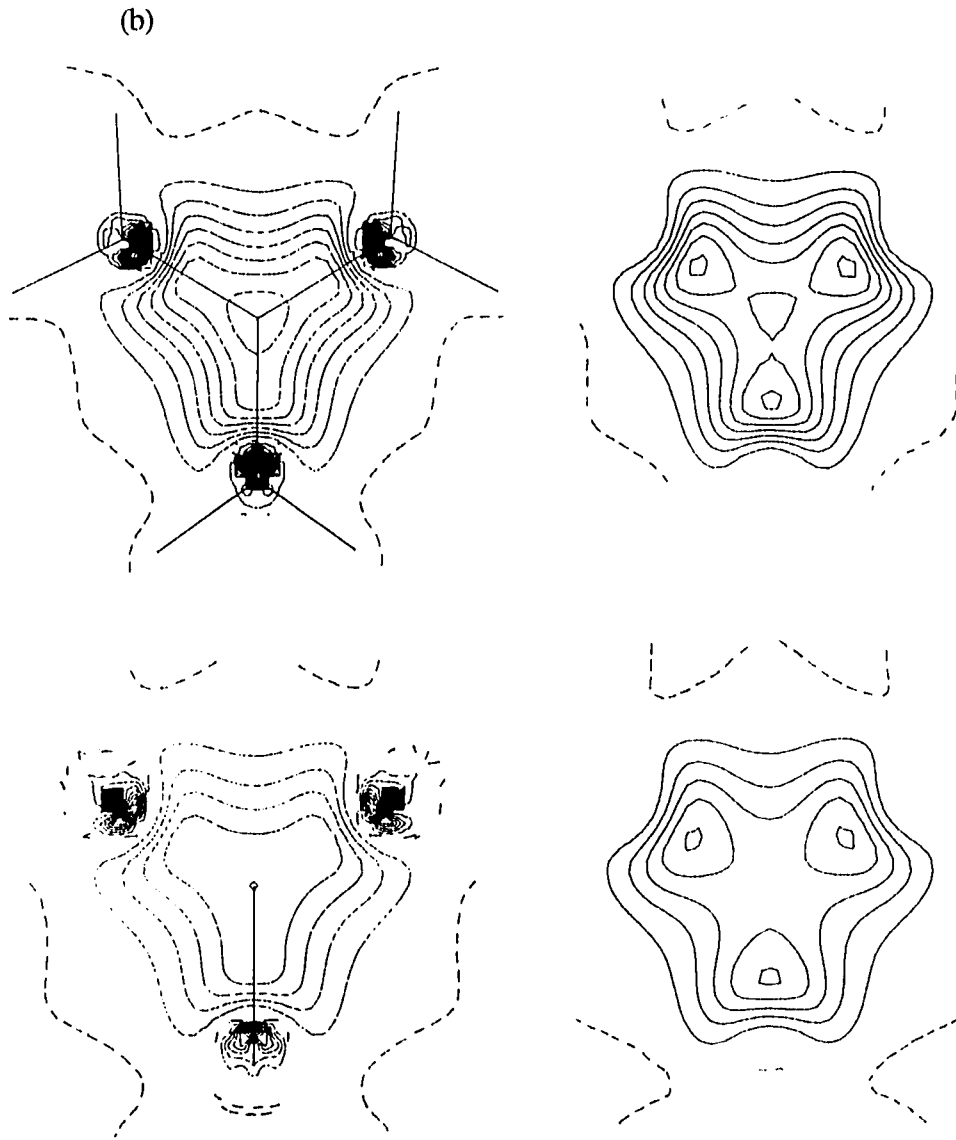


Fig. 6.—continued.

CHAPTER 3. STRUCTURES AND BONDING OF GROUP IV SULFUR AND OXYGEN PROPELLANE DERIVATIVES

A paper published in and reprinted with permission from

J. Am. Chem. Soc. **1991**, 113, 7924-7929

Copyright 1991 American Chemical Society

Kiet A. Nguyen, Marshall T. Carroll and Mark S. Gordon

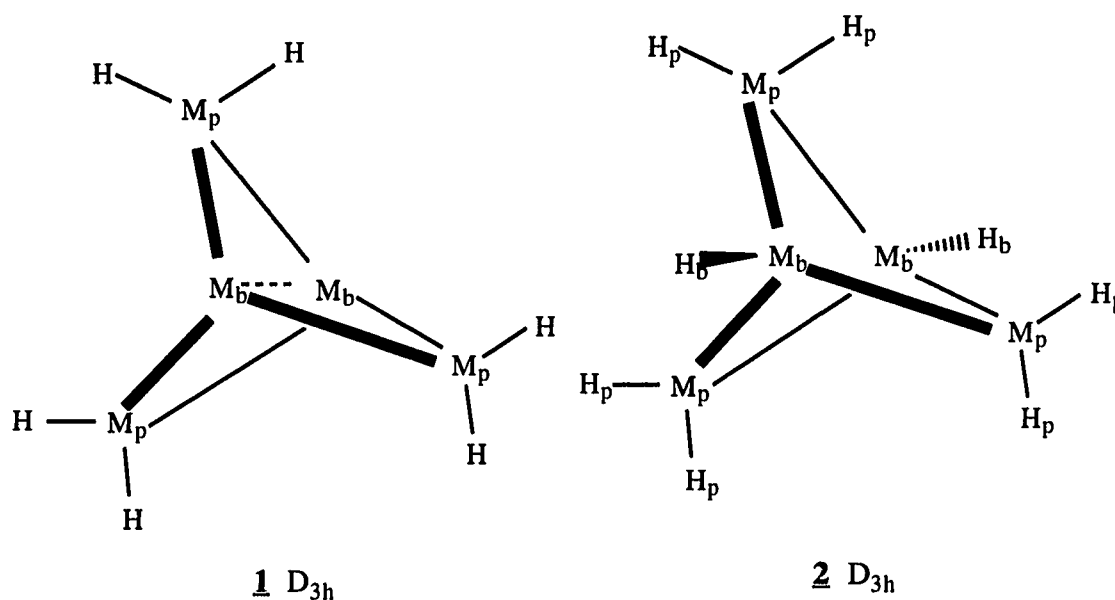
Abstract

The RHF, ROHF, and GVB structures and energetics of group IV 2,4,5-trioxa[1.1.1]metallapropellanes, 2,4,5-trithia[1.1.1]metallapropellanes, and their bicyclopentane analogues have been determined from ab initio molecular orbital theory using both the 6-31G(d) basis set for all-electron calculations and the valence basis set with effective core potentials (ECP) developed by Stevens, Basch and Krauss. Although they have extremely short bridgehead distances, these species possess fairly large natural orbital occupation numbers in the lowest unoccupied molecular orbitals, indicating significant diradical character. Structures and other properties determined by ECP calculations are in good agreement with the 6-31G(d) all-electron calculations.

I. Introduction

Considerable attention has been given to Group IV propellanes (**1**) ($M = C, Si, Ge, Sn$) and their derivatives in an effort to understand the nature of the bridgehead bonds (M_b-M_b). Despite a highly strained "inverted" tetrahedral arrangement at the bridgehead atoms, the simplest propellane ($M = C$) was successfully synthesized by Wiberg and co-workers.¹ This reactive compound (reacting rapidly with various reagents at the bridgehead positions²) with an experimental M_b-M_b bridgehead distance (1.60 \AA)³ that is

slightly longer than the peripheral M_b-M_p bond (1.52 Å) and much shorter than the bridgehead bond (1.84 Å)⁴ in bicyclo[1.1.1]pentane (**2**), has been a subject of discussion among both experimentalists^{2,3,5} and theoreticians.^{1,6,7-12} The silicon,^{6,13-15} germanium,^{15,16a} and tin¹⁵ analogues have also been theoretically investigated. Experimentally, pentasila[1.1.1]propellane is not known, although a derivative (1,3-bis(4-*tert*-butyl-2,6,-diisopropylphenyl)-2,2,4-tetra-isopropylbicyclo[1.1.1]pentasilane) of bicyclo[1.1.1]pentasilane has been synthesized recently.^{16b} For germanium, neither the bicyclo form (**2**) nor the propellane form (**1**) has been



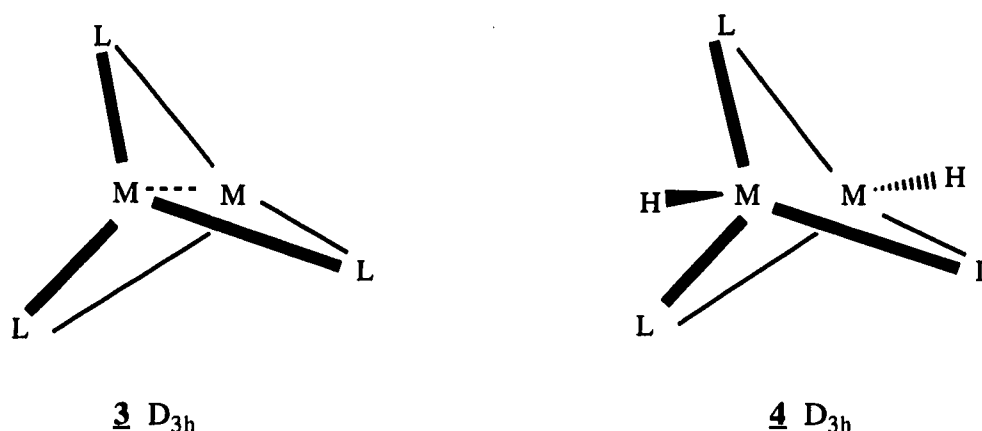
experimentally observed.

Recently, an investigation of the structure and bonding of pentastanna[1.1.1]propellane and the analogues in group IV has been carried out in this laboratory using the 3-21G(d) basis set and two different sets of effective core potentials

developed by Stevens, Basch and Krauss (SBK) and Wadt and Hay (WH). The singlet states were investigated at the restricted Hartree-Fock (RHF) and at the two configuration self-consistent field (TCSCF) levels of theory, while the triplet state was analyzed using the unrestricted Hartree-Fock (UHF) method.¹⁵ The calculated structure of **1** ($M = \text{Sn}$) is consistent with the X-ray crystal structure of 2,2,4,4,5,5-hexakis(2,6-diethylphenyl)pentastanna[1.1.1]propellane.^{15,16c} The RHF/3-21G(d) distance between the bridgehead atoms in **1** (3.463 Å) is much longer than that between the bridgehead and peripheral tin atoms (2.876 Å) and essentially the same as the corresponding M_b-M_b distance in **2**. Similarly, the X-ray bridgehead distance (M_b-M_b) of 3.367 Å of 2,2,4,4,5,5-hexakis(2,6-diethylphenyl)pentastanna[1.1.1]propellane is almost identical to that of its pentastannabicyclo[1.1.1]pentane analogue ($M_b-M_b = 3.361$ Å).^{15,16c} Thus, the experimental and theoretical evidence places the existence of a bridgehead (M_b-M_b) bond in **1** in doubt when $M \neq \text{C}$. It is interesting that TCSCF calculations for **1** show only a slight increase in diradical character upon going from $M = \text{C}$ to Sn. Furthermore, localization of the valence molecular orbitals using the method developed by Foster and Boys,¹⁷ gives rise to localized M_b-M_b orbitals for all four parent [1.1.1]propellane species ($M = \text{C}, \text{Si}, \text{Ge}, \text{Sn}$). Although no **bond critical point**¹² (a saddle point in the total electron density indicating the existence of a bond between two atoms in a molecule) has been located between the bridgehead atoms for the [1.1.1]metallapropellane systems ($M_b = M_p = \text{Si}, \text{Ge}, \text{Sn}$), slight differences in the charge densities of these systems can affect the absence or presence of M_b-M_b bond critical points in these species.¹⁵ The electron density surfaces for these systems, therefore, are very flat, especially around the bridgehead regions. The existence of M_b-M_b bond orbitals for $M_b = M_p = \text{Si}, \text{Ge}$ or Sn, despite the absence of bond critical points, supports this notion. This suggests that changes in the nature of the

peripheral groups might increase or decrease the strengths of the M_b-M_b bonding interactions in 1.

Accordingly, Nagase^{13,16a} and others¹⁰ have suggested that substitution of more electronegative groups (oxygen, CH_2 groups) at the peripheral positions could stabilize the central M_b-M_b interaction for $M = Si$ and Ge . Ab initio calculations for the oxygen



derivatives of Si and Ge propellanes (**3**) and bicyclopentanes (**4**), with $M = Si, Ge$ and $L = O$, have been performed^{16a,b} using RHF/6-31G(d) and RHF/3-21G(d) wavefunctions. For Si, M-M distances in *both* **3** (2.060 Å) and **4** (2.089 Å) are predicted to be extremely short compared to the M_b-M_b distance (2.719 Å) of 1 ($M = Si$) and the M_b-M_b distance (2.915 Å) in 2 ($M = Si$), calculated at the same level of theory⁴. Contractions of similar magnitude are found for $M = Ge$ where RHF/3-21G(d) predicts the bridgehead distance in **3** to be 0.623 Å shorter than that in 1 (2.883 Å), and the bridgehead distance in **4** to be 0.803 Å shorter than that in 2 (3.025 Å).⁵ These results were taken as evidence that electronegative substitution at the peripheral centers does indeed stabilize the bridgehead bond and therefore the [1.1.1]propellanes as well. Similar trends have been found for $M_2C_3H_6$ and $M_2C_3H_8$ ($M = Si$), where the MH_2 groups in 1 and 2 are replaced by the

more electronegative CH₂ groups.¹⁰ To date, no calculations have been reported on the oxapropellane derivatives (**3** and **4**) with M = C and Sn. To our knowledge, neither the group IV 3,4,5-trioxa[1.1.1]propellanes **3** nor their bicyclopentane analogues **4** (M_b = C, Si, Ge and Sn) have been observed experimentally. Other related compounds that have been synthesized are [Sn(OtBu)₃Tl]^{16d} **3** (M = Sn and Tl, L = OtBu) and [Sn(OtBu)₃In]^{16e} **3** (M = Sn and In, L = OtBu).

Although the extremely short distances between the central bridgehead atoms in compounds **3** and **4** may be an indication of the existence of a bond, shorter distances do not always correspond to stable bonding interactions.¹⁸ Likewise, significant bonding interactions can occur between atoms separated by long internuclear distances.^{15,19a} It is significant in this regard that substitution of L = O leads to a large decrease in the M_b-M_b distance in *both* **3** and **4**, since one does not expect the bridgehead atoms to be bonded in the latter. Furthermore, in view of the unusual nature of the bonding in [1.1.1]propellanes and their derivatives, the importance of a multi-configurational description of the wavefunction must be assessed. This has been done previously for the parent compounds **1** and **2**,¹⁵ but not for the derivatives of **3** and **4**. Therefore, multi-configurational wavefunctions are used in the present paper to probe the nature of the bridgehead interaction. Here, we report results of the second, third, fourth and fifth period group IV 2,4,5-trioxa[1.1.1]propellane and 2,4,5-trithia[1.1.1]propellane derivatives, as well as their [1.1.1]bicyclopentane analogues. That is, M = C, Si, Ge, Sn and L = O, S. The all-electron results for Si₂O₃ and H₂Si₂O₃ have recently been presented in the context of other SiO compounds,^{19b} but are included here for comparison to other propellanes and bicyclopentanes.

II. Computational Approach

For carbon and silicon, structures were determined with the 6-31G(d) basis set²⁰ using analytical energy gradients with restricted Hartree-Fock²¹ (RHF) and restricted open shell Hartree-Fock²² (ROHF) wavefunctions for closed shell singlets and open shell triplets, respectively. In addition, TCSCF²³ calculations have been carried out on the singlets to ascertain the diradical character in these compounds; such calculations have been shown to be useful in characterizing the nature of the bridgehead bonds in propellanes.^{6,15,19b} Quantitative measurement of the diradical character is given by the CI orbital coefficients. The natural orbital occupation number (NOON) is defined as twice the square of the CI coefficient. In our TCSCF, the highest occupied molecular orbital (HOMO) and the lowest unoccupied molecular orbital (LUMO) are included in the active space. Effective core potential (ECP²⁴) calculations (with the SBK basis set²⁵) at the RHF, ROHF and TCSCF levels were also carried out using the same d orbital exponents as in the all-electron calculations. Structures were verified as minima by their positive definite Hessians (matrices of energy second derivatives), obtained analytically for all-electron calculations and from finite differences of the analytically determined gradients for ECP calculations. These ab initio electronic structure calculations were performed using the GAMESS²⁶ quantum chemistry program.

The nature of the bonding in the compounds of interest has been investigated using the electron density analysis developed by Bader and co-workers^{12, 27,28} as part of their theory of atoms in molecules. It has been found necessary to include an additional set of d functions on the M atoms to eliminate spurious non-nuclear maxima in the total charge density.²⁹ In the present work, the d orbital exponents used for this purpose are 1.6000, 0.4000 (C), 0.7900, 0.1975 (Si), 1.6000, 0.4000 (O) and 1.3000, 0.3250 (S). The density analysis has been discussed in detail elsewhere,^{12,27,28} and only a few key points

will be given here. A critical point in the charge density is a point at which the gradient of the charge density vanishes ($\nabla\rho(\mathbf{r})=0$). A bond critical point (\mathbf{r}_b) exists between two atoms if there is a saddle point in the electron density $\rho(\mathbf{r})$ between the two atoms. At this point the hessian of $\rho(\mathbf{r})$ has one positive eigenvalue along the bond axis and two negative eigenvalues along the axes orthogonal to the bond axis. The existence of a bond critical point implies the existence of a bond path (a line linking the two nuclei along which charge density is a maximum with respect to any lateral displacement) and the two atoms are said to be bonded. The hessian at a ring critical point (\mathbf{r}_r) has two positive and one negative eigenvalues, with the density $\rho(\mathbf{r}_r)$ at the ring critical point being smaller than that at all of the surrounding bond critical points. The hessian at a cage critical point has three positive curvatures and $\rho(\mathbf{r})$ is a local minimum at this point. If an M_b-M_b bond is present in a [1.1.1] propellane system, one expects a bond critical point between the two bridgehead atoms, as well as three ring critical points, one on the face of each three-membered ring. The absence of such a bond critical point suggests that there is no "formal bond" connecting these two atoms.^{12,27,28} However, such arguments may not reflect the existence of very flat electron density surfaces.¹

III. Results and Discussion

A. Carbon and Silicon compounds

The RHF, ROHF and TCSCF geometries of the propellanes **3** and RHF geometries of the bicyclopentanes **4** are listed in Table I and Table II. Both all-electron and ECP calculations were carried out for $M = \text{C, Si}$ and $L = \text{O, S}$. At all levels of theory (RHF, ROHF and TCSCF), ECP bond lengths are within 0.02 Å of the 6-31G(d) all-electron calculations; bond angles agree to within a degree. Thus, as noted earlier,¹⁵ the ECP wavefunctions provide a consistently reasonable description of complex molecular geometries.

At the RHF/6-31G(d) level, the M_b-M_b bridgehead distance in **3** ($M = C, L = O$) is only 0.09 Å shorter than the bridgehead distance of 1.543 Å in [1.1.1]propellane.¹ In contrast, the analogous difference is 0.60 Å when $M = Si$. As discussed earlier by Nagase and co-workers,^{13b} the 2.096 Å bridgehead Si-Si distance in **3** is in fact much shorter than the 2.353 Å single Si-Si bond distance in disilane³⁰ and is actually less than 2.143 Å double Si=Si bond distance in disilene.³¹ The bonding of **3** ($M = Si, L = O$) was therefore explained in terms of a π -complex model,³² with each peripheral oxygen and two bridgehead silicon atoms forming a T-shaped structure instead of a conventional three-membered ring. This assertion was based solely on the RHF bond distances and not on an analysis of electron density. In the sulfur analogues (Table I), the RHF/6-31G(d) C-C bridgehead distance (1.551 Å) is similar to that of [1.1.1]propellane (1.543 Å). In **3** ($M = Si, L = S$), the RHF/6-31G(d) Si-Si bridgehead distance (2.356 Å) is within the normal range of single Si-Si bond distances; however, this is still considerably shorter than the Si-Si bridgehead (2.719 Å) distance in pentasila[1.1.1]propellane.¹⁰

Thus, for $M = Si$, the M-M bridgehead distances in both the trioxa and trithia compounds **3** are predicted to be much shorter than the corresponding distances in the parent propellanes **1**, at the RHF level of theory. This raises two questions: (1) Do the shorter M-M bond distances correspond to stronger bonding interactions? (2) Are RHF wavefunctions adequate to describe these species? With regard to the former point, the geometry of compound **3** (with $M = C, Si$ and $L = O$) may be highly constrained by the peripheral atoms in order to maintain the strong C-O and Si-O interactions and minimize O-O repulsions. Support for this is provided by noting that, in general, no significant increase is found in the M-M distances upon hydrogen additions at the bridgehead positions to form the corresponding bicyclopentane (**4**: $M = C, L = O$) systems (Table II). This suggests that either there are very strong M-M bonding interactions in *both* oxo derivatives

(**3** and **4**) or there is little M-M bonding in **3** and no formal bridgehead bond in **4** with $L = O$. The latter would mean that the shorter bridgehead distance in these systems relative to $L = M$, could simply be a result of geometrical constraint. Indeed, the geometries of the sulfur analogues of **3** and **4** reinforce exactly that interpretation. Furthermore, the C-C bond critical point ($L = O$) almost coalesces with the surrounding ring critical points, implying a very flat distribution of charge in this central region (Figure 1). When $L = S$, however, the distribution is not as flat (Figure 2); the magnitude of the charge density $\rho(\mathbf{r})$ at the bond critical point is much larger than at the surrounding ring critical points. This difference in $\rho(\mathbf{r})$ (between the bond critical point and ring critical point) when $L = S$ is an order of magnitude larger than when $L = O$.

To assess the reliability of the RHF description of these compounds, TCSCF calculations were performed on the singlet states of **3**. This leads to two interesting results. First (Table I), TCSCF has little effect on the M-M distances, except in the case of **3** ($M = C, L = S$), where the TCSCF C-C bridgehead distance lengthens compared to the RHF value with the same basis set. Second, the TCSCF natural orbital occupation numbers (NOON) listed in Table III are quite large. The NOON are a convenient measure of the percent diradical character. The silicon derivative **3** ($M = Si, L = O$) has the highest percent diradical character (36%). The analogous value for the corresponding carbon compound is 18%. In contrast, the diradical character in [1.1.1]propellane **1** is 10% for $M_b = M_p = C$ and 14% for $M_b = M_p = Si$, at the same levels of theory.¹⁵ The larger diradical character in **3** than in **1** diminishes the utility of interpretation based on RHF wavefunctions. The percent diradical character of **3** when $M = C$ and $L = S$ (9%) is almost identical to that of the parent propellane; the corresponding value (21%) for the silicon analogue ($M = Si, L = S$) is significantly larger than that of pentasilapropellane **1** ($M_p = M_b = Si$). Thus, going from C to Si, the percent diradical character approximately doubles for both the sulfur and

oxygen propellane derivatives. The percent diradical character values obtained from all-electron calculations for carbon and silicon with $L = O$ and S using the 6-31G(d) basis set are essentially identical to those predicted by ECP.

Having established the importance of TCSCF descriptions of these systems, it is useful to analyze the total charge density derived from these wavefunctions. Figures 1-4 display relief maps of the total charge density in both the σ_h [containing the three peripheral atoms (L) in **3** and **4**] and the σ_v [containing one peripheral atom (L) and two bridgehead atoms (M) in **3** and **4**] planes. Since the σ_h plane bisects the bridgehead M-M axes, any concentration of charge density [$\rho(\mathbf{r})$] in the bridgehead regions will produce a bump. Accumulation of charge density in the bridgehead regions in the σ_v plane will only produce a saddle, since $\rho(\mathbf{r})$ at nuclei are always greater than $\rho(\mathbf{r})$ in bonding and nonbonding regions. For both carbon propellane derivatives, there is a significant accumulation of charge between the two carbon nuclei. Indeed, a bond critical point is located (as was the case for the parent propellane). However, in the bicyclopentane compounds, there is relatively little charge density distributed in the bridgehead regions.

In the silicon propellane derivatives, the distribution of electron density in the bridgehead region is flat (Figure 3-4). The fact that there is little charge accumulated between the two silicon nuclei and more charge accumulated along the Si-O and Si-S bonds does not support the proposal^{13b} of a T-shaped bonding mechanism for the pentasilapropellane trioxa and trithia derivatives. Also, note that addition of two hydrogens across the bridgehead does not result in any significant change in the amount of charge density between the bridgehead silicons (Figures 3-4). No Si-Si bond critical point is found in these silicon compounds.

Further evidence for the large diradical character in **3** is provided by ROHF calculations on the corresponding triplet states, obtained via an excitation of one electron

from the M-M bonding orbital (σ) to its anti-bonding MO (σ^*). The singlet-triplet splittings for these species are compiled in Table IV. Note the good agreement between all-electron and ECP methods and also that the singlet is more stable than the triplet in all cases. Further, replacement of O by S leads to a stabilization of the singlet over the triplet by 17.7 kcal/mol for M = C and 13.3 kcal/mol for M = Si. This is consistent with the greater diradical character found in the oxo than in the thia compounds. Thus, it is seen that as the L group (L = O and S) decreases in electronegativity relative to M (M = C and Si), the closed shell character of the system increases. Not unexpectedly, inspection of the HOMO and LUMO plots (Figure 5) shows that in the bridgehead region, the electron density is polarized to a greater extent towards the peripheral atoms as the electronegativity of L increases. This apparently results in a smaller singlet-triplet splitting for L = O. The more electronegative oxygen polarizes electron density to a greater extent than does sulfur. These observations suggest that except for 2,4,5-trithia[1.1.1]propellane, single determinant wavefunction treatments may not be appropriate for these species.

B. Germanium and Tin Compounds

Since ECP calculations compare favorably with full ab initio results, only ECP results are reported for the heavier atoms. The most interesting electronic structural features found for C and Si are those in the trioxa species, so we limit ourselves to these and omit discussion of the sulfur analogs. The results of structures, energetics and the TCSCF NOON of the germanium and tin trioxa[1.1.1]propellane derivatives are listed in Tables I-IV along with the carbon and silicon analogs. Because the essential conclusions drawn for Ge and Sn compounds (**3**, **4** with M = Ge, Sn and L = O) are the same as those discussed above for C and Si, only the key features of these species will be addressed.

In both the germanium and tin analogs of **3** (L = O) extremely short bridgehead M-M distances are found at the RHF, ROHF and TCSCF levels of theory. These bridgehead

M-M distances are not significantly affected by the additions of hydrogens across the bridgehead centers (cf. Table I & II). Indeed, the differences between the M-M distances in the propellanes **3** and the bicyclopentane **4** analogs are less than 0.1 Å for both M = Ge and Sn. Furthermore, differences among the three levels of theory (RHF, ROHF and TCSCF) in the corresponding M-M bridgehead distances are within 0.1 Å. These results are similar to those found in the silicon analogues of **3** and **4**. The RHF/SBK(d) geometric results for **3** (M = Ge, L = O) and the corresponding bicyclopentane analogue are essentially identical to those calculated by Nagase and Kudo^{13a} using the 3-21G(d) basis set at RHF level of theory. The percent diradical character and the singlet-triplet splittings for Sn (28%, 22.0 kcal mol⁻¹) and Ge (25%, 29 kcal mol⁻¹) are also similar to those discussed above (36%, 20.7 kcal mol⁻¹) for the Si analog of **3**.

IV. Conclusions

In this study, ab initio molecular orbital theory has been used to investigate the structure and bonding of sulfur and oxygen propellane derivatives (**3**) and their bicyclopentane analogues (**4**) with RHF, ROHF and TSCF wavefunctions. We have found that the M = Si, Ge and Sn species possess unusually short bridgehead distances. However, this does not result in significant bonding interactions, as shown by the TCSCF calculations and total density plots. For M = C, TCSCF calculations and total density analyses suggest substantial bridgehead bonding only in the L = S system. We have found excellent agreement in structures and energetics between ECP calculations and the 6-31G(d) all-electron calculations.

Acknowledgment

The computations described in this work were performed on the North Dakota State University IBM 3090/200E vector computer, obtained in part with the aid of a joint study agreement between IBM and NDSU, and on the Cray-2 at the National Center for

Supercomputing Applications Champaign, Illinois. This work was supported in part by a grant from the National Science Foundation (CHE-8911911). We thank Walter Stevens, Morris Krauss and Harold Basch for making their ECPs available to us prior to publication.

References

- (1) Wiberg, K. B.; Bader, R. F. W.; Lau, C. D. H. *J. Am. Chem. Soc.* **1987**, 109, 985.
- (2) Wiberg, K. B.; Waddell, S. T. *J. Am. Chem. Soc.* **1990**, 112, 2194.
- (3) (a) Wiberg, K. B.; Walker, F. H., *J. Am. Chem. Soc.* **1982**, 104, 5239. (b) Wiberg, K. B.; Dailey, W. P.; Walker, F. H.; Waddell, S. T.; Crocker, L. S.; Newton, M. D. *J. Am. Chem. Soc.* **1985**, 107, 7247.
- (4) Wiberg, K. B.; Wendoloski, J. J. *J. Am. Chem. Soc.* **1982**, 104, 5679.
- (5) Wiberg, K. B. *Chem. Rev.* **1989**, 89, 975.
- (6) Schleyer, P. v. R.; Janoschek, R. *Angew. Chem. Int. Ed. Engl.* **1987**, 26, 1267.
- (7) Stohrer, W. D.; Hoffmann, R. *J. Am. Chem. Soc.* **1972**, 94, 779.
- (8) Newton, M. D.; Schulman, J. M. *J. Am. Chem. Soc.* **1972**, 94, 773.
- (9) Jackson, J. E.; Allen, L. C. *J. Am. Chem. Soc.* **1984**, 106, 591.
- (10) Kitchen, D. B.; Jackson, J. E.; Allen, L. C. *J. Am. Chem. Soc.* **1990**, 112, 3408.
- (11) Epiotis, N. D. *J. Am. Chem. Soc.* **1984**, 106, 3170.
- (12) Bader, R. F. W.; Nguyen-Dang, T. T.; Tal, Y. *Rep. Prog. Phys.* **1981**, 44, 893.
- (13) (a) Nagase, S.; Kudo, T. *Organometallics* **1987**, 6, 2456. (b) Nagase, S.; Kudo, T.; Kurakake, T. *J. Chem. Soc., Chem. Commun.* **1988**, 1063.
- (14) Schoeller, W. W.; Dabisch, T.; Busch, T. *Inorg. Chem.* **1987**, 26, 4383.
- (15) Gordon, M. S.; Nguyen, K. A.; Carroll, M. T. *Polyhedron* **1991** in press.
- (16) (a) Nagase, S.; Kudo, T. *Organometallics* **1988**, 7, 2534. (b) Kabe, Y.; Kawase, T.; Okada, J. *Angew. Chem. Int. Ed. Engl.* **1990**, 29, 794. (c) Sita, L. R.;

- Kinnshita, I. *J. Am. Chem. Soc.* **1990**, 112, 8839. (d) Veith, M.; Rösler, R. *Angew. Chem.* **1982**, 94, 867; *Angew. Chem. Int. Ed. Engl.* **1982**, 21, 858. (e) Veith, M.; Kunze, K. *Angew. Chem. Int. Ed. Engl.* **1991**, 30, 95.
- (17) Foster, J. M.; Boys, S. F. *Rev. Mod. Phys.* **1963**, 32, 300.
- (18) Gordon, M. S.; Packwood, T. J.; Carroll, M. T.; Boatz, J. A. *J. Phys. Chem.* **1991**, 95, 4332.
- (19) (a) Gordon, M. S.; Carroll, M. T.; Jensen, J.; Davis, L. P.; Burggraf, L. W.; Guidry, M. *Organometallics*, submitted. (b) Schmidt, M. W.; Nguyen, K. A.; Gordon, M. S.; Montgomery, J. A., Jr. *J. Am. Chem. Soc.* **1991** in press.
- (20) (a) Hehre, W. J.; Ditchfield, R.; Pople, J. A. *J. Chem. Phys.* **1971**, 51, 2257. (b) Gordon, M. S. *Chem. Phys. Lett.* **1980**, 76, 163. (c) Hariharan, P. C.; Pople, J. A. *Theoret. Chim. Acta.* **1973**, 28, 213.
- (21) Roothaan, C. C. J. *Rev. Mod. Phys.* **1951**, 23, 69.
- (22) Hsu, H.; Davidson, E. R.; Pitzer, R. M. *J. Chem. Phys.* **1976**, 65, 609.
- (23) Goddard, W. A. III.; Dunning, T. H.; Hunt, W. J.; Hay, P. J. *Acc. Chem. Res.* **1973**, 6, 368.
- (24) Kahn, L. R.; Baybutt, P.; Truhlar, D. G. *J. Chem. Phys.* **1976**, 65, 3826.
- (25) Stevens, W. J.; Basch, H.; Krauss, M. *J. Chem. Phys.* **1984**, 81, 6026.
- (26) Schmidt, M. W.; Baldrige, K. K.; Boatz, J. A.; Jensen, J. H.; Koseki, S.; Gordon, M. S.; Nguyen, K. A.; Windus, T. L.; Elbert, S. T. *QCPE Bulletin, GAMESS, Indiana University* **1990**, 10, 52.
- (27) Bader, R. F. W.; Nguyen-Dang, T. T.; *Adv. Quant. Chem.* **1981**, 14, 63.
- (28) Bader, R. F. W. *Acc. Chem. Res.* **1985**, 18, 9.
- (29) Boatz, J. A.; Gordon, M. S. *J. Phys. Chem.* **1989**, 93, 3025.

- (30) Francl, M. M.; Pietro, W. J.; Hehre, W. J.; Binkley, J. S.; Gordon, M. S.; DeFrees, D. J.; Pople, J. A. *J. Chem. Phys.* **1982**, 77 3654.
- (31) Krogh-Jespersen, K. *J. Phys. Chem.* **1982**, 86, 1492.
- (32) (a) Dewar, M. J. S.; Ford, G. P. *J. Am. Chem. Soc.* **1979**, 101, 783. (b) Cremer, D.; Kraka, E. *J. Am. Chem. Soc.* **1985**, 107, 3800.

Table I. Geometries and Energies (E(SCF) in Hartree, E(ZPE) in kcal mol⁻¹) of M₂L₃ (M = C, Si, L = O, S) systems; internuclear distances are in Angstroms and angles are in degrees.

Systems	wave function	basis set	E(SCF)	E(ZP)	Distances		Angles	
					M-M	M-L	M-M-L	M-L-M
C ₂ O ₃	RHF	(a)	-300.04260	11.7	1.456	1.393	58.5	60.0
		(b)	-57.79064	11.6	1.481	1.405	58.2	63.6
	ROHF	(a)	-299.99056	12.7	1.561	1.415	56.5	67.0
		(b)	-57.73889	12.7	1.581	1.425	56.3	67.4
	TCSCF	(a)	-300.09461	13.0	1.487	1.397	57.8	64.3
		(b)	-57.84260	12.9	1.511	1.408	57.6	64.9
C ₂ S ₃	RHF	(a)	-1268.08384	9.0	1.524	1.779	64.6	50.7
		(b)	-40.60722	9.0	1.551	1.785	64.2	51.5
	ROHF	(a)	-1267.97886	8.2	1.937	1.848	58.4	63.2
		(b)	-40.50348	8.5	1.935	1.848	58.4	63.2
	TCSCF	(a)	-1268.11107	8.8	1.616	1.786	63.1	53.8
		(b)	-40.63564	8.9	1.640	1.792	62.8	54.5
Si ₂ O ₃	RHF	(a)	-802.40206	7.9	2.096	1.720	52.4	75.1
		(b)	-54.58636	8.0	2.088	1.716	52.5	75.0
	ROHF	(a)	-802.42694	9.1	2.078	1.711	52.6	74.8
		(b)	-54.61042	9.1	2.071	1.707	52.7	74.7
	TCSCF	(a)	-802.45925	9.1	2.084	1.711	52.5	75.0
		(b)	-54.64346	9.1	2.076	1.707	52.6	74.9
Si ₂ S ₃	RHF	(a)	-1770.41900	5.1	2.347	2.117	57.4	65.3
		(b)	-37.36838	5.2	2.356	2.182	57.3	65.3
	ROHF	(a)	-1770.40068	5.4	2.360	2.192	57.4	65.1
		(b)	-37.34904	5.5	2.366	2.197	57.4	65.2
	TCSCF	(a)	-1770.45409	6.0	2.357	2.176	57.2	65.6
		(b)	-37.40328	6.0	2.363	2.180	57.2	65.6
Ge ₂ O ₃	RHF	(b)	-54.44186	6.3	2.269	1.817	51.4	77.2
	ROHF	(b)	-54.43481	7.1	2.233	1.807	51.8	76.3
	TCSCF	(b)	-54.48166	7.1	2.250	1.806	51.5	77.1
Sn ₂ O ₃	RHF	(b)	-53.56479	5.6	2.600	1.998	49.4	81.2
	ROHF	(b)	-53.56632	6.2	2.556	1.984	49.9	80.2
	TCSCF	(b)	-53.60142	6.2	2.577	1.985	49.5	81.0

Notes: (a) 6-31G(d), (b) SBK(d)

Table II. Geometries and RHF Energies (E(SCF) in Hartree, E(ZPE) in kcal mol⁻¹) of M₂L₃H₂ (M = C,Si,Ge,Sn and L = O, S) systems; internuclear distances are in Angstroms and angles are in degrees.

System	Basis set	E(SCF)	E(ZPE)	Distances			Angles		
				M-M	M-L	M-H	M-M-L	M-L-M	L-M-H
C ₂ O ₃ H ₂	a	-301.32584	30.3	1.601	1.417	1.073	55.6	68.8	124.4
	b	-59.07698	30.3	1.622	1.427	1.077	55.4	69.3	124.3
C ₂ S ₃ H ₂	a	-1269.30504	25.0	2.023	1.846	1.076	56.8	66.4	123.2
	a	-41.82728	25.4	2.020	1.846	1.080	56.8	66.3	123.2
Si ₂ O ₃ H ₂	a	-803.68372	21.0	2.067	1.703	1.452	56.7	74.7	127.3
	b	-55.86794	21.0	2.060	1.700	1.452	52.7	74.6	127.3
Si ₂ S ₃ H ₂	a	-1771.64243	16.9	2.363	2.176	1.462	57.1	65.8	122.9
	b	-38.59101	16.9	2.373	2.181	1.464	57.0	65.9	123.0
Ge ₂ O ₃ H ₂	b	-55.66231	18.2	2.225	1.795	1.499	51.7	76.6	128.3
Sn ₂ O ₃ H ₂	b	-54.75728	15.8	2.546	1.971	1.668	49.8	80.5	130.0

^a6-31G(d). ^bSBK(d)

Table III. TCSCF coefficients and natural orbital occupation numbers (NOON) for M_2O_3 and M_2S_3 systems.

Systems	Basis set	TCSCF coefficients		NOON	
		HOMO	LUMO	HOMO	LUMO
C_2O_3	a	0.954	-0.300	1.820	0.179
	b	0.934	-0.301	1.819	0.181
C_2S_3	a	0.978	-0.207	1.914	0.086
	b	0.977	-0.212	1.910	0.090
Si_2O_3	a	0.905	-0.426	1.637	0.363
	b	0.906	-0.424	1.640	0.360
Si_2S_3	a	0.946	-0.324	1.790	0.210
	b	0.947	-0.323	1.792	0.208
Ge_2O_3	b	0.936	-0.352	1.752	0.248
Sn_2O_3	b	0.928	-0.372	1.724	0.276

^a6-31G(d). ^bSBK(d)

Table IV. Singlet—Triplet splittings for M_2L_3
(M = C, Si, L = O,S) systems

System	$\Delta E, \text{kcal-mol}^{-1}$ (TCSCF-ROHF)	
	6-31G(d)	SBK(d)
C_2O_3	65.3	65.0
C_2S_3	83.0	82.9
Si_2O_3	20.3	20.7
Si_2S_3	33.5	34.0
Ge_2O_3		29.4
Sn_2O_3		22.0

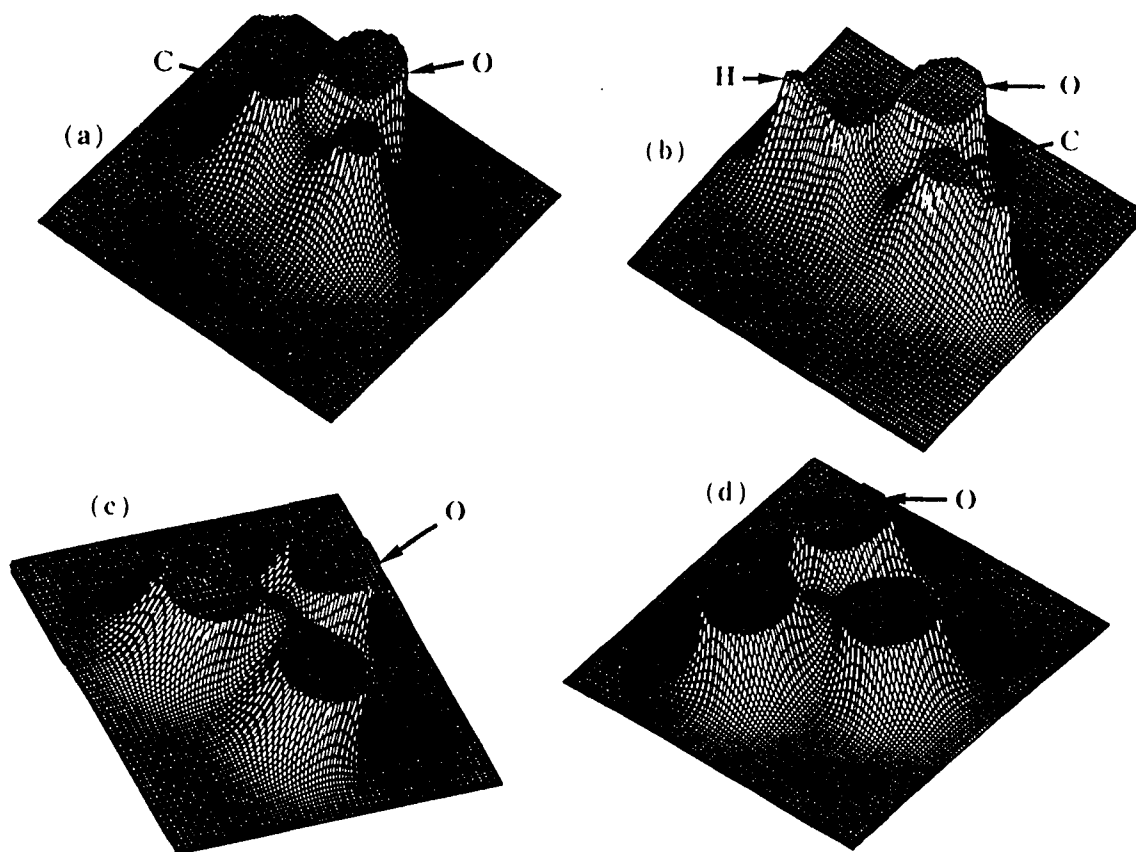


Figure 1. Relief maps of the charge distributions of C_2O_3 (a, c) and $C_2O_3H_2$ (b, d) systems in the σ_v (a, b) and σ_h (c, d) planes using the TCSCF/6-31G(2d)//TCSCF/6-31G(d) with the charge density cutoff of 0.32 au and 0.22 au for the σ_v and σ_h plane, respectively. These maps are very similar in form to those generated by using the RHF/6-31G(2d)//RHF/6-31G(d) wavefunctions.

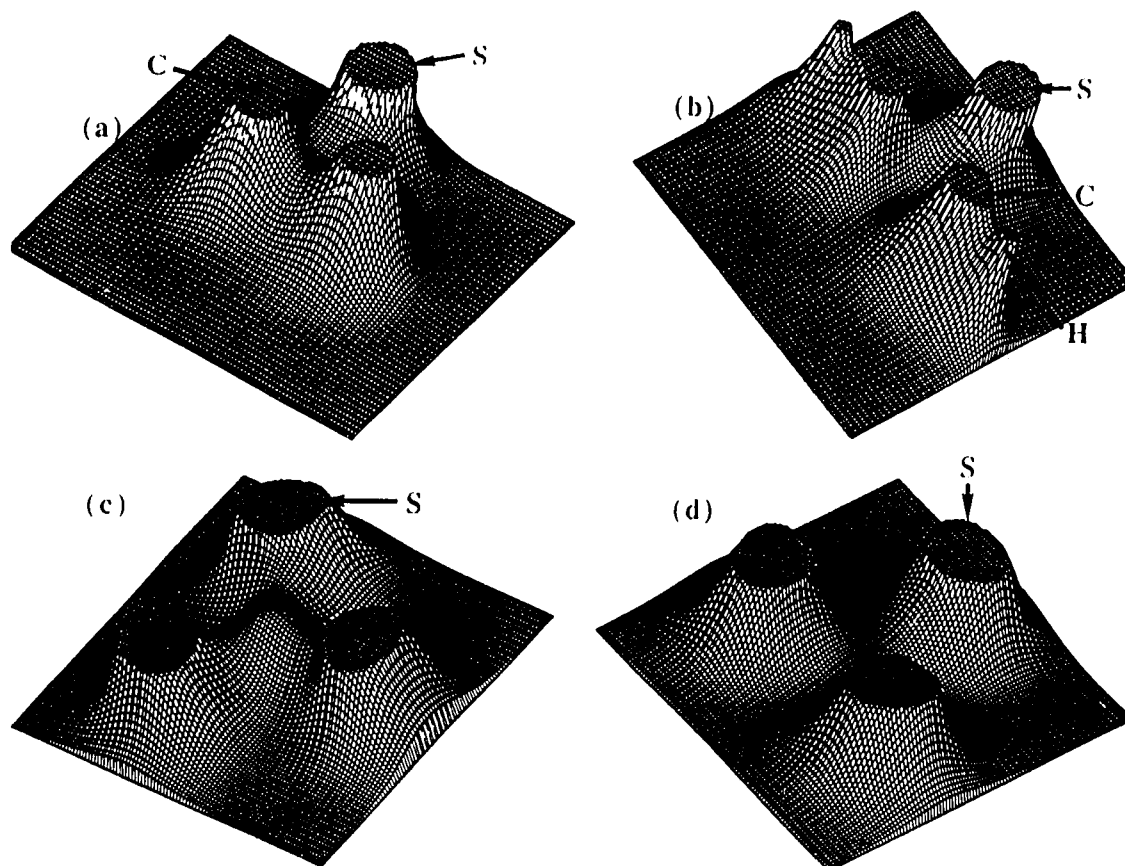


Figure 2. Relief maps of the charge distributions of C_2S_3 (a, c) and $C_2S_3H_2$ (b, d) systems in the σ_v (a, b) and σ_h (c, d) planes using the TCSCF/6-31G(2d)//TCSCF/6-31G(d) with the charge density cutoff of 0.32 au and 0.22 au for the σ_v and σ_h plane, respectively. These maps are very similar in form to those generated by using the RHF/6-31G(2d)//RHF/6-31G(d) wavefunctions.

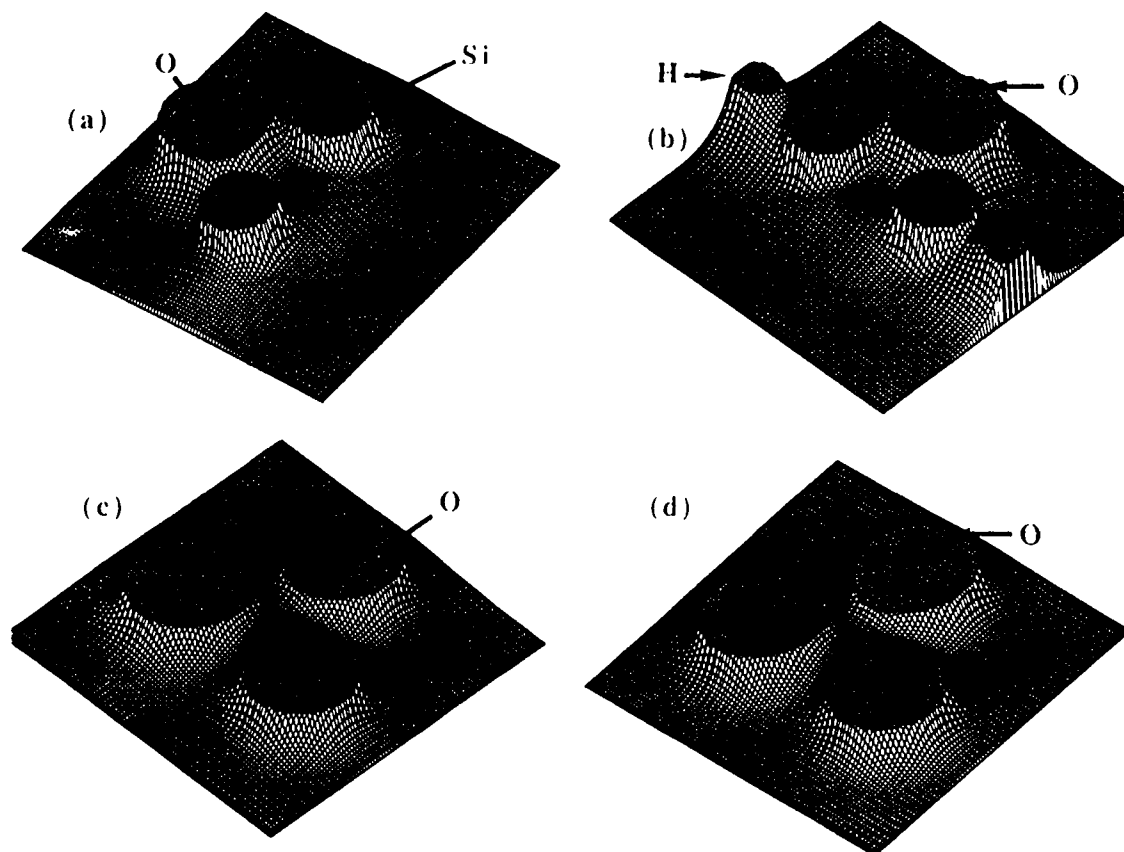


Figure 3. Relief maps of the charge distributions of Si_2O_3 (a, c) and $\text{Si}_2\text{O}_3\text{H}_2$ (b, d) systems in the σ_v (a, b) and σ_h (c, d) planes using the TCSCF/6-31G(2d)//TCSCF/6-31G(d) with the charge density cutoff of 0.15 au and 0.10 au for the σ_v and σ_h plane, respectively.

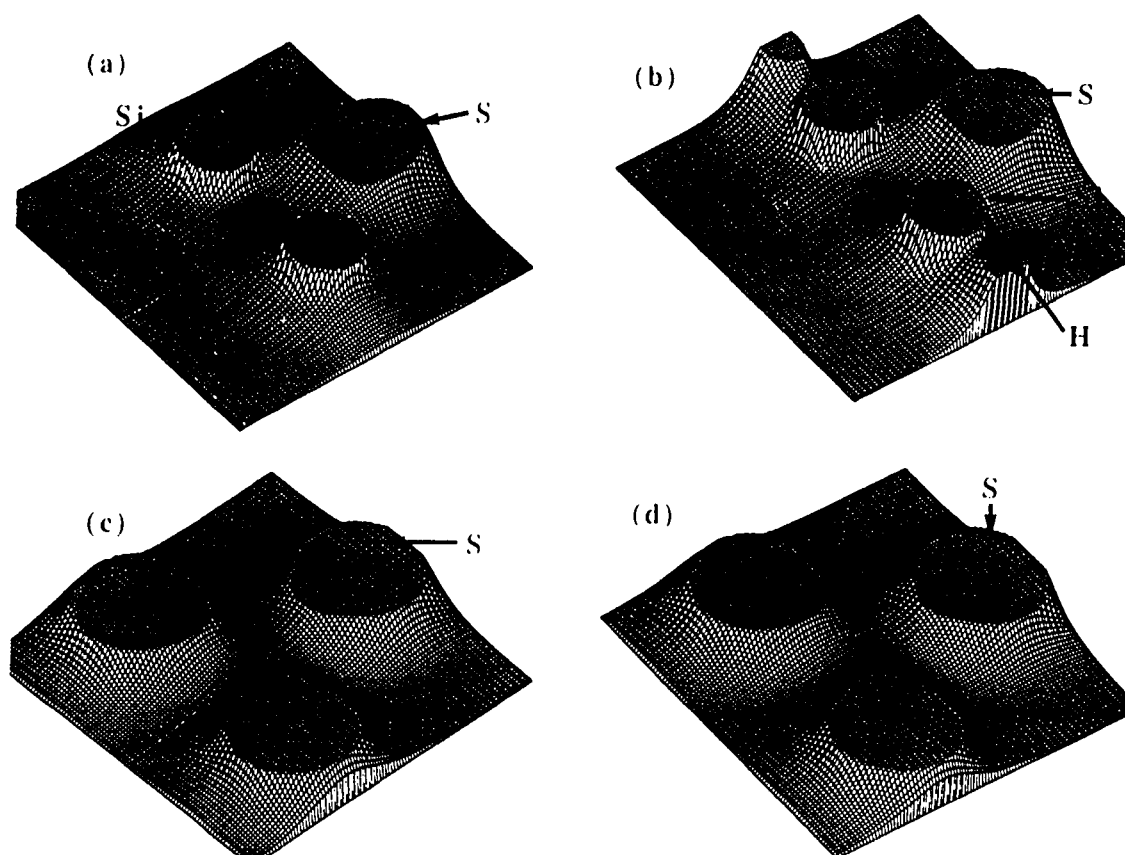


Figure 4. Relief maps of the charge distributions of Si_2S_3 (a, c) and $\text{Si}_2\text{S}_3\text{H}_2$ (b, d) systems in the σ_v (a, b) and σ_h (c, d) planes using the TCSCF/6-31G(2d)//TCSCF/6-31G(d) with the charge density cutoff of 0.15 au and 0.10 au for the σ_v and σ_h plane, respectively.

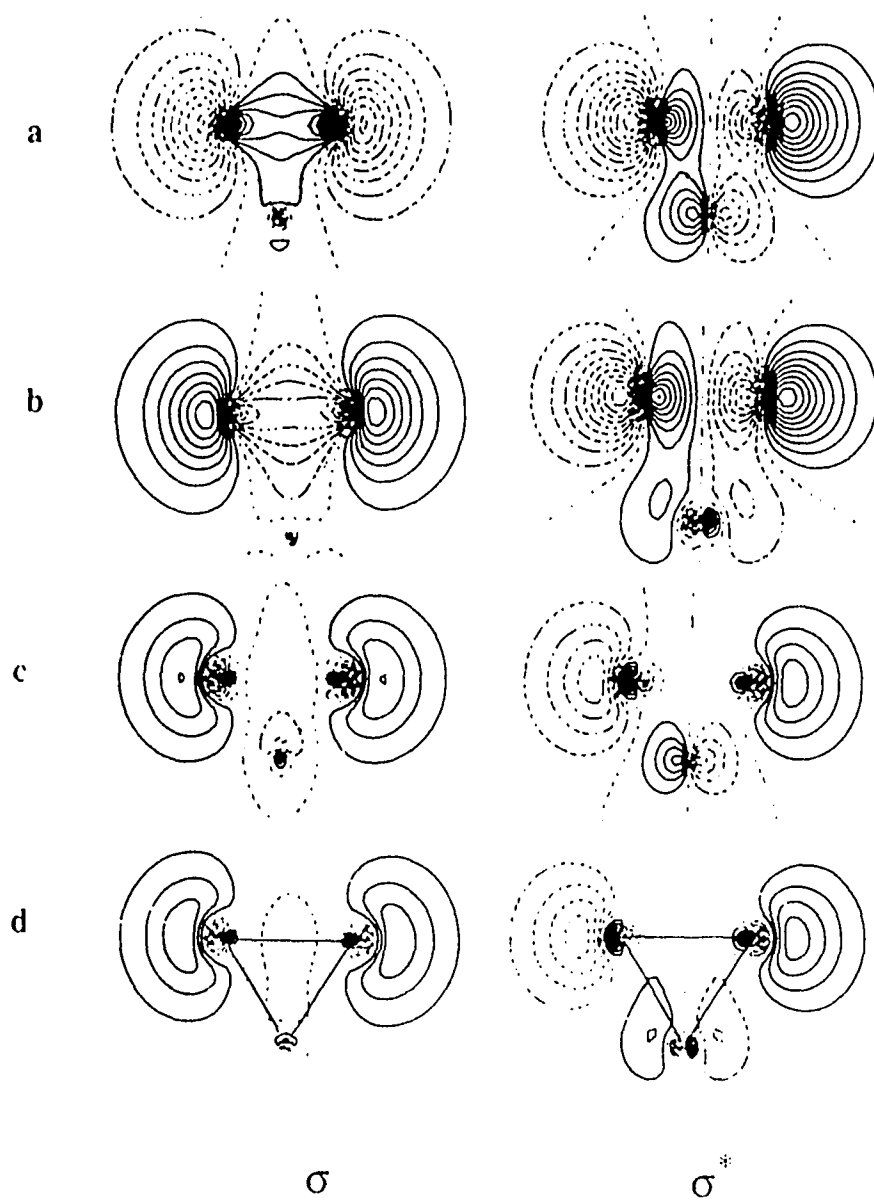


Figure 5. Contour plots of the HOMO and LUMO orbitals of C_2O_3 (a), C_2S_3 (b), Si_2O_3 (c) and Si_2S_3 (d) using TCSCF/6-31G(2d)//TCSCF/6-31G(d) wavefunctions.

CHAPTER 4: STRUCTURES, BONDING AND ENERGETICS OF N₂O₂ ISOMERS

A paper to be submitted to Journal of Physical Chemistry

Kiet A. Nguyen, Mark S. Gordon, John A. Montgomery Jr., and H. Harvey Michels

Abstract

The structures and energetics of the N₂O₂ isomers are predicted at several levels of theory. Both single reference and multi-reference based correlated methods were used to determine the structures and relative energies. Four high energy minima were located above 2NO with the QCISD(T)/6-311+G(2df)//MP2/6-311+G(d) (PT2F/6-311+G(2df)//MCSCF/6-31G(d)) relative energies of ca. 38 (51), 46 (51), 61 (74), 69 (74), and 68 (80) kcal/mol for 1,2-diaza-3,4-dioxocyclobutene (**1**), bond stretch bicyclodiazoxane (**2**), a-N₂O₂ (**3**), and bicyclodiazoxane (**5**), respectively. The effect of basis sets on structures are small within a given level of theory. The MCSCF structures agree reasonably with those of MP2.

I. Introduction

Contrary to considerable experimental¹⁻¹⁷ and theoretical¹⁸⁻²³ interest in the weakly bound nitric oxide (NO)₂ dimers, few calculations^{21,24,25} and experiments²⁶ have been reported on the possible existence of other isomers of N₂O₂ (see Figure 1). Recent interest in these high energy isomers has arisen due to their potential applications as new high energy density materials (HEDM).

To be useful as potential fuels, metastable species must be rather high in energy relative to their more stable isomers and to potential decomposition products (e.g., NO + NO, N₂ + O₂, N + NO₂ or N₂O + O in the case of N₂O₂). In addition to a large

thermodynamic exothermicity, these species must be kinetically stable, both adiabatically (that is, relative to an energy barrier on a singlet potential energy surface) and non-adiabatically (so that decomposition via coupling to a repulsive (e. g., triplet) state is unlikely). In the present work, we examine several high energy isomers of N_2O_2 , with particular emphasis on the molecular structure, fundamentals of bonding and energetics relative to alternative decomposition products. The kinetic stabilities of these species are dealt with separately.^{25b-d}

The only isomer of N_2O_2 that has been characterized experimentally¹⁻¹⁷ is the weakly bound cis-ONNO dimer, that lies 1-2 kcal/mol lower than $\text{NO} + \text{NO}$. It is clear from previous theoretical studies that a proper representation of the structure and relative energy of this isomer requires a multi-reference configuration interaction (MR-CI) treatment. The focus of this work is on the high energy and more covalently bound isomers 1-5, shown in Figure 1.

Several calculations have already been performed on the isomer of interest here. Using an SCF plus limited CI calculation, Bardo²¹ predicted the existence of a metastable cyclodiazoxene (1) lying 43.8 kcal/mol above the cis NO dimer. The D_{2h} cyclic isomer (2) was predicted to be a minimum at the RHF/6-31G(d) level of theory by Zandwijk et al.²⁴ Michels and Montgomery^{25a} have found that, at both the SCF and CISD/6-31G(d) levels of theory, the asymmetric (a- N_2O_2) planar OONN (3) isomer is a minimum on the N_2O_2 potential energy surface, with a 119.5 kcal mol⁻¹ enthalpy of formation. These authors also found a dioxirane-like C_{2v} (4) minimum energy RHF/6-31G(d) structure that lies 36 kcal/mol above the asymmetric minimum and is separated from the lower energy isomer (a- N_2O_2) by a small (<1 kcal/mol) barrier.

Very recently, Wodtke and co-workers²⁶ detected resonances in their molecular beam SEP experiments that suggest the existence of high energy N_2O_2 isomers. Indeed,

there are several such isomers that might be potential energy minima, some of which may correspond to those shown schematically in Figure 1. Because of their interest as possible new fuels and the fascinating recent experiments,²⁶ the molecular and electronic structures, nature of chemical bonding, and relative energies of these species are investigated using *ab initio* electronic structure theory.

II. Methods of Calculation

The structures of the N₂O₂ isomers have been predicted at both the SCF and MP2²⁷ levels of theory, using the 6-31G(d)²⁸, 6-311G(d)²⁹, and 6-311+G(d)^{29,30} basis sets. Additional sets of d and f functions were also used to study the basis set effects at the SCF level of theory. Because many of the structures displayed in Figure 1 may have significant diradical character that require a multi-configurational description, geometries were also evaluated with fully optimized reaction space (FORS) MCSCF³¹ wave functions.

Structures were obtained with the use of the analytically determined gradients encoded in the GAMESS³² (SCF and MCSCF) and GAUSSIAN88³³ (SCF, CISD, MP2) program systems. The structures were verified to be either minima or transition states by evaluating the appropriate matrix of energy second derivatives (hessian) either analytically (SCF with GAMESS, MP2 with CADPAC³⁴) or from finite differences of the analytically determined gradients (MCSCF from GAMESS).

MCSCF wave functions correlate all the bonds in the N₂O₂ isomers. The active space used consists of five doubly occupied (bonding MOs) and five empty anti-bonding MOs making up the FORS-MCSCF(10,10) (10 electrons in 10 orbitals) wavefunction. This corresponds to 5048, 2584, 9996, 5068, 4936 spin adapted configuration state functions (CFS) for structures 1- 5, respectively (or 19404 CSFs without symmetry). The starting MOs for these calculations were constructed by localizing the occupied orbitals

within each symmetry and then modifying these appropriately for the corresponding anti-bonding orbitals.

The final energetics were determined with single point calculations using the second order multi-reference perturbation theory (PT2)³⁵ and the GAUSSIAN-1³⁶ (G1) and GAUSSIAN-2³⁷ (G2) methods. PT2 calculations using two different types of Møller-Plesset-like partitioning were carried out using the MOLCAS-2 program.³⁵ The PT2D partitioning includes only the diagonal part of the one-electron operator in the zeroth-order Hamiltonian while PT2F also includes all non-diagonal elements. Only the former one is invariant to orbital transformations. The G1 and G2 procedures are based on MP2/6-31G(d) geometries. G1 energies are obtained from MP4(SDTQ)³⁸/6-311G(d,p), with additional improvements in basis sets and level of correlation, assuming that they are additive beyond the MP2/6-311G(d,p) level. The basis set corrections include: corrections due to diffuse-sp [$\Delta E(+)$] and polarization functions (d and f type) [$\Delta E(2df)$] for non-hydrogen atoms. Correlation corrections beyond MP4(SDTQ) were obtained using the QCISD(T)³⁹ method with the 6-311G(d,p) basis set, $\Delta E(QCI)$. The combined energies [$E(\text{MP4}/6\text{-}311\text{G}(\text{d},\text{p}) + \Delta E(+) + \Delta E(2df) + \Delta E(\text{QCI}))$], plus a "higher level correction" using an empirical formula

$$\Delta E(\text{HLC}) = -0.19n_{\alpha} - 5.96n_{\beta}$$

yield the G1 energies. Here, n_{α} and n_{β} are the number of α and β electrons, respectively. The G2 method includes a correction [$E(\Delta)$] for non-additivity of diffuse-sp and 2df basis set extensions used in the G1 method, an addition of a third set of d-functions and a second set of p-functions, and a modification of the higher level correction (HLC) used to correct for the remaining basis set deficiencies.

The nature of the bonding in the N_2O_2 isomers has been analyzed with the aid of the atoms in molecules (AIM) electron density analysis.⁴⁰ The density analysis has been

discussed in detail elsewhere,⁴⁰ and only a few key points will be given here. A critical point in the charge density is a point at which the gradient of the charge density vanishes ($\nabla\rho(\mathbf{r})=0$). A bond critical point (\mathbf{r}_b) exists between two atoms if there is a saddle point in the electron density $\rho(\mathbf{r})$ between two atoms. At such a point the hessian of $\rho(\mathbf{r})$ has one positive eigenvalue along the bond axis and two negative eigenvalues along the axes orthogonal to the bond axis. The existence of a bond critical point implies the existence of a bond path (a line linking two nuclei along which the charge density is a maximum with respect to any lateral displacement) and the two atoms are said to be bonded. The hessian of $\rho(\mathbf{r})$ at a ring critical point (\mathbf{r}_r) has two positive and one negative eigenvalues, with density $\rho(\mathbf{r}_r)$ at the ring critical point being smaller than that at all surrounding bond critical points. If an N-N bond is present in structure **5** (bicyclodiazoxane), one expects a bond critical point between the two bridgehead atoms, as well as two ring critical points, one on the face of each three-membered ring.

III. Results and Discussion

The structural and energetic information are tabulated separately for each isomer in Table Ia-e, illustrating the effects of different levels of theory. The SCF structures were optimized with the 6-31G(d) basis and the valence triple zeta series obtained by the systematic expansion of the 6-311G basis set with different types of polarization and diffuse functions yielding the following basis sets: 6-311G(d), 6-311G(2d), 6-311+G(d), 6-311+G(2d), 6-311G(2df) and 6-311+G(2df). Differences in predicted geometries among these basis sets are generally small for a given isomer. Deviations among these basis sets are generally less 0.02Å for bond lengths and less than a degree for bond angles, with the exception of structure **5** where the differences in the O-O distance (0.09Å) and the O-O-N (1.24°) angle between the 6-31G(d) and the 6-311G(d) basis sets are somewhat larger. Generally, the larger basis sets decrease O-O distances as expected. Similar to the

SCF results, structures obtained from three different basis sets [6-31G(d), 6-311G(d) and 6-311+G(d)] at the MP2 level of theory are in good agreement with one another. Since MP2 introduces anti bonding character into the various bonds, the general effect of adding MP2 into the geometry determination is a lengthening of the bonds. The same is true for MCSCF geometries.

In the next three subsections, we discuss results of the SCF, MP2 and MCSCF calculations with the 6-31G(d) basis set, since the basis set effects appear to be small, based on the discussion in the previous paragraph. These results will be discussed in the structures and bonding (section A) and energetics (section B) sections. The calculated structures are presented in three subsections (SCF, MP2 and MCSCF), starting with the single determinant SCF subsection. The bonding of these compounds is examined using the MCSCF/6-31G(d) wavefunctions.

A. Structures and Bonding

1. SCF

The geometrical parameters of the N₂O₂ isomers (**1-5**) are listed in Table Ia-e, respectively, along with the total energies at the SCF, MP2, QCISD and MCSCF levels of theory with several basis sets. The four-membered ring (**1**) structure calculated at RHF/6-31G(d) has (see Table Ia): N-O = 1.351Å, O-O = 1.398Å, and an N-N distance essentially identical to the N=N double bond in HN=NH. These bond distances and bond angles are about 0.1Å shorter and 2° smaller, respectively than those obtained earlier by Bardo.²¹ The bicyclodiazoxane structure (**5**) is a minimum on the SCF potential energy surface. This C_{2v} structure possesses an N-N bond (1.322Å) that is shorter than the N-N single bond in hydrazine (1.426Å, H₂N-NH₂) and longer than the N=N double bond in diimide (HN=NH, 1.216Å),⁴¹ at the same level of theory. The N-O distance of 1.402Å in **5** is similar the N-O distance of 1.413Å⁴² in hydroxylamine (H₂N-OH). Like bicyclobutane^{25c}

and silabicyclobutane species⁴³, **5** also has a bond stretch isomer (**2**).²⁴ This planar structure with D_{2h} symmetry possesses a much longer N-N distance of 1.876Å. This is compensated by a shorter N-O distance (1.302Å).

The two unusual structures **3** and **4** that had been considered earlier by Michels and Montgomery^{25a} are also included in Table I. The N-N bond length in **4** is shorter than expected for a double bond, while the O-O distance is about the O-O single bond length. The a-N₂O₂ structure **3** has very short N-N and N-O distances, and an unusually long O-O distance.

2. MP2

One generally expects the introduction of correlation corrections to increase bond distances due to the addition of antibonding character into the wavefunction. This is illustrated in the MP2 geometries in Tables Ia-e. For the short bond bicyclodiazoxane isomer (**5**), increases of 0.07Å and 0.08Å from SCF distances are observed with the 6-31G(d) basis set at the MP2 level of theory for the N-N and N-O bond distances, respectively. At this level of theory, structure (**5**) has one imaginary frequency of 164i cm⁻¹ (see Figure 2a), indicating a transition state instead of a local minimum. MP2/6-31G(d) predicts the bond stretch isomer (**2**) to be a minimum on the potential energy surface with a distance of 2.012Å for the N-N bond and 1.396Å for the N-O bond. This is a 0.136Å increase for the N-N distance relative to RHF/6-31G(d). At this level of theory, the N-N bond in **2** is greater than that in **5** by 0.617Å.

For the other three isomers [dioxirane-like (**4**), asymmetric (**3**) and the cyclic four membered ring (**1**)], non trivial bond lengthenings are found for the O-O distances (**4** ~ 0.2Å, **3** and **1** ~ 0.1Å) (see Table Ia, Ic, Id). Similar results were also found with the 6-311G(d) and 6-311+G(d) basis sets for all N₂O₂ isomers, upon introduction of correlation at the MP2 level of theory.

3.MCSCF

Correct descriptions of unusual molecular structures frequently need to be examined with more flexible wave functions.^{44,45,25a,25c} In these unusual bonding environments, multi-configuration wavefunctions may be essential to ensure correct descriptions when such species have large diradical character.

The MCSCF geometries obtained with the 6-31G(d) basis set are also listed in Tables Ia-e. Structural agreement between MCSCF and MP2 is quite good for structures **1**, **2**, and **5**. For structure **4**, the difference in predicted O-O distance is 0.07Å, and in **3** this disagreement is 0.1Å. Other structural parameters are in reasonable agreement. The MCSCF/6-31G(d) structures for **2** and **5** were reported in an earlier study^{25c} and are included here for completeness. The MCSCF/6-31G(d) hessian of **5** is positive definite, indicating that it is a minimum on the PES, not a transition state as predicted by MP2. Structure **2** is a bond stretch isomer of bicyclodiazoxane (**5**). The O-N-N-O dihedral angle of 107.0° in **5** is flattened to 180° to form **2**, together with a much longer N-N bond (1.970Å), suggesting that there may be significant configurational mixing.

The amount of configurational mixing can be assessed by examining the occupation numbers of the natural orbitals (NOONs) of the MCSCF wave function. In contrast to the largely closed shell nature of the N-N bond in **5** (with NOONs of 1.9600 and 0.0405 in the bonding and anti-bonding MOs, respectively), the NOONs in the N-N bonding and anti-bonding MOs of **2** are 1.8051 and 0.1945, respectively. However, sums of all the NOONs in the anti-bonding MOs (that is, the net population in orbitals outside of the closed shell, Hartree-Fock configuration) for **2** and **5** are quite similar: 0.3508 and 0.3351, respectively. These NOONs are significantly larger than the corresponding NOONs of 0.1970 in 2NO. The σ -like N-N bonding orbitals in bicyclodiazoxane (**5**) become π -like in **2** as illustrated by the natural orbitals shown in Figure 3e (i, j) and Figure

3b (g, h) for isomer **5** and **2**, respectively. In fact, the total density analysis reveals a symmetric four-membered ring like arrangement for **2** (see Figure 4a: bottom left). This is verified by the four equivalent N-O bond critical points and one ring critical point at the center of **2** (see Table II and Figure 4a). Figure 4a (bottom) displays the total density of bicyclodiazoxane (**5**) in the plane containing one peripheral oxygen and two bridgehead nitrogen atoms, revealing only one of the two equivalent three-membered rings making up the bicyclo system with two N-O and one N-N bond critical points and a ring critical point.

Structure **4**, a minimum at both the SCF and MP2 levels of theory, is predicted to be a transition state (with an imaginary frequency of $187i \text{ cm}^{-1}$) at the MCSCF level. From the imaginary normal mode, **4** appears to be a symmetric transition state leading to a-N₂O₂ (**3**) (see Figure 2b). The optimized MCSCF/6-31G(d) bond lengths and bond angles of **3** are within 0.1 \AA and 1° of the results obtained earlier at the MR-CISD(4,4)/TZP level of theory.^{25b} The natural orbitals and their corresponding NOONs reveal some mixing at the transition structure (**4**) leading to **3** (see Figure 3d). The N-O and O-O anti-bonding MOs' of **3** each has a NOON greater than 0.1. Despite the unusual structure, a-N₂O₂ (**3**) has the smallest amount of configurational mixing among the four isomers (0.2258 electron in the anti-bonding MOs), as shown in Figure 3c. The total density plots displayed in Figure 4a (bottom right) and Figure 4b (top), confirm the bonding nature revealed by the structural information of **3** and **4**, respectively. The short N-N bonds in **3** and **4** result in considerable charge density accumulation in the those regions, in contrast to the densities in the regions containing of the stretched O-O bonds (Table 2).

Natural orbitals and total density plots confirm the cyclic nature of **1** (see Figure 3a and Figure 4a: top). There are four N-N MOs (σ, σ^*, π , and π^*) with density of 0.496 au at the bond critical point. The N-N distance (1.247 \AA) of the cyclic N₂O₂ is similar to the N-N bond in HN=NH while the N-O (1.431 \AA) and O-O (1.539 \AA) bonds are closer to

those of bicyclodiazoxane and *a*-N₂O₂ (**3**), respectively. These distances are within 0.05 Å of the corresponding MP2 values.

C. Energetics

The calculated relative energies—with reference to 2NO—of all N₂O₂ isomers are listed in Table IIIa-b. G2 relative energies are 41.7, 47.3, 63.8, 71.4 and 69.3 kcal/mol for **1-5**, respectively. The corresponding G1 energetics are generally within 2.5 kcal mol⁻¹ of the G2 values. QCISD(T)/6-311+G(2df) relative energies are essentially identical to those predicted by G1 and G2. Since the unrestricted Hartree-Fock⁴⁶ (UHF) wave function for NO is only slightly spin-contaminated ($\langle S^2 \rangle = 0.7737$) the differences between the projected⁴⁷ (PMPn) and unprojected (MPn) relative energies for the MP series are small, 5.0 and 3.0 kcal/mol for MP2 and MP4, respectively. The PMP4 relative energies are converged to within 1 kcal/mol of the QCISD(T) values, except for structure **2** and **4** where the QCISD(T)-PMP4 differences are 4.7 and 3.7 kcal/mol, respectively. Since the QCISD(T), G1 and G1 methods have been shown to have excellent agreement with experiment for cases in which MP4 was inadequate,^{36,37,48} the QCISD(T) relative energies for these isomers may be closer to the correct results. A correction for spin contamination of the UHF wave functions is likely to bring the G1, G2 and QCISD(T)/6-311+G(2df)//MP2/6-311G+(d) relative energies into closer agreement with the multireference PT2F/6-311+G(2df)//MCSCF/6-31G(d) relative energies. The basis set dependence of PT2F and MCSCF relative energies are small (less than 3 kcal/mol for the worst case) upon going from 6-31G(d) to 6-311+G(2df) (see Table IIIb). Note that all levels of theory beyond the simple MCSCF predict all structures **1-5** to be high in energy relative to 2NO and also predict structures **3, 4, 5** to be 15-20 kcal/mol higher than **1** and **2**.

IV. Summary and Conclusion

Several levels of *ab initio* molecular orbital theory have been used to predict the structures and energetics of N₂O₂ isomers. Four high energy isomers were located above 2NO with the QCISD(T)/6-311+G(2df)//MP2/6-311+G(d) (PT2F/6-311+G(2df)//MCSCF/6-31G(d)) relative energies of ca. 38 (51), 46 (51), 61 (74), 69 (74), and 68 (80) kcal/mol for cyclodiazoxene (1), bond stretch bicyclodiazoxane (2), *a*-N₂O₂ (3), and bicyclodiazoxane (5), respectively. The effect of basis sets on structures are small within a given level of theory. The MCSCF structures agree reasonably with those of MP2.

Of the four metastable (thermodynamically) species, *a*-N₂O₂ has been shown to dissociate via the spin-forbidden channel *a*-N₂O₂ (¹A') → N₂O (X ¹Σ⁺) + O (³P).^{25b} Study of the kinetic stability of the other isomers with respect to spin-allowed and spin-forbidden processes is in progress.

Acknowledgment

This collaborative research was supported in part by grants from: the Air Force Office of Scientific Research under the High Energy Density Materials Initiative to KAN and MSG, the AF Phillips Laboratory under Contract F04611-90-C-0009 to JAM and HHM. Calculations described in this work were performed on an IBM RS6000/530 (obtained through an AFOSR grant to MSG) at North Dakota State University, on an IBM RS6000/350 generously provided by Iowa State University, on an IBM RS6000/350 at United Technologies Research Center, and on the Cray-2 at the National Center for Supercomputing Applications, Champaign, Illinois.

References

- (1) Smith, A. L.; Keller, W. E.; Johnston, H. L. *J. Chem. Phys.* **1951**, 19, 189.
- (2) (a) Lipscomb, W. N.; Wang, F. E.; May, W. R.; Lippert, Jr. E. L. *Acta. Crystallogr.* **1961**, 14, 1100. (b) Lipscomb, W. N. *J. Chem. Phys.* **1971**, 54, 3659.
- (3) Guillory, W. A.; Hunter, C. E. *J. Chem. Phys.* **1969**, 50, 3516.
- (4) (a) Dinerman, C. E.; Ewing, G. E. *J. Chem. Phys.* **1970**, 53, 626. (b) Dinerman, C. E.; Ewing, G. E. *J. Chem. Phys.* **1971**, 54, 3660.
- (5) (a) Naitoh, Y.; Fujimura, Y.; Honma, K.; Kajimoto, O. *Chem. Phys. Lett.* **1993**, 205, 423. (b) Naitoh, Y.; Fujimura, Y.; Kajimoto, O.; Honma, K. *Chem. Phys. Lett.* **1993**, 190, 135.
- (6) Kajimoto, O.; Honma, K.; Kobayashi, T. *J. Phys. Chem.*, **1985**, 89, 2725.
- (7) Billingsley, J.; Callear, A. B. *Trans. Faraday Soc.* **1971**, 67, 589.
- (8) During, J. R.; Griffin, M. G. *J. Raman. Spectrosc.* **1976**, 5, 273.
- (9) Anderson, A.; Lassier-Govers, B. *Chem. Phys. Lett.* **1977**, 50, 124.
- (10) Forte, E.; van den Bergh, H. *Chem. Phys.* **1978**, 30, 325.
- (11) (a) Kumar, V.; Verma, U. P.; Pandey, A. M. *J. Mol. Struct.* **1978**, 49, 411. (b) Ohlsen, J. R.; Lanne, J. *J. Am. Chem. Soc.* **1978**, 100, 6948.
- (12) Western, C. M.; Langridge, P. R. R.; Howard, B. J.; Novick, S. E. *Mol. Phys.* **1981**, 44, 145.
- (13) Kukolich, S. G. *J. Mol. Spectrosc.* **1983**, 98, 80.
- (14) Menoux, V.; LeDoucen, R.; Haleusler, C.; Deroche, J. C. *Can. J. Phys.* **1984**, 62, 322.
- (15) Sodeau, J. R.; Withnall, R. *J. Chem. Phys.* **1985**, 89, 4484.

- (16) (a) Casassa, M. P.; Woodward, A. M. Stephenson; J. C.; King, D. S. *J. Chem. Phys.* **1986**, 85, 6235. (b) Casassa, M. P.; Stephenson, J. C.; King, D. S. *J. Chem. Phys.* **1988**, 89, 1966.
- (17) Fischer, I.; Strobel, A.; Staecker, J.; Niedner-Schatteburg, G. Muller-Dethlefs, K.; Bondybey, V. E. *J. Chem. Phys.* **1992**, 96, 7171.
- (18) (a) Williams, J. E.; Murrell, J. N. *J. Am. Chem. Soc.* **1971**, 93, 7149. (b) Vladimiroff, T. *J. Am. Chem. Soc.* **1972**, 94, 8250. (c) Skancke, P. N.; Boggs, J. E. *Chem. Phys. Lett.* **1973**, 21, 316. (d) Skaarup, S.; Skancke, P. N.; Boggs, J. E. *J. Am. Chem. Soc.* **1976**, 98, 6106. (e) Lee, T. J.; Rice, J. E.; Scuseria, G.; Schaefer, H. *Theore. Chim. Acta (Berl.)* **1989**, 75, 81. Harcourt, R. D. *J. Mol. Struct. (Theochem)* **1990**, 65, 253. (f) Cole, S. J.; Bartlett, R. J. unpublished results.
- (19) Benzel, M. A.; Dykstra, E. C.; Vincent, M. A. *Chem. Phys. Lett.* **1981**, 78, 139.
- (20) Ha, Tae-K. *Theore. Chim. Acta (Berl.)* **1981**, 58, 125.
- (21) Bardo, R. D. *J. Phys. Chem.* **1982**, 86, 4658.
- (22) Bock, C.; Trachtman, M.; Schmiedekamp, A.; George, P.; Chin, T. S. *J. Comp. Chem.* **1983**, 4, 379.
- (23) Neilin, C. J.; Bagus, P. S.; Behm, J.; Brundel, C. R. *Chem. Phys. Lett.* **1984**, 105, 58.
- (24) Zandwijk, v. G. Janssen, R. A. J.; Buck, H. M. *J. Am. Chem. Soc.* **1990**, 112, 4155.
- (25) (a) Michels, H. H.; Montgomery, Jr. J. A. *J. Chem. Phys.* **1988**, 88, 7248. (b) Nguyen, K. A.; Gordon, M. S.; Montgomery, Jr. J. A.; Michels, H. H.; Yarkony, D. R. *J. Chem. Phys.* **1993**, 98, 3845. (c) Nguyen, K.; Gordon, M. S.; Boatz, J.

- A. *J. Am. Chem. Soc.* **1993** submitted. (d) Nguyen, K. A.; Chaban, G.; Gordon, M. S.; Montgomery, Jr. J. A.; Michels, H. H.; Yarkony, D. R. to be published.
- (26) (a) Yang, X.; Kim, E. H.; Wodtke, A. M. *J. Chem. Phys.* **1992**, *96*, 5111. (b) Yang, Price, J. M.; Mack, J. A.; Morgan, C. G.; Rogaski, C. A.; McGuire, D.; X.; Kim, E. H.; Wodtke, A. M. *J. Phys. Chem.* **1993**, *97*, 3944.
- (27) Pople, J. A.; Krishnan, R.; Schlegel, H. B.; Binkley, J. S.; *Int. J. Quant. Chem.* **1979**, *S13*, 225.
- (28) Hehre, W. J.; Ditchfield, R.; Pople, J. A. *J. Chem. Phys.* **1972**, *56*, 2257.
- (29) Krishnan, R.; Binkley, J. S.; Seeger, R.; Pople, J. A. *J. Chem. Phys.* **1980**, *72*, 650.
- (30) Clark, T.; Chandrasekhar, J.; Spitznagel, G. W., Schleyer, P. v. R. *J. Comp. Chem.* **1983**, *4*, 294.
- (31) Lengsfeld, B. H. III; *J. Chem. Phys.* **1980**, *73*, 382. Yarkony, D. R. *Chem. Phys. Lett.* **1981**, *77*, 634. Ruedenberg, K.; Schmidt, M. W.; Dombek, M. M.; Elbert, S. T. *Chem. Phys.* **1982**, *71*, 41,51 65; Lam, B.; Schmidt, M. W.; Ruedenberg, K. *J. Phys. Chem.* **1985**, *89*, 2221.
- (32) GAMESS (General Atomic and Molecular Electronic Structure System): (a) Schmidt, M. W.; Baldrige, K. K.; Boatz, J. A.; Jensen, J. H.; Koseki, S.; Gordon, M. S.; Nguyen, K. A.; Windus, T. L.; Elbert, S. T. *QCPE Bulletin*, **1990**, *10*, 52. (b) Schmidt, M. W.; Baldrige, K. K.; Boatz, J. A.; Elbert, S. T.; Gordon, M. S.; Jensen, J. H.; Koseki, S.; Matsunaga, N.; Nguyen, K. A.; Su, S. Windus, T. L. *J. Comp. Chem.* **1993**, *14*, 1347.
- (33) GAUSSIAN88, Frisch, M. J.; Head-Gordon, M.; Schlegel, B. H.; Raghavachari, K.; Binkley, J. S.; Gonzalez, C.; Defrees, D. J.; Fox, D. J.; Whiteside, R. A.;

- Seeger, R.; Melius, C. F.; Baker, J. Martin, R.; Kahn, L. R.; Stewart, J. J. P.; Fluder, E. M.; Topiol, S. Pople, J. A. Gaussian, Inc., Pittsburgh, PA, **1988**.
- (34) Amos, R. D.; Rice J. E., 'CADPAC: The Cambridge Analytic Derivatives Package', issue 4.0, Cambridge, 1987.
- (35) (a) Anderson, K. Malmqvist, P.-Å., Roos, B. O. *J. Chem. Phys.* **1992**, 96, 1218.
(b) Anderson, K. Malmqvist, P.-Å., Roos, B. O. *J. Phys. Chem.* **1990**, 94, 5483.
(c) Anderson, K.; Fülcher, M. P.; Lindh, R.; Malmqvist, P.-Å.; Olsen, J.; Roos, B. O.; Sadlej, A. J.; Wilmark, P.-O. MOLCAS version 2, User's Guide; University of Lund, Sweden, 1991.
- (36) Pople, J. A.; Head-Gordon, M.; Fox, D. J.; Raghavachari, K.; Curtiss, L. A. *J. Chem. Phys.* **1989**, 90, 5622.
- (37) Curtiss, L. A.; Raghavachari, K.; Trucks, G. W.; Pople, J. A. *J. Chem. Phys.* **1991**, 94, 7221.
- (38) (a) Moller, C.; Plesset, M. S.; *Phys. Rev.* **1934**, 46, 618. (b) Krishnan, R.; Frisch, M. J.; Pople, J. A. *J. Chem. Phys.* **1980**, 72, 4244. (c) Barlett, R. J.; Sekino, H.; Purvis, G. D. *Chem. Phys. Lett.* **1983**, 98, 66.
- (39) Pople, J. A.; Head-Gordon, M.; Raghavachari, K. *J. Phys. Chem.* **1987**, 87, 5968.
- (40) (a) Bader, R. F. W.; Nguyen-Dang, T. T. *Adv. Quant. Chem.* **1981**, 14, 63. (b) Bader, R. F. W.; Nguyen-Dang, T. T.; Tal, Y. *Rep. Prog. Phys.* **1981**, 44, 893.
(c) Bader, R. F. W. *Acc. Chem. Res.* **1985**, 18, 9. (d) Bader, R. F. W. *Chem. Rev.* **1991**, 91, 893.
- (41) Schmidt, M. W.; Gordon, M. S. *Inorg. Chem.* **1986**, 25, 248.
- (42) Schmidt, M. W.; Truong, P. N.; Gordon, M. S. *J. Am. Chem. Soc.* **1987**, 109, 5217.
- (43) Boatz, J. A.; Gordon, M. S. *J. Phys. Chem.* **1989**, 93, 2888.

- (44) Schmidt, M. W.; Nguyen, K. A.; Gordon, M. S.; Montgomery, Jr. J. A. *J. Am. Chem. Soc.* **1991**, 113, 5998.
- (45) Nguyen, K. A.; Carroll, M. T.; Gordon, M. S. *J. Am. Chem. Soc.* **1991**, 113, 7924.
- (46) Pople, J. A.; Nesbet, R. K. *J. Phys. Chem.* **1954**, 22, 571.
- (47) Schlegel, H. B. *J. Phys. Chem.* **1986**, 84, 4530.
- (48) Raghavachari, K.; Trucks, G. W. *J. Chem. Phys.* **1991**, 91, 2457.

Table Ia. Structures, total energies (in au) of cyclodiazoxene (**1**).

Level	Energy	Bond length			Angle
		N-N	N-O	O-O	O-O-N
RHF/6-31G(d)	-258.356361	1.2162	1.3510	1.3975	93.85
RHF/6-311G(d)	-258.421803	1.2133	1.3427	1.3807	93.57
RHF/6-311G(2d)	-258.436501	1.2115	1.3486	1.3903	93.80
RHF/6-311+G(d)	-258.426866	1.2134	1.3429	1.3810	93.58
RHF/6-311+G(2d)	-258.439994	1.2114	1.3479	1.3896	93.79
RHF/6-311G(2df)	-258.447486	1.2112	1.3451	1.3859	93.72
RHF/6-311+G(2df)	-258.451147	1.2112	1.3444	1.3851	93.71
MP2/6-311G(d)	-259.071100	1.2845	1.3923	1.4875	94.18
MP2/6-311G(d)	-259.238762	1.2769	1.3745	1.4600	93.82
MP2/6-311+G(d)	-259.251533	1.2773	1.3756	1.4644	93.90
MCSCF/6-31G(d)	-258.579867	1.2469	1.4308	1.5393	95.86

Table Ib. Structures, total energies (au) of bond stretch bicyclodiazoxane (2).

Level	Energy	Bond length		Angle	
		N-N	N-O	N-O-N	O-N-O
RHF/6-31G(d)	-258.291376	1.8762	1.3021	92.19	87.81
RHF/6-311G(d)	-258.388654	1.8657	1.2953	92.14	87.86
RHF/6-311G(2d)	-258.400881	1.8703	1.2988	92.11	87.89
RHF/6-311+G(2d)	-258.404710	1.8699	1.2985	92.11	87.89
RHF/6-311G(2df)	-258.413103	1.8666	1.2963	92.11	87.89
RHF/6-311+G(2df)	-258.417150	1.8665	1.2961	92.12	87.88
MP2/6-31G(d)	-259.088768	2.0123	1.3962	92.22	87.78
MP2/6-311G(d)	-259.279048	1.9838	1.3772	92.14	87.85
MP2/6-311+G(d)	-259.288677	1.9860	1.3789	92.13	87.87
MCSCF/6-31G(d)	-258.536838	1.9701	1.3651	92.38	87.62

Table Ic. Structures, total energies (in au) of a-N₂O₂ (**3**).

Level	Energy	Bond length			Angle	
		N-N	N-O	O-O	O-O-N	N-N-O
RHF/6-31G(d)	-258.348838	1.0844	1.2024	1.7574	103.97	179.51
RHF/6-311G(d)	-258.417315	1.0787	1.1901	1.8014	106.20	179.62
RHF/6-311G(2d)	-258.431015	1.0734	1.2001	1.7089	104.22	179.35
RHF/6-311+G(d)	-258.424318	1.0774	1.1944	1.7590	106.45	179.66
RHF/6-311+G(2d)	-258.436977	1.0726	1.2017	1.6863	104.80	179.48
RHF/6-311G(2df)	-258.442081	1.0732	1.1955	1.6900	104.67	179.42
RHF/6-311+G(2df)	-258.448070	1.0724	1.1971	1.6693	105.22	179.47
MP2/6-31G(d)	-259.027820	1.1547	1.2273	1.5303	103.59	179.49
MP2/6-311G(d)	-259.223431	1.1466	1.2137	1.5249	105.67	179.47
MP2/6-311+G(d)	-259.238295	1.1453	1.2166	1.5104	106.36	179.74
CISD/6-31G(d)	-258.932499	1.1072	1.2240	1.5817	102.87	179.34
QCISD/6-31G(d)	-259.032783	1.1257	1.2472	1.5722	101.39	179.50
MCSCF/6-31G(d)	-258.552040	1.1166	1.2706	1.6285	98.19	179.70

Table Id. Structures, total energies (in au) of (4).

Level	Energy	Bond length			Angle
		N-N	N-O	O-O	N-N-O
RHF/6-31G(d)	-258.287006	1.1268	1.3520	1.4786	146.85
RHF/6-311G(d)	-258.352989	1.1231	1.3420	1.4572	147.12
RHF/6-311G(2d)	-258.368546	1.1159	1.3512	1.4723	146.99
RHF/6-311+G(d)	-258.356572	1.1234	1.3413	1.4588	147.06
RHF/6-311+G(2d)	-258.372557	1.1159	1.3497	1.4714	146.97
RHF/6-311G(2df)	-258.380592	1.1169	1.3455	1.4660	146.99
RHF/6-311+G(2df)	-258.384666	1.1169	1.3438	1.4649	146.97
MP2/6-31G(d)	-259.025810	1.1377	1.4882	1.5881	147.75
MP2/6-311G(d)	-259.216905	1.1300	1.4681	1.5785	147.48
MP2/6-311+G(d)	-259.228004	1.1296	1.4711	1.5814	147.49
MCSCF/6-31G(d)	-259.520464	1.1247	1.5236	1.6514	147.18

Table Ie. Structures, total energies (in au) of bicyclodiazoxane (**5**).

Level	Energy	Bond length		Angle		Dihedral
		N-N	N-O	N-O-N	O-N-O	N-O-N-O
RHF/6-31G(d)	-258.291376	1.3221	1.4021	56.26	91.16	56.93
RHF/6-311G(d)	-258.359403	1.3183	1.3927	56.50	91.25	56.69
RHF/6-311G(2d)	-258.368283	1.3216	1.4005	56.31	91.18	56.89
RHF/6-311G(d)	-258.364259	1.3187	1.3926	56.52	91.24	56.68
RHF/6-311+G(2d)	-258.371766	1.3217	1.3998	56.34	91.21	56.84
RHF/6-311G(2df)	-258.381813	1.3179	1.3960	56.33	91.25	56.33
RHF/6-311+G(2df)	-258.385715	1.3178	1.3952	56.36	91.27	56.79
MP2/6-31G(d)	-259.025183	1.3948	1.4843	56.05	91.37	56.97
MP2/6-311G(d)	-259.216565	1.3805	1.4642	56.25	91.63	56.64
MP2/6-311+G(d)	-259.227356	1.3819	1.4658	56.24	91.53	56.71
QCISD/6-31G(d)	-259.022616	1.3729	1.4701	55.67	91.43	57.23
MCSCF/6-31G(d)	-258.534178	1.3951	1.4837	56.09	90.36	57.58

Table II. Bond, ring and cage critical point analysis of N_2O_2 isomers using the MCSCF(10,10)/6-31G(d). All values are in atomic units.

Systems	Bond A-B	$\rho(\mathbf{r})$	$\nabla^2\rho(\mathbf{r})$
1	N-N	0.4960	-0.1349
	N-O	0.3080	-0.4090
	O-O	0.1492	-0.4368
	Ring ^a	0.09496	0.8045
2	N-O	0.3589	-0.6429
	Ring ^a	0.1166	1.0033
3	N-N	0.5885	-0.1677
	N-O	0.4297	-0.5758
	O-O	0.1492	0.4368
4	N-N	0.5885	-0.1850
	N-O	0.2370	0.0495
	O-O	0.1556	0.3222
	Ring ^a	0.1298	0.7392
5	N-N	0.3364	-0.5605
	N-O	0.2621	-0.0798
	Ring ^a	0.2139	0.5745

^asee text

Table III. Relative energies (kcal/mol) of N₂O₂ isomers with reference to 2NO.

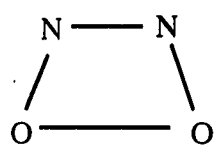
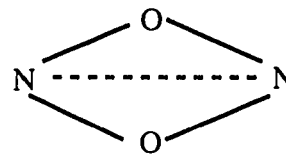
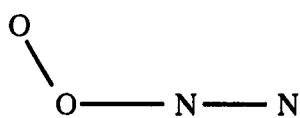
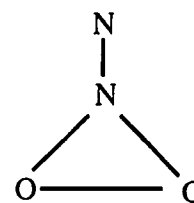
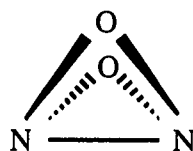
(a)

Systems	MP2 ^a	MP4 ^a	PMP2 ^a	PMP4 ^a	QCISD(T) ^b	G1	G2
1	34.3	35.8	39.3	38.8	38.3	39.5	41.7
2	24.2	37.8	29.2	40.8	45.5	46.1	47.3
3	55.8	56.6	60.8	59.6	60.5	62.1	63.8
4	60.9	62.2	65.9	65.2	68.9	69.0	71.4
5	60.4	63.5	65.4	66.5	67.0	68.0	69.3

(b)

Systems	6-31G(d)//6-31G(d)		6-311+G(2d)//6-31G(d)		6-311+G(2df)//6-31G(d)	
	MCSCF	PT2F	MCSCF	PT2F	MCSCF	PT2F
1	43.4	49.4	44.4	52.9	43.6	51.2
2	71.0	49.0	71.7	48.7	71.1	51.0
3	60.3	79.3	57.1	75.5	56.8	73.8
4	78.7	76.2	79.0	75.3	78.6	73.6
5	71.2	77.3	73.2	81.9	72.4	79.7

^aMP4(SDTQ)/6-3111+G(2df)//6-311+G(d). ^bQCISD(T)/6-311+G(2df)//MP2/6-311G+(d)

**1** C_{2v} **2** D_{2h} **3** C_s **4** C_{2v} **5** C_{2v} Figure 1. N_2O_2 structural isomers

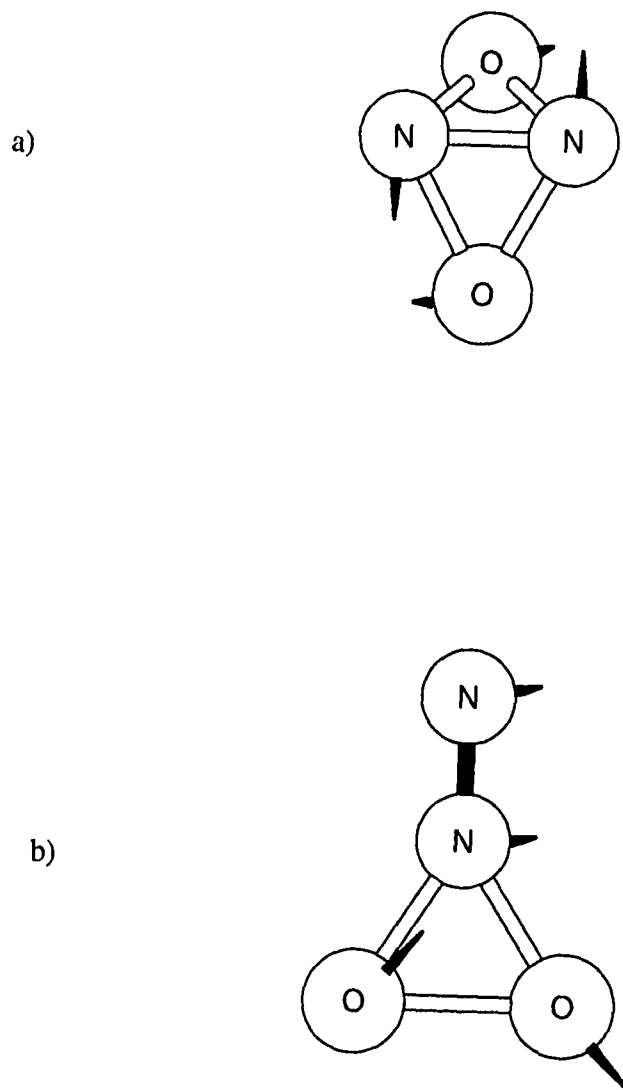
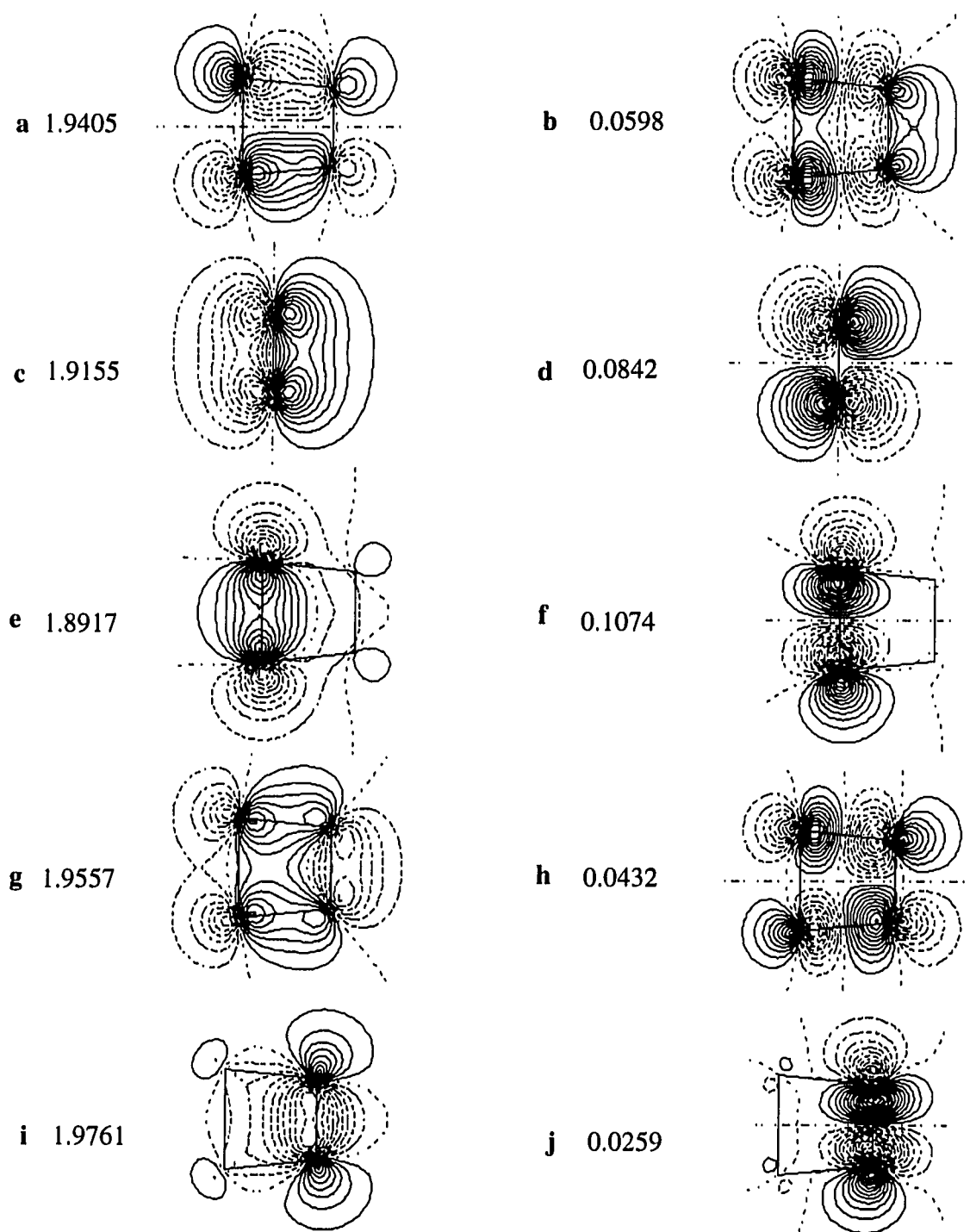
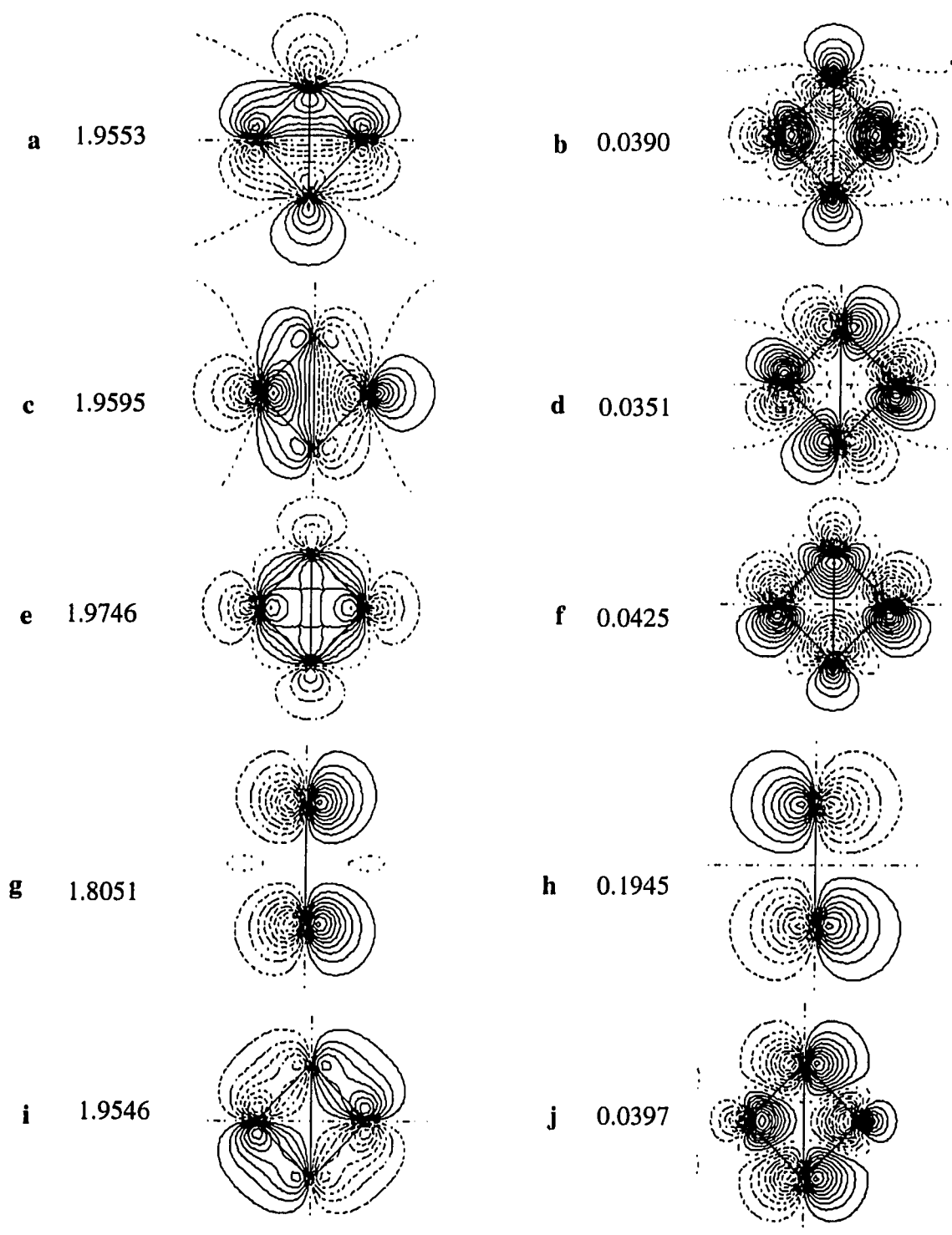


Figure 2. a) MP2/6-31G(d) Imaginary Normal Mode ($164i \text{ cm}^{-1}$) of **5**.
b) MCSCF/6-31G(d) Imaginary Normal ($187i \text{ cm}^{-1}$) Mode of **4**.



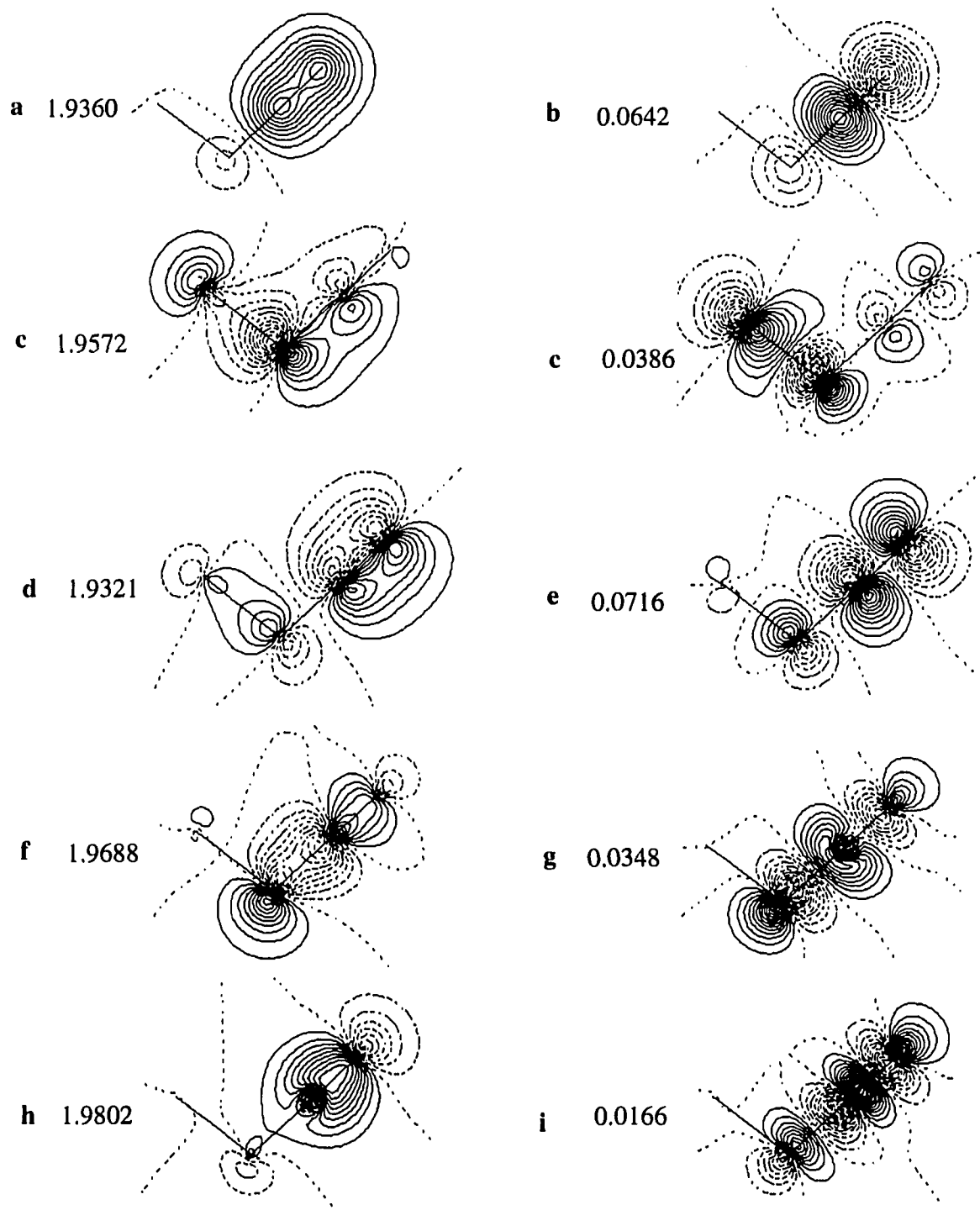
Structure 1

Figure 3a. Correlated reaction orbitals of the optimized (10,10) MCSCF/6-31G(d) wave function in the $\sigma_v(xz)$ (a, b, e, f, h, i, j) and σ_v above the xy-plane (c, d) (numerical value = occupation numbers).



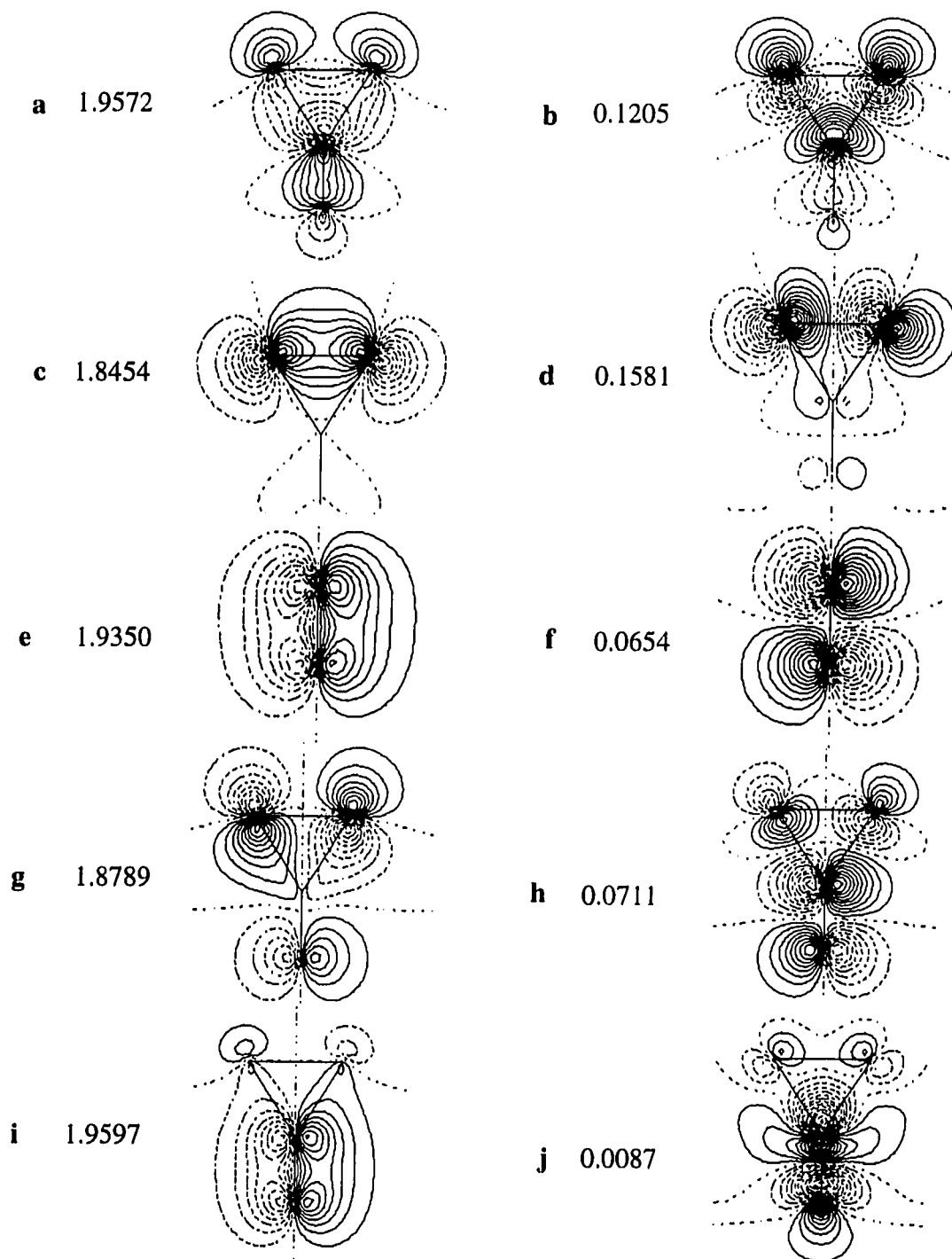
Structure 2

Figure 3b. Correlated reaction orbitals of the optimized (10,10) MCSCF/6-31G(d) wave function in the $\sigma_h(xy)$ (a, b, c, d, e, f, i, j) and $\sigma_v(xz)$ (g, h) planes (numerical value = occupation numbers).



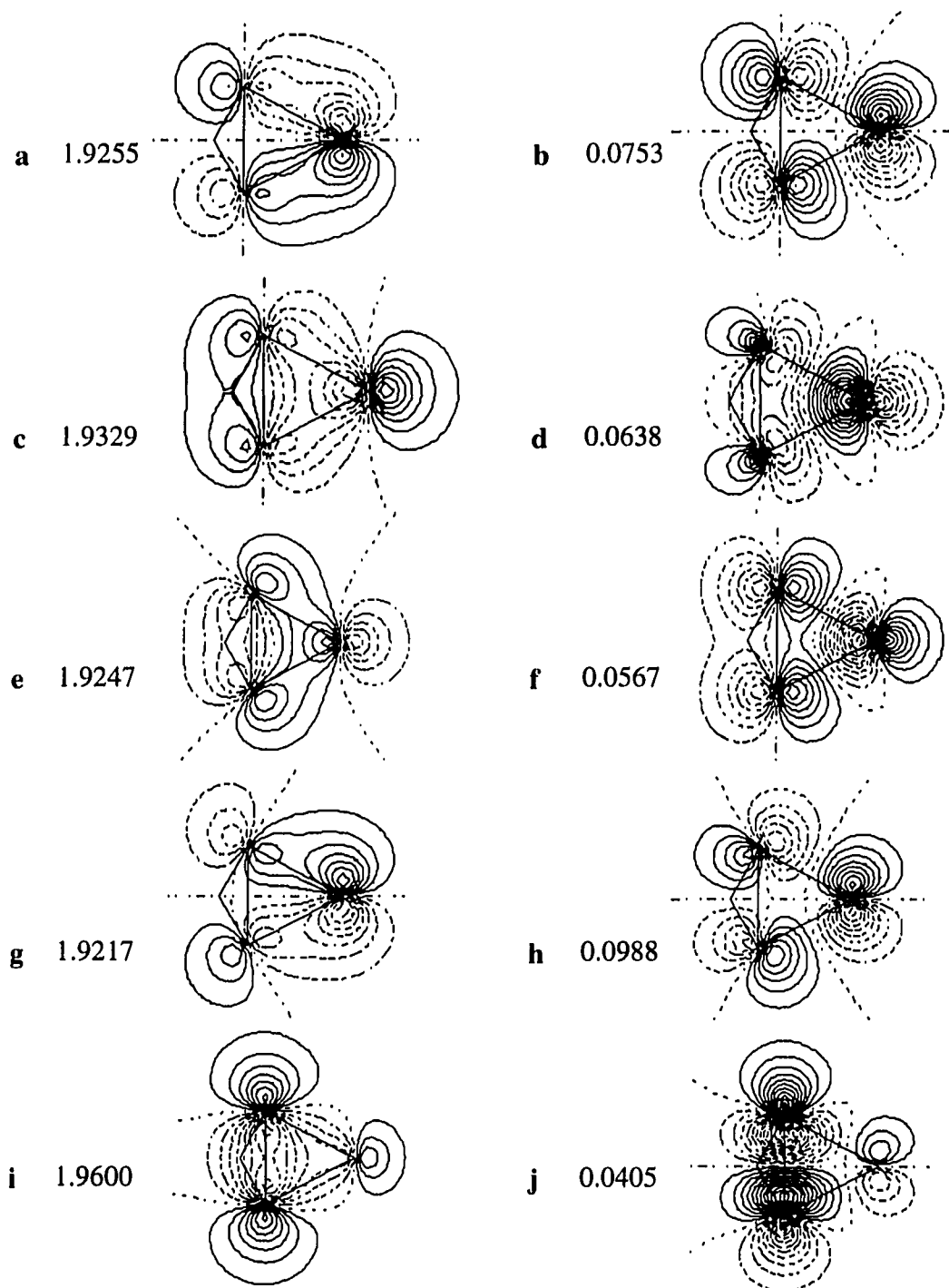
Structure 3

Figure 3c. Correlated orbitals of the optimized (10,10) MCSCF/6-31G(d) wave function in the XY-plane (a, b, c and d were plotted at 0.5au above the XY-plane). (numerical value = occupation numbers).



Structure 4

Figure 3d. Correlated reaction orbitals of the optimized (10,10) MCSCF/6-31G(d) wave function in the $\sigma_v(yz)$ (a, b, c, d, g, h, i, j) and $\sigma_v(xz)$ (e, f) plane (numerical value = occupation numbers).



Structure 5

Figure 3e. Correlated orbitals of the optimized (10,10) MCSCF/6-31G(d) wave function in the planes containing two bridgehead nitrogen atoms and one of two peripheral oxygen atoms (numerical value = occupation numbers).

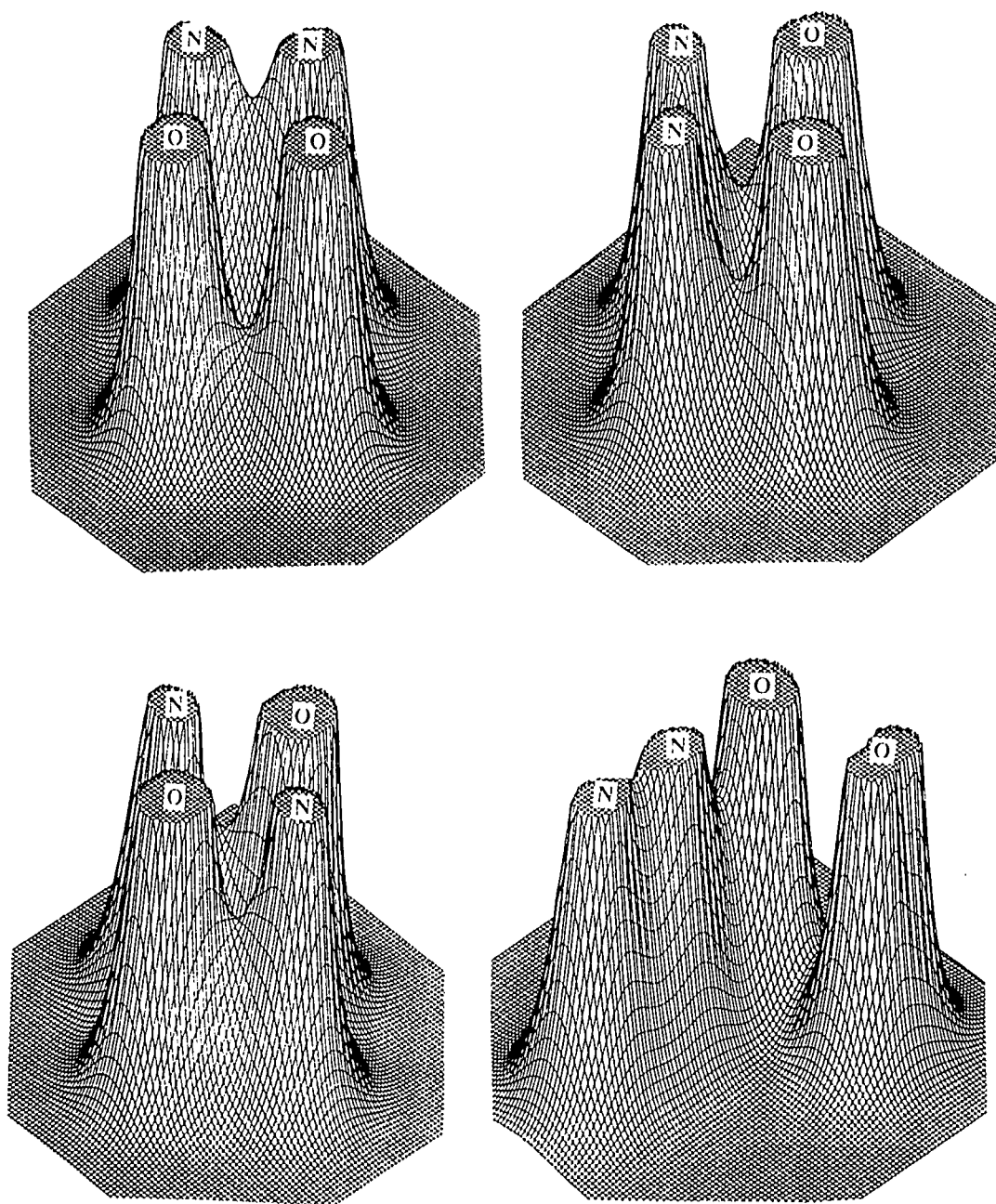


Figure 4a. Relief maps of the charge distributions of : 1-cyclodiazoxene (top right and top left) in the σ_v plane. 2-bond stretch bicyclodiazoxane (bottom left) and σ_h plane. 3-a- N_2O_2 (bottom right) in the in the σ_h plane. The charge density cutoff is 0.60 au.

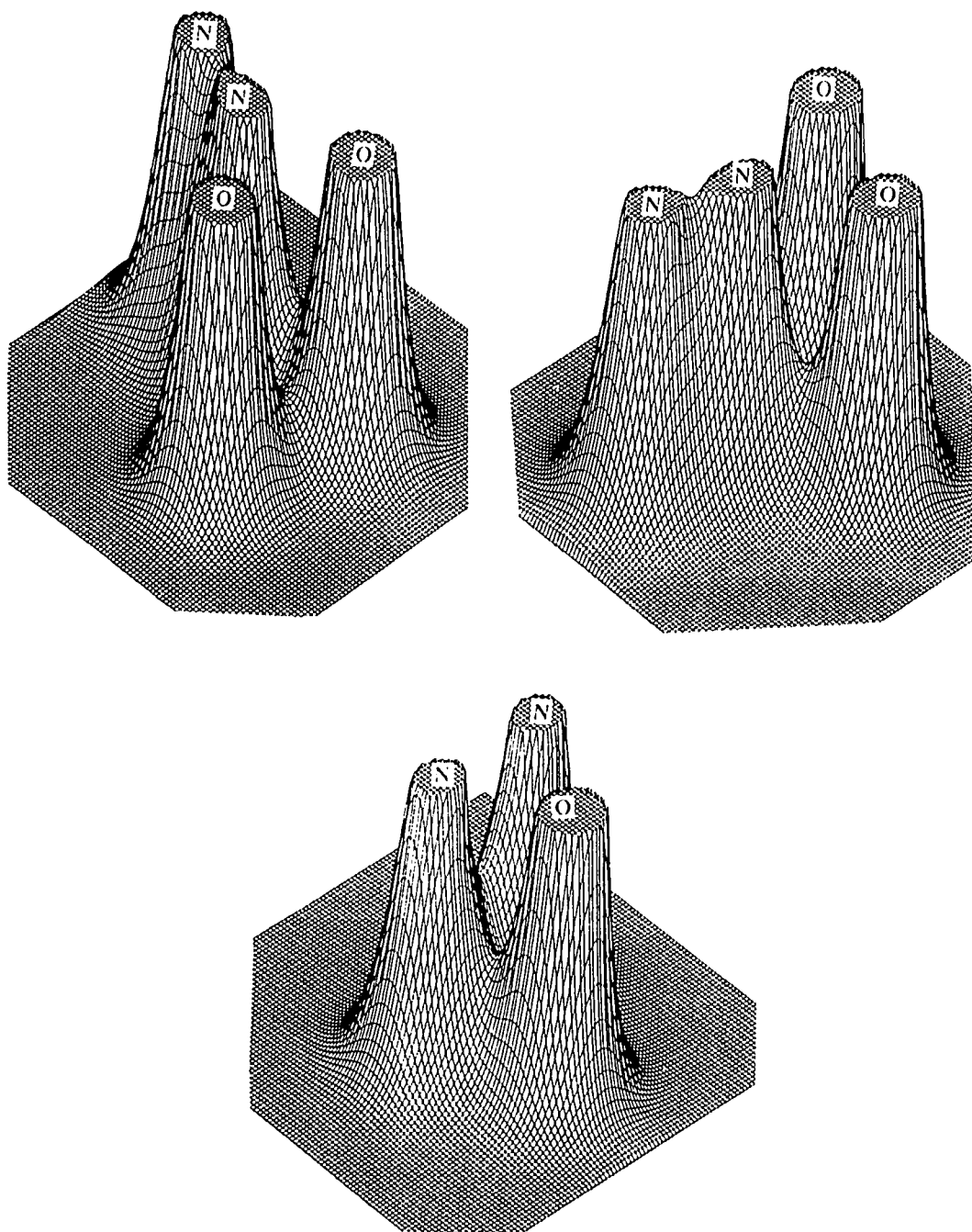


Figure 4b. Relief maps of the charge distributions of: **4** (top right and top left) in the σ_v plane. **5**-bicyclodiazoxane (bottom) in a plane containing two bridgehead nitrogen atoms and one peripheral oxygen atom. The charge density cutoff is 0.60 au.

CHAPTER 5: THE INVERSION OF BICYCLOBUTANE AND BICYCLODIAZOXANE

A paper submitted to Journal of The American Chemical Society

Kiet A. Nguyen, Mark S. Gordon, and Jerry A. Boatz

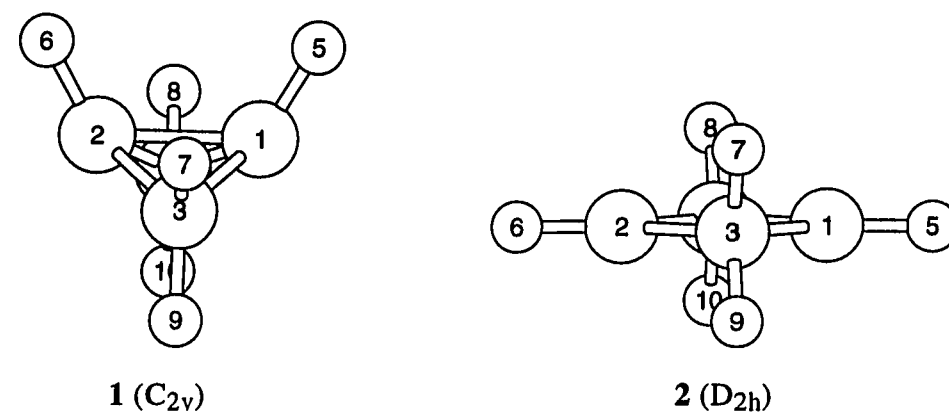
Abstract

Multi-configurational wavefunctions were used to study the inversion processes of bicyclobutane (C_4H_6) and its isoelectronic congener bicyclodiazoxane (N_2O_2). The barriers are about 50 (47) and 40 (32) kcal/mol, respectively as calculated with multi-reference CI (second order multi-reference perturbation theory). Multi-configurational descriptions of these systems with simpler GVB wavefunctions were also carried out. Good agreement between GVB and MCSCF is obtained for geometries. The GVB energetics are not reliable, but relative energies obtained at GVB geometries, using higher levels of theory, provide a reasonable representation of the potential energy surface.

I. Introduction

In the presence of a proton source, such as an alcohol, bicyclobutane (**1**) can be produced from the thermal conversion of the anion derived from cyclopropanecarboxaldehyde tosylhydrazone.^{1a} The irradiation of butadiene also produces bicyclobutane.^{1b} The molecular and electronic structure of this compound,² as well as the reactions³ it can undergo, have been the subject of both experimental and theoretical investigations. In particular, two competing processes that **1** can undergo are the inversion to an equivalent isomer and the isomerization to butadiene. This work is concerned with the former process.

An early paper related to bicyclobutane inversion was the two configurational self-consistent field (TCSCF) calculation by Feller, Davidson, and Borden^{3d} on dimethylene bicyclobutane, using the STO-3G basis set.⁴ These authors verified the planar structure of the transition state by diagonalizing the matrix of energy second derivatives (hessian) and demonstrating that this matrix has just one negative eigenvalue. They found significant mixing at the transition state between the $\dots a_1^2$ and $\dots b_1^2$ configurations, where the a_1 and b_1 orbitals are the highest occupied (HOMO) and lowest unoccupied (LUMO) in the SCF configuration.



The first calculation of the inversion of bicyclobutane was done by Gassman and co-workers^{3b} using one pair [GVB-P(1)] generalized valence bond⁵ wave functions (equivalent to the TCSCF wavefunction) within the PRDDO approximation.⁶ An analysis of the inversion potential energy surface (PES) suggested that the transition state structure has C_{2v} symmetry, such that the bridgehead hydrogens are out of the plane of the four carbons, leading to a 30 kcal/mol "barrier", in agreement with the experimental value (26 kcal/mol) for a substituted compound in which the bridgehead (H_5 and H_6) and two of four peripheral (H_9 and H_{10} , or H_7 and H_8) hydrogens are replaced with phenyl (C_5H_6)

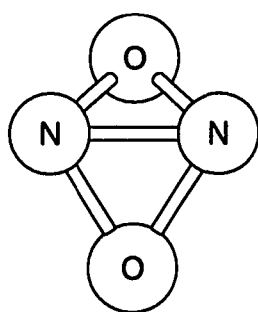
and methylcarboxylate groups, respectively.⁷ The C_{2v} structure was found to be 4 kcal/mol lower in energy than the planar D_{2h} structure (**2**); however, the hessian was not calculated to verify that the C_{2v} structure is indeed a transition state. The bridgehead C-C bond length at the C_{2v} structure was predicted to be 2.017Å, leading to significant diradical character. Even though the proposed transition structure has C_{2v} symmetry, the authors suggested that the inversion requires motion through a planar D_{2h} (**2**) structure.

Schleyer and co-workers⁸ also considered bicyclobutane with GVB-P(1) wave functions, using the 3-21G basis set;⁹ however, only the minimum and D_{2h} structures were examined. No hessian calculations were performed, since the authors asserted that the inversion motion must go through the D_{2h} structure. The latter structure is predicted to have a C-C bridgehead distance of 2.103Å and significant diradical character. The predicted SCF and GVB "barriers" are 90 and 30 kcal/mol, respectively.

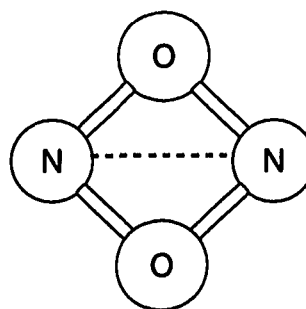
The most recent theoretical study of bicyclobutane inversion was performed by Collins, Dutter, and Rauk (CDR)^{10b} with restricted Hartree-Fock (RHF) wave functions and the 6-31G(d) basis set.¹¹ The authors verified their D_{2h} (**2**) transition state by diagonalizing the hessian. Their MP3/6-31G(d)¹² barrier at the RHF geometry is 82.4 kcal/mol (including zero point energy corrections), similar to the RHF value obtained by Schleyer and co-workers. A configuration interaction calculation including all single and double excitation (CISD) gave essentially the same result. The authors attributed the disparity between their results and those from experiment to either substituent effects or the triplet state playing a role in the inversion process.

Very recently, bicyclodiazoxane (**3**), an isoelectronic analog of bicyclobutane, has been suggested as a possible high energy density (HEDM) material,¹³ based on calculations using both SCF and GVB wave functions with the 6-31G(d) basis set. Although recent experiments by Wodtke and co-workers^{14,15} have inferred the possible

existence of (3) and its bond stretch isomer (4) as well as other N_2O_2 isomers, little is known about bicyclodiazoxane.



3 (C_{2v})



4 (D_{2h})

In the present study, the inversion process of both bicyclobutane and bicyclodiazoxane will be examined in detail at several levels of theory using multi-configurational wave functions.

II. Methods of Calculation

Several levels of multi-configurational wave function have been used in this work. The active space for the TCSCF calculations consisted of the HOMO and LUMO in the SCF configuration, corresponding to the bridgehead bonding and anti-bonding (N-N or C-C σ and σ^*) orbitals. This is the smallest reference space required to insure a proper qualitative description of species having large biradical character, as in the case of structures in the transition state region of the bicyclobutane inversion.^{3d,3b,8} To quantitatively account for the changes in the bicyclobutane and bicyclodiazoxane rings upon inversion, the reference space is expanded by combining five doubly occupied bonding MOs and their corresponding anti-bonding MOs, creating the five perfect pairs GVB [GVB-P(5)] wave function and 19404 spin adapted configuration state functions

(CFS) making up the 10 orbitals and 10 electrons MCSCF [MCSCF(10,10)] wave function. These 10 active orbitals correspond to: 1) five C-C bonding and anti-bonding MOs of bicyclobutane; 2) one N-N and four N-O bonding and anti-bonding MOs of bicyclic diazoxane. The GVB-P(5) wave function ignores interactions between correlated pairs. These interactions are included in the full MCSCF(10,10) or CASSCF(10,10) wave function.

The multi-configurational description of geometries and energetics evaluated with TCSCF, multiple pair generalized valence bond⁵ (GVB) and fully optimized reaction space (FORS) MCSCF¹⁶ wave functions were calculated using the GAMESS¹⁷ quantum chemistry program system. Structures were obtained with the use of the analytically determined gradients. Minima and transition states were verified by evaluating the appropriate matrix of energy second derivatives (hessian) from finite differences of the analytically determined gradients. TCSCF Hessians were evaluated analytically. The final energies were obtained by performing single point internally contracted multi-reference CI (MRCI)¹⁸ calculations (including all single and double excitations from active orbitals of the MCSCF(10,10) reference space), using the MCSCF(10,10) wave functions to define the reference space [MRCI(10,10)//MCSCF(10,10)]. It has been demonstrated that internally contracted MRCI calculations are in close agreement with the corresponding uncontracted or second order CI (SOC) results.¹⁸ MRCI calculations were done using the MOLPRO¹⁸ codes.

In addition, second order perturbation theory calculations with the CASSCF(10,10) wave function as the reference space (PT2) were also carried out to assess the effect of dynamic electron correlation that is not included in the MRCI(10,10). PT2¹⁹ calculations of two different type of Møller-Plesset-like partitioning were carried out using the MOLCAS-2 program.²⁰ The PT2D partitioning includes only the the

diagonal part of the one-electron operator in the zeroth-order Hamiltonian while PT2F also includes all non-diagonal elements. Only the former one is invariant to orbital transformations. PT2F has been shown to give accurate energetics for a number of systems containing first-row-atoms.²¹

In order to properly connect each transition state with its corresponding minima on the potential energy surface, minimum energy paths (MEP) were traced by following the paths of steepest descents in mass-weighted cartesian coordinates^{22,23} using the concept of intrinsic reaction coordinate^{22,24} (IRC). The reaction paths (MEPs) were generated using the second order Gonzalez-Schlegel (GS2)²⁵ method encoded in GAMESS.¹⁷ The initial step off the saddle point was taken by following the imaginary normal mode with a 0.12 amu^{1/2}bohr step. Other points on the MEP were located with a stepsize of 0.17 amu^{1/2}bohr ($\Delta s = 0.17$ amu^{1/2}bohr).

All geometry searches and IRC calculations were done with the 6-31G(d) basis set.¹¹ MRCI and CASPT2 calculations were carried out using the 6-31G(d)¹¹, 6-311G(d,p)²⁶ and 6-311+G(2d)²⁷ basis sets.

III. Results and Discussion

1. Bicyclobutane

The two central issues to be resolved are the nature of the inversion transition state(s) and the height of the inversion barrier. Consequently, initial calculations focused on structures **1** and **2**, starting with the structural and bonding issues. The C_{2v} structure **1** is verified to be a minimum on the bicyclobutane PES by its positive definite hessian at three different levels of theory, GVB-P(1), GVB-P(5) and MCSCF(10,10), using the 6-31G(d) basis set. The C-C bond distances obtained at all three levels of theory compare favorably with the experimentally determined bridgehead C₁-C₂ and peripheral C₁-C₃ bond distances of 1.497Å and 1.498Å, respectively (see Table I).²⁸ Our highest

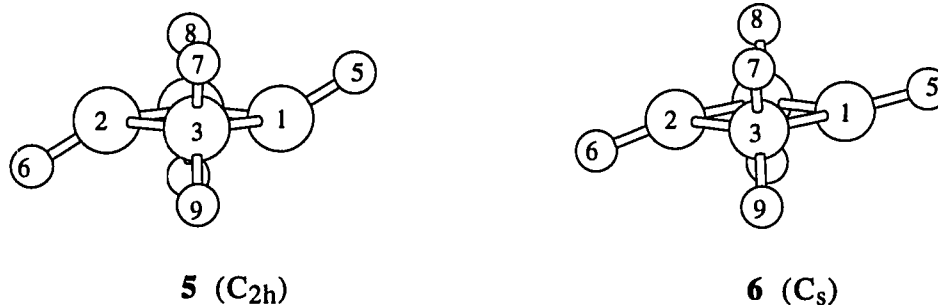
correlated level of theory [MCSCF(10,10)/6-31G(d)] overestimates the bridgehead and peripheral C₁-C₃ distances by 0.024Å and 0.021Å, respectively. Since there is little configurational mixing at this geometry, good agreement with geometries predicted by earlier RHF and MP2 calculations is also obtained.^{10c,d}

At all levels of theory the D_{2h} structure (**2**) is predicted to have a C₁-C₃ bridgehead distance greater than 2Å. Although the three levels of theory agree in their prediction of bond distances and bond angles for structure **2** to within 0.03Å and 0.5°, respectively, MCSCF(10,10) finds **2** to be a transition state with one 346i cm⁻¹ imaginary frequency, while GVB-P(1) and GVB-P(5) incorrectly predict **2** to have two imaginary frequencies. The normal mode corresponding to the imaginary frequency at the MCSCF(10,10) transition state is displayed in Figure 1a. The small MCSCF(10,10) imaginary frequency (cf. 829i cm⁻¹ obtained by RHF with the same basis set^{10c}) signifies a wide potential barrier as verified by IRC calculations (see Figure 2a).

The IRC was traced from **2** to **1**, by following the path of steepest descents starting at the transition state (**2**). These IRC calculations verify that the D_{2h} transition state (**2**), indeed, connects with the reactant (**1**). Figure 2a displays structures along the IRC to illustrate the structural rearrangement in the inversion process. Near the transition state, the IRC is quite flat (as expected from the small imaginary frequency) and involves mostly the bending of the bridgehead hydrogens. In fact, as the molecule proceeds from the transition state (**2**) through 33 steps on the IRC, with the two bridgehead hydrogens simultaneously bending to an H₅-C₁-C₂ angle of 11.2°, the energy drops only to 2.3 kcal/mol below the transition state (**2**). The remainder of the MEP involves bending of the bridgehead hydrogens as well as the peripheral carbons. Energetically, the MCSCF(10,10)/6-31G(d) inversion transition state (**2**) is 46.8 kcal/mol (with zero point corrections included) above bicyclobutane (**1**) (see Table II). A single point correction

with MRCI(10,10)/6-31G(d) and PT2F/6-31G(d) increases this barrier only slightly to 50.2 and 48.2 kcal/mol, respectively. MRCI(10,10) and PT2F calculations with the larger 6-311G(d,p) basis set reduce the barrier to 50.1 and 47.4 kcal/mol, respectively (see Table II and III). Note that the barrier of 46.1 kcal/mol obtained from an MCSCF(10,10) single point energy at the GVB-P(5) geometry (MCSCF(10,10)//GVB-P(5)) is in excellent agreement with the MCSCF(10,10)//MCSCF(10,10) barrier (see Table II).

Inversion of bicyclobutane via a bond stretched isomer (**5**) is another possible route. The primary difference between structures **2** and **5**, in addition to the longer C₁C₂ distance in **5** (Table I), is in the staggered, non-planar arrangement of the hydrogens in the minimum **5**. A transition state (**6**) with C_s symmetry is found to have a long C₁-C₂ bridgehead bond and a C₃-C₁-C₂-C₄ dihedral angle near 180°. This structure has two bridgehead hydrogen and carbon



atoms lying in the σ_h plane (contains H₆, C₂, C₁ and H₅) and an MCSCF(10,10) imaginary frequency of 280i cm⁻¹. The GVB levels of theory also predict **6** to be a transition state. The normal mode corresponding to the MCSCF(10,10) imaginary frequency is displayed in Figure 1b (the GVB normal modes are very similar). The IRC displayed in Figure 2b connects the shallow minimum **5**, via a small barrier **6**, with

bicyclobutane **1**. Initially, descending from the transition state (**6**) involves upward bending of one bridgehead hydrogen (H_6). This is followed by synchronous bending of the two bridgehead hydrogens and two peripheral carbons similar to the inversion IRC discussed above. The MCSCF(10,10)/6-31G(d) bond stretch transition state (**6**) lies 47.0 kcal/mol above bicyclobutane, only 0.2 kcal/mol higher than the inversion barrier (**2**). Since the bond stretch intermediate (**5**) is lower than **6** by less than 1 kcal/mol (0.8 and 0.2 kcal/mol with and without zero point correction, respectively), inversion of bicyclobutane via this two-step mechanism may be competitive. A single point correction with MRCI(10,10) (PT2F) increases the bond stretch barrier ($1 \leftrightarrow 6$) to 54.3 (48.5) kcal/mol, only 0.2 (0.2) kcal/mol above (below) the intermediate **5** prior to the addition of zero point corrections. With zero point corrections, the transition state **6** actually falls to 0.8 (1.3) kcal/mol *below* **5** at the MRCI (PT2F) level of theory. Changes in the MRCI and PT2F barrier **6** (and relative energies of **5**) are less than 1 kcal/mol upon going from the 6-31G(d) to 6-311G(d,p) basis set (see Tables II and III). This again illustrates the flatness of this part of the potential energy surface. The key point is that **2**, **5** and **6** have very similar energies at the MCSCF, MRCI, and PT2 levels of theory.

The bridgehead C_1-C_2 bond length at the global bicyclobutane minimum (**1**) is a "normal" 1.504Å as noted in earlier papers.^{3b,8} In contrast, the value of C_1-C_2 is greater than 2Å in structures **2**, **5** and **6**, suggesting significant configurational mixing. The amount of configurational mixing in the transition region may be assessed by examining the occupation numbers of the natural orbitals (NOONs) of the various multi-configurational wave functions. For RHF wave functions, the NOONs are 2 for occupied orbitals and 0 for virtual orbitals. The deviations from these values in multi-configurational wave functions may therefore be taken as a measure of "diradical character".

The MCSCF(10,10) natural orbitals (NO's) are displayed in Figure 3 for each of the four structures of interest. The orbitals labeled **i** and **j** correspond to the C₁-C₂ bridge bond and are the HOMO and LUMO in the RHF and GVB-P(1) wave functions. The NOON for these NO's are close to 2.0 and 0.0, respectively, in structure **1**, but become nearly 1.0 (true diradicals) in structures **2**, **5**, and **6**. This strong diradical character was noted in the earlier reports by Gassman et. al.^{3b} and by Schleyer and co-workers⁸, based on small basis set GVB calculations. It is clear from these results that single configuration-based methods can not properly account for the bicyclobutane inversion process in a qualitative manner. Attempts to correct the single configuration results with MP2 or CISD apparently provide little improvement.^{10b}

The remaining eight NO's displayed in Figure 3 correspond to the four bridgehead-peripheral (C₁-C₃, C₁-C₄, C₂-C₃, C₂-C₄) bonds in bicyclobutane. These NO's remain nearly closed shell in nature throughout the inversion process.

2. Bicyclodiazoxane

Like silabicyclobutane,²⁹ bicyclodiazoxane (**3**) has a bond stretch isomer (**4**). The geometrical parameters of bicyclodiazoxane (**3**), its long bond isomer (**4**) and the transition state (**7**) connecting them are listed in Table IV. At all three [GVB-P(1), GVB-P(5) and MCSCF(10,10)] levels of theory, both isomers are minima on the potential energy surface. The C_{2v} bicyclodiazoxane structure possesses an N-N bond [1.377 Å at MCSCF(10,10)] that is shorter than the N-N single bond in hydrazine [1.447 Å (experiment)] and somewhat longer than the N=N double bond in HN=NH (experimentally determined to be 1.252 Å).³⁰ The MCSCF(10,10)/6-31G(d) N-O distance of 1.484 Å in **3** is similar to the experimentally determined N-O distance of 1.453 Å³⁰ in H₂N-OH.

At the MCSCF(10,10)/6-31G(d) level of theory, the planar structure (**4**) with D_{2h} symmetry possesses a much longer N-N distance of 1.970Å; this is accompanied by a shorter N-O distance (1.365Å). Similar to bicyclobutane, the large N-N bridgehead distance in **4** suggests significant configurational mixing (Figure 4b). The bonding and anti-bonding NN orbitals (**g** and **h** in Figure 4b) have NOON values of 1.8051 and 0.1945, respectively, for this isomer. In contrast, the values in **3** are 1.9600 and 0.0405, respectively (**i** and **j** in Figure 4a). Note also the qualitative difference in these two orbitals upon stretching the NN bond from **3** to **4**.

The bond stretch transition state (**7**) connecting **3** and **4** has a long N-N bond distance. At the MCSCF(10,10) level of theory, the N-N distance in this transition state structure lengthens to 1.893Å, 0.498Å longer than the N-N distance in bicyclodiazoxane (**3**) and only 0.077Å shorter than the N-N bond in the long bond (**4**) bicyclodiazoxane; however, the 132.2° O-N-N-O dihedral angle of the transition state remains closer to that of bicyclodiazoxane (107.0°) (**3**). As expected, the long N-N distance in the transition state signifies large configurational mixing as shown by the MCSCF NOON's listed in Figure 4c. The N-N bonding (**i**) and antibonding (**j**) orbitals of the MCSCF(10,10)/6-31G(d) wave function have NOON's of 1.2671 and 0.7340, respectively (see Figure 4c).

Inspecting the natural orbitals (in Figure 4 a, b and c) reveals interesting features of the bonding in reactant, transition state and product. Note that the N-N bonding and anti-bonding orbitals of **3** (**i** and **j**) are sigma-like, confirming the normal single N-N bond. Since the O-N-N-O dihedral angle of bicyclodiazoxane (**3**) is flattened from 107.0° to 180° to form the long bond isomer (**4**) with a much longer N-N bond, the bonding and anti-bonding orbitals corresponding to the stretched N-N bond become π -like as shown in Figure 4b [**4(g,h)**]. In the planar arrangement of **4**, a π -lone pair on each oxygen can participate in the bonding to provide extra stability for this 6 π -electrons system.³¹ The

differences in bonding between bicyclodiazoxane and the inversion transition state (**4**) are more subtle. While the N-N bonding and anti-bonding MOs are in transition from σ to π type, the N-O bonding MO's in the transition state (**7**) structure resemble those of bicyclodiazoxane. Although the N_2O_2 natural orbitals are qualitatively similar to those in bicyclobutane, there are significant differences. Whereas bicyclobutane is essentially a pure diradical in its transition state region, the diradical character is much smaller in (**7**), though still significant.

It is clear from the MCSCF(10,10) imaginary normal mode ($1150i\text{ cm}^{-1}$) of the bond stretch transition state (**7**) displayed in Figure 5 that **7** connects isomers **3** and **4**. An intrinsic reaction coordinate (IRC) traced from **7** to both **3** and **4**—by following the the path of steepest descents starting at the transition state (**7**)—verify that **3** connects **4** via **7**. The MCSCF(10,10)/6-31G(d) energy at each point on the IRC is displayed in Figure 6.

The total and relative energies for the N_2O_2 structures are listed in Tables V and VI, using the 6-31G(d) and 6-31+G(2d) basis sets, respectively. It is interesting that all levels of theory predict that the stability of isomer **4** is competitive with that of isomer **3**, even though the long N-N distance and the diradical character discussed above suggest the N-N bond is at least partially broken. The MCSCF(10,10) level of theory predicts the two isomers to be similar in energy, and the MRCI(10,10) energies based on this MCSCF(10,10) wave function have little effect on this result.

The most striking result in Tables V and VI is that the PT2F calculations predict a much greater stability for **4** than do the MCSCF(10,10) or the corresponding MRCI results: For the same basis set and size of the active space, PT2F predicts **4** to be nearly 30 kcal/mol more stable than **3**. The primary difference between the internally contracted MRCI(10,10) and PT2F for a given basis set is that whereas the MRCI(10,10) wave function simply includes contractions of single and double excitations of all active orbitals

from the configurations generated by the (10,10) active space, PT2F correlates *all* valence orbitals. In effect, PT2F includes all valence orbitals in the dynamic correlation. The fact that this makes a very large difference for N₂O₂ and virtually no difference for bicyclobutane suggests that the oxygen π lone pairs mentioned earlier play an important role in stabilizing **4**. To explore this possibility, the MCSCF(10,10) active space was expanded to: 1) MCSCF(18,14) by adding all the lone pairs except for the π lone pairs on the oxygens; 2) MCSCF(14,12) by adding the π lone pairs on each O, since these are most likely to interact with the π system in **4**. As seen in Table V, this expanded active space brings the MCSCF relative energies in close agreement with the PT2F results while the MCSCF(18,14) is in closer agreement with MCSCF(10,10). Unfortunately, we are unable to perform the full valence MCSCF and MRCI calculation from the MCSCF(14,12) and MCSCF(18,14) reference functions. However, based on the results from the smaller active space, the MRCI is unlikely to modify the MCSCF prediction significantly.

With regard to the barrier height (**3** \rightarrow **4**), the MRCI and MCSCF(10,10) calculations again predict essentially the same barrier of ca. 41 kcal/mol. Both the PT2F and MCSCF(14,12) calculations reduce the barrier to ca. 34 kcal/mol, so the effect of the O π lone pairs is much smaller here (ca. 7 kcal/mol) than for the isomerization energy (ca. 30 kcal/mol).

Table VI lists the MCSCF(10,10), MRCI(10,10) and PT2F total and relative energies for the N₂O₂ structures calculated with the larger 6-311+G(2d) basis set. The effect on relative energies upon going from 6-31G(d) to 6-311+G(2d) is small; the largest deviation is 3 kcal/mol obtained from MRCI(10,10). The PT2F calculations find a 31.8 kcal/mol inversion barrier, with zero point corrections included.

IV. Summary and Conclusion

The inversion process of bicyclobutane and its isoelectronic analog bicyclodiazoxane have been examined at several levels of theory. At the highest level of theory (PT2F/6-311G(d,p)//MCSCF(10,10)/6-31G(d) and PT2F/6-311+G(2d)//MCSCF(10,10)/6-31G(d) for bicyclobutane and bicyclodiazoxane, respectively), barriers of 47.4 and 31.8 kcal/mol are obtained for the inversion of bicyclobutane and bicyclodiazoxane, respectively. Inversion of the latter system follows a two-step process via a D_{2h} bond stretch isomer. The bicyclobutane inversion process involves a transition region which contains three nearly isoenergetic stationary points at about 47 kcal/mol above the minimum. The calculated (PT2F) inversion barrier for bicyclobutane is much higher than that observed experimentally for a highly substituted analog. The origin of this difference must be some combination of the difference in substituents and a less than complete atomic basis set.

Relative energies predicted at the GVB levels of theory are unreliable, although the energetics with MCSCF or MRCI wave function at the GVB geometries deviates only slightly from the predicted energetics at MCSCF geometries.

Acknowledgment

This research was supported in part by a grant (90-0052) from the Air Force Office of Scientific Research, under the High Energy Density Materials Initiative, and in part by a grant from the National Science Foundation (CHE-8911911). Calculations described in this work were performed on an IBM RS6000/530 (obtained through an AFOSR grant to MSG) at North Dakota State University, on an IBM RS6000/350 generously provided Iowa State University, and on the Cray-2 at the National Center for Supercomputing Applications, Champaign, Illinois.

References

- (1) (a) Wiberg, K. B.; Lavanish, J. M. *J. Am. Chem. Soc.* **1966**, 88, 365. (b) Srinivasan, R.; Levi, A. A.; Haller, I. J. *Phys. Chem.* **1969**, 69, 1775.
- (2) Pomerantz, M.; Abrahamson, E. W. *J. Am. Chem. Soc.* **1966**, 88, 3970.
- (3) (a) Wiberg, K. B. *J. Am. Chem. Soc.* **1983**, 105, 1227. (b) Gassman, P. G.; Greenlee, M. L.; Dixon, D. A.; Richtsmeier, S.; Gougoutas, J. Z. *J. Am. Chem. Soc.* **1983**, 105, 5865. (c) Wiberg, K. B.; Bonneville, G.; Dempsey, R. *Isr. J. Chem.* **1983**, 23, 85. (d) Golberg, A. H.; Doherty, D. H. *J. Am. Chem. Soc.* **1983**, 105, 284. (e) Feller, D.; Davidson, E. R.; Borden, W. T. *J. Am. Chem. Soc.* **1982**, 104, 1216.
- (4) Hehre, W. J.; Stewart, R. F.; Pople, J. A. *J. Chem. Phys.* **1969**, 51, 2657.
- (5) Goddard, W. A. III; Dunning, T. H.; Hunt, W. J.; Hay, P. J. *Acc. Chem. Res.* **1973**, 6, 368.
- (6) Halgren, T. A.; Lipscomb, W. N. *J. Chem. Phys.* **1973**, 58, 1569.
- (7) (a) D'Yakanov, I. A.; Razen, V. V.; Komendantov, M. I. *Tetrahedron Lett.* **1966**, 1127, 1135. (b) Woodward, R. B.; Dalrymple, D. L. *J. Am. Chem. Soc.* **1969**, 91, 4612.
- (8) Budzelaar, P. H. M.; Kraka, E.; Cremer, D.; Schleyer, P. v. R. *J. Am. Chem. Soc.* **1986**, 108, 561.
- (9) (a) Binkley, J. S.; Pople, J. A.; Hehre, W. J. *J. Am. Chem. Soc.* **1980**, 102, 1980. (b) Gordon, M. S.; Binkley, J. S.; Pople, J. A.; Pietro, W. J.; Hehre, W. J. *J. Chem. Phys.* **1982**, 104, 2997.
- (10) (a) Wiberg, K. B.; Bader, R. F. W.; Lau, C. D. H. *J. Am. Chem. Soc.* **1987**, 109, 985, 1001. (b) Politzer, P.; Kirschenheuter, G. P.; Alster, J. *J. Am. Chem. Soc.* **1987**, 106, 4211. (c) Collins, S.; Dutler, R.; Rauk, A. *J. Am. Chem. Soc.* **1987**,

- 109, 2564. (d) Walters, V. A.; Hadad, C. M.; Thiel, Y. Colson, S. D.; Wiberg, K. B.; Johnson, P. M.; Foresman, J. B., *J. Am. Chem. Soc.* **1991**, 113, 4782.
- (11) (a) Hariharan, P. C.; Pople, J. A., *Theoret. Chim. Acta.* **1973**, 28, 213. (b) Gordon, M. S. *Phys. Lett.* **1980**, 76, 2997.
- (12) Krishnan, R.; Frisch, M. J.; Pople, J. A. *J. Chem. Phys.* **1980**, 72, 4244.
- (13) Gordon, M. S.; Windus, T. L.; Nguyen, K. A.; Matsunaga, N. Potential Energy Surfaces and Dynamics of Potential HEDM Molecules, in Proceedings of The High Energy Density Materials Contractors Conference.; AFOSR, Washington, DC, 1991.
- (14) Yang, X.; Kim, E. H.; Wodtke, A. M. *J. Chem. Phys.* **1992**, 96, 5111.
- (15) Yang, Price, J. M.; Mack, J. A.; Morgan, C. G.; Rogaski, C. A.; McGuire, D.; X.; Kim, E. H.; Wodtke, A. M. *J. Phys. Chem.* **1993**, 97, 3944.
- (16) (a) Lengsfeld, B. H. III; *J. Chem. Phys.* **1980**, 73, 382. (b) Jarkony, D. R. *Chem. Phys. Lett.* **1981**, 77, 634. (c) Ruedenberg, K.; Schmidt, M. W.; Dombek, M. M.; Elbert, S. T. *Chem. Phys.* **1982**, 71, 41,51 65. (d) Lam, B.; Schmidt, M. W.; Ruedenberg, K. *J. Phys. Chem.* **1985**, 89, 2221. (e) Werner, H.-J.; Knowles, P. *J. J. Chem. Phys.* **1985**, 82, 5053. (f) Werner, H.-J.; Knowles, P. *J. Chem. Phys. Lett.* **1985**, 115, 259.
- (17) GAMESS (General Atomic and Molecular Electronic Structure System): (a) Schmidt, M, W.; Baldrige, K. K.; Boatz, J. A.; Jensen, J. H.; Koseki, S.; Gordon, M. S.; Nguyen, K. A.; Windus, T. L.; Elbert, S. T. *QCPE Bulletin*, **1990**, 10, 52. (b) Schmidt, M, W.; Baldrige, K. K.; Boatz, J. A.; Elbert, S. T.; Gordon, M. S.; Jensen, J. H.; Koseki, S.; Matsunaga, N.; Nguyen, K. A.; Su, S. Windus, T. L.; *J. Comp. Chem.* **1993**, 14, 1347.

- (18) (a) Werner, H.-J.; Knowles, P. J. *J. Chem. Phys.* **1988**, 89, 5803. (b) Werner, H.-J.; Knowles, P. J. *Chem. Phys. Lett.* **1988**, 145, 514. MOLPRO is written by Werner, H.-J.; Knowles, P. J. with contributions by Almlöf, J.; Amos, R. D.; Elbert, S. T.; Taylor, P. R.
- (19) (a) Anderson, K. Malmqvist, P.-Å., Roos, B. O. *J. Chem. Phys.* **1992**, 96, 1218. (b) Anderson, K. Malmqvist, P.-Å., Roos, B. O. *J. Phys. Chem.* **1990**, 94, 5483.
- (20) Anderson, K.; Fülcher, M. P.; Lindh, R.; Malmqvist, P.-Å.; Olsen, J.; Roos, B. O.; Sadlej, A. J.; Wilmark, P.-O. MOLCAS version 2, User's Guide; University of Lund, Sweden, 1991.
- (21) (a) Anderson, K. Roos, B. O. *Int. J. Quantum Chem.* **1993**, 45, 591. (b) Serrano-Andres, L.; Merchan, M.; Nebot-Gil, I.; Roos, B. O.; Fülcher, M. *J. Am. Chem. Soc.* **1993**, 115, 6184. (c) Borowski, B.; Anderson, K. Malmqvist, P.-Å., Roos, B. O. *J. Chem. Phys.* **1992**, 97, 5569. (d) Anderson, K.; Roos, B. O. *Chem. Phys. Lett.* **1992**, 191, 507. (e) errano-Andres, L.; Merchan, M.; Fülcher, M.; Roos, B. O. *Chem. Phys. Lett.* **1993**, 211, 125.
- (22) (a) Fukui, K. *Acc. Chem. Res.* **1981**, 14, 363. (b) Fukui, K. *Pure Appl. Chem.* **1982**, 54, 1825. (c) Fukui, K. *Int. J. Quantum Chem. Sym.* **1981**, 15, 633.
- (23) (a) Marcus, R. A.; *J. Chem. Phys.*, **1966**, 45, 4493. (b) Marcus, R. A. *J. Chem. Phys.* **1968**, 49, 2610. (c) Truhlar, D. G.; Kuperman, A. *J. Am. Chem. Soc.* **1971**, 93 1840. (d) Schaefer, H. F. III. *Chem. Britain.* **1975**, 11, 227.
- (24) (a) Ishida, K.; Morokuma, K.; Komornicki, A. *J. Chem. Phys.* **1977**, 66, 2153. (b) Muller, K. *Engew. Chem., Int. Ed. Engl.* **1980**, 19, 1. (c) Schmidt, M. W.; Gordon, M. S.; Dupuis, M. *J. Am. Chem. Soc.* **1985**, 107 2585. (d) Garrett, B. C.; Redmon, M. J.; Steckler, R.; Truhlar, D. G.; Baldrige, K. K.; Bartol, D.; Schmidt, M. W.; Gordon, M. S. *J. Phys. Chem.* **1988**, 92, 1476.

- (25) Gonzalez, C.; Schlegel, H. B. *J. Chem. Phys.* **1989**, *90*, 2154; *J. Phys. Chem.* **1990**, *94*, 2154; *J. Chem. Phys.* **1991**, *90*, 5853.
- (26) (a) Krishnan, R.; Binkley, J. S.; Seeger, R.; Pople, J. A. *J. Chem. Phys.* **1980**, *72*, 650. (b) Clark, T.; Chandrasekhar, J.; Spitznagel, G. W.; Schleyer, P. von R. *J. Comput. Chem.* **1983**, *4*, 294.
- (27) Frish, M. J.; Pople, J. A.; Binkley, J. S. *J. Chem. Phys.* **1984**, *80*, 3265.
- (28) Cox, K. W.; Harmony, M. D.; Nelson, G.; Wiberg, K. G. *J. Phys. Chem.* **1969**, *50*, 5107. (b) Cox, K. W.; Harmony, M. D.; Nelson, G.; Wiberg, K. G. *J. Phys. Chem.* **1970**, *53*, 858.
- (29) (a) Boatz, J. A.; Gordon, M. S. *J. Phys. Chem.* **1988**, *92*, 3037.
30. (b) Harmony, M. D.; Laurie, V. W.; Kuczkowski, R. L.; Schwendeman, R. H.; Ramsay, D. A.; Lovas, F. J.; Lafferty, W. J.; Maki, A. G.; *J. Phys. Chem. Ref. Data* **1979**, *8*, 619.
- (31) Zandwijk, v. G.; Janssen, R. A. J.; Buck, H. M., A. *J. Am. Chem. Soc.* **1990**, *112*, 4155.

Table I. MCSCF(10,10), GVB-P(5) (in parentheses) and GVP-P(1) (in brackets) geometrical parameters of C_4H_6 systems, calculated with the 6-31G(d) basis set.

Systems	1 ^a	2 ^b	5 ^a	6 ^c
symmetry	C_{2v}	D_{2h}	C_{2h}	C_s
	Bond distances (Å)			
C_1C_2	1.521 (1.485) [1.504]	2.088 (2.092) [2.059]	2.168 (2.147) [2.121]	2.113 (2.110) [2.079]
C_1C_3	1.519 (1.516) [1.485]	1.555 (1.542) [1.519]	1.555 (1.546) [1.524]	1.553 (1.548) [1.525]
H_5C_1	1.069 (1.071) [1.070]	1.073 (1.072) [1.072]	1.078 (1.076) [1.078]	1.074 (1.074) [1.075]
H_7C_3	1.078 (1.079) [1.079]	1.087 (1.088) [1.089]	1.085 (1.086) [1.087]	1.087 (1.089) [1.089]
H_9C_3	1.080 (1.082) [1.082]	1.087 (1.088) [1.089]	1.085 (1.086) [1.087]	1.087 (1.087) [1.088]
	Bond Angles (deg)			
$H_5C_1C_3$	129.7 (131.0) [130.0]	132.3 (132.7) [132.7]	122.7 (126.2) [124.3]	130.0 (128.7) [128.2]
$H_7C_3C_1$	116.6 (116.6) [117.0]	115.6 (115.5) [115.7]	113.5 (114.8) [114.3]	115.6 (115.4) [115.5]
$H_9C_3C_1$	119.2 (120.1) [119.3]	115.6 (115.5) [115.7]	113.5 (114.8) [115.5]	114.8 (114.9) [115.1]
	Dihedral Angles (deg)			
$C_4C_1C_2C_3$	122.1 (119.4) [122.4]	180.0 (180.0) [180.0]	180.0 (180.0) [180.0]	179.8 (178.4) [178.6]

^aa minimum at all levels of theory. ^bMCSCF(10,10): a transition state, GVB-P(1) and GVB-P(5): two imaginary frequencies. ^ca transition state at all levels of theory. distances: $C_2C_3=1.550$ (1.540) [1.516], $H_6C_2=1.073$ (1.072) [1.072]; angles: $H_6C_2C_1=131.6$ (132.7) [132.8], $H_7C_3C_2=114.8$ (114.9) [115.2], $H_7C_3C_2=114.9$ (116.0) [116.1].

Table II. 6-31G(d) Total (au) and Relative Energies (kcal/mol⁻¹) of C₄H₆ Structures.^a

Systems	wavefunction	Total Energies	Relative Energies	
			ΔE	ΔH_0^b
1	GVB-P(1)//GVB-P(1) ^c	-154.88832 (57.6)	0.0	0.0
	GVB-P(5)//GVB-P(5) ^c	-154.94873 (57.2)	0.0	0.0
	MCSCF(10,10)//GVB-P(5)	-154.98823	0.0	0.0
	MCSCF(10,10)//MCSCF(10,10) ^c	-154.98904 (57.0)	0.0	0.0
	MRCI(10,10)//MCSCF(10,10)	-155.11561	0.0	0.0
	PT2F//MCSCF(10,10)	-155.41188	0.0	0.0
2	GVB-P(1)//GVB-P(1) ^d	-154.82383 (54.0)	40.5	36.9
	GVB-P(5)//GVB-P(5) ^d	-154.88526 (53.3)	39.8	35.9
	MCSCF(10,10)//GVB-P(5)	-154.90852	50.0	46.1
	MCSCF(10,10)//MCSCF(10,10) ^e	-154.90874 (53.4)	50.4	46.8
	MRCI(10,10)//MCSCF(10,10)	-155.02990	53.8	50.2
	PT2F//MCSCF(10,10)	-155.32929	51.8	48.2
5	GVB-P(1)//GVB-P(1) ^c	-154.82613 (55.6)	39.0	37.0
	GVB-P(5)//GVB-P(5) ^c	-154.88676 (54.7)	38.9	36.4
	MCSCF(10,10)//GVB-P(5)	-154.90928	49.5	47.0
	MCSCF(10,10)//MCSCF(10,10) ^c	-154.90976 (54.6)	49.7	47.3
	MRCI(10,10)//MCSCF(10,10)	-155.02934	54.1	51.7
	PT2F//MCSCF(10,10)	-155.32864	52.2	49.8
6	GVB-P(1)//GVB-P(1) ^e	-154.82452 (54.7)	40.0	37.1
	GVB-P(5)//GVB-P(5) ^e	-154.88580 (54.0)	39.5	36.3
	MCSCF(10,10)//GVB-P(5)	-154.49452	51.3	47.8
	MCSCF(10,10)//MCSCF(10,10) ^e	-154.908858 (53.5)	50.5	47.0
	MRCI(10,10)//MCSCF(10,10)	-155.02914	54.3	50.8
	PT2F//MCSCF(10,10)	-155.32897	52.2	48.5

^aZero point energies in parentheses. ^bIncluding zero point vibrational energies. ^cMinimum. ^dTwo imaginary frequencies. ^eTransition state.

Table III. 6-311G(d,p) Total (au) and Relative Energies (kcal/mol⁻¹) of the MCSCF(10,10)/6-31G(d) C₄H₆ Structures

Systems	wavefunction	Total Energies	Relative Energies	
			ΔE	ΔH_0^a
1	MCSCF(10,10)	-155.02648	0.0	0.0
	MRCI(10,10)	-155.16516	0.0	0.0
	PT2F(10,10)	-155.57630	0.0	0.0
2	MCSCF(10,10)	-154.94551	50.8	47.2
	MRCI(10,10)	-155.07963	53.7	50.1
	PT2F	-155.49495	51.0	47.4
5	MCSCF(10,10)	-154.94681	50.0	47.6
	MRCI(10,10)	-155.07910	54.0	51.6
	PT2F	-155.49423	51.5	49.1
6	MCSCF(10,10)	-154.94544	50.8	47.3
	MRCI(10,10)	-155.07884	54.2	50.7
	PT2F	-155.49452	51.3	47.8

^aIncluding zero point vibrational energies.

Table IV. MCSCF(10,10), GVB-P(5) (in parentheses) and GVB-P(1) (in brackets) geometrical parameters of Bicyclodiazoxane short (**3**), long (**4**) and the isomerization transition state (**7**), calculated with the 6-31G(d) basis set.

System	Symetry	Bond length		Angle		Dihedral O-N-N-O
		N-N	N-O	N-O-N	O-N-O	
3	C_{2v}	1.395	1.484	56.1	90.4	107.0
		(1.367)	(1.484)	(54.9)	(90.4)	(106.2)
		[1.377]	[1.399]	[59.0]	[90.6]	[109.5]
4	D_{2h}	1.970	1.365	92.4	87.6	0.0
		(1.963)	(1.362)	(92.2)	(87.8)	(0.0)
		[1.908]	[1.324]	[92.3]	[87.7]	[0.0]
7	C_{2v}	1.893	1.469	80.2	88.7	132.2
		(1.849)	(1.465)	(78.3)	(88.0)	(127.2)
		[1.757]	[1.397]	[77.9]	[88.7]	[128.1]

Table V. 6-31G(d) Total (au) and Relative Energies (kcal/mol⁻¹) of N₂O₂ systems.^a

Systems	wavefunction	Total Energies	Relative Energies	
			ΔE	ΔH_o^b
3	GVB-P(1)//GVB-P(1)	-258.31983 (8.6)	0.0	0.0
	MRCI//GVB-P(1)	-259.07037	0.0	0.0
	GVB-P(5)//GVB-P(5)	-258.45966 (6.3)	0.0	0.0
	MCSCF(10,10)//GVB-P(5)	-258.53367	0.0	0.0
	MCSCF(10,10)//MCSCF(10,10)	-258.53418 (7.1)	0.0	0.0
	MCSCF(14,12)//MCSCF(10,10)	-258.54973	0.0	0.0
	MCSCF(18,14)//MCSCF(10,10)	-258.56589	0.0	0.0
	MRCI(10,10)//MCSCF(10,10)	-258.64461	0.0	0.0
	PT2F//MCSCF(10,10)	-259.01246	0.0	0.0
4	GVB-P(1)//GVB-P(1)	-158.37943 (10.3)	-37.4	-35.7
	MRCI//GVB-P(1)	-259.11996	-31.1	-29.4
	GVB-P(5)//GVB-P(5)	-258.48113 (8.8)	-13.5	-13.3
	MCSCF(10,10)//GVB-P(5)	-258.53680	-2.0	0.5
	MCSCF(10,10)//MCSCF(10,10)	-258.53684 (8.6)	-1.7	-0.2
	MCSCF(14,12)//MCSCF(10,10)	-258.59527	-28.6	-27.1
	MCSCF(18,14)//MCSCF(10,10)	-258.55721	5.4	6.9
	MRCI(10,10)//MCSCF(10,10)	-258.64373	0.5	2.0
	PT2F//MCSCF(10,10)	-259.06004	-29.9	-28.4
7	GVB-P(1)//GVB-P(1)	-258.28464 (7.4)	22.1	20.9
	MRCI//GVB-P(1)	-259.02201	30.3	29.1
	GVB-P(5)//GVB-P(5)	-258.41031 (5.7)	31.0	30.4
	MCSCF(10,10)//GVB-P(5)	-258.46857	40.9	40.3
	MCSCF(10,10)//MCSCF(10,10)	-258.46538 (5.7)	43.2	41.8
	MCSCF(14,12)//MCSCF(10,10)	-258.49494	34.4	33.0
	MCSCF(18,14)//MCSCF(10,10)	-258.51016	35.0	33.6
	MRCI(10,10)//MCSCF(10,10)	-258.57620	42.9	41.5
	PT2F//MCSCF(10,10)	-258.95739	34.6	33.2

^aZero point energies in parentheses. ^bIncluding zero point vibrational energies.

Table VI. 6-311+G(2d)//MCSCF(10,10)/6-31G(d) Total (au) and Relative Energies (kcal/mol⁻¹) of N₂O₂ systems.

Systems	wavefunction	Total Energies	Relative Energies	
			ΔE	ΔH_0^a
3	MCSCF(10,10)	-258.61422	0.0	0.0
	MRCI(10,10)	-258.74345	0.0	0.0
	PT2F	-259.27059	0.0	0.0
4	MCSCF(10,10)	-258.61949	-3.3	-1.8
	MRCI(10,10)	-258.74744	-2.5	-1.0
	PT2F	-259.31999	-31.0	-29.5
7	MCSCF(10,10)	-258.54707	42.1	40.7
	MRCI(10,10)	-258.67712	41.6	40.2
	PT2F	-258.95739	33.2	31.8

^aIncluding zero point vibrational energies.

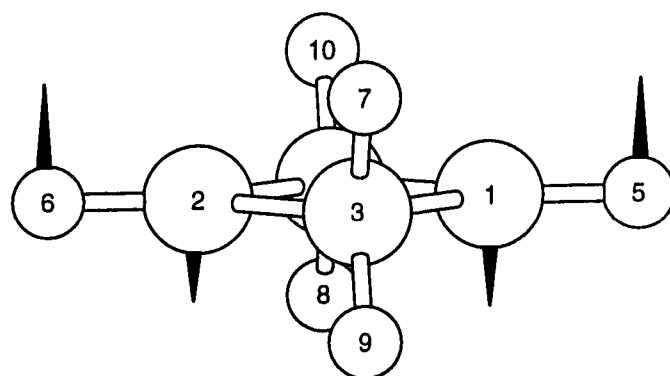
**2**

Figure 1a. MCSCF(10,10)/6-31G(d) Imaginary Normal Mode ($346i \text{ cm}^{-1}$) for **2**.

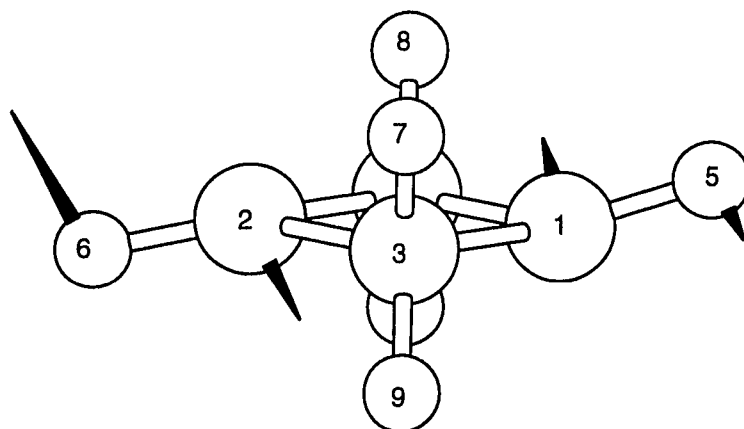
**6**

Figure 1b. MCSCF(10,10)/6-31G(d) Imaginary Normal Mode ($280i \text{ cm}^{-1}$) for **6**.

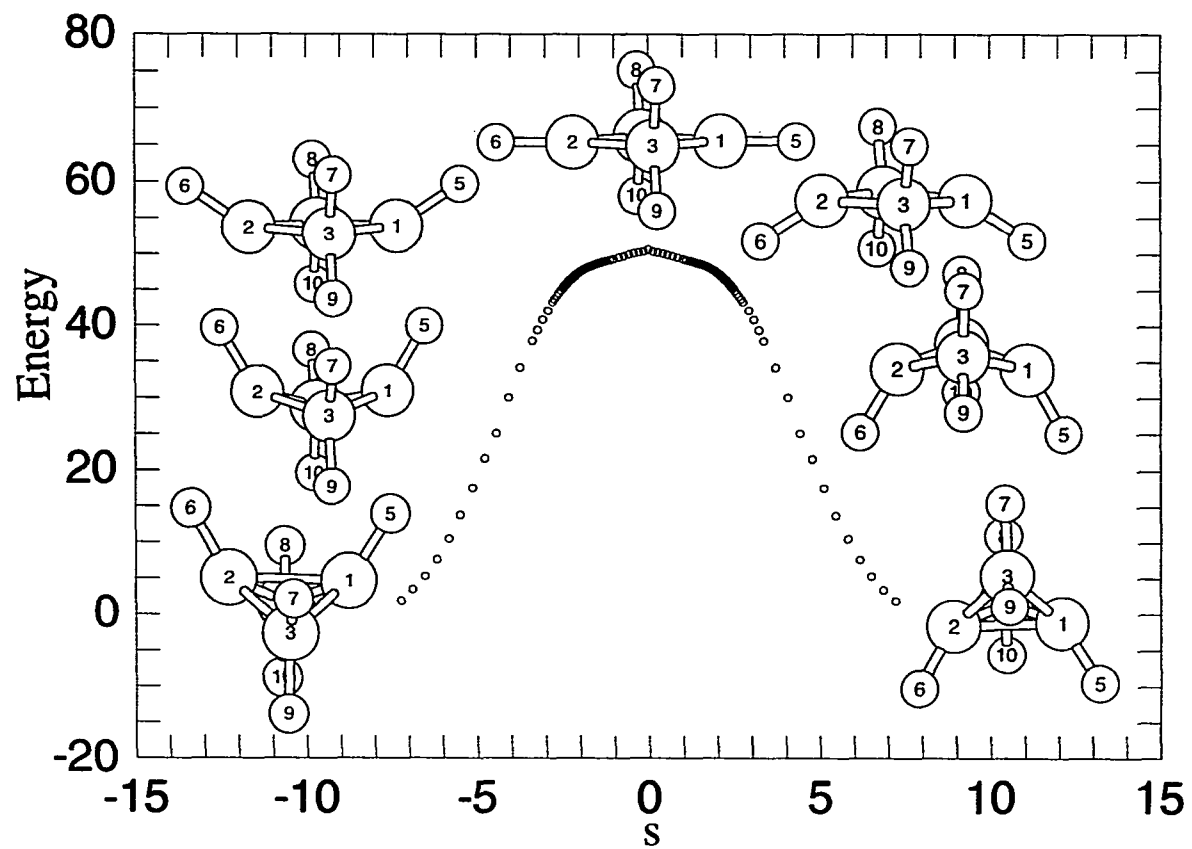


Figure 2a. Inversion IRC of bicyclobutane calculated with MCSCF(10,10)/6-31G(d); energy in kcal/mol, s in $\text{amu}^{1/2} \cdot \text{bohr}$. The structures displayed along the IRC are for the transition state 2 (top), and for points 33, 66 and 72 for the forward ($s > 0$) and backward ($s < 0$) directions.

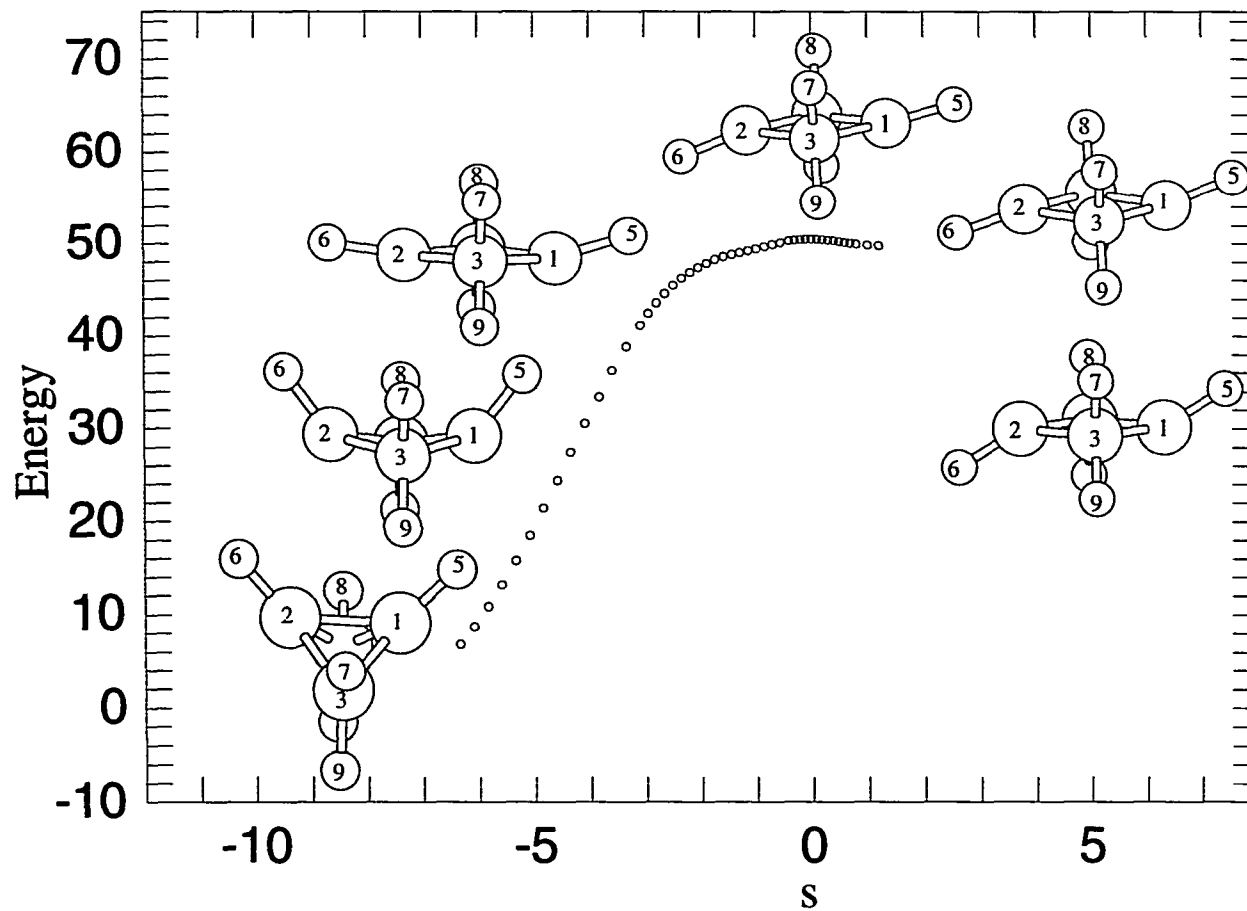


Figure 2b. Bond stretch IRC of bicyclobutane, calculated with MCSCF(10,10)/6-31G(d); energy in kcal/mol, s in $\text{amu}^{1/2} \cdot \text{bohr}$. The structures displayed along the IRC are of the transition state 6 (top), forward ($s > 0$): points 2 and 10, backward ($s < 0$): points 10, 20 and 30.

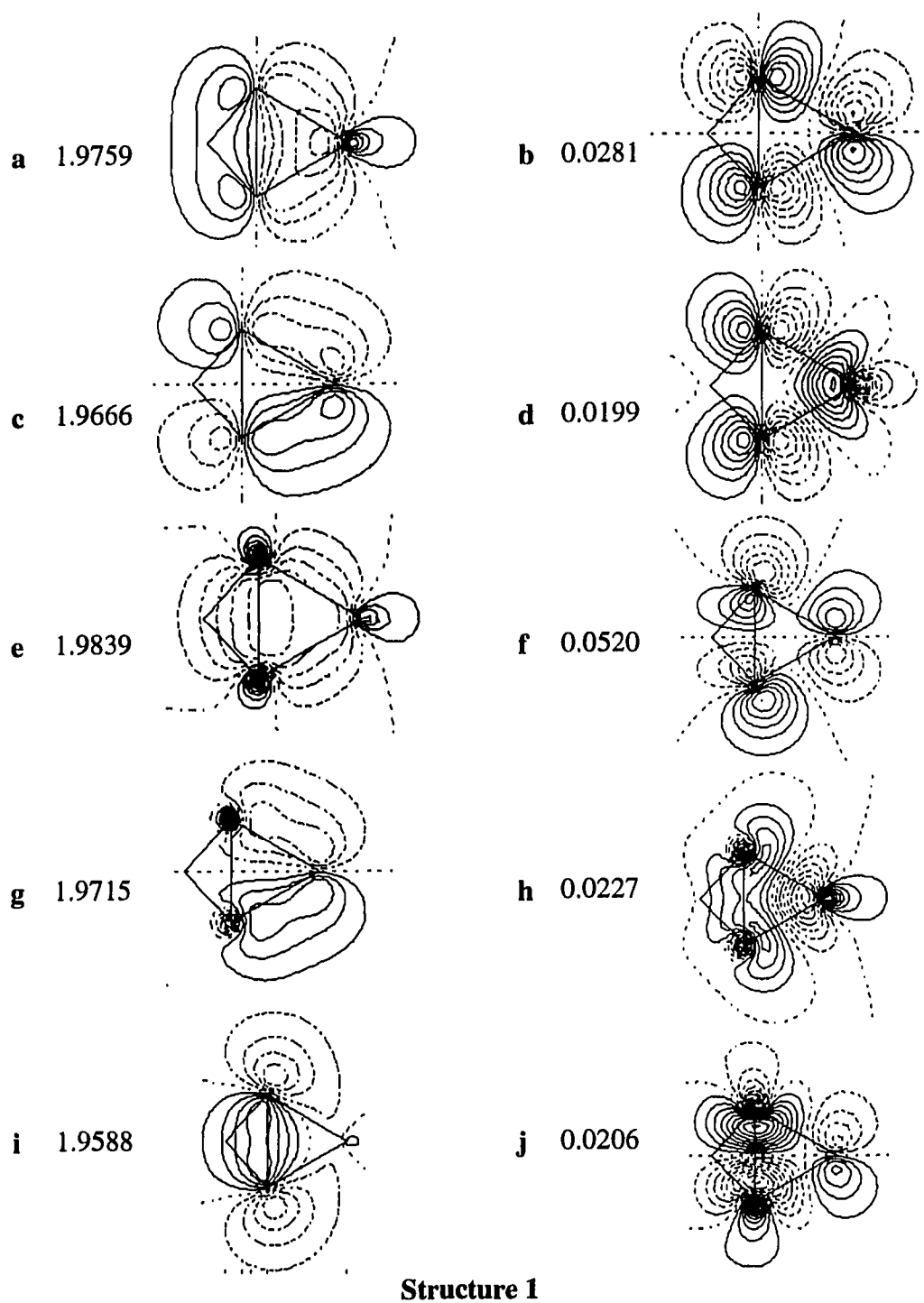


Figure 3a. Contour plots of the bicyclobutane correlated reaction orbitals of the optimized MCSCF(10,10)/6-31G(d) wave function in the planes that are made up by two bridgehead atoms and one of two peripheral atoms (numerical values = occupation numbers).

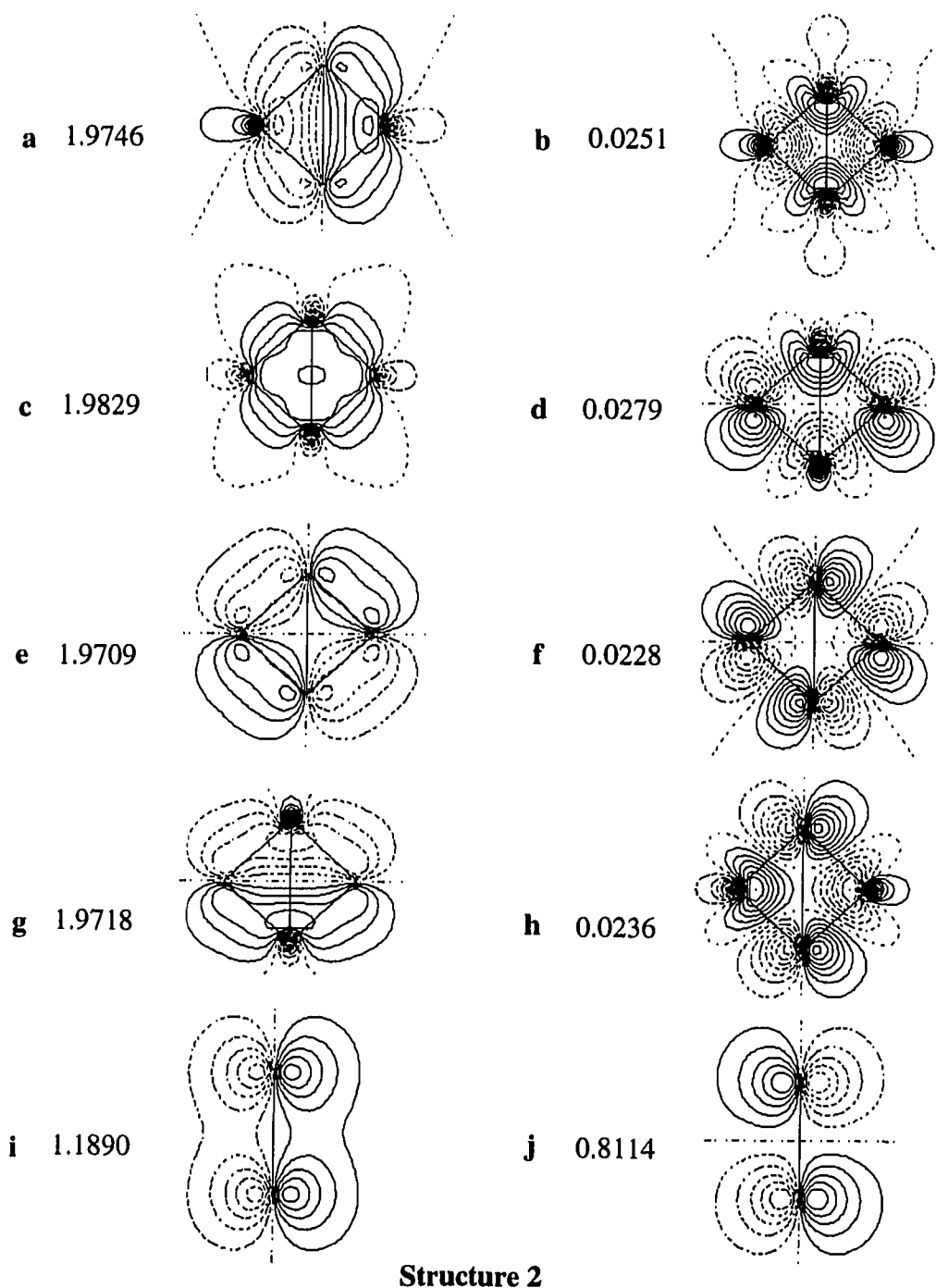
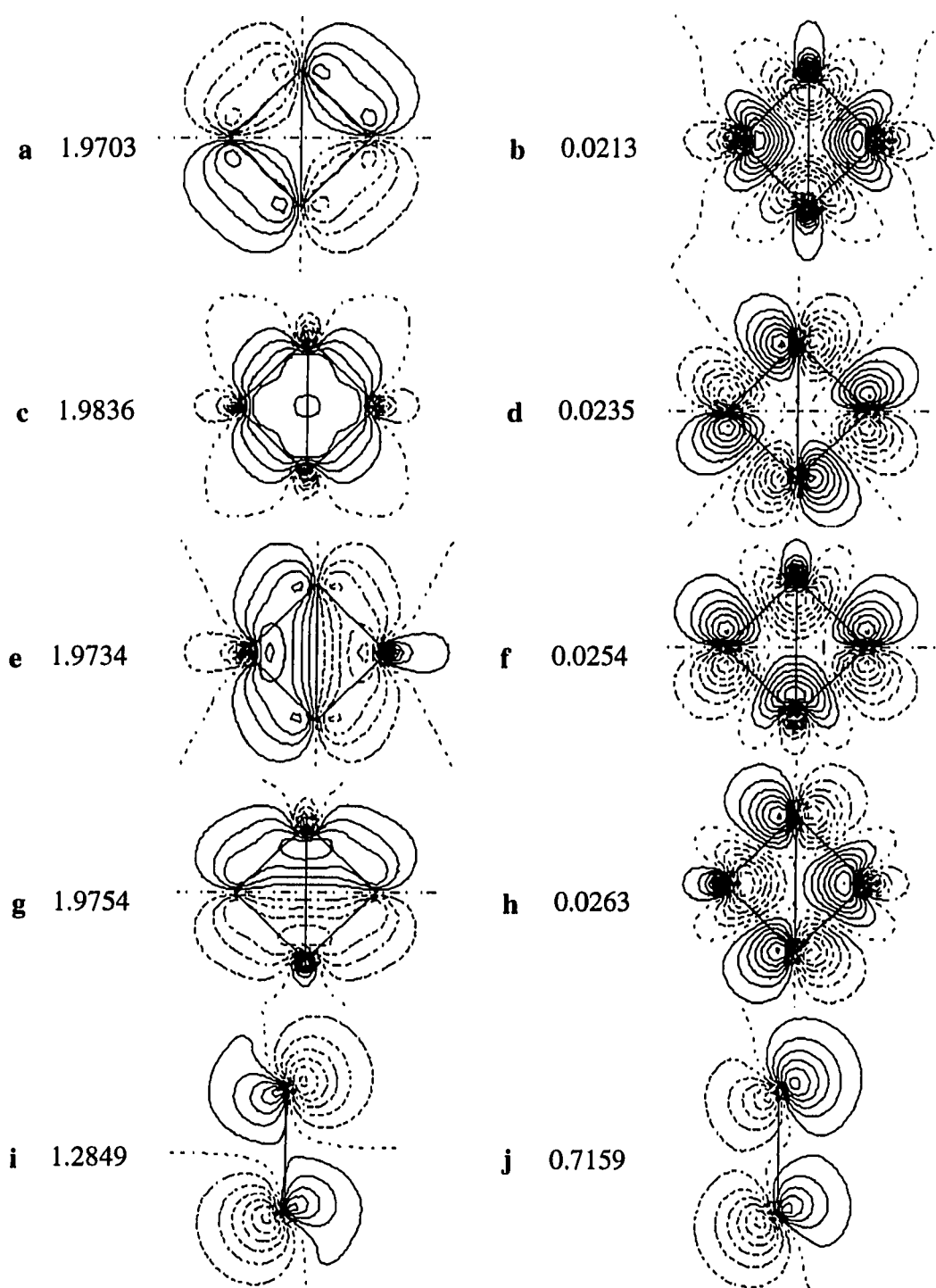
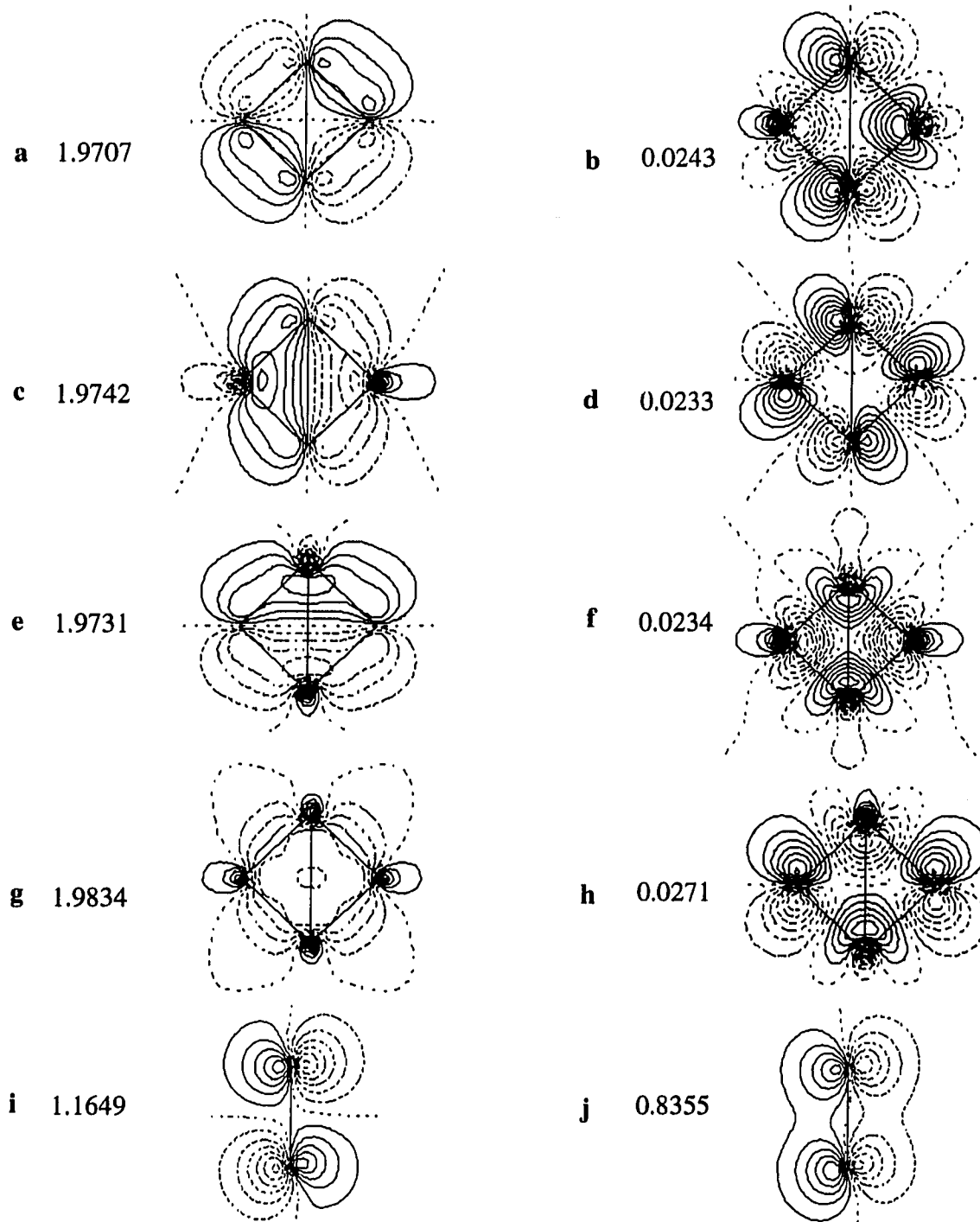


Figure 3b. Contour plots of the bicyclobutane correlated reaction orbitals of the optimized MCSCF(10,10)/6-31G(d) wave function in the $\sigma_h(xy)$ (a-h) and $\sigma_v(yz)$ (i, j) planes (numerical values = occupation numbers).



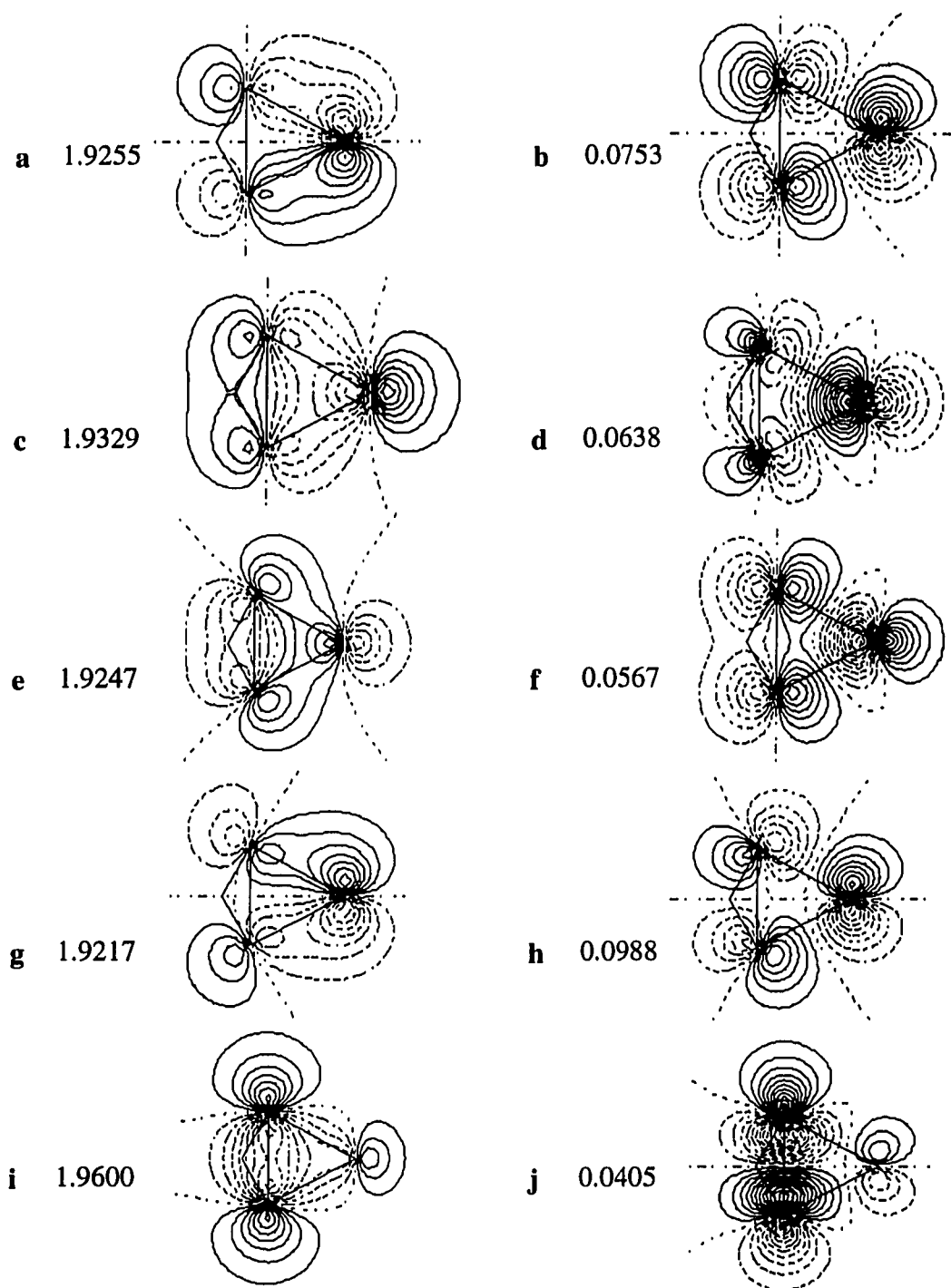
Structure 5

Figure 3c. Contour plots of the bicyclobutane correlated reaction orbitals of the optimized MCSCF(10,10)/6-31G(d) wave function in the YZ (a-h) and $\sigma_h(x,y)$ (i-j) planes (numerical values = occupation numbers) numerical values = occupation numbers).



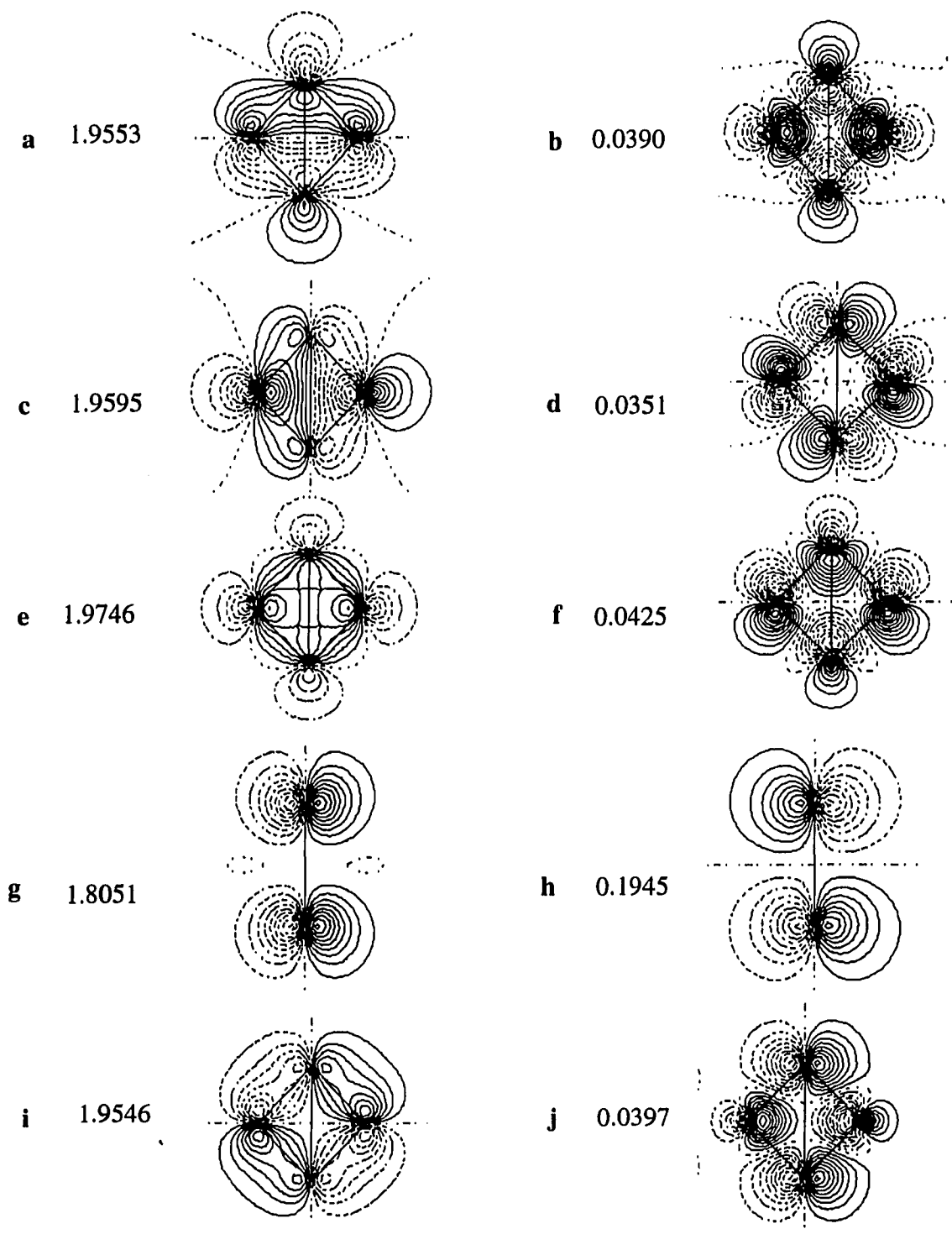
Structure 6

Figure 3d. Contour plots of the bicyclobutane correlated reaction orbitals of the optimized MCSCF(10,10)/6-31G(d) wave function in the $\sigma_h(xy)$ plane (i,j) and in the planes (a-h) that are made up by two bridgehead atoms and one of two peripheral atoms (numerical values = occupation numbers).



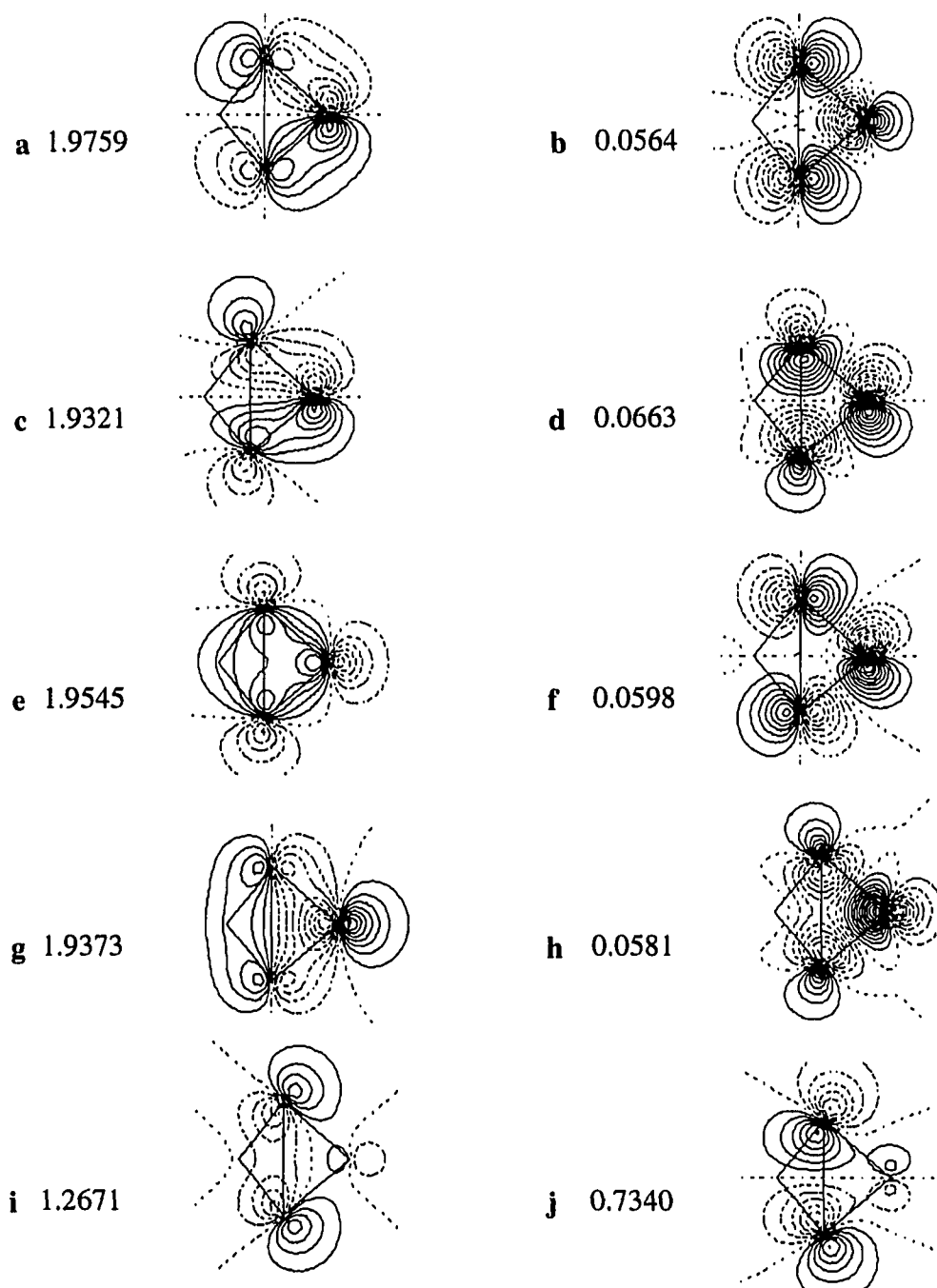
Structure 3

Figure 4a. Correlated orbitals of the optimized (10,10) MCSCF/6-31G(d) wave function in the planes containing two bridgehead nitrogen atoms and one of two peripheral oxygen atoms (numerical values = occupation numbers).



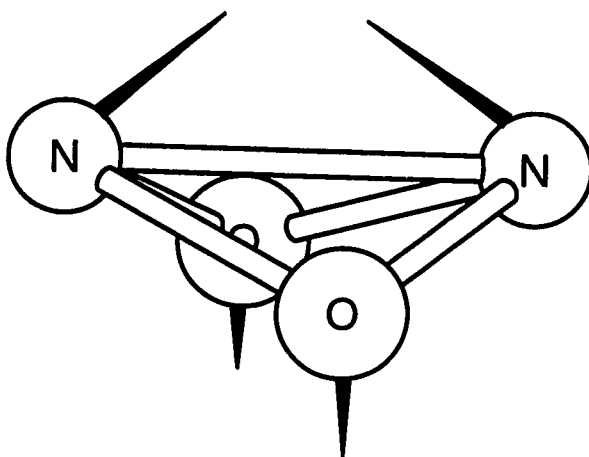
Structure 4

Figure 4b. Correlated reaction orbitals of the optimized (10,10) MCSCF/6-31G(d) wave function in the $\sigma_h(xy)$ (a, b, c, d, e, f, i, j) and $\sigma_v(xz)$ (g, h) planes (numerical values = occupation numbers).



Structure 7

Figure 4c. Contour plots of the correlated reaction orbitals of the optimized MCSCF(10,10)/6-31G(d) wave function in the planes that are made up by two bridge head atoms and one of two peripheral atoms (numerical value = occupation numbers).



7

Figure 5. MCSCF(10,10)/6-31G(d) Imaginary Normal Mode ($1150i \text{ cm}^{-1}$) for 7.

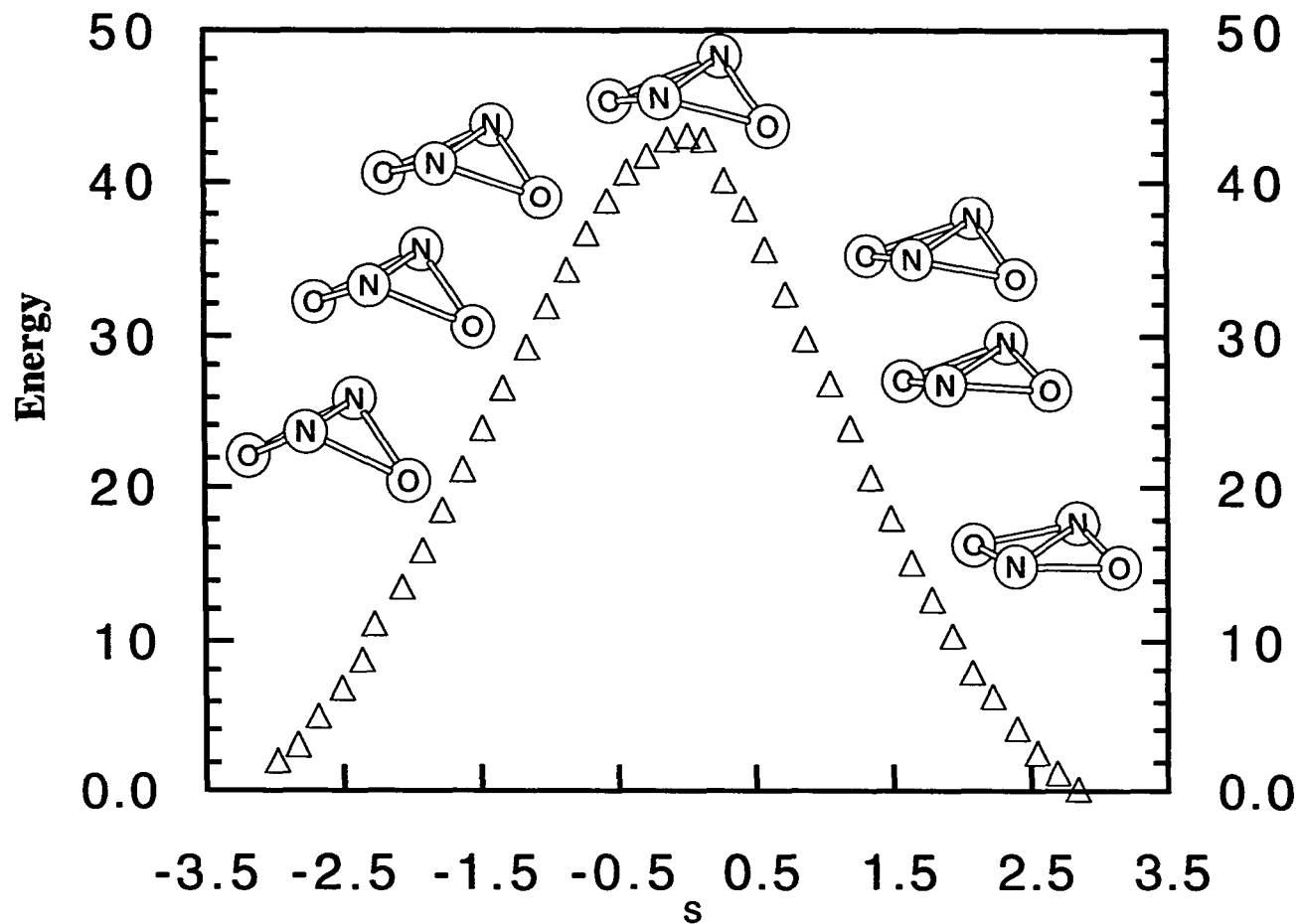


Figure 6. Bicyclodiazoxane bond stretch IRC calculated with MCSCF(10,10)/6-31G(d); energy in kcal/mol, s in amu^{1/2}.bohr. The structures displayed along the IRC are of the transition state (top), point 5, 10, and 16 in the forward and reverse direction.

CHAPTER 6. THE ISOMERIZATION OF BICYCLOBUTANE TO BUTADIENE

A paper submitted to The Journal of The American Chemical Society

Kiet A. Nguyen and Mark S. Gordon

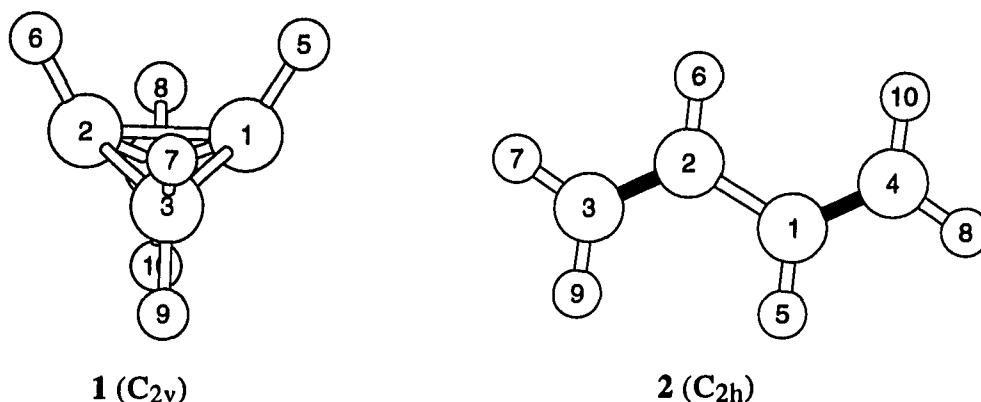
Abstract

Multi-configurational wave functions were used to study the (1) concerted conrotatory, (2) concerted disrotatory, and (3) nonconcerted isomerization processes of bicyclobutane (C_4H_6) to butadiene. The barriers for (1), (2), and (3) are about 42, 56, and 116 kcal/mol, respectively as calculated with the second order multi-reference perturbation theory (PT2). The barriers obtained from the multi-reference CI (MRCI) are within 1 kcal/mol of the those predicted by PT2. The predicted conrotatory barrier is within 1 kcal/mol of the experimentally measured barrier. The predicted stereochemistry is in agreement with the experimental observations.

Introduction

Bicyclobutane (**1**) has received extensive study both experimentally¹⁻⁶ and theoretically.⁷⁻¹⁰ In a recent paper^{10c} we have examined the inversion process of bicyclobutane using the internally contracted multireference configuration interaction (MRCI) method¹¹ and second-order perturbation theory with a complete active space self-consistent field (CASSCF)¹² reference function (PT2).¹³ In this paper, we consider the isomerization reaction of bicyclobutane to butadiene (**2**).

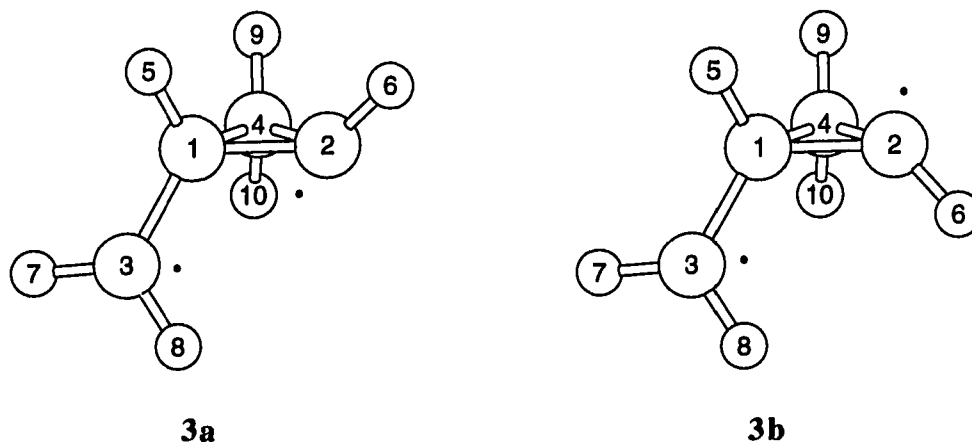
Numerous theoretical and experimental studies have been carried out to help unravel the energetics and pathways of this reaction. Experimentally, a thermolysis study of bicyclobutane has suggested that isomerization of **1** to **2** occurs with the central bond



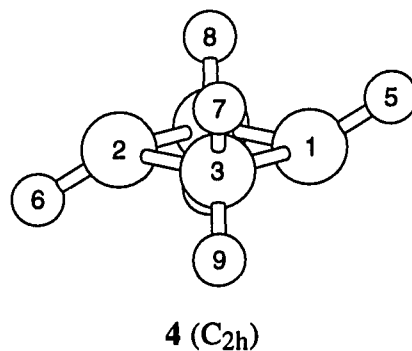
remaining intact, while two opposite peripheral C-C bonds are broken.³ An activation energy of 40.6 kcal/mol⁴ is needed to drive this reaction. Studies of bicyclobutane derivatives⁵ have found that the isomerization follows a highly stereoselective concerted process. A labeling study⁶ of a deuterated bicyclobutane (one of the *exo*-hydrogens H₇ or H₈ is deuterium labeled) has inferred that thermal rearrangement of **1** follows a concerted process with the two methylene groups moving in a conrotatory fashion, as predicted by Woodward-Hoffmann rules.⁷

Theoretically, Dewar and Kirschner^{9a} have predicted that isomerization of **1** is a stepwise process involving the cyclopropylcarbinyl biradical intermediate (**3**), based on results from the two configurational CI calculations within the MINDO/3 approximation. The rate determining step was predicted to be a ring opening of **1** to form **3** which subsequently dissociates into **2** without significant activation. The authors have argued that the stereochemistry of the reaction is maintained due the rapid interconversion of **3** to **2** compared to the formation of **3** from **1**.

Recent results from the *ab initio* MP2/3-21G calculations by Shevlin and Mckee^{9b} have suggested that ring opening of bicyclobutane (**1**) to form butadiene (**2**) follows an asynchronous one-step pathway with a transition state (MP4(SDTQ)//6-31G(d)//MP2/3-21G barrier = 43.6 kcal/mol) having one C-C peripheral bond lengthened by 0.783Å and the other by 0.088Å compared to **1**. The MP2/6-31G(d)//MP2/3-21G relative thermodynamic



stabilities of various biradicals were also considered by Shevlin and Mckee. All the biradicals investigated were found to be higher in energy relative to the transition state. Thus, the stepwise mechanism was ruled out. These calculations, however, were performed using single determinant based methods that are inadequate for describing species having large diradical character.^{9a,10} In the present work, the isomerization of bicyclobutane to butadiene is examined in detail using multi-configurational wave functions. Multi-configurational wave functions have the necessary flexibility to properly describe diradical intermediates such as **3**⁹ and **4**.^{4c-e,10c} In this way, structures **1-4** and the associated transition states can be described in an accurate and consistent manner. The intermediate **4** has been examined in our previous study



of the inversion of bicyclobutane.^{10c} To gain a better understanding of the stereochemistry and to ensure proper connections of all transition states with the corresponding minima, we apply the concept of intrinsic reaction coordinate (IRC)¹⁴ to follow the steepest descent paths from the transition states in both directions.

II. Methods of Calculation

Since the isomerization of bicyclobutane to butadiene involves breaking a least two opposite peripheral C-C bonds, our multi-configurational wave function for this process would require an active space of at least 4 orbitals and 4 electrons [i.e., MCSCF(4,4)]. To completely account for all changes in the bicyclobutane ring system, the reference space is expanded by combining five doubly occupied C-C bonding MOs and their corresponding antibonding MOs, creating 19404 spin adapted configuration state (CFS) functions (for C₁ symmetry) making up the 10 orbitals and 10 electrons complete active space (CAS) MCSCF¹⁴ [MCSCF(10,10)] wave function.

The MCSCF(10,10) determinations of geometries were performed using the 6-31G(d) basis set. Structures were obtained with the use of the analytically determined gradients encoded in the GAMESS¹⁵ quantum chemistry program system. Minima and transition states were verified by evaluating the appropriate matrix of energy second derivatives (hessian), using finite differences of the analytically determined gradients. The final energetics were obtained from MRCI¹¹ calculations (including all single and double excitations from the active orbitals of the MCSCF(10,10) reference space), using the MCSCF wave functions to define the reference space. All MRCI calculations were done using the MOLPRO^{16,11} codes.

In addition, second order perturbation theory calculations with the CASSCF(10,10) wave function as the reference space (PT2)¹³ were also carried out to assess the effect of dynamic electron correlation that is not included in the MRCI(10,10). PT2 calculations of

two different type of Møller-Plesset-like partitioning were carried out using the MOLCAS-2 program.¹⁷ The PT2D partitioning includes only the diagonal part of the one-electron operator in the zeroth-order Hamiltonian while PT2F also includes all non-diagonal elements. Only the latter one is invariant to orbital transformations.

The IRC was traced by following the path of steepest descents in the mass-weighted Cartesian coordinates.^{18,19} The reaction paths were generated using the second order Gonzalez-Schlegel (GS2)²⁰ method encoded in GAMESS.¹⁵ The initial step off the saddle point was taken by following the imaginary normal mode with a 0.12 amu^{1/2}bohr step. Other points on the IRC were located with a stepsize of 0.17 amu^{1/2}bohr ($\Delta s = 0.17$ amu^{1/2}bohr).

All geometry searches and IRC calculations were done with the 6-31G(d) basis set.¹¹ Since the basis set dependence upon going from 6-31G(d) to 6-311G(d,p)²¹ was shown to be small in MRCI and PT2F calculations for the inversion process of bicyclobutane,^{10c} only the 6-31G(d) basis set is used for all correlated calculations in this study.

III. Results and Discussion

The MCSCF, MRCI and PT2F total and relative energies of all stationary points on the isomerization surface are listed in Table I. The MCSCF(10,10)/6-31G(d) geometric parameters of these species are given Figure 1. Whenever available, the experimental geometric parameters are given in parentheses for comparisons. In general, correlated MCSCF bond distances are slightly longer compared to the experimentally determined values. Our MCSCF(10,10) calculations overestimate the experimental²² bridgehead (C₁-C₂) and peripheral (C₁-C₃) distances of bicyclobutane (**1**) by 0.024Å and 0.021Å, respectively (see Figure 1). Similarly, MCSCF (10,10) bond distances for butadiene (**2**) are about 0.01-0.03 angstroms longer than the experimental values.²³ Energetically, the exothermicity of the isomerization **1** → **2** has been experimentally measured to be 26 ± 2

kcal/mol.²⁴ The calculated MCSCF(10,10) exothermicity is 41.3 kcal/mol, including corrections for the vibrational zero point energy (ZPE). To include dynamic electron correlation, MRCI(10,10)//MCSCF(10,10) calculations with all CH MOs frozen were carried out, resulting in an exothermicity of 32.4 kcal/mol. The full PT2 based on the same MCSCF(10,10) wave function has the advantage that all valence MOs are correlated. This level of theory, PT2F//MCSCF(10,10) yields an isomerization enthalpy of -26.0 kcal/mol. This PT2F result is in excellent agreement with the experimental exothermicity value. The *cis*-butadiene conformation (**5**) is not a minimum on the MCSCF(10,10)/6-31G(d) potential energy surface. Rather, this structure, with one imaginary frequency of 130i cm⁻¹, corresponds to the rotational transition state leading to the *gauche*-butadiene (**6**) isomer. At the PT2F level of theory, the *cis*-butadiene transition state is predicted to be 3.6 kcal/mol (with ZPE correction) above the *trans*-butadiene (**2**) conformer. A similar ΔH value is obtained with MRCI (see Table I). The *gauche* conformer of butadiene (**6**) is a minimum on the MCSCF(10,10)/6-31G(d) potential energy surface. The *gauche* isomer is predicted to be 0.8 (0.7) kcal/mol below *cis* and 2.8 (2.6) kcal/mol above the *trans* at the PT2F (MRCI) level of theory. So, the orbitals that are frozen in the MRCI calculations have little effect on the relative energies of the three butadiene conformers. The relative energies are essentially identical to the MP2/6-31G(d)//MP2/6-31G(d) predictions by Wiberg et al.²⁴

Three transition states, **7**, **8** and **9**, were located on the MCSCF(10,10)/6-31G(d) potential energy surface. Structures **7** and **8** correspond to the transition states for the asynchronous concerted mechanisms in which the methylene groups move in conrotatory and disrotatory fashions, respectively. Transition state **9** corresponds to the non-concerted isomerization process with a diradical intermediate **4** which can be readily converted to bicyclobutane without significant activation.^{10c} The geometric parameters and relative energies of these transition states are also given in Table I and Figure 1, respectively. The

IRCs traced from these transition states to the corresponding minima are displayed in Figures 2-4, and the three competing processes are considered in the next three subsections.

A. Conrotatory Ring Opening

At all levels of theory, ring opening of bicyclobutane (**1**) via the conrotatory transition state **7** is predicted to be the lowest in energy among the three barriers found. At the MCSCF(10,10) level of theory, the conrotatory barrier (**7**) is located at 39.7 kcal/mol above the reactant bicyclobutane, with ZPE included. PT2F//MCSCF(10,10) and MRCI/MCSCF(10,10) slightly increase this barrier to 41.5 kcal/mol. This is in excellent agreement with the experimentally measured barrier of 40.6 kcal/mol.⁴

At the transition state (**7**), the C₂-C₃ peripheral bond (2.258 Å) is completely broken while the other C₁-C₃ peripheral distance (1.456 Å) is only 0.063 Å shorter than the C-C peripheral distance in the reactant bicyclobutane. The ring opening is accompanied by a distortion of the H₅-C₁-C₂-H₆ dihedral angle to 128° away from the eclipsed position at the equilibrium structure (**1**) (see **7**, Figure 1). In the opposite ring, the C₁-C₄ distance increases to 1.560 Å, and C₂-C₄ decreases to 1.495 Å.

The connection of bicyclobutane with the conrotatory transition state **7** and *gauche*-butadiene (**6**) is verified by the IRC calculations. Figure 2 displays the structural rearrangements along the IRC in this isomerization process. Notice that while one bridgehead hydrogen (H₅) bends away from an eclipsed position relative to H₆, the two methylene groups move in a conrotatory fashion in the ring opening process. This leads to the final stereochemistry of butadiene with H₈ and H₇ (*exo*-hydrogens of bicyclobutane) having H-C-C-C dihedral angles of 0° (*cis*) and 180° (*trans*), respectively (see Figure 2). So if both peripheral *exo*-hydrogens (H₈, H₇) were labeled with deuteriums, the final product would be referred to as *gauche*-butadiene-1-*cis*-4-*trans*-d₂, as predicted by the IRC calculation in Figure 2, where the “1” and “4” refer to the carbons vicinal to H₈ and H₇,

respectively. If the one of peripheral *exo*-hydrogens (H_8 , H_7) was deuterated, an equal mixture of *gauche*-butadiene-*cis*-1-d (for D_8) and *gauche*-butadiene-*trans*-1-d (for D_7) would be obtained. Furthermore, since the *gauche-trans* rotational barrier is less than 3 kcal/mol,²⁴ the final experimentally observed products are likely to contain an equal mixture of *trans*-butadiene-*cis*-1-d and *trans*-butadiene-*trans*-1-d, as has been found in labeling studies.⁶ The predicted stereochemistry of the products is also consistent with experimental observations in the pyrolysis studies of *exo*, *exo*- and *exo*, *endo*-dimethyl substituted bicyclobutane derivatives.⁵

Although the conrotatory mechanism is consistent with the major product from the pyrolysis of *exo,exo*- and *exo,endo*-dimethyl substituted bicyclobutane derivatives,⁵ the observed diene conformations are stereoselective, not stereospecific with minor side products. Furthermore, the pyrolysis of *endo*-monomethylated bicyclobutane (H_9 or H_{10} is replaced by a CH_3 group) and *exo*-monomethylated bicyclobutane (H_7 or H_8 is replaced by a CH_3 group) leads to over 90% *trans*-1,3-pentadiene (dihedral $CH_3-C-C-C = 180^\circ$). Following the IRC in Figure 2, the *exo*-monomethylated form (with $H_7 = CH_3$), apparently for steric reasons, favors the conrotatory ring opening with an initial C-C cleavage from the methyl substituted cyclopropane ring of bicyclobutane, while the *endo*-monomethylated form (with $H_{10} = CH_3$) may prefer the conrotatory ring opening with an initial C-C cleavage from the unsubstituted side. Since each of these mechanisms for *exo*- and *endo*-monomethylated bicyclobutane will lead to the same product, explicit calculations on the monomethyl derivatives are needed to distinguish between competing energetics.

B. Disrotatory Ring Opening

The disrotatory ring opening barrier (**8**) is located at 52.4 kcal/mol above bicyclobutane on the MCSCF(10,10)/6-31G(d) potential energy surface. MRCI and PT2F dynamic electron correlation corrections give 56.7 and 56.3 kcal/mol, respectively, for this

barrier when ZPE corrections are included. This is about 15 kcal/mol higher than the conrotatory isomerization barrier, obtained at the same levels of theory. At the transition state (**8**), the C₁-C₃ bond in one cyclopropane ring is completely broken (C₁-C₃ = 2.591 Å), while the all C-C distances in the opposite cyclopropane ring are only slightly changed from their values in bicyclobutane (Figure 1). In contrast to the conrotatory transition state (**7**), **8** has two bridgehead hydrogens (H₅ and H₆) nearly eclipsed with each other.

The IRC displayed in Figure 3 connects bicyclobutane (**1**) with *gauche*-butadiene via transition state **8**. In the disrotatory ring opening, the methylene groups rotate in opposite directions asynchronously. The disrotatory rotation of the two methylene groups gives rise to the *gauche*-butadiene-1-*trans*-4-*trans*-d₂ (H₈-C₄-C₁-C₂ and H₇-C₃-C₂-C₁ dihedral angles are 180°) if the two *exo*-hydrogens are deuterium labeled. The opposite (*cis*) stereochemistry would be obtained for *endo*-deuterated bicyclobutane. The reaction mechanism resulting in this type of stereoselectivity for the disrotatory ring opening of bicyclobutane is likely to be a minor path, since the competing conrotatory process with different stereoselectivity has a significantly lower barrier (15 kcal/mol lower). Furthermore, the *exo*- and *endo*-hydrogens of bicyclobutane can be scrambled by the inversion process^{10c} with a barrier of about 8 kcal/mol lower than the disrotatory ring opening barrier.

The barrier for disrotatory ring opening constrained to C₂ symmetry (**9**) is located at 85.7 kcal/mol above bicyclobutane. This structure (**9**, Figure 1) is not a true transition state as characterized by the two imaginary eigenvalues of the force constant matrix.

C. Stepwise Mechanism

The diradical structure **4** has been speculated to be an intermediate for the stepwise isomerization bicyclobutane to butadiene in photolysis studies.^{10c-e} Structure **4**—a minimum on the MCSCF(10,10)/6-31G(d) potential energy surface—lying about 50 kcal/mol above bicyclobutane—has been found to isomerize back to bicyclobutane without

any significant barrier.^{10c} Despite careful searches, the diradical intermediates **3a** and **3b** were not found.

Since the isomerization of bicyclobutane to butadiene via intermediate **4** requires the breaking (at least partially) of another C-C peripheral bond in addition to the central bridgehead C₁-C₂ bond, the barrier may be significantly higher than the concerted pathways. This barrier (**10**) is indeed found by PT2F to lie 116.4 kcal/mol (including ZPE correction) above bicyclobutane. The barrier predicted by MRCI is about 1 kcal/mol higher than that of PT2F.

The reaction path for the **4** ↔ **6** isomerization via transition state **10** is displayed in Figure 4. At the transition state (**10**), the bridgehead hydrogens (H₅ and H₆) remain staggered, and the bridgehead C₁-C₂ and the peripheral C₂-C₃ bonds are lengthened to 2.535 Å and 2.794 Å, respectively.

The initial descent from the transition state **10** toward butadiene involves, mostly, the shortening of the bridgehead C₁-C₂ bond and the rotation of one methylene group. This is followed by the conrotatory rotations of the two methylene groups. Since the intermediate **4** scrambles the peripheral hydrogens via an inversion barrier of less than 1 kcal/mol^{10c}, this isomerization process is not stereoselective.

D. Bonding

The large increase in C-C bond distances at the transition states suggests significant configurational mixing may occur. The amount of configurational mixing in the transition states may be assessed by examining the natural orbital occupation numbers (NOONs) of the MCSCF wave functions. For RHF wave functions, the NOONs are 2 for occupied orbitals and 0 for virtual orbitals. The deviations from these values in multi-configurational wave functions may therefore be taken as a measure of "diradical character".

The MCSCF(10,10) natural orbitals (NOs) of bicyclobutane, butadiene, transition states, and other structures of interest are displayed in Figures 5-11. The orbitals labeled **g** and **h** displayed in the plane containing two bridgehead and one peripheral atoms correspond to the bonding and antibonding orbitals of the broken C-C peripheral bond in the transition states **7** and **8**. The NOONs for these NOs are nearly 1.0 (true diradicals) in structure **8** (Figure 8), whereas for structure **7**, these occupation numbers are ~ 1.75 and 0.25, respectively. The diradical character of **7** is lower compared to **8** due, in part, to the developing π -bond character nearly perpendicular to the plotting plane. However, there is still significant configurational mixing in the conrotatory transition state **7** compared to the relatively closed shell nature of bicyclobutane (**1**) and butadiene (**6**) (see Figures 5-6). The concerted breaking of two C-C peripheral bonds in structure **9** also creates a significant amount of diradical character (with the two C-C antibonding MOs having NOONs of 0.2 and 0.4 electrons).

In contrast to the closed shell nature of the C-C bridgehead bond in all structures discussed above, the NOONs of orbitals **i** and **j** become nearly 1 in the bond stretch isomer (**4**, Figure 10) and the nonconcerted transition state (**10**, Figure 11). The NOONs of orbitals **g** and **h** corresponding to the C₃-C₂ peripheral bond, are also close to 1 at the transition state structure **10**. The remaining four NOs correspond to the two other bridgehead-peripheral bonds in the all bicyclo arrangements (**a-d**); these NOs remain nearly closed shell in nature throughout the isomerization process. It is interesting that there appears to be a correlation between the diradical character of the three transition states (as measured by the population of antibonding orbitals) and the height of the corresponding barrier. From the strong diradical character noted above, the isomerization process of bicyclobutane can not be treated in a consistent manner with single configuration-based methods.

IV. Summary and Conclusion

The isomerization process of bicyclobutane has been examined using multi-configurational based wave functions. The ca. 42 kcal/mol conrotatory barrier obtained by PT2F/6-31G(d)//MCSCF(10,10)/6-31G(d) and MRCI(10,10)/6-31G(d)//MCSCF(10,10)/6-31G(d) is within 1 kcal/mol of experiment and of one another. Barriers for the concerted disrotatory and stepwise isomerization processes are ca. 56 kcal/mol and 116 kcal/mol, respectively, so the bicyclobutane to butadiene isomerization is predicted to proceed primarily via the concerted conrotatory mechanism. This conclusion is in agreement with the experimental observations^{5,6} that the reaction proceeds in a concerted manner, but disagrees with previous semi-empirical calculations that predict a stepwise mechanism.^{9a} Earlier *ab initio* calculations^{9b} using single configuration wavefunctions also predict a concerted mechanism with a barrier of about 44 kcal/mol.

Excellent agreement with the experimental exothermicity of the isomerization of bicyclobutane to butadiene was obtained for PT2F, but not for MRCI(10,10), since the frozen core approximation for CH bonds is less valid in the latter. The predicted stereochemistry is in agreement with the experimental observations. For this system, there appears to be a correlation between the amount of diradical character in the transition state (conrotatory < disrotatory < nonconcerted) and the height of the associated energy barrier. This emphasizes the need for multi-configurational based methods for a consistent treatment of the isomerization process.

Acknowledgment

This research was supported in part by a grant from the Air Force Office of Scientific Research, under the High Energy Density Materials Initiative (92-0226), and in part by a grant from the National Science Foundation (CHE-9313717). Calculations described in this work were performed on an IBM RS6000/530 (obtained through an AFOSR grant to MSG)

at North Dakota State University, on an IBM RS6000/350 generously provided Iowa State University, on the Cray-C90 at the DoD High Performance Computing Center USAE Waterways Experiment Station, and on the Cray-2 at the National Center for Supercomputing Applications, Champaign, Illinois.

References

- (1) Bent, G. D. *J. Chem. Phys.* **1992**, 96, 8084.
- (2) Walters, V. A.; Hadad, C. M.; Thiel, Y.; Colson, S. D.; Wiberg, K. B.; Johnson, P. M.; Foresman, J. B. *J. Am. Chem. Soc.* **1990**, 113, 4782.
- (3) Blanchard, E. P. Jr.; Carncross, A. *J. Am. Chem. Soc.* **1966**, 88, 487.
- (4) (a) Frey, H. M.; Stevens, I. D. R. *Trans. Faraday Soc.* **1965**, 61, 90. (b) Srinivasan, R.; Levi, A.; Haller, I. *J. Phys. Chem.* **1965**, 58, 1775. (c) Becknell, A. F. Berson, J. A.; Srinivasan, R. *J. Am. Chem. Soc.* **1985**, 107, 1076. (d) Adam, W.; Oppenlander, T.; Zang, G. *J. Am. Chem. Soc.* **1985**, 107, 3921. (e) Adam, W.; Oppenlander, T. *Angew. Chem., Int. Ed. Engl.* **1986**, 25, 661 and references cited therein.
- (5) Closs, G. L.; Pfeffer, P. E. *J. Am. Chem. Soc.* **1968**, 90, 2452.
- (6) Wiberg, K. B.; Lavanish, J. M. *J. Am. Chem. Soc.* **1966**, 88, 5272.
- (7) Woodward, R. B.; Hoffman, R. *The Conservation of Orbital Symmetry*; Verlag Chemie, Academic Press: New York, 1970.
- (8) Wiberg, K. B. *Tetrahedron* **1968**, 24, 1083. (symmetric transition state)
- (9) (a) Dewar, M. J. S.; Kirschner, S. *J. Am. Chem. Soc.* **1975**, 97, 2931. (b) Shevlin, P. B.; Mckee, M. L. *J. Am. Chem. Soc.* **1988**, 110, 1666.
- (10) (a) Schmidt, M. W.; Nguyen, K. A.; Gordon, M. S.; Montgomery, Jr. J. A. *J. Am. Chem. Soc.* **1991**, 113, 5998. (b) Nguyen, K. A.; Carroll, M. T.; Gordon, M. S. *J.*

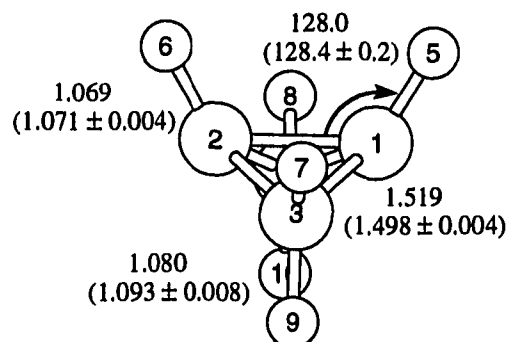
- Am. Chem. Soc.* **1991**, 113, 7924. (c) Nguyen, K. A.; Gordon, M. S.; Boatz, J. A. *J. Am. Chem. Soc.* **1994**, submitted
- (11) (a) Werner, H.-J.; Knowles, P. J. *J. Chem. Phys.* **1988**, 89, 5803. (b) Werner, H.-J.; Knowles, P. J. *Chem. Phys. Lett.* **1988**, 145, 514.
- (12) (a) Lengsfeld, B. H. III; *J. Chem. Phys.* **1980**, 73, 382. (b) Jarkony, D. R. *Chem. Phys. Lett.* **1981**, 77, 634. (c) Ruedenberg, K.; Schmidt, M. W.; Dombek, M. M.; Elbert, S. T. *Chem. Phys.* **1982**, 71, 41,51 65. (d) Lam, B.; Schmidt, M. W.; Ruedenberg, K. *J. Phys. Chem.* **1985**, 89, 2221. (e) Werner, H.-J.; Knowles, P. J. *J. Chem. Phys.* **1985**, 82, 5053. (f) Werner, H.-J.; Knowles, P. J. *Chem. Phys. Lett.* **1985**, 115, 259.
- (13) (a) Anderson, K. Malmqvist, P.-Å., Roos, B. O. *J. Chem. Phys.* **1992**, 96, 1218. (b) Anderson, K. Malmqvist, P.-Å., Roos, B. O. *J. Phys. Chem.* **1990**, 94, 5483.
- (14) (a) Ishida, K.; Morokuma, K.; Komornicki, A. *J. Chem. Phys.* **1977**, 66, 2153. (b) Muller, K. *Engew. Chem., Int. Ed. Engl.* **1980**, 19, 1. (c) Schmidt, M. W.; Gordon, M. S.; Dupuis, M. *J. Am. Chem. Soc.* **1985**, 107 2585. (d) Garrett, B. C.; Redmon, M. J.; Steckler, R.; Truhlar, D. G.; Baldrige, K. K.; Bartol, D.; Schmidt, M. W.; Gordon, M. S. *J. Phys. Chem.* **1988**, 92, 1476. (e). Baldrige, K. K.; Gordon, M. S.; Steckler, R.; Truhlar, D. G. *J. Phys. Chem.* **1989**, 93, 5107.
- (15) GAMESS (General Atomic and Molecular Electronic Structure System): a) Schmidt, M. W.; Baldrige, K. K.; Boatz, J. A.; Jensen, J. H.; Koseki, S.; Gordon, M. S.; Nguyen, K. A.; Windus, T. L.; Elbert, S. T. *QCPE Bulletin*, **1990**, 10, 52. b) Schmidt, M. W.; Baldrige, K. K.; Boatz, J. A.; Elbert, S. T.; Gordon, M. S.; Jensen, J. H.; Koseki, S.; Matsunaga, N.; Nguyen, K. A.; Su, S. Windus, T. L.; *J. Comp. Chem.* **1993**, 14, 1347.

- (16) MOLPRO is written by Werner, H.-J.; Knowles, P. J. with contributions by Almlöf, J.; Amos, R. D.; Elbert, S. T.; Taylor, P. R.
- (17) Anderson, K.; Fülischer, M. P.; Lindh, R.; Malmqvist, P.-Å.; Olsen, J.; Roos, B. O.; Sadlej, A. J.; Wilmark, P.-O. MOLCAS version 2, User's Guide; University of Lund, Sweden, 1991.
- (18) (a) Fukui, K. *Acc. Chem. Res.* **1981**, 14, 363. (b) Fukui, K. *Pure Appl. Chem.* **1982**, 54, 1825. (c) Fukui, K. *Int. J. Quantum Chem. Sym.* **1981**, 15, 633.
- (19) (a) Marcus, R. A.; *J. Chem. Phys.*, **1966**, 45, 4493. (b) Marcus, R. A. *J. Chem. Phys.* **1968**, 49, 2610. (c) Truhlar, D. G.; Kuperman, A. *J. Am. Chem. Soc.* **1971**, 93 1840. (d) Schaefer, H. F. III. *Chem. Britain.* **1975**, 11, 227.
- (20) Gonzalez, C.; Schlegel, H. B. *J. Chem. Phys.* **1989**, 90, 2154; *J. Phys. Chem.* **1990**, 94, 2154; *J. Chem. Phys.* **1991**, 90, 5853.
- (21) (a) Krishnan, R.; Binkley, J. S.; Seeger, R.; Pople, J. A. *J. Chem. Phys.* **1980**, 72, 650. (b) Clark, T.; Chandrasekhar, J.; Spitznagel, G. W.; Schleyer, P. von R. *J. Comput. Chem.* **1983**, 4, 294.
- (22) Bock, C. W.; Panchenko, Y. N. *J. Mol. Struct.* **1989**, 187, 69.
- (23) Cox, K. W.; Harmony, M. D.; Nelson, G.; Wiberg, K. G. *J. Phys. Chem.* **1969**, 50, 5107. (b) Cox, K. W.; Harmony, M. D.; Nelson, G.; Wiberg, K. G. *J. Phys. Chem.* **1970**, 53, 858.
- (24) Wiberg, K. B.; Rosenberg, R. E. *J. Am. Chem. Soc.* **1990**, 112, 1509.

Table I. 6-31G(d) Total (au) and Relative Energies of Bicyclobutane (**1**), *trans*-Butadiene (**2**), Bicyclobutane Bond Stretch Isomer (**4**), *cis*-Butadiene (**5**), *gauche*-Butadiene (**6**), Conrotatory Transition State (**7**), Disrotatory Transition State (**8**), Second Order Stationary point (**9**), and Nonconcerted Transition State (**10**).^a

Structure	Wave function	Total Energy	Relative Energy	
			ΔE	ΔH_0^b
1	MCSCF(10,10)//MCSCF(10,10)	-154.98904 (57.0)	0.0	0.0
	MRCI(10,10)//MCSCF(10,10)	-155.11561	0.0	0.0
	PT2F//MCSCF(10,10)	-155.41188	0.0	0.0
2	MCSCF(10,10)//MCSCF(10,10)	-155.05286 (55.7)	-40.0	-41.3
	MRCI(10,10)//MCSCF(10,10)	-155.16525	-31.0	-32.4
	PT2F//MCSCF(10,10)	-155.45117	-24.7	-26.0
4	MCSCF(10,10)//MCSCF(10,10)	-154.90976 (54.6)	49.7	47.3
	MRCI(10,10)//MCSCF(10,10)	-155.02934	54.1	51.6
	PT2F//MCSCF(10,10)	-155.32864	52.2	49.8
5	MCSCF(10,10)//MCSCF(10,10)	-155.04803 (55.7)	-37.0	-38.3
	MRCI(10,10)//MCSCF(10,10)	-155.16525	-27.8	-29.1
	PT2F//MCSCF(10,10)	-155.45117	-21.1	-22.4
6	MCSCF(10,10)//MCSCF(10,10)	-155.04846 (55.5)	-37.3	-38.8
	MRCI(10,10)//MCSCF(10,10)	-155.16067	-28.3	-29.8
	PT2F//MCSCF(10,10)	-155.44642	-21.7	-23.2
7	MCSCF(10,10)//MCSCF(10,10)	-154.92153 (54.3)	42.4	39.7
	MRCI(10,10)//MCSCF(10,10)	-155.04519	44.2	41.5
	PT2F//MCSCF(10,10)	-155.34147	44.2	41.5 ^c
8	MCSCF(10,10)//MCSCF(10,10)	-154.89930 (53.0)	56.3	52.4
	MRCI(10,10)//MCSCF(10,10)	-155.01880	60.7	56.7
	PT2F//MCSCF(10,10)	-155.31575	60.3	56.3
9	MCSCF(10,10)//MCSCF(10,10)	-154.84849 (50.9)	82.1	88.2
	MRCI(10,10)//MCSCF(10,10)	-154.96976	91.5	85.4
	PT2F//MCSCF(10,10)	-155.26560	91.8	85.7
10	MCSCF(10,10)//MCSCF(10,10)	-154.81374 (50.8)	110.0	107.8
	MRCI(10,10)//MCSCF(10,10)	-154.92515	119.5	117.3
	PT2F//MCSCF(10,10)	-155.22285	118.8	116.4

^aZero point vibrational energies are in parentheses; molecule numbering system is given in Figure 1. ^bIncluding zero point correction. ^cExperimental barrier = 40.6 kcal/mol (reference 4).

1 (C_{2v}) BicyclobutaneDistances (in Å)

$$r(7,3) = 1.078 (1.093 \pm 0.008)$$

$$r(1,2) = 1.521 (1.497 \pm 0.003)$$

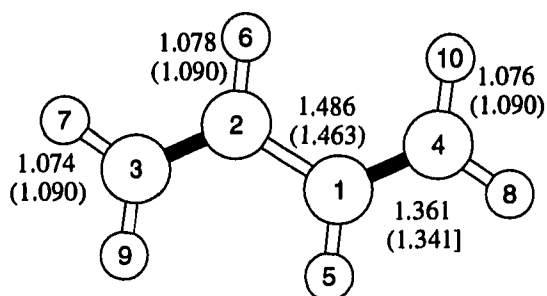
Angles (in degrees)

$$\alpha(7,3,9) = 114.5 (115.6)$$

$$\beta(3,1,2,4) = 122.1$$

$$\beta(7,3,2,1) = 106.8$$

$$\beta(9,3,2,1) = -108.9$$

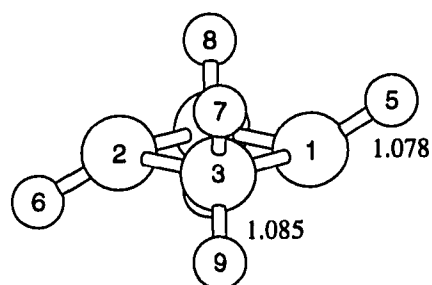
2 (C_{2h}) *trans*-ButadieneAngles (in degrees)

$$\alpha(7,3,2) = 121.5 (121.8)$$

$$\alpha(9,3,2) = 121.1 (121.8)$$

$$\alpha(5,1,4) = 119.8 (121.8)$$

$$\alpha(4,1,2) = 123.8 (123.3)$$

4 (C_{2h}) Bicyclobutane Bond Stretch IsomerDistances (in Å)

$$r(1,3) = 1.555$$

$$r(1,2) = 2.168$$

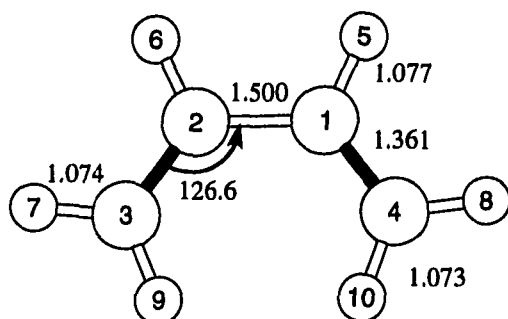
Angles (in degrees)

$$\alpha(5,1,2) = 140.8$$

$$\alpha(5,1,3) = 122.7$$

$$\alpha(7,3,1) = 113.5$$

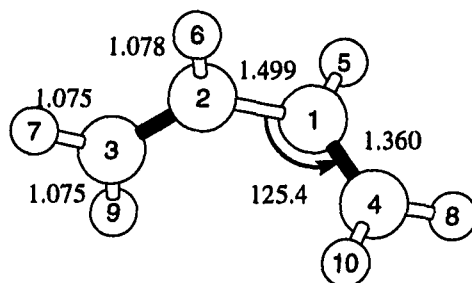
Figure 1. MCSCF(10,10)/6-31G(d) structures of C₄H₆ isomers. Experimental values are in parentheses.

5 (C_{2v}) *cis*-ButadieneAngles (in degrees)

$\alpha(7,3,2) = 120.7$

$\alpha(9,3,2) = 122.6$

$\alpha(5,1,4) = 118.0$

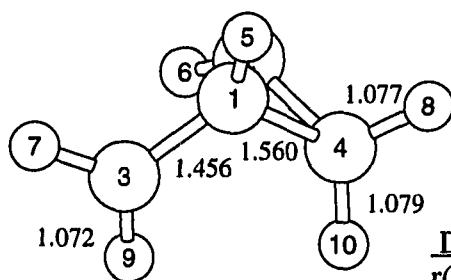
6 (C_2) *gauche*-ButadieneAngles (in degrees)

$\alpha(7,3,2) = 121.0$

$\alpha(9,3,2) = 122.0$

$\alpha(5,1,4) = 116.0$

$\omega(4,1,2,3) = 31.4$

7 (C_1) Concerted Conrotatory Transition State for the $1 \rightleftharpoons 6$ Isomerization ReactionDistances (in Å)

$r(1,2) = 1.518$

$r(1,3) = 2.258$

$r(2,4) = 1.495$

$r(1,5) = 1.074$

$r(2,6) = 1.074$

$r(3,7) = 1.075$

Angles (in degrees)

$\alpha(3,1,2) = 98.7$

$\alpha(4,1,2) = 58.1$

$\alpha(5,1,2) = 124.1$

$\alpha(6,2,1) = 128.0$

$\alpha(7,3,1) = 121.2$

$\alpha(8,4,1) = 113.0$

$\alpha(9,3,1) = 119.7$

$\alpha(10,4,1) = 119.1$

$\omega(3,1,2,4) = -108.4$

$\omega(3,1,2,6) = 12.7$

$\omega(5,1,2,4) = 110.5$

$\omega(5,1,2,6) = 128.0$

$\omega(2,1,3,7) = -105.0$

$\omega(2,1,3,9) = 62.3$

$\omega(3,1,4,8) = -166.5$

$\omega(3,1,4,10) = -26.9$

Figure 1.-Continued

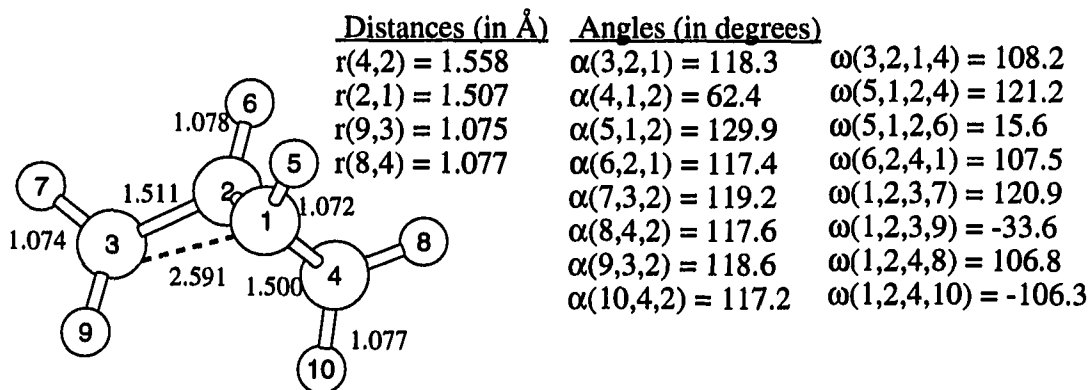
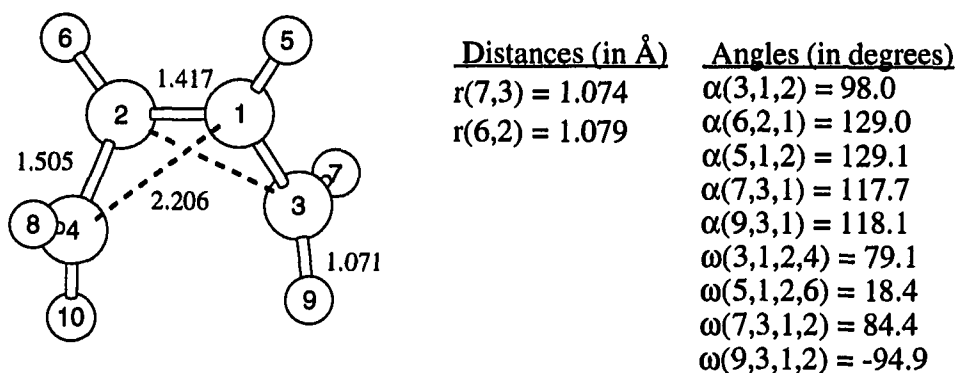
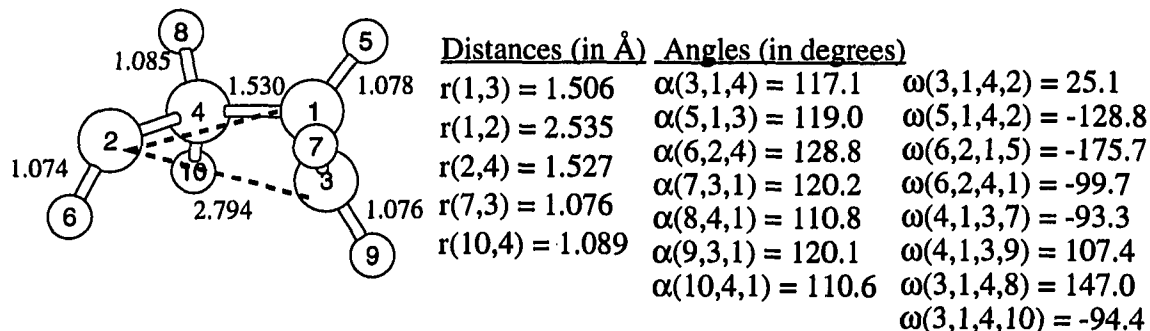
8 (C₁) Concerted Disrotatory Transition state for the 1 ⇌ 6 Isomerization Reaction

9 (C₂) Second Order Stationary Point (two imaginary frequencies)

10 (C₁) Nonconcerted Transition State for the 1 ⇌ 4 ⇌ 6 Isomerization Reaction


Figure 1.-Continued

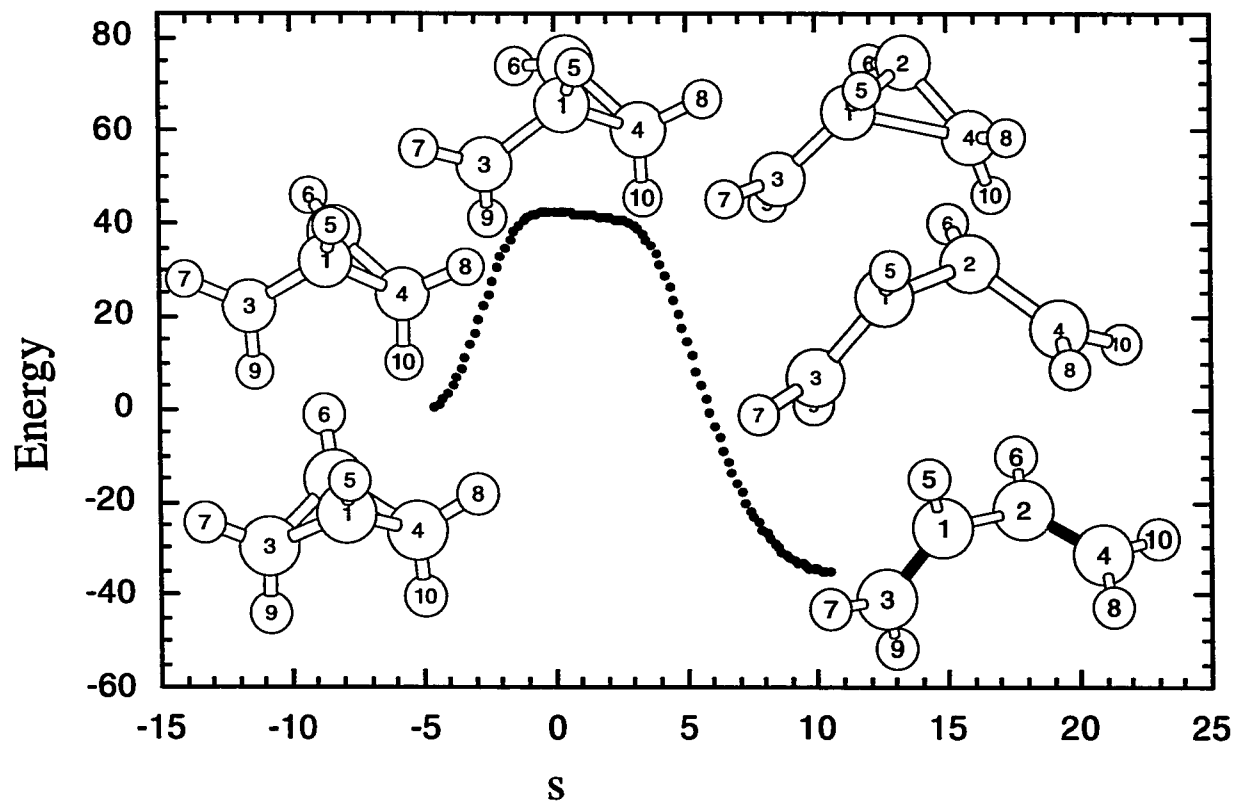


Figure 2. MCSCF(10,10)/6-31G(d) IRC for the bicyclobutane \leftrightarrow gauche-1,3-butadiene reaction; energy in kcal/mol; s in $\text{amu}^{1/2} \cdot \text{bohr}$. The structures displayed along the IRC are of the transition state (top), forward ($s > 0$): point 25, 45 and 64, backward ($s < 0$): point 14 and 28.

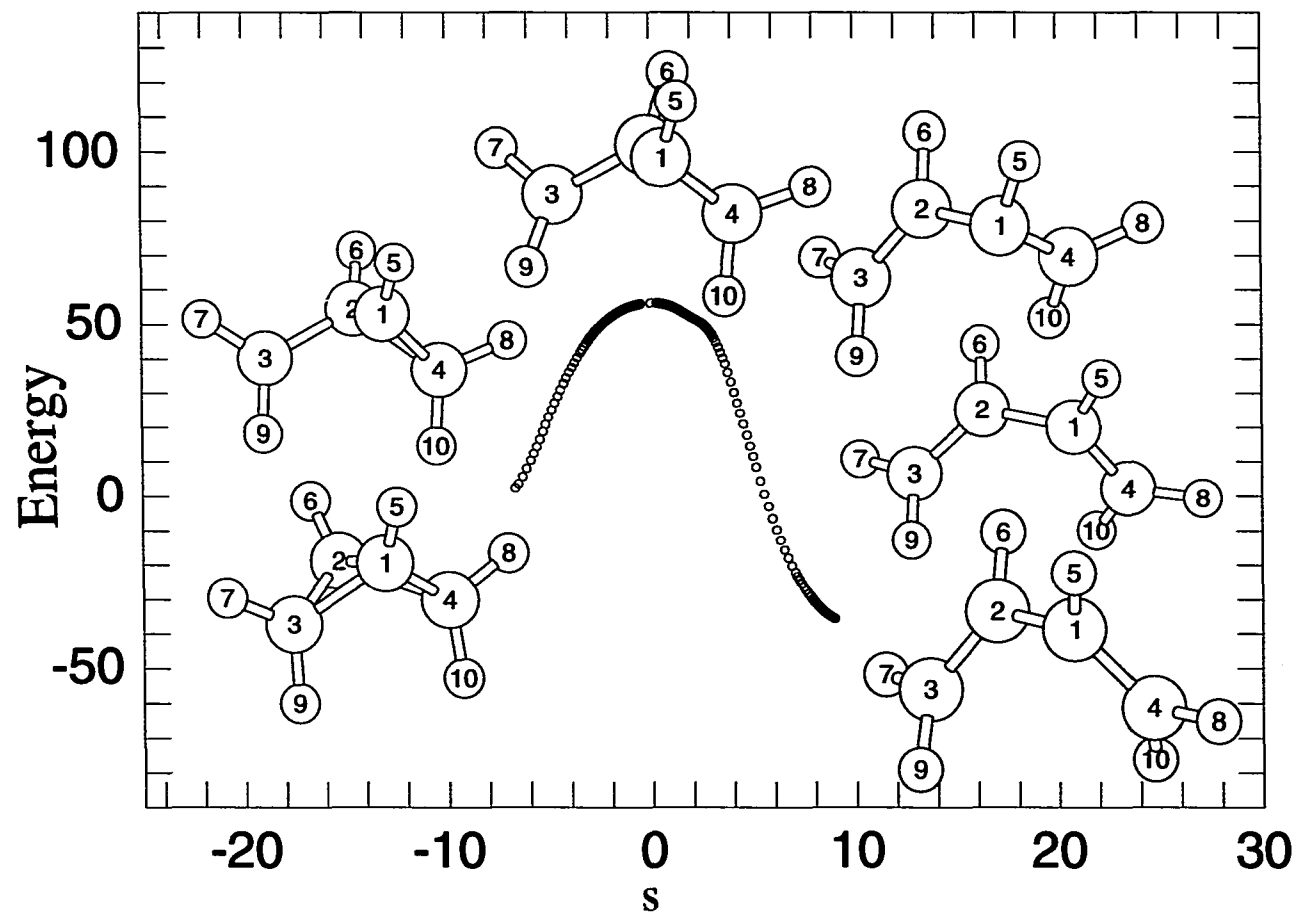


Figure 3. MCSCF(10,10)/6-31G(d) IRC for the bicyclobutane \leftrightarrow *gauche*-1,3-butadiene reaction; energy in kcal/mol; s in $\text{amu}^{1/2} \cdot \text{bohr}$. The structures displayed along the IRC are of the transition state (top), forward ($s > 0$): point 70, 80 and 100, backward ($s < 0$): point 60 and 75.

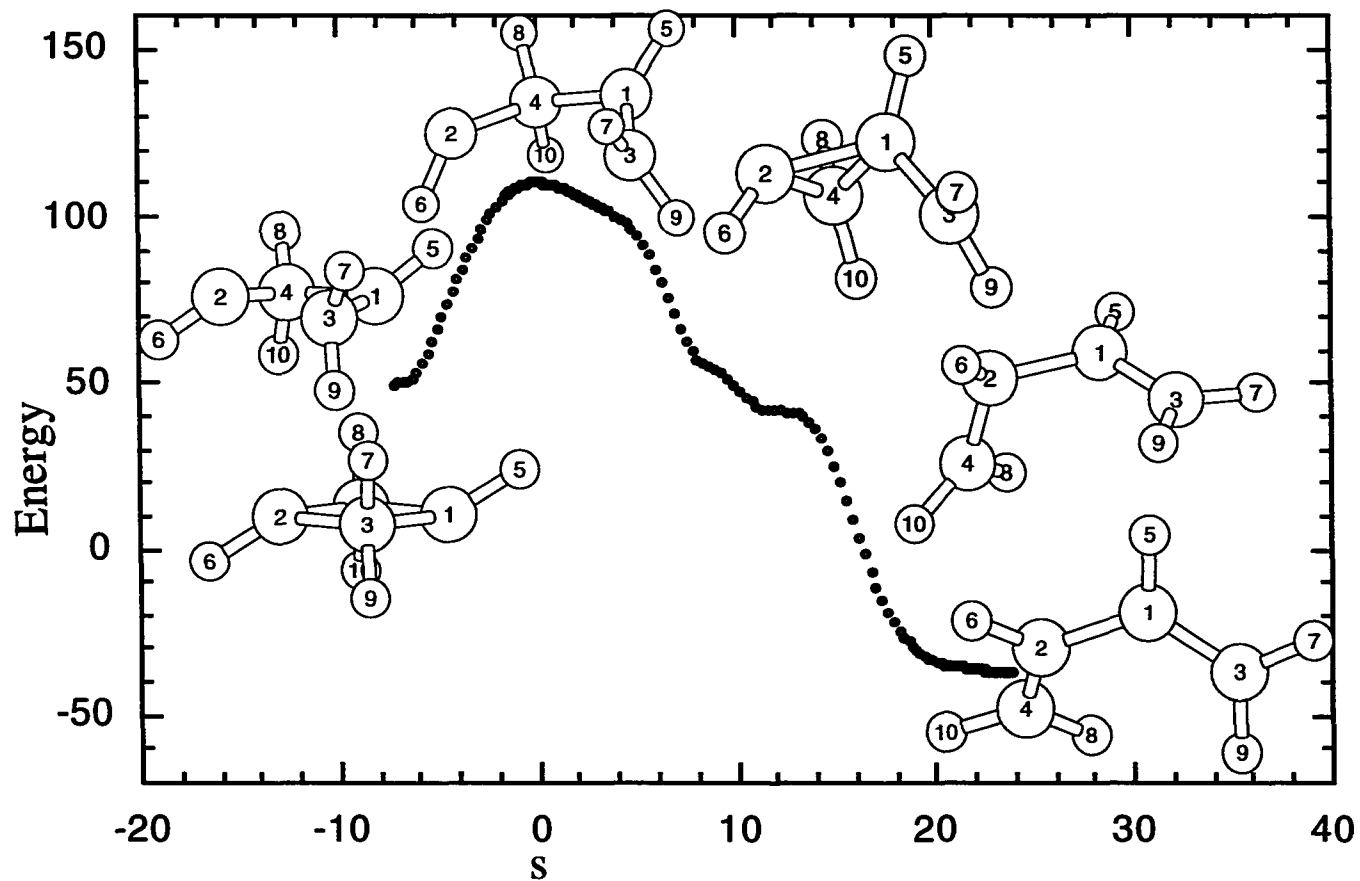


Figure 4. MCSCF(10,10)/6-31G(d) IRC for the bicyclobutane \leftrightarrow gauche-1,3-butadiene reaction; energy in kcal/mol; s in $\text{amu}^{1/2} \cdot \text{bohr}$. The structures displayed along the IRC are of the transition state (top), forward ($s > 0$): point 60, 85 and 122; backward ($s < 0$): point 36 and 43.

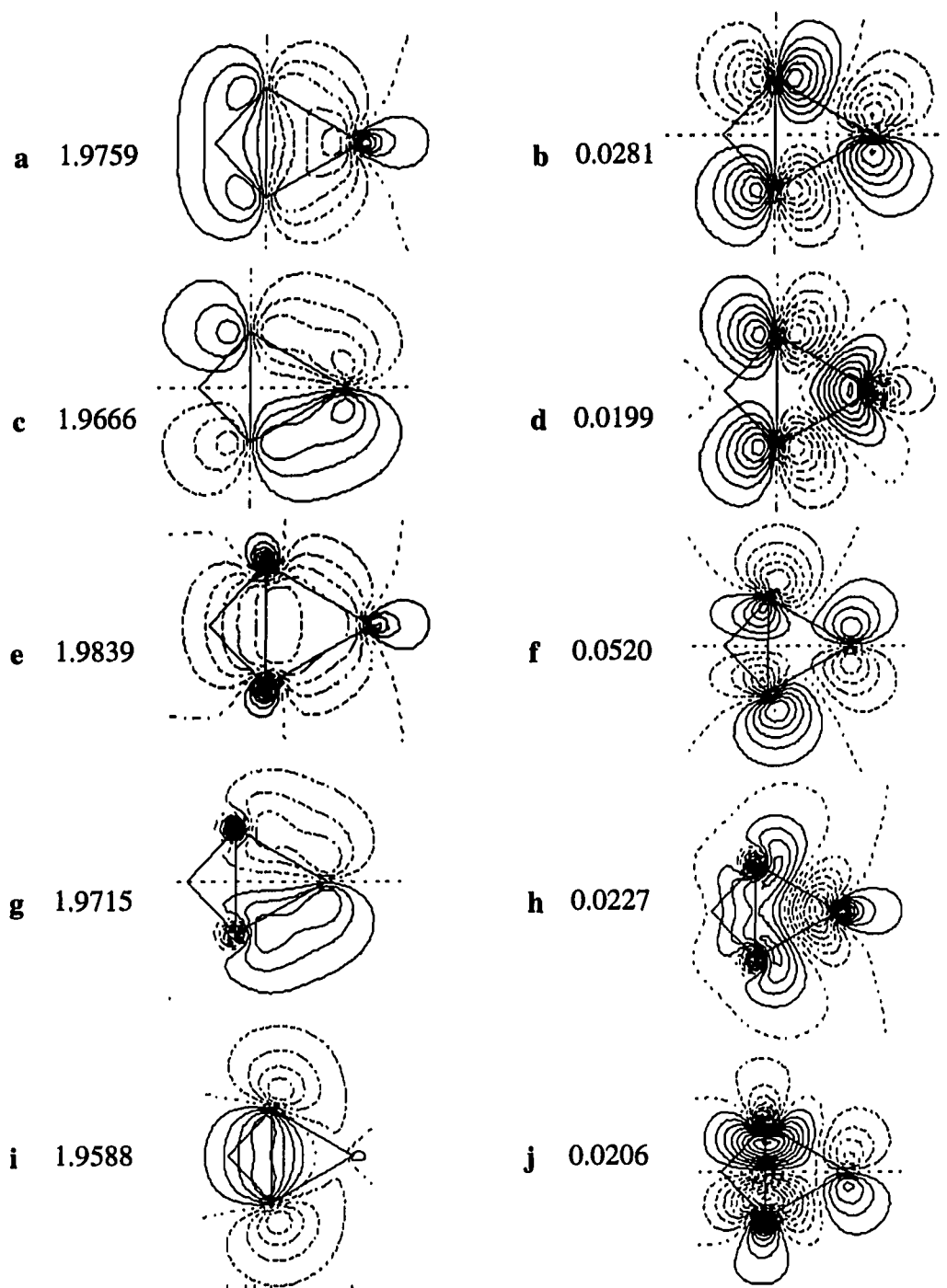


Figure 5. Contour plots of bicyclobutane (**1**) correlated reaction orbitals of the optimized MCSCF(10,10)/6-31G(d) wave function in the planes that are constructed from two bridge head atoms and one of two peripheral atoms (numerical values = occupation numbers).

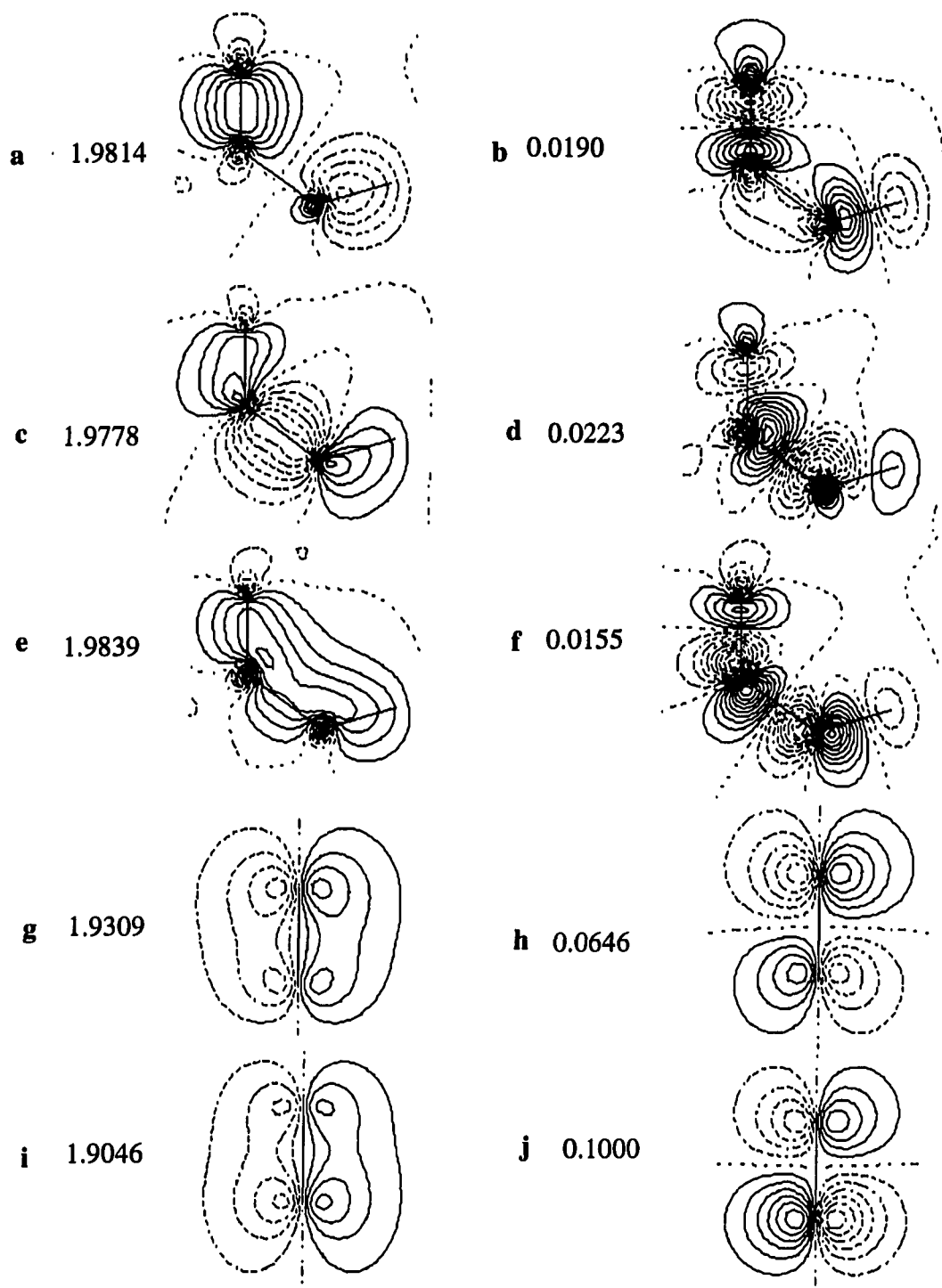


Figure 6. Contour plots of the *gauche*-butadiene (**6**) correlated reaction orbitals of the optimized MCSCF(10,10)/6-31G(d) wave function in the $C_1-C_2-C_3$ plane (a-h) and the planes bisecting $H_{10}-C_4-H_8$ (g-h) and $H_9-C_3-H_7$ (i-j) (numerical values = occupation numbers).

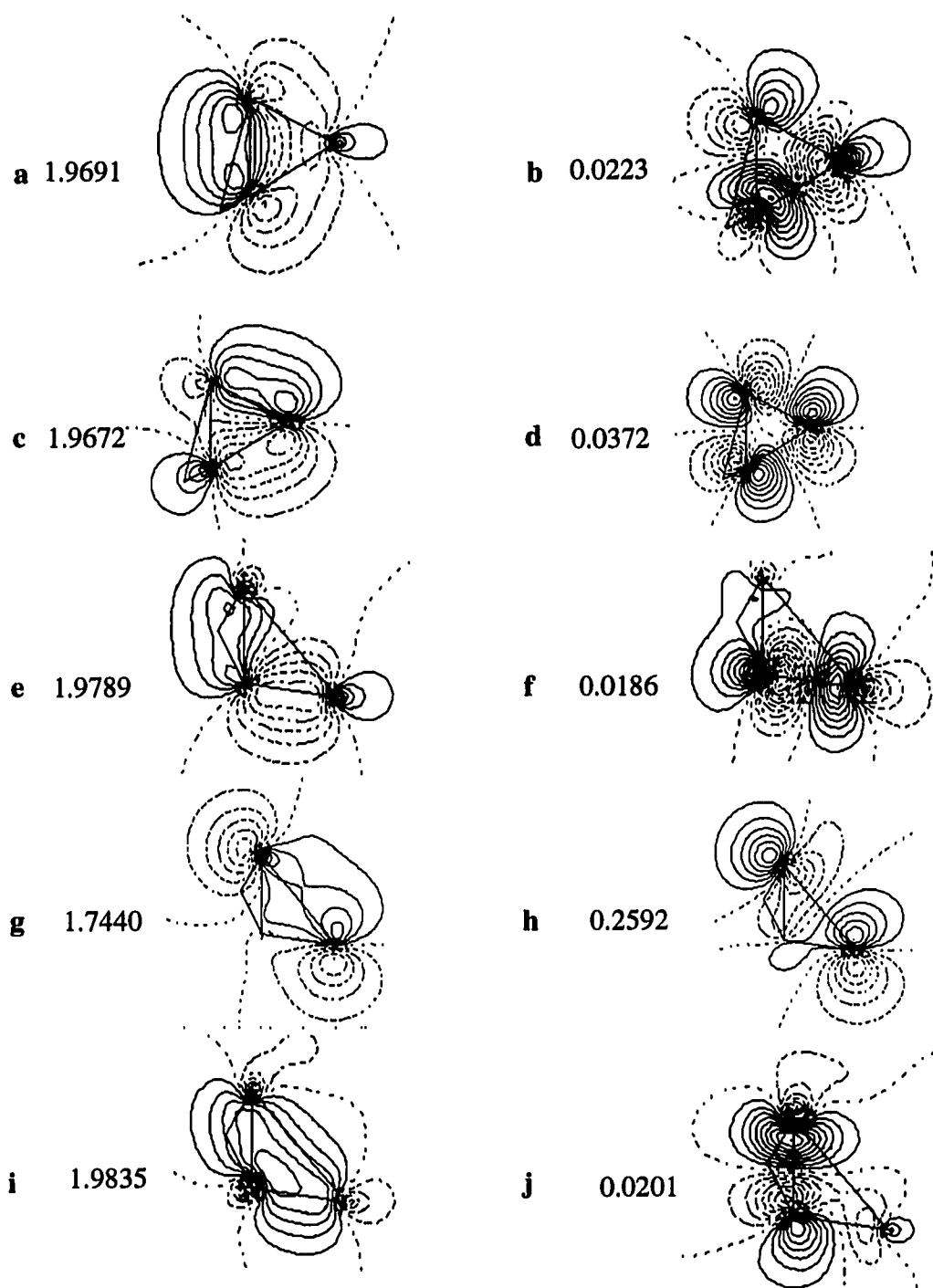


Figure 7. Contour plots of the conrotatory transition state (7) correlated reaction orbitals of the optimized MCSCF(10,10)/6-31G(d) wave function in the planes that are constructed from two bridge head atoms and one of two peripheral atoms, 1-2-4-plane: a-d; 1-2-3-plane: e-j (numerical values = occupation numbers).

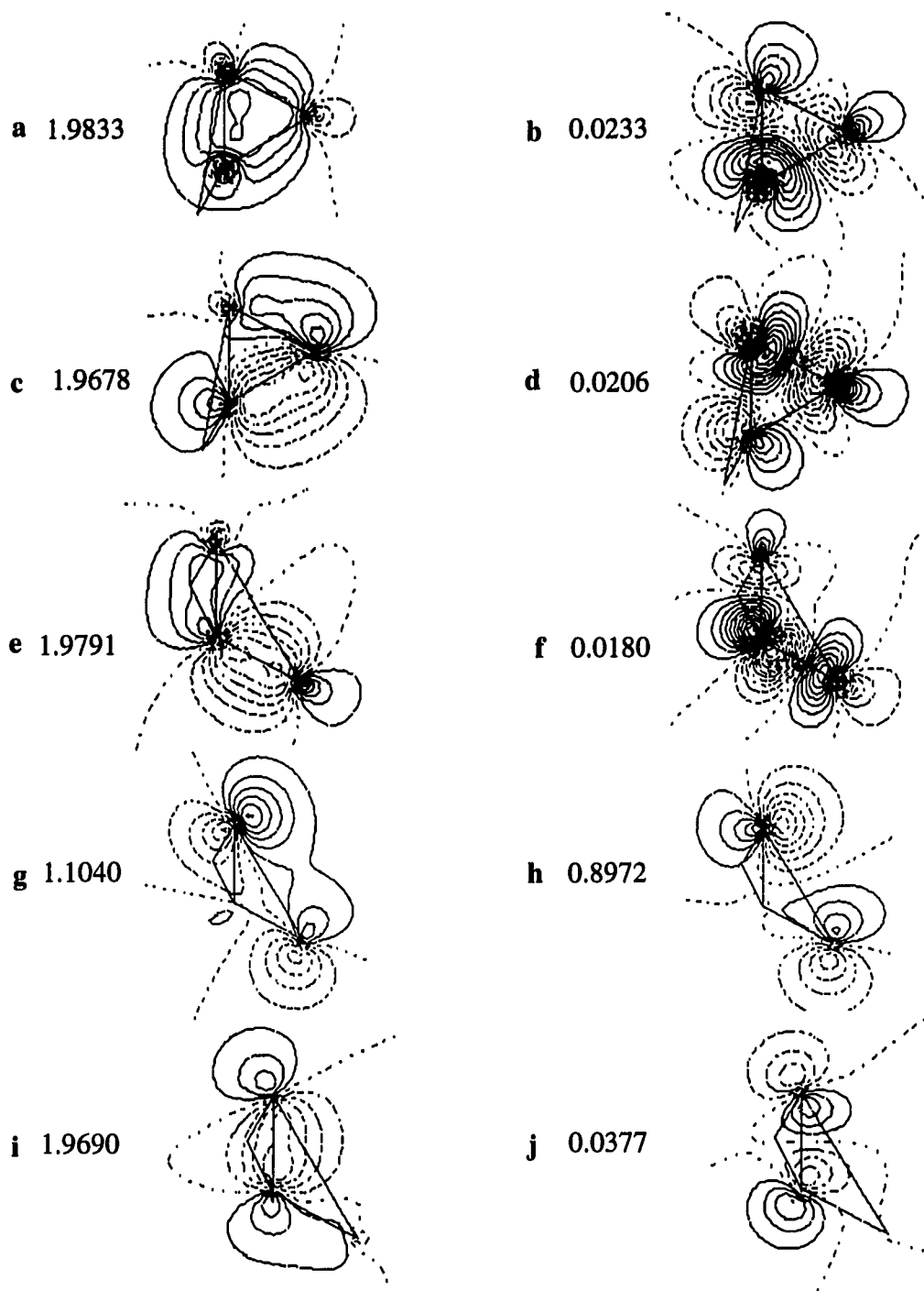


Figure 8. Contour plots of the disrotatory transition state (**8**) correlated reaction orbitals of The optimized MCSCF(10,10)/6-31G(d) wave function in the planes that are constructed from two bridge head atoms and one of two peripheral atoms, 1-2-4-plane: a-d; 1-2-3-plane: e-j (numerical values = occupation numbers).

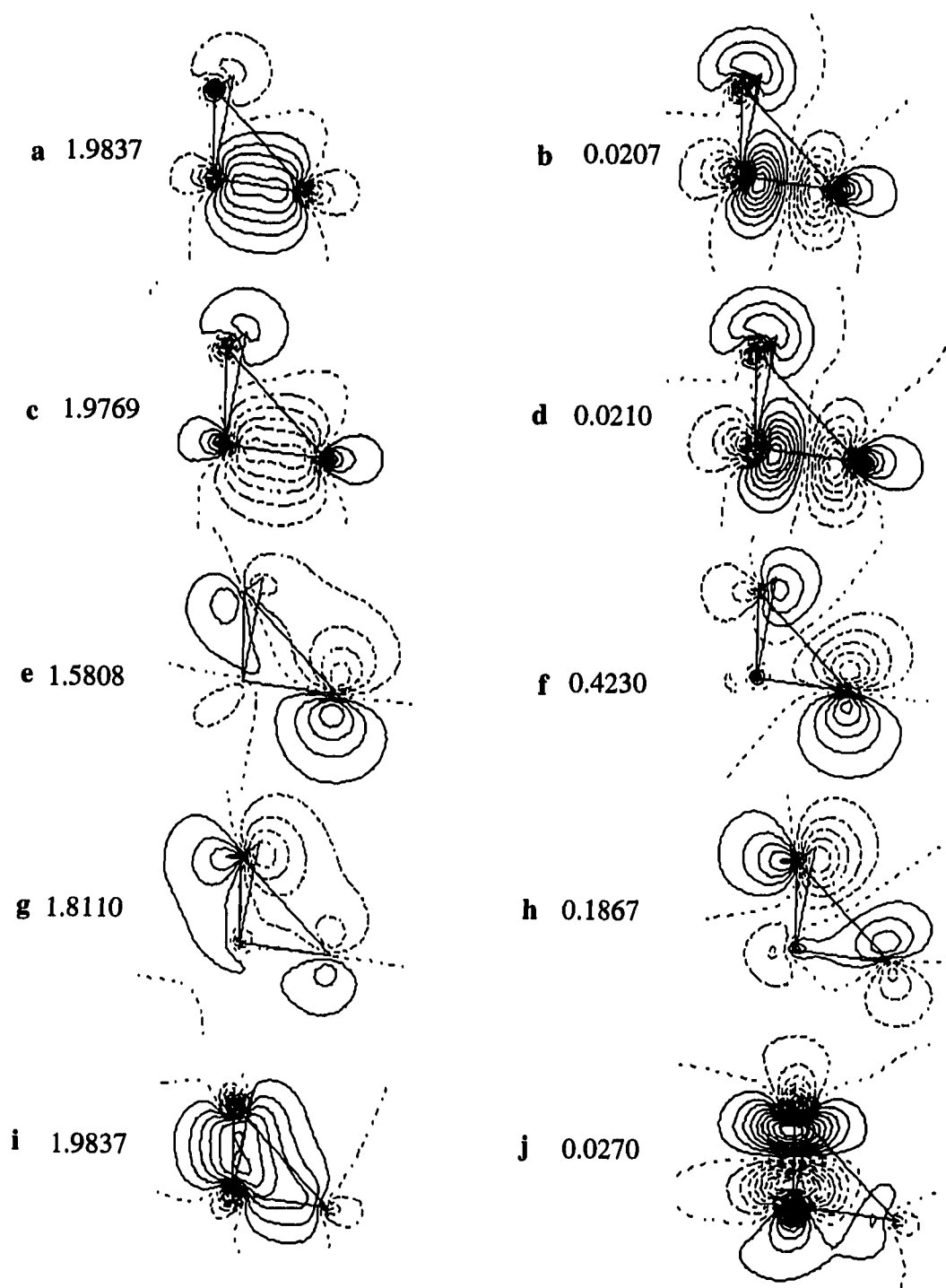


Figure 9. Contour plots of the second order stationary point (9) correlated reaction orbitals of the optimized MCSCF(10,10)/6-31G(d) wave function in the planes that are constructed from two bridge head atoms and one of two peripheral atoms (numerical values = occupation numbers).

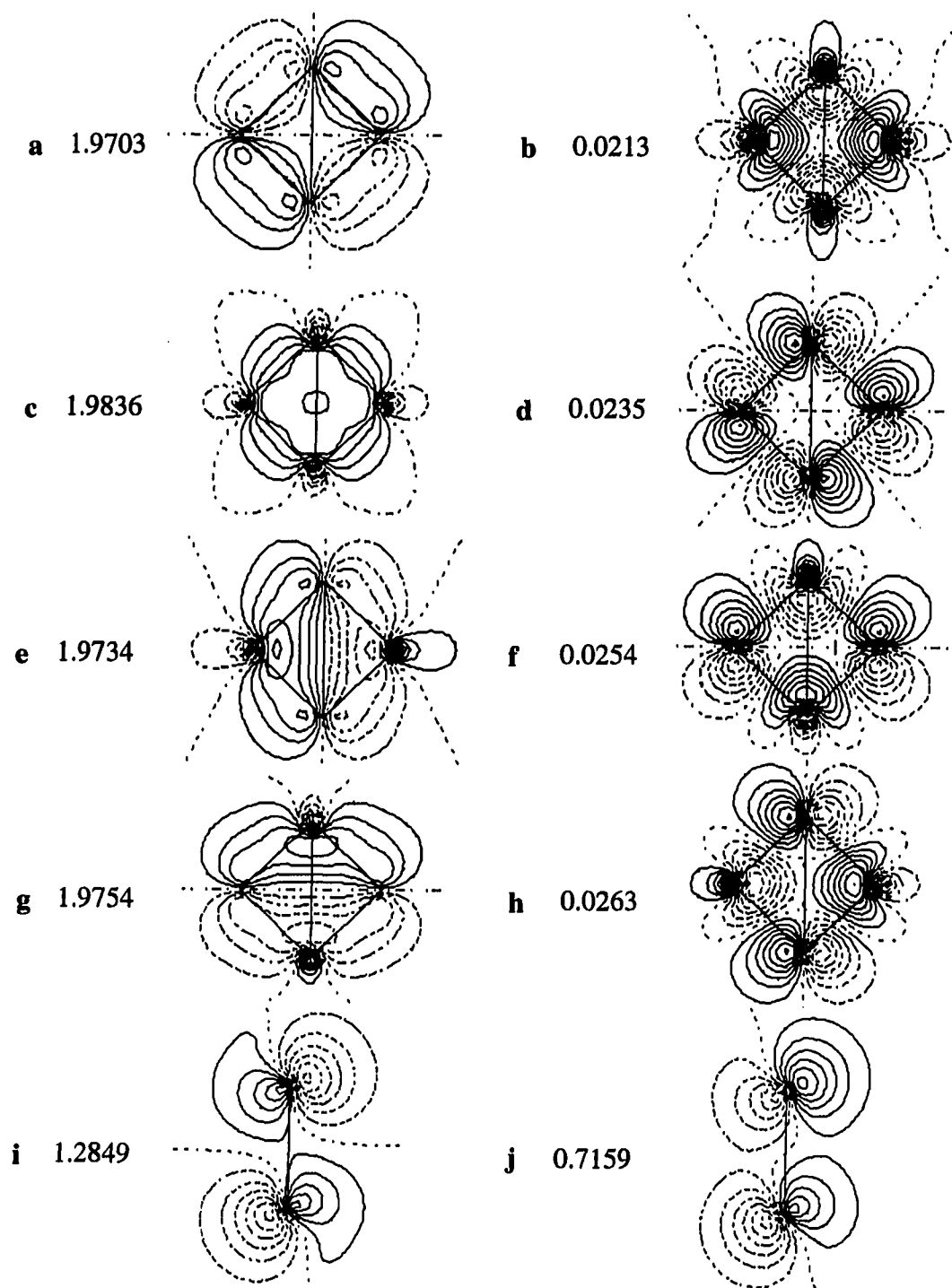


Figure 10. Contour plots of the bicyclobutane bond stretch isomer (**4**) correlated reaction orbitals of the optimized MCSCF(10,10)/6-31G(d) wave function in the YZ (a-h) and $\sigma_h(x,y)$ (i-j) (numerical values= occupation numbers).

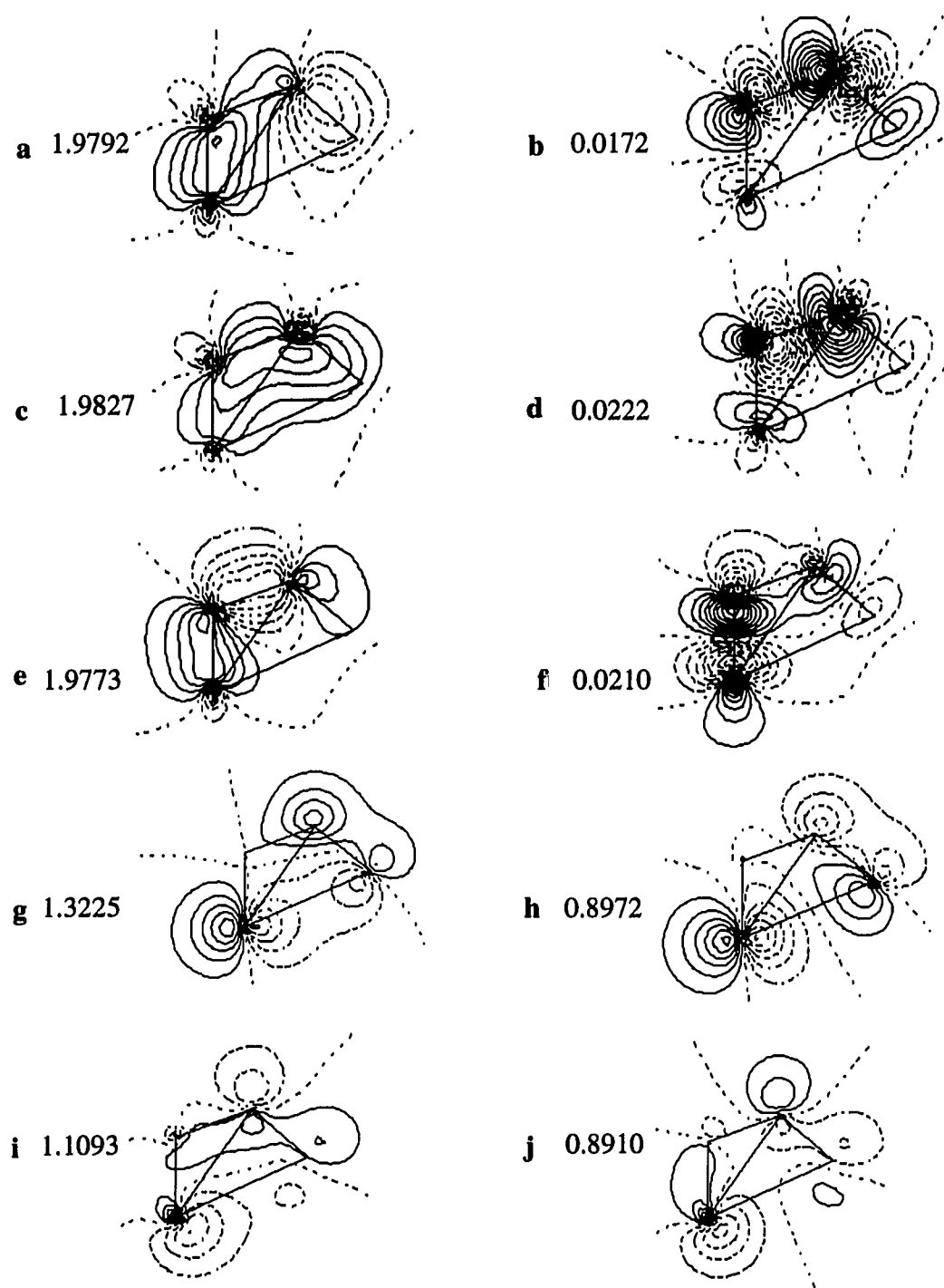


Figure 11. Contour plots of the nonconcerted transition state (**10**) correlated reaction orbitals of the optimized MCSCF(10,10)/6-31G(d) wave function in the planes that are constructed from two bridge head atoms and one of two peripheral atoms, 1-2-4-plane: a-h; 1-2-3-plane: g-j (numerical values = occupation numbers).

**CHAPTER 7. STABILIZATION OF β POSITIVE CHARGE BY SILICON,
GERMANIUM, OR TIN**

A paper published in and reprinted with permission from

Organometallics **1991**, 10, 2798-2803

Copyright 1991 American Chemical Society

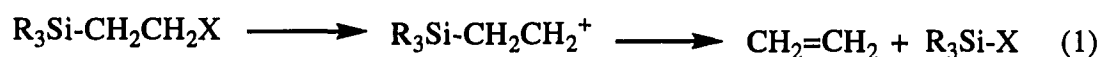
Kiet A. Nguyen, Mark S. Gordon, Gen-tai Wang, and Joseph B. Lambert

Abstract

Ab initio molecular orbital theory is used to study the β effect of carbon, silicon, germanium, or tin on the carbenium ions in $H_2R'M-CH_2-CHR^+$ ($R' = H$, $R = H$ and CH_3). The relative stabilization energies of carbenium ions provided by M ($M = C, Si, Ge,$ and Sn) were determined by calculating the energy change in an isodesmic reaction using MP2/3-21G(d) (at SCF/3-21G* geometries) and MP2/6-31G(d) (at SCF/6-31G(d) geometries) wavefunctions. The magnitude of the β effect is predicted to increase in the order $C < Si < Ge < Sn$. For $R = H$, the nonvertical cyclic structure is favored for the cations, whereas methyl substitution appears to stabilize the vertical acyclic arrangement.

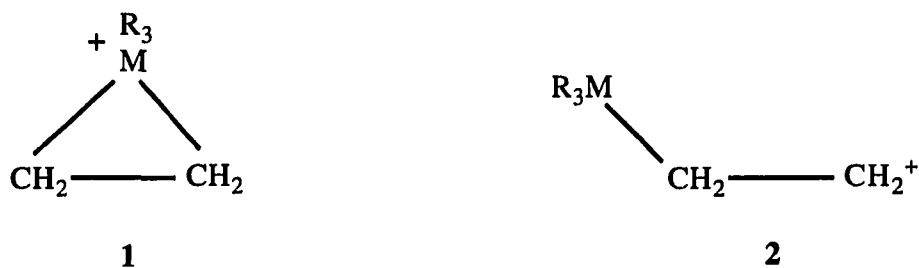
Introduction

In either the liquid or gas phase, a C-Si bond provides a strongly stabilizing interaction with a developing or fully formed empty p orbital at the β position to silicon (Si-C-C⁺).²⁻⁵ The overall reaction is an E₁ elimination (eq #1) formation of



a carbocation by rate-determining loss of the nucleofuge X). Several alternative mechanisms either have been proved to be absent or can be removed from the reaction pathway by suitable choice of conditions. Rate-determining loss of the electrofuge through the Si-C bond cleavage (E_{1cb}) has not been supported by solvent studies. Rate-determining nucleophilic attack of the solvent or a base on silicon (analogous to an E_2 mechanism) or on the C-X bond (S_N2) likewise has been eliminated as a viable alternative because the reaction is independent of solvent nucleophilicity.^{5,6}

The β effect of silicon thus is manifested primarily in an E_1 like mechanism, in which departure of the nucleofuge is rate determining (eq 1). The effect arises because the high polarizability and electropositivity of silicon enable it to stabilize the electron-deficient intermediate. Two modes of stabilization, differing in the geometry of the intermediate, have been considered: (1) The silicon atom moves toward the positive charge and forms a full C-Si bond to the carbon atom from which the nucleofuge departed. The movement may be in concert with this departure, so that the reaction is analogous to neighboring group participation or epoxide formation. The result is the formation of a bridged ion such as **1**

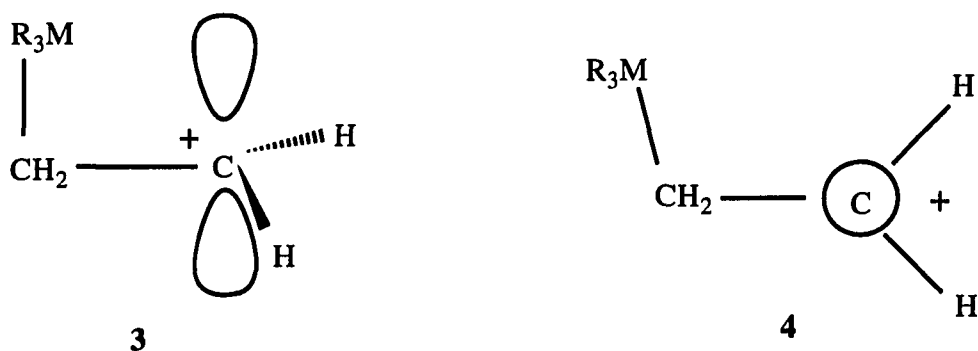


(M = Si). This pathway has been termed *nonvertical* because of the movement of the silicon atom. (2) Full charge develops on carbon, and stabilization of this electron deficiency occurs by hyperconjugation between the highly polarizable C-M bond (M = Si)

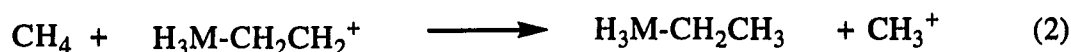
and the empty p orbital (2). This unbridged pathway has been termed *vertical* because stabilization requires little movement of the silicon atom.⁷

Both bridged and unbridged models are consistent with the preponderance of evidence.⁵ The optimal stereochemistry for nonvertical participation involves a 180° dihedral angle between electrofuge and nucleofuge, i. e., the Si-C-C-X unit has the antiperiplanar arrangement. This stereochemistry is required in order to place the internal nucleophile (silicon) backside to the breaking C-X bond during formation of the three-membered ring (1). Likewise, the antiperiplanar geometry is optimal for σ - π conjugation in the nonbridged cation 2, since all the orbitals lie in the same plane and have the optimal relative phases.

Earlier calculations attempted to compare the bridged with the open forms⁸ and the β -silyl with the α -silyl system.⁹ Jorgensen and co-workers¹⁰ carried out calculations on the primary system for three geometries: the bridged form 1 and two versions of the open form 2. In one open form (3) the empty p orbital is parallel to the β M-C bond (M = Si),



and in the other (4) these two orbitals are orthogonal. It is expected that full hyperconjugation could occur in 3 but not in 4. The β effect was assessed by calculation of the energy change of the isodesmic reaction (eq 2, M = Si) at the



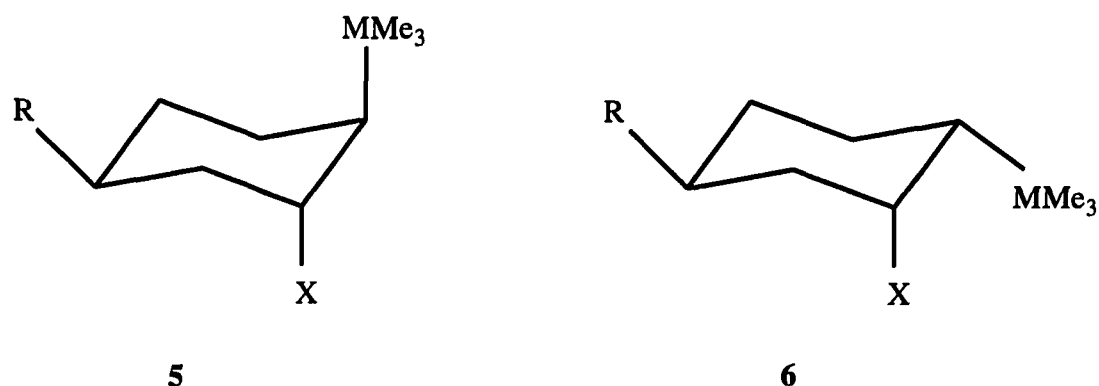
MP3/6-31G(d)//SCF/3-21G* level for the three geometries. The cyclic form (**1**, R = H) had the largest stabilization in this comparison to CH_3^+ (74.4 kcal mol⁻¹), followed closely by the parallel structure **3** (72.0 kcal mol⁻¹), and distantly by the orthogonal form **4** (42.4 kcal mol⁻¹). The parallel open form was not a minimum but was transformed into the slightly more stable bridged form on geometry optimization. Hyperconjugative overlap in the parallel open form **3** is improved by geometric distortions from the neutral parent or from the orthogonal form. The C-C bond is shorter in **3** (1.360 Å) than that in **4** (1.443 Å), and the Si-C-C angle is smaller (94.3° vs 119.6°). Thus, the Si leans toward the empty p orbital.

A measure of the β effect was obtained by comparing the energy of $\text{H}_3\text{Si-CH}_2\text{CH}_2^+$ with that of $\text{H-CH}_2\text{CH}_2^+$. For the parallel geometry, the silicon system is 38 kcal mol⁻¹ more stable (a measure of all interactions), and for the orthogonal geometry, the silicon system is only 8.9 kcal mol⁻¹ more stable (a measure of angle-independent contributions such as induction).

Ibrahim and Jorgensen¹¹ carried out similar calculations at the MP2/6-31G(d)//SCF/6-31G(d) level for secondary and tertiary systems, in order to assess the effect of substitution at carbon. The secondary β effect was estimated by comparison of $\text{SiH}_3\text{-CH}_2\text{-C}^+\text{HCH}_3$ with $\text{H-CH}_2\text{C}^+\text{HCH}_3$. The open parallel form analogous to **3** was found to have a β effect of 22.1 kcal mol⁻¹ compared with 18.2 kcal mol⁻¹ for the bridged form and 38 kcal mol⁻¹ for the parallel primary system. The primary system has higher electron demand, so that stabilization is greater. Furthermore, in the secondary case the bridged form is not an energy minimum but relaxes to the open form. However, force

constant matrices were not diagonalized in references 10 or 11 to verify the existence of minima.

No calculations have previously been carried out for the β effect in germanium or tin systems, but a few experimental results have been reported.^{12,13} The cyclohexane framework offers two stereochemical relationships between the electrofugal metal (M) and the nucleofuge (X). The diaxial arrangement in the 1,2-trans isomer **5** is antiperiplanar and hence is optimal for either vertical or nonvertical participation.



The cis isomer **6** offers the gauche arrangement between groups, in which only a diminished vertical participation is possible. Experimental measurements of the rates of solvolysis of these compounds for silicon (R = H), germanium (R = H), and tin (R = H for cis and trans but also R = *tert*-butyl for trans) were carried out by Lambert et al.^{12,13} Rate ratios were calculated for the trifluoroacetate in 97% trifluoroethanol at 25.0°C, compared with 1.0 for cyclohexyl. In the cis series (R = H), the rate acceleration was observed to be 3.3×10^4 for Si, 4.6×10^5 for Ge, and 1.3×10^{11} for Sn. In the trans series (R = H), the rate accelerations were 5.7×10^9 for Si, 1.0×10^{11} for Ge, and $\gg 10^{14}$ for Sn.

In the present study, calculations of geometries and energies of carbocations carrying β germanium or tin, as well as carbon and silicon ($\text{H}_2\text{R}'\text{M}-\text{CH}_2\text{CHR}^+$, R = H and

CH₃), are being carried out in order to assess these very substantial differences within the Group IV series. Two questions are of prime interest in this study. (1) How is the stabilization of positive charge affected as M varies from C to Sn? (2) How does the presence of bulky substituents (in this case methyl groups) affect the relative stabilities of **1** vs **2**?

Computational Methods

All structures were optimized using analytical energy gradients with the 3-21G* basis set¹⁴ at the SCF level of theory¹⁵ (SCF/3-21G*). For M = C and Si, the larger 6-31G(d) basis set¹⁶ was also incorporated when locating optimal structures for these compounds. This level of theory has been shown to give good agreement with experiment for complex species, such as pentastanna[1.1.1]propellane.¹⁷ Single point correlation corrections were done with the 6-31G(d) basis for C and Si, and 3-21G(d) for Ge and Sn, using the second (MP2) order many body perturbation theory formulated by Pople and co-workers.¹⁸ The 3-21G(d) basis set adds a set of d functions to each C, whereas 3-21G* omits these functions. For M = C and Si, only valence electrons were correlated. MP2 single point corrections were also carried out with the 6-31G(d) basis set at SCF/6-31G(d) optimized geometries (MP2/6-31G(d)//SCF/6-31G(d)) for M = C and Si. Minima were identified by diagonalizing the force constant matrices (hessians) to verify that they are positive definite. The energy change (ΔE) for the isodesmic reaction¹⁹ (eq 2, with M = C, Si, Ge, and Sn) was used to assess the β effect for both the bridged (**1**) form (nonvertical pathway) and two open (vertical pathway) forms (**3** and **4**). Stabilization energies upon methyl substitution were also determined by the isodesmic reactions **3** and **4** for M = C and Si.



Ab initio electronic structure calculations were performed using the GAMESS²⁰ and GAUSSIAN86²¹ quantum chemistry programs.

Results and Discussion

The structures of $\text{H}_3\text{M}-\text{CH}_2-\text{CHR}^+$ cations and their neutral counterparts are shown in Figures 1-4. Three geometrical systems, bridged form **1**, open form **3** (empty p orbital is parallel to the β M-C bond), and open form **4** (orbitals are orthogonal), were fully optimized for $\text{R} = \text{H}$ and $\text{M} = \text{C}, \text{Si}, \text{Ge},$ and Sn at the SCF/3-21G* level of theory. The results are shown in Figures 1, 3, and 4. The structures of an open form with C_s symmetry and an unrestricted C_1 form for $\text{R} = \text{CH}_3$, $\text{M} = \text{C}, \text{Si}$ are given in Figures 5 and 6.

Consider first the predicted structures for the species $\text{H}_3\text{MCH}_2\text{CH}_2^+$ ($\text{M} = \text{C}, \text{Si}, \text{Ge}, \text{Sn}$). If a nonvertical pathway is defined as one having a C-Si bond formation to stabilize the electron-deficient intermediate, these can occur via the bridged and parallel structures in Figures 1 and 3. In all cases, both parallel (**3**) and bridged (**1**) structures are almost identical in energy (see Table I and II). Geometrically, both **1** and **3** consist of a cyclic complex between MH_3^+ ($\text{M} = \text{C}, \text{Si}, \text{Ge},$ or Sn) and ethylene. At the SCF/3-21G* level of theory, parallel (**3**) forms of $\text{M} = \text{C}$ and Si are verified minima. The larger basis set 6-31G(d), however, predicts the bridged form to be the minimum structure for $\text{M} = \text{Si}$. The bridged forms are the most favorable SCF/3-21G* configurations for Ge and Sn .

The calculated total energies and zero point vibrational energies of all species are given in Table I. For both vertical and nonvertical pathways, MP2/3-21G(d)//SCF/3-21G* and SCF/3-21G*//SCF/3-21G* stabilization energies of the $\text{H}_3\text{MCH}_2\text{CH}_2^+$ ($\text{M} = \text{C}, \text{Si}, \text{Ge}$

and Sn) cations compared to CH_3^+ in the isodesmic reaction (eq 2) are provided in Table IIa; the MP2/6-31G(d)//SCF/6-31G(d) and SCF/6-31G(d)//6-31G(d) values are in Table IIb (for M = C and Si). The stabilization energies of methyl substituted $\text{H}_3\text{M}-\text{CH}_2\text{CH}^+\text{Me}$ cations, obtained from reactions 3 and 4, are reported in Table IIIa,b. A larger value for ΔE indicates a greater stabilization energy: The corresponding substituent is better able to stabilize the positive charge. These stabilization energies increase substantially upon the addition of correlation corrections, except for the high-lying orthogonal structures.

Turning to the energetics for reaction 2, the MP2/3-21G(d)//SCF/3-21G* stabilization energies (Table IIa) increase from 48 to 69 to 77 to 89 kcal mol⁻¹, upon proceeding vertically in group IV from C to Sn, where the most stable structure is used as reference in each case. For C and Si, increasing the basis set to 6-31G(d) has little effect on the relative stabilization energies (see Table IIb), or on the relative energies of the open and bridged forms.

Jorgensen and co-workers,¹⁰ with SCF calculations on the $\text{H}_3\text{MCH}_2\text{CH}_2^+$ (M = C, Si) systems with the 3-21G* basis set (Si d exponent = 0.45) reported the following: (a) for M = C, the parallel form **3** is lower in energy compared to the orthogonal form **4**; (b) for M = Si, the bridged form **1** and the parallel form **3** were almost identical in energy; however single point MP2/6-31G(d)//SCF/3-21G* calculations favored the bridged structure by 2.4 kcal mol⁻¹. MP2/6-31G(d)//SCF/3-21G* stabilization energies of 49.0 and 70.0 kcal mol⁻¹, obtained from reaction 2 were predicted for the parallel form **3** of C and the bridged form **1** for Si. These findings are in agreement with the results given in Table IIb.

Placing the methyl group on the positively charged carbon could preferentially stabilize the acyclic structure due to steric hinderance. For M = C (Figure 5), the acyclic structure with C₁ symmetry (**5b**) is the lowest in energy on both the SCF/3-21G* and the

SCF/6-31G(d) potential energy surfaces. In this C_1 structure, one CH_3^+ -C bond lengthens by 0.45 Å and the other shortens by 0.1 Å when the methyl group is added (cf. Figure 3 (3a)), as predicted at the SCF/6-31G(d) level of theory. Compared to the planar C_s structure, the C_1 structure is 1.5 kcal mol⁻¹ lower at the MP2/6-31G(d)//6-31G(d) level (cf. Table IIIa). For M = Si, the SCF/6-31G(d) distance between the positively charged carbon and silicon increases by 0.32 Å when the methyl group is added (cf. Figures 5 (5d) and 3 (3b)) to form the C_1 structure. This C_1 configuration (5d) is 17.2 kcal mol⁻¹ (19.9 kcal mol⁻¹) lower than C_s configuration (5c) at the MP2/6-31G(d)//SCF/6-31G(d) (MP2/3-21G(d)//SCF/3-21G*) level of theory (see Table IIIa). The stabilization energies of the C_1 configurations of $H_3MCH_2CH^+Me$ (M = C, Si) (5b and 5d) compared to CH_3^+ , using reaction (3), increase to 63 kcal mol⁻¹ for C and to 80 kcal mol⁻¹ for Si at the MP2/6-31G(d)//SCF/6-31G(d) level of theory, so both stabilization energies increase about 10 kcal mol⁻¹ upon methyl substitution. Thus, methyl substitution at the positively charged carbon provides a constant stabilization energy while the β effect increases in energy upon going from C to Si. A comparison of the C_1 configuration of $H_3MCH_2CH^+Me$ (M = C, Si) energetics with a secondary cation $CH_3CH^+CH_3$ in eq 4 using the MP2/6-31G(d)//SCF/6-31G(d) wavefunction, also gives a 17 kcal mol⁻¹ increase in stability upon going from C (3.4 kcal mol⁻¹) to Si (20.6 kcal mol⁻¹) (see Table IIIb).

Calculations of the bridged structures with a methyl group replacing a hydrogen at the M position were also carried out using both SCF/3-21G* and SCF/6-31G(d) wavefunctions. For M = Si, this cyclic structure (Figure 6. (6b)) is a minimum on the potential energy surface. Energetically, 6b is 28.3 kcal mol⁻¹ above the C_1 structure (5d) at the MP2/6-31G(d)//SCF/6-31G(d) level. Thus, methyl substitution substantially stabilizes the open (vertical) form relative to the unsubstituted parent compound. For M = C, the cyclic form is a transition state at both 6-31G(d) and 3-21G* levels, with imaginary

frequencies of 91.8i and 98.7i cm^{-1} , respectively. Germanium and tin are expected to behave similarly to silicon. These calculations were omitted in the interest of conserving computational resources.

Conclusion

An investigation of the β effect of group IV elements, including the first such calculations on germanium and tin, on the carbenium ion $\text{H}_3\text{MCH}_2\text{CHR}^+$ ($\text{R} = \text{H}$ and CH_3) has shown that the thermodynamics of this effect are consistent with the observed kinetics, although the trend is not as dramatic. This suggests that the nature of the transition state(s) for reaction 1 as a function of M also plays an important role. The magnitude of the β effect is predicted to increase steadily upon going from C to Sn in group IV. The nonvertical cyclic configuration (**1**) with C_s symmetry is the most favorable one for $\text{R} = \text{H}$. Methyl substitution, however, appears to stabilize the vertical acyclic form with C_1 symmetry, and one expects other hydrocarbon substituents to behave similarly to methyl. For carbon and silicon, increasing the basis set from 3-21G* to 6-31G(d), has little effect on the relative stabilization energies, but correlation corrections have a considerable effect.

Acknowledgment

This work was supported by the National Science Foundation (Grant No. CHEM-8910841 to Northwestern University and Grant No. CHEM89-11911 to North Dakota State University) and by the Donors of the Petroleum Research Fund administered by the American Chemical Society, and by the Air Force Office of Scientific Research (90-0050). These calculations were performed in part on the North Dakota State University IBM 3090 (aided by a joint study agreement with IBM) and on the NDSU Quantum Chemistry VAX 8530 (funded by a grant from the Air Force Office of Scientific Research).

References

- (1) (a) North Dakota State University. (b) Northwestern University.
- (2) Ushakov, S. N.; Itenberg, A. M. *Zh. Obshch. Khim.* **1937**, 7, 2495.
- (3) Sommer, L. H.; Whitmore, F. C. *J. Am. Chem. Soc.* **1946**, 68, 485.
- (4) Sommer, L. H.; Dorfman, E.; Goldberg, G. M.; Whitmore, F. C. *J. Am. Chem. Soc.* **1946**, 68, 488.
- (5) For a comprehensive review, see: Lambert, J. B. *Tetrahedron* **1990**, 46, 2677.
- (6) Lambert, J. B.; Wang, G.-t.; Finzel, R. B.; Teramura, D. H. *J. Am. Chem. Soc.* **1987**, 109, 7838.
- (7) Hanstein, W.; Berwin, H. J.; Traylor, T. G. *J. Am. Chem. Soc.* **1970**, 92, 829.
- (8) Eabron, C.; Feichtmayr, F.; Horn, M.; Murrell, J. N. *J. Organomet. Chem.* **1974**, 77, 39.
- (9) Apeloig, Y.; Karni, M.; Stanger, A.; Schwarz, H.; Drewello, R.; Czekay, G. *J. Chem. Soc., Chem. Commun.* **1987**, 989.
- (10) Wierschke, S. G.; Chandrasekhar, J.; Jorgensen, W. L. *J. Am. Chem. Soc.* **1985**, 107, 1496.
- (11) Ibrahim, M. R.; Jorgensen, W. L. *J. Am. Chem. Soc.* **1989**, 111, 819.
- (12) Lambert, J. B.; Wang, G.-t. *Tetrahedron Lett.* **1988**, 29, 2551.
- (13) Lambert, J. B.; Wang, G.-t.; Teramura, D. H. *J. Org. Chem.* **1988**, 53, 5422.
- (14) Binkley, J. S.; Pople, J. A.; Hehre, W. J. *J. Am. Chem. Soc.* **1980**, 102, 939.
- (15) Roothan, C. C. *J. Rev. Mod. Phys.* **1951**, 23, 69.
- (16) (a) Hariharan, P. C.; Pople, J. A. *Theoret. Chim. Act.* **1973**, 28, 213. (b) Francl, M. M.; Pietro, W. J.; Hehre, W. J.; Binkley, J. S.; Gordon, M. S.; DeFrees, J. D.; Pople, J. A. *J. Chem. Phys.* **1982**, 77, 3654.
- (17) Gordon, M. S.; Nguyen, K. A.; Carroll, M. T. *Polyhedron*, in press.

- (18) (a) Møller, C.; Plesset, M. S. *Phys. Rev.* **1934**, 46, 618. (b) Pople, J. A.; Binkley, J. S.; Seeger, R. *Int. J. Quantum Chem. Symp.* **1976**, 10, 1. (c) Pople, J. A.; Seeger, R.; Krishnan, R. *Int. J. Quantum Chem. Symp.* **1977**, 11, 149. (d) Krishnan, R.; Pople, J. A. *Int. J. Quantum Chem.* **1978**, 14, 91. (e) Krishnan, R.; Frisch, M. J.; Pople, J. A. *J. Chem. Phys.* **1980**, 72, 4244.
- (19) Hehre, W. J.; Ditchfield, R.; Random, L.; Pople, J. A. *J. Am. Chem. Soc.* **1970**, 92, 4796.
- (20) (a) Dupuis, M.; Spangler, D.; Wendoloski, J. J. *National Resource for Computational in Chemistry Software Catalog*; University California, Berkley, CA, 1980, Prog. QG01. (b) Schmidt, M. W.; Boatz, J. A.; Baldrige, K. K.; Koseki, S.; Gordon, M. S.; Elbert, S. T.; Lam, B. *QCPE Bulletin*, **1978**, 7, 115.
- (21) GAUSSIAN86: Frisch, M. J.; Binkley, J. S.; Schlegel, H. B.; Ragahvachari, K.; Melius, C. F.; Kahn, L. R.; DeFrees, D. J.; Seeger, R.; Whiteside, R. A.; Rohlfing, C. M.; Fox, D. J.; Fleuder, E. M.; Pople, J. A. Carnegie-Mellon Quantum Chemistry Publishing Unit, Pittsburgh, PA 1984.

Table Ia. Total energies (au) of $\text{H}_3\text{MCH}_2\text{CH}_2^+$, CH_3^+ , $\text{H}_3\text{MCH}_2\text{CH}_3$, and CH_4 (M=C, Si, Ge, and Sn).

Molecule	SCF/3-21G*//SCF/3-21G*	MP2/3-21G(d)//SCF/3-21G*	Zero-Point Energy ^d
$\text{H}_3\text{CCH}_2\text{CH}_2^+$ (1a)	-116.70535	-117.17936	60.7
$\text{H}_3\text{CCH}_2\text{CH}_2^+$ (3a)	-116.70533	-117.17513	60.7 ^b
$\text{H}_3\text{CCH}_2\text{CH}_2^+$ (4a)	-116.69731	-117.15963	59.3
$\text{H}_3\text{SiCH}_2\text{CH}_2^+$ (1b)	-366.54943	-366.94272	52.7 ^a
$\text{H}_3\text{SiCH}_2\text{CH}_2^+$ (3b)	-366.54993	-366.93968	52.7 ^b
$\text{H}_3\text{SiCH}_2\text{CH}_2^+$ (4b)	-366.51144	-366.88900	50.3
$\text{H}_3\text{GeCH}_2\text{CH}_2^+$ (1c)	-2144.60238	-2145.01138	51.7 ^b
$\text{H}_3\text{GeCH}_2\text{CH}_2^+$ (3c)	-2144.60227	-2145.01118	51.6
$\text{H}_3\text{GeCH}_2\text{CH}_2^+$ (4c)	-2144.54899	-2144.94488	48.8
$\text{H}_3\text{SnCH}_2\text{CH}_2^+$ (1d)	-6075.84007	-6076.26042	49.3 ^b
$\text{H}_3\text{SnCH}_2\text{CH}_2^+$ (3d)	-6075.84002	-6076.26042	49.3
$\text{H}_3\text{SnCH}_2\text{CH}_2^+$ (4d)	-6075.77081	-6076.17916	46.2 ^c
CH_3^+	-39.00913	-39.13771	20.8 ^b
$\text{H}_3\text{CCH}_2\text{CH}_3$ (2a)	-117.61330	-118.10362	69.6 ^b
$\text{H}_3\text{SiCH}_2\text{CH}_3$ (2b)	-367.43059	-367.83605	60.5 ^b
$\text{H}_3\text{GeCH}_2\text{CH}_3$ (2c)	-2145.46612	-2145.89046	59.0 ^b
$\text{H}_3\text{SnCH}_2\text{CH}_3$ (2d)	-6076.68413	-6077.12061	56.7 ^b
CH_4	-39.97688	-40.14319	30.1 ^b

^aBecomes positive definite at the SCF/6-31G(d) level of theory.

^bPositive definite force-field; others have one imaginary frequency.

^cTwo imaginary frequencies

^dZero-point energies (kcal mol^{-1}) calculated at the SCF/3-21G*//SCF/3-21G* level.

Table Ib. Total energies (au) of $\text{H}_3\text{MCH}_2\text{CH}_2^+$, $\text{H}_3\text{MCH}_2\text{CH}_3$ (M=C and Si), CH_3^+ , and CH_4 , optimized at SCF/6-31G(d).

Molecule	SCF/6-31G(d)//SCF/6-31G(d)	MP2/6-31G(d)//SCF/6-31G(d)	Zero-Point Energy ^d
$\text{H}_3\text{CCH}_2\text{CH}_2^+$ (1a)	-117.35917	-117.73738	61.2
$\text{H}_3\text{CCH}_2\text{CH}_2^+$ (3a)	-117.35941	-117.73756	61.3 ^b
$\text{H}_3\text{SiCH}_2\text{CH}_2^+$ (1b)	-368.42800	-368.75295	52.9 ^b
$\text{H}_3\text{SiCH}_2\text{CH}_2^+$ (3b)	-368.42782	-368.75264	52.8
$\text{H}_3\text{CCH}_2\text{CH}_3$ (2a)	-118.26365	-118.65997	69.4 ^b
$\text{H}_3\text{SiCH}_2\text{CH}_3$ (2b)	-369.30209	-369.64672	60.3 ^b
CH_3^+	-39.23064	-39.32515	21.2 ^b
CH_4	-40.19517	-40.33245	30.0 ^b

^bPositive definite force-field; others have one imaginary frequency.

^dZero-point energies (kcal mol^{-1}) calculated at the SCF/6-31G(d)//SCF/6-31G(d) level.

Table Ic. Total energies (au) of $\text{H}_3\text{MCH}_2\text{CH}^+\text{Me}$, $\text{H}_3\text{MCH}_2\text{CH}_2\text{Me}$ (M=C and Si), and $\text{CH}_3\text{CH}^+\text{CH}_3$, optimized at SCF/3-21G*.

Molecule	SCF	MP2	Zero-Point Energy ^d
	3-21G*//SCF/3-21G*	3-21G(d)//SCF/3-21G*	
$\text{H}_3\text{CCH}_2\text{CH}^+\text{Me}$ (5a)	-155.54916	-156.17687	78.6
$\text{H}_3\text{CCH}_2\text{CH}^+\text{Me}$ (5b)	-155.55302	-156.18141	79.6b
$\text{H}_3\text{SiCH}_2\text{CH}^+\text{Me}$ (5c)	-405.36312	-405.90638	69.4
$\text{H}_3\text{SiCH}_2\text{CH}^+\text{Me}$ (5d)	-405.39063	-405.94140	71.5
$\text{H}_2\text{MeCCH}_2\text{CH}_2^+$ (6a)	-155.53123	-155.88873	80.1 ^b
$\text{H}_2\text{MeSiCH}_2\text{CH}_2^+$ (6b)	-405.39859	-405.74305	72.3
$\text{H}_3\text{CCH}_2\text{CH}_2\text{Me}$ (1e)	-156.43247	-157.08578	88.8b
$\text{H}_3\text{SiCH}_2\text{CH}_2\text{Me}$ (1f)	-406.25018	-406.81905	79.7b
$\text{CH}_3\text{CH}^+\text{CH}_3$	-116.72644	-117.19191	59.6b

b Positive definite force-field; others have one imaginary frequency.

d Zero-point energies (kcal mol⁻¹) calculated at the SCF/3-21G*//SCF/3-21G* level.

Table Id. Total energies (au) of $\text{HMCH}_2\text{CH}^+\text{Me}$, $\text{H}_3\text{MCH}_2\text{CH}_2\text{Me}$ ($\text{M} = \text{C}$ and Si), and $\text{CH}_3\text{CH}^+\text{CH}_3$, optimized at SCF/6-31G(d)

Molecule	SCF/6-31G(d)//SCF/6-31G(d)	MP2/6-31G(d)//SCF/6-31G(d)	Zero-Point Energy ^d
$\text{H}_3\text{CCH}_2\text{CH}^+\text{Me}$ (5a)	-156.41912	-156.91356	78.5
$\text{H}_3\text{CCH}_2\text{CH}^+\text{Me}$ (5b)	-156.42062	-156.91776	79.6 ^b
$\text{H}_3\text{SiCH}_2\text{CH}^+\text{Me}$ (5c)	-407.45535	-407.89784	69.3
$\text{H}_3\text{SiCH}_2\text{CH}^+\text{Me}$ (5d)	-407.48127	-407.93406	71.4 ^b
$\text{H}_2\text{MeCCH}_2\text{CH}_2^+$ (6a)	-156.39853	-156.90811	80.5
$\text{H}_2\text{MeSiCH}_2\text{CH}_2^+$ (6b)	-407.47259	-407.88895	72.5
$\text{H}_3\text{CCH}_2\text{CH}_2\text{Me}$ (1e)	-157.29841	-157.82553	88.6 ^b
$\text{H}_3\text{SiCH}_2\text{CH}_2\text{Me}$ (1f)	-408.33717	-408.81301	79.5 ^b
$\text{CH}_3\text{CH}^+\text{CH}_3$	-117.38116	-117.74550	59.6 ^b

^bPositive definite force-field; others have one imaginary frequency.

^dZero-point energies calculated at the SCF/6-31G^{*}//SCF/6-31G^{*}, are in kcal mol⁻¹.

Table II. Energy differences (in kcal mol⁻¹, zero point correction included) for the isodesmic reaction (2).

(a) M = C, Si, Ge, and Sn

Molecule	SCF	MP2	no. of imag freq
	6-31G(d)//SCF/6-31G(d)	6-31G(d)//SCF/6-31G(d)	
H ₃ CCH ₂ CH ₂ ⁺ (1a)	37.1	50.6	1
H ₃ CCH ₂ CH ₂ ⁺ (3a)	37.1	47.9	0
H ₃ CCH ₂ CH ₂ ⁺ (4a)	33.5	39.6	1
H ₃ SiCH ₂ CH ₂ ⁺ (1b)	52.8	68.9 ^a	1
H ₃ SiCH ₂ CH ₂ ⁺ (3b)	53.1	67.0	0
H ₃ SiCH ₂ CH ₂ ⁺ (4b)	31.4	37.9	1
H ₃ GeCH ₂ CH ₂ ⁺ (1c)	63.3	77.3	0
H ₃ GeCH ₂ CH ₂ ⁺ (3c)	63.3	77.3	1
H ₃ GeCH ₂ CH ₂ ⁺ (4c)	32.7	38.5	1
H ₃ SnCH ₂ CH ₂ ⁺ (1d)	75.7	89.3	0
H ₃ SnCH ₂ CH ₂ ⁺ (3d)	75.7	89.3	1
H ₃ SnCH ₂ CH ₂ ⁺ (3d)	35.4	41.4	2

(b) M = C and Si

Molecule	SCF	MP2	no. of imag freq
	6-31G(d)//SCF/6-31G(d)	6-31G(d)//SCF/6-31G(d)	
H ₃ CCH ₂ CH ₂ ⁺ (1a)	37.1	52.6	1
H ₃ CCH ₂ CH ₂ ⁺ (3a)	37.1	52.6	0
H ₃ SiCH ₂ CH ₂ ⁺ (1b)	53.3	69.9	0
H ₃ SiCH ₂ CH ₂ ⁺ (3b)	53.3	69.8	1

^a Becomes positive definite at the SCF/6-31G(d) level of theory.

Table III. Energy differences (in kcal mol⁻¹, zero point correction included)

(a) Isodesmic reaction (3) with M=C and Si.

Molecule	SCF		MP2	
	3-21G*//	6-31G(d)//	3-21G(d)//	6-31G(d)//
	SCF/3-21G*	SCF/6-31G(d)	SCF/3-21G*	SCF/6-31G(d)
H ₃ CCH ₂ CH ⁺ Me (5a)	53.9	61.5	54.8	61.1
H ₃ CCH ₂ CH ⁺ Me (5b)	55.3	63.3 ^b	54.6 ^b	62.7 ^b
H ₃ SiCH ₂ CH ⁺ Me (5c)	51.6	59.2	53.3	59.3
H ₃ SiCH ₂ CH ⁺ Me (5d)	66.8	79.1 ^b	67.4 ^b	79.8 ^b

(b) Isodesmic reaction (4) with M=C and Si.

Molecule	SCF		MP2	
	3-21G*//	6-31G(d)//	3-21G(d)//	6-31G(d)//
	SCF/3-21G*	SCF/6-31G(d)	SCF/3-21G*	SCF/6-31G(d)
H ₃ CCH ₂ CH ⁺ Me (5a)	2.4	2.3	2.0	1.9
H ₃ CCH ₂ CH ⁺ Me (5b)	3.8	2.1 ^b	3.8 ^b	3.4 ^b
H ₃ SiCH ₂ CH ⁺ Me (5c)	0.2	1.1	-0.3	0.3
H ₃ SiCH ₂ CH ⁺ Me (5d)	15.3	15.0 ^b	19.6 ^b	20.6 ^b

^bPositive definite force-field; others have one imaginary frequency.

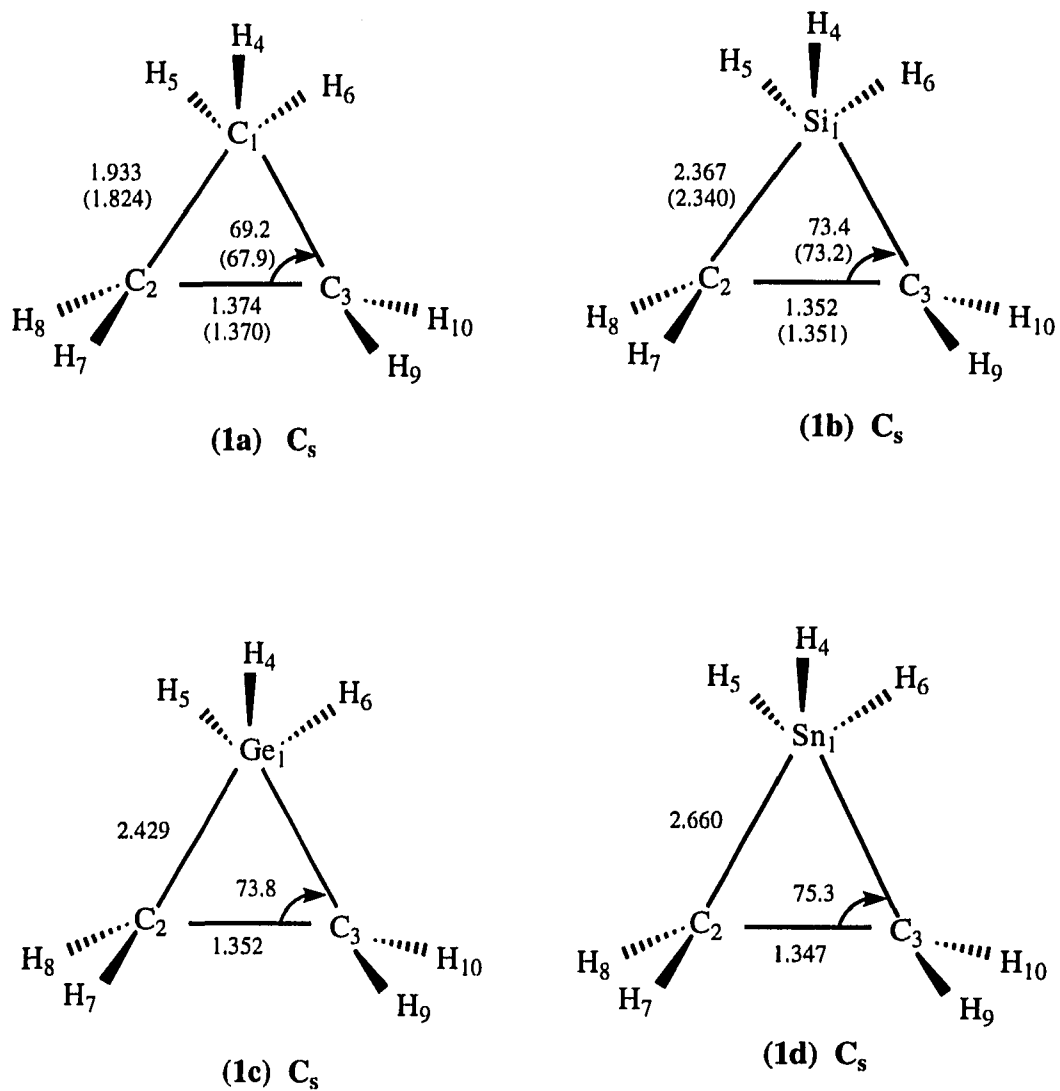


Figure 1. SCF/3-21G* structures of bridged (1) $H_3MCH_2CH_2^+$ ($M = C, Si, Ge, Sn$); SCF/6-31G(d) values are in parentheses; bond lengths are in angstroms; angles are in degrees.

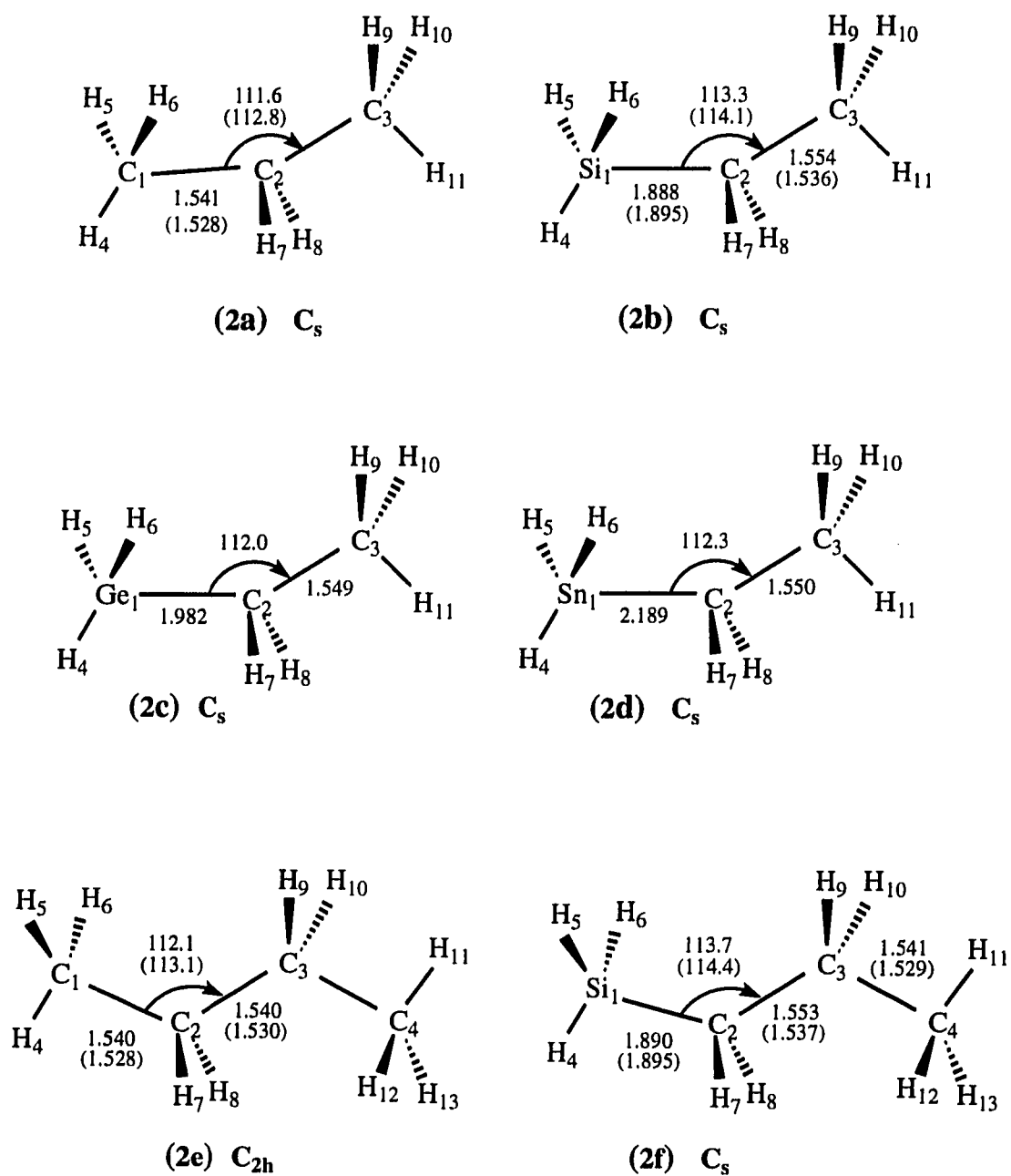


Figure 2. SCF/3-21G* structures of neutral species; SCF/6-31G(d) values are in parentheses; bond lengths are in angstroms, angles are in degrees.

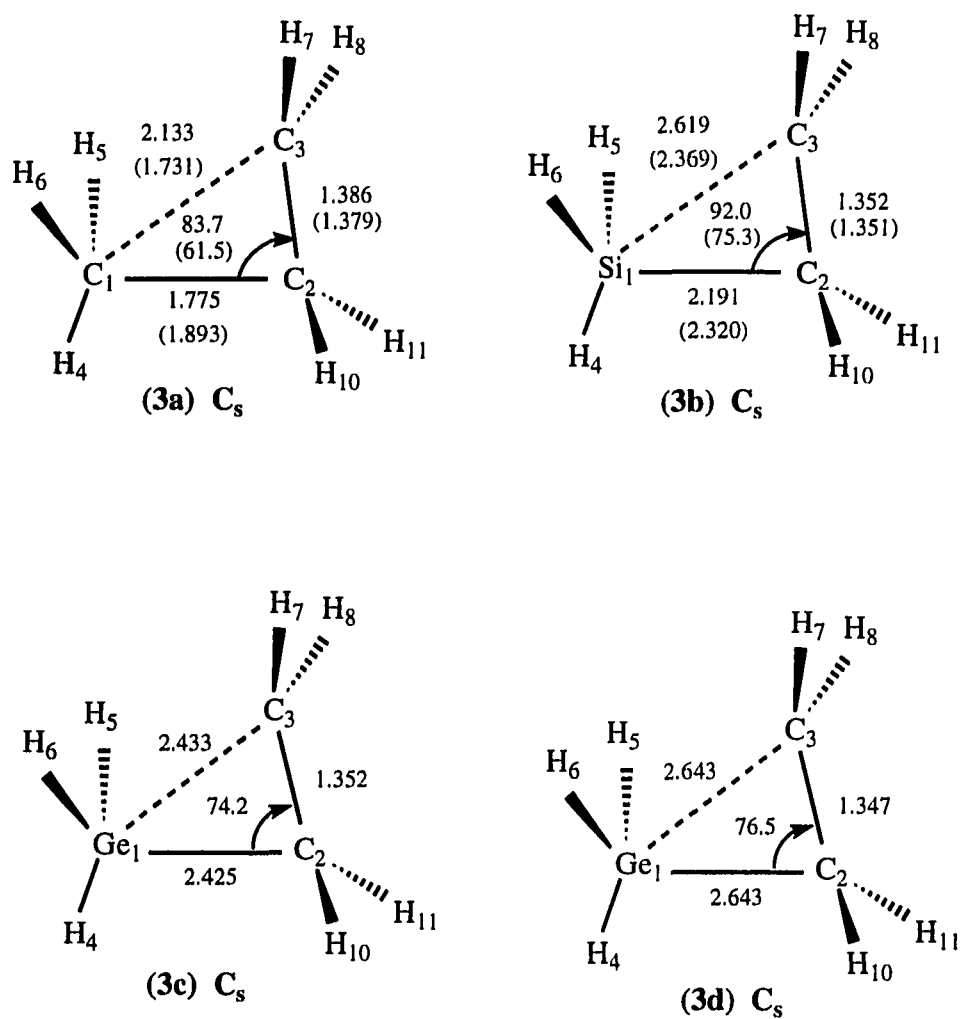


Figure 3. SCF/3-21G* structures of parallel (3) $H_3MCH_2CH_2^+$ ($M = C, Si, Ge, Sn$); bond lengths are in angstroms, angles are in degrees; SCF/6-31G(d) values are in parentheses.

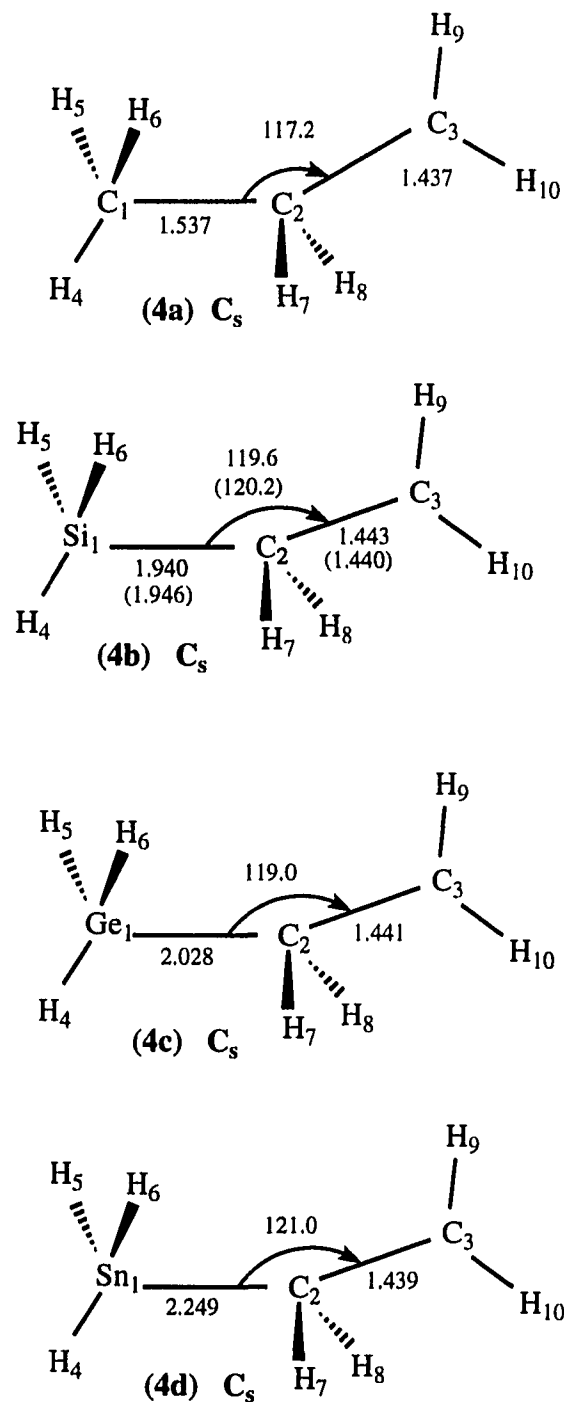


Figure 4. SCF/3-21G * structures of orthogonal (4) $H_3MCH_2CH_2^+$ ($M=C, Si, Ge, Sn$); bond lengths are in angstroms; angles are in degrees; SCF/6-31G(d) values are in parentheses.

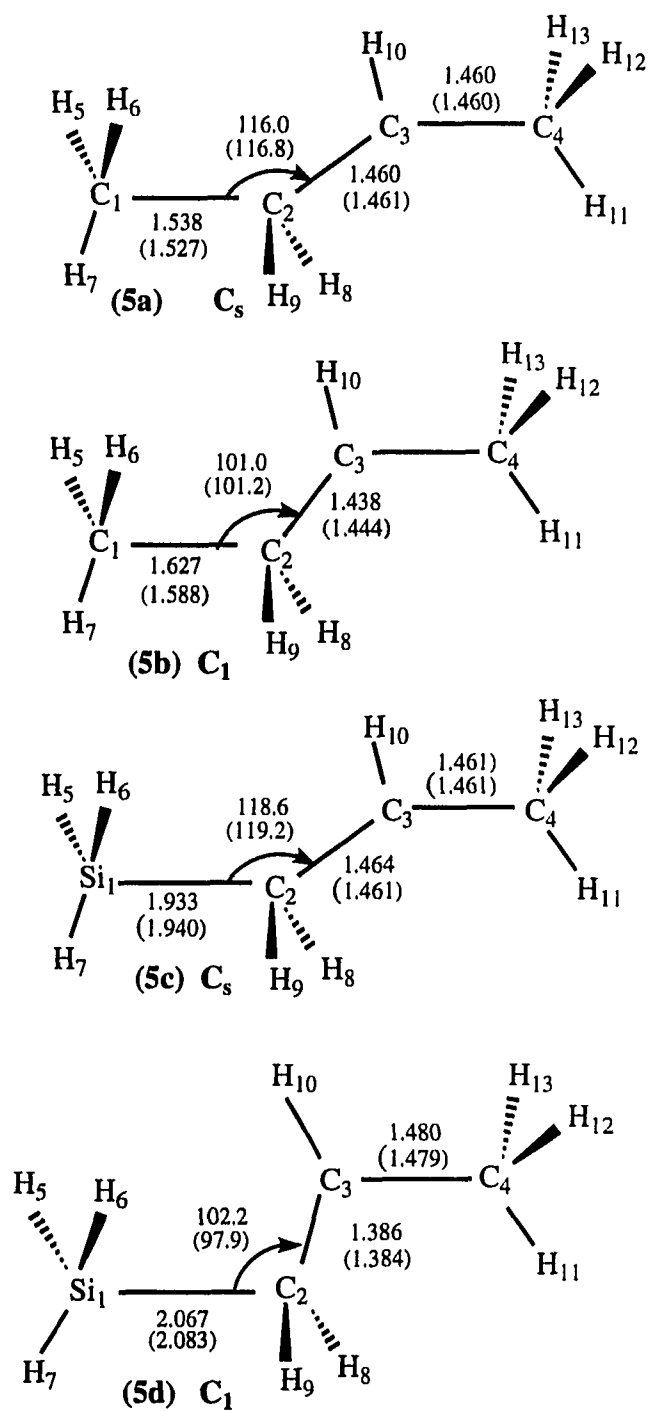


Figure 5. SCF/3-21G* structures of $H_3MCH_2CH^+CH_3$ ($M = C, Si$). SCF/6-31G(d) values are in parentheses; bond lengths are in angstroms; angles are in degrees. (c) $R(1,3) = 2.368$ (2.345); (d) $R(1,3) = 2.722$ (2.655).

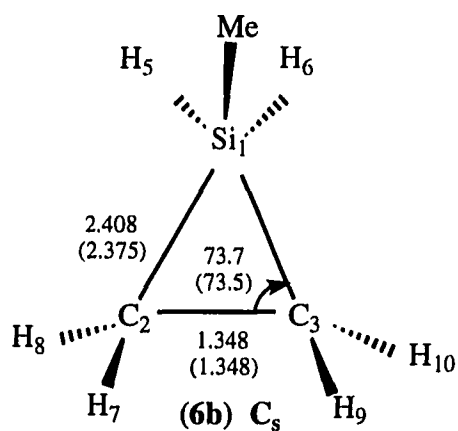
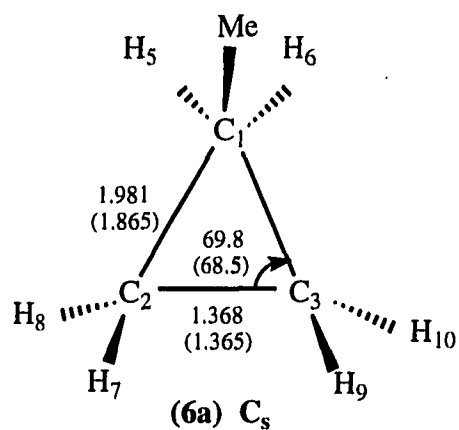


Figure 6. SCF/3-21G^{*} structures of bridged (1) $\text{MeH}_2\text{MCH}_2\text{CH}_2^+$ ($\text{M} = \text{C}, \text{Si}$); SCF/6-31G(d) values are in parentheses; bond lengths are in angstroms; angles are in degrees.

CHAPTER 8. MECHANISMS AND ENERGETICS OF THE REACTION OF Si⁺ WITH CH₃-SiH₃

A paper submitted to Journal of Physical Chemistry

Kiet A. Nguyen, Mark S. Gordon, and Krishnan Raghavachari

Abstract

An *ab initio* quantum chemical study of the reactions of Si⁺ with methylsilane has been carried out: SCF/6-31G(d) wavefunctions were used to predict structures of the possible products and transition states; relative energies were obtained by means of single point electron correlation corrections with fourth order perturbation theory using the larger 6-31G(d,p) basis set. Three different mechanisms involving initial complex formation, followed by insertion of Si⁺ into Si-C, Si-H and C-H bonds leading to the eliminations of H₂ and other products, have been investigated in detail. This involves the detailed mapping of Si₂CH₆⁺, Si₂CH₅⁺ and Si₂CH₄⁺ potential energy surfaces. Results of the calculations are compared with the experimental observations of Mandich et al, Mayer et al and Kickel et al. Good agreement with experiments is obtained.

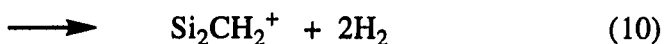
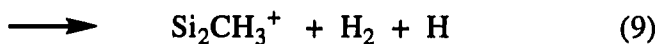
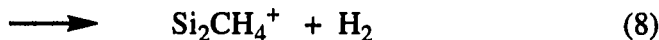
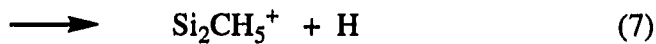
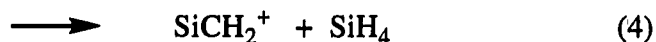
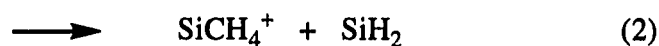
Introduction

As the demands of silicon device fabrications grow, the advantage in expanding our knowledge of silicon chemistry is clear. Gas phase studies of small silicon cluster ions with different reagents have proven valuable in understanding chemical deposition and etching.¹ In particular, the potential energy surfaces for the reactions of Si⁺ with several small molecules have been the subject of considerable attention.² Of interest in the present work is the reaction of Si⁺ with methylsilane (CH₃SiH₃). This reaction has been the subject of several experimental studies.^{3,4,5} Along with other positive ion-molecule reactions, the

reaction of Si^+ with methylsilane was first studied sixteen years ago in a tandem mass spectrometer by Mayer and Lampe.³ Two predominant products, SiCH_3^+ and SiCH_5^+ , were observed, along with very small amounts of Si_2H_3^+ , Si_2CH_2^+ and Si_2CH_4^+ . The first two ion products (SiCH_3^+ and SiCH_5^+) were found to be formed in an endothermic reaction of ground state Si^+ (^2P) with methylsilane. Recently, Mayer and Lampe⁶ have reported that the ions SiCH_3^+ and SiCH_5^+ comprised 52% and 39%, respectively, of the ionic products in the reaction of Si^+ with methylsilane. In that study, Si^+ was allowed to react with CH_3SiH_3 at a collision energy of 1.2 eV in a tandem mass spectrometry apparatus. Labeling studies have found no scrambling of H and D in the ion products. In contrast, an experimental study of the reaction of Si^+ with methylsilane under low pressure in the ion trap cell of a FTMS (Fourier Transform Mass Spectrometer), performed by Mandich, Reents and Bondebey⁴ yielded only Si_2CH_4^+ and SiCH_3^+ ; no other ionic products were found at thermal energies.

The most recent study of the reaction of Si^+ with methylsilane was performed by Kickel, Fisher and Armentrout with kinetic energies ranging from thermal to 10 eV, using guided ion beam mass spectrometry.⁵ Ten different ionic products were observed (1-10), with SiCH_3^+ (reaction 3) and Si_2CH_4^+ (reaction 8) being the major ionic products at thermal energy. Reaction 8 was found to be exothermic, in agreement with previous observations of both Mayer and Lampe³ and Mandich et al.⁴ Reaction 3 was also found to be exothermic. This conclusion is consistent with the observations of Mandich et al.,⁴ but disagrees with findings made by Mayer and Lampe.³ Above 1 eV, Kickel et al. found SiCH_5^+ (reaction 1) to be the major ionic product. This endothermic reaction was also observed by Mayer and Lampe³, but not by Mandich et al.⁴ since their experiments were carried out at thermal energies. When isotopically labeled silicons ($^{30}\text{Si}^+$) were used as reactant ion, 73% of

CH_3Si^+ ions were found to be unlabeled, in good agreement with the 84% obtained by Reents and Mandich. Reaction 1 was reported to produce exclusively labeled $^{30}\text{Si-H}$.



So, it appears that the initially labeled Si^+ eventually appears in the neutral products.

The structures of many of these ionic products, as well as important intermediates and transition states that provide information relevant to reaction mechanisms for the exothermic channels, have been examined by Raghavachari,⁷ using the 6-31G(d) basis set at the unrestricted Hartree-Fock (UHF) level of theory. This study also provided energetic information for the ground state potential energy surface using full fourth order Møller-Plesset perturbation [MP4(SDTQ)]⁸ theory. These single point corrections were done with the larger 6-31G(d,p) basis set.⁹

Two low-energy channels were found in the previous theoretical study, corresponding to reactions (3) and (8). Reaction 8 was predicted to proceed without barrier to an initial interaction complex of Si^+ with one Si-H bond of methylsilane, leading to a binding energy of 29 kcal/mol for this ion-molecule complex. The insertion of Si^+ into an

Si-H bond of methylsilane and a subsequent 1,2-H₂ elimination step have transition states that are predicted to lie 19 and 11 kcal/mol below the separated Si⁺ and CH₃-SiH₃ species, respectively. The exothermic formation of the final product CH₃-SiH-Si⁺, therefore, has no overall barrier. One other H₂ elimination pathway, the 1,1-H₂ elimination from [H₃C-SiH₂-SiH]⁺ (**1**) leading to H₃C-Si-SiH⁺, was predicted to have an overall barrier of 3 kcal/mol. Thermodynamically, formation of H₃C-Si-SiH⁺ is predicted to be about 8 kcal/mol less favorable than the isomeric CH₃-SiH-Si⁺ ion.

The second exothermic channel, leading to the formation of CH₃Si⁺ (reaction 3), was predicted to proceed by simple Si-Si bond cleavage from the [H₃C-Si-SiH₃]⁺ cation intermediate. Steps leading to this key [H₃C-Si-SiH₃]⁺ cation intermediate were predicted to follow two different paths: 1) direct Si⁺ insertion into the Si-C bond of methylsilane with a barrier that lies just 6 kcal/mol below the reactants; 2) stepwise 1,2-H migrations from the (**1**). The two transition states involved in the hydrogen migrations producing [H₃C-SiH-SiH₂]⁺ and [H₃C-Si-SiH₃]⁺ ionic intermediates were predicted to have barriers that are 33 and 30 kcal/mol below the reactants. These results are consistent with the labeling experiments, since there are two channels leading to [H₃C-Si-SiH₃]⁺ in which two silicons are scrambled.

Since most of the transition states on the potential energy surface of the reaction of Si⁺ with methylsilane have no symmetry, it is not clear which reactants and products they connect. In the present work, we apply the concept of intrinsic reaction coordinate (IRC)^{10,11} to follow the steepest descent paths from the transition states to insure proper connections of all reactants and products. IRC calculations are also carried out to analyze the potential energy surfaces of Si₂CH₄⁺ and Si₂CH₅⁺ which involve both cyclic and acyclic intermediates that were not considered in the previous study.⁷ We also explore other channels for the products formed from Si₂CH₆⁺, Si₂CH₅⁺ and Si₂CH₄⁺ intermediates to

investigate new experimental results from studies by Kickel, Fisher and Armentrout⁵ and by Mayer and Lampe.⁶

Computational Methods

To avoid the effects of spin contamination expected from unrestricted Hartree-Fock (HF) wavefunctions, geometry optimizations and transition state searches of all open-shell ion species were determined at the restricted open-shell HF¹² (ROHF) level of theory with both the 3-21G*¹³ and the 6-31G(d)¹⁴ basis sets. Geometrical parameters obtained from the 6-31G(d) basis set are reported in parentheses in all figures. All stationary points were verified to be either minima or transition states on the potential energy surface (PES) using the analytically determined hessian (matrix of energy second derivatives) encoded in the GAMESS quantum chemistry program package.¹⁵

The minimum energy path (MEP) was traced from each transition states to the corresponding reactants or products to insure correct connections of reactants with products. The MEP was traced by following the path of steepest descents in the mass-weighted Cartesian coordinates^{10,16} using the concept of intrinsic reaction coordinate^{10,11} (IRC). The reaction paths were generated using the fourth order Runge-Kutta^{11d} (RK4) or the second order Gonzalez-Schlegel^{11e} (GS2) methods in GAMESS. Except for the initial step off the saddle point of 0.1 amu^{1/2}.bohr, other points on the IRC were located with stepsizes of 0.15 amu^{1/2}.bohr.

The final energetics were determined by single point calculations at the SCF geometries using the complete fourth-order Moller-Plesset (MP4) perturbation theory⁸ with the larger 6-31G(d,p)⁹ basis set. At this correlated level of theory, contributions from single, double, triple, and quadruple excitations from the UHF determinant were spin-projected¹⁷, (e.g., for a doublet state, contaminations could come from quartet and higher states) since UHF wave functions are not eigenfunctions of the total spin (S^2) operator.

These single point calculations were performed using the GAUSSIAN88¹⁸ and GAUSSIAN90¹⁹ quantum chemistry program packages.

Results and Discussion

The structures, energetics and reaction mechanisms of reactions 1-10 are discussed in sections 1-7. Structures of the reactants, products, intermediates and transition states with solid lines showing their connections are displayed in Figures 1-6. Total and relative energies are listed in Tables Ia-e and IIa-f. The relative energies of Si_2CH_4^+ (**1a-1g**), Si_2CH_5^+ (**2a-2g**) and Si_2CH_6^+ (**3a-3n**) isomers are listed in Tables Ia, Ib and Ic, respectively. Table Id lists the barriers for: 1) The insertion of Si^+ into C-H, Si-H and Si-C bonds of methylsilane (**4a-4c**); 2) Different isomerization reactions of Si_2CH_6^+ ions (**5a-5i**); 3) Subsequent H_2 -elimination reactions from Si_2CH_6^+ (**6a-6g**). The processes leading to the formation of Si_2CH_4^+ (reaction 8) are discussed in sections 1 and 2. Section 3 discusses the H_2 -elimination and isomerization pathways of different Si_2CH_4^+ ions leading to formation of Si_2CH_2^+ ions (reaction 10). The barriers for these H_2 -elimination (**7a-7b**) and isomerization (**8a-8d**) reactions are listed in Table Ia. Sections 4, 5 and 6 discuss reaction 7 (Si_2CH_5^+), reaction 9 (Si_2CH_3^+) and reaction 4 (SiCH_2^+), respectively. Table Ie listed the relative energies of various simple bond cleavage processes, reactions 1, 2, 3, 5, 6, and 7. The reaction mechanisms for these reactions are discussed in section 7.

1. Si_2CH_6^+

A. Complex formation

Although Si_2CH_6^+ ions were not observed, these addition complexes are important ionic intermediates involved in the formation of virtually all the observed products. The structures and energetics of the Si_2CH_6^+ isomers and transition states associated with the isomerization and subsequent decomposition processes, can provide valuable information regarding the detailed mechanisms of the ion-molecule reactions. Formation of these

intermediates begins with the initial ion-molecule interactions of Si^+ with methylsilane. Three ion-molecule complexes were found on the Si_2CH_6^+ potential energy surface, as the result of the interaction of Si^+ with methylsilane on the silicon (**3i** and **3k** in Figure 1a) and carbon (**3l** in figure 1c) ends of the molecule.

At the PUMP4/6-31G(d,p) level of theory, Si^+ interacts most favorably with two hydrogens (**3k**) forming a double bridged complex on the silicon end of methylsilane. This results in a binding energy of 33.8 kcal/mol relative to the separated reactants ($\text{Si}^+ + \text{CH}_3\text{SiH}_3$). A single bridged complex between Si^+ and one Si-H (**3i**) is found to be 28.3 kcal/mol below the separated reactants (Figure 1a). The latter result compares favorably to the 28.9 kcal/mol obtained previously by Raghavachari⁷ at a similar level of theory. It is also worth noting that **3i** and **3k** are essentially identical in energy at the SCF level of theory (Table Ia). These complexes have Si-H bonds that are lengthened significantly compared to the normal (1.457Å) Si-H bond of methylsilane. At the ROHF/6-31G(d) level of theory, Si-H bridged distances are calculated to be 1.629Å and 1.547Å for **3i** and **3k**, respectively.

A transition state connecting **3i** and **3k**, structure **5h**, was located (see Figure 1a). At the ROHF/6-31G(d) level of theory, **5h** lies only 1.3 kcal/mol above **3i**. However, single point corrections at the PUMP4/6-31G(d,p) level of theory lower the barrier by 2.3 kcal/mol, placing the transition state **5h** 1.0 kcal/mol below the reactant **3i**. Higher levels of theory may be necessary to accurately determine the structure and energetics of **5h**, if it exists at all. It is possible that of the three stationary points (**3i**, **3k**, **5h**) only **3k** exists at the highest level of theory.

Interaction of Si^+ with methylsilane on the carbon side is less favorable. Only one complex in which Si^+ interacts primarily with carbon (**3l**), was found (see Figure 1c). This structure lies 19.2 kcal/mol below the separated reactants of Si^+ and $\text{CH}_3\text{-SiH}_3$, at the PUMP4/6-31G(d,p) level of theory. Although this ion-molecule complex has the highest

energy among all complexes found, it may be an important intermediate for high energy channels, as discussed below.

B. Insertion reactions

From the three ion-molecule complexes (**3i**, **3l** and **3k**), the next possible steps in the reaction involve either the insertion of Si^+ into a bond of methylsilane (Si-H, C-Si and C-H) or various bond cleavages and abstractions. The latter types of reactions may have no reverse barriers. A C-Si bond cleavage from complex **3l** can result in the formation of the experimentally observed $\text{CH}_3\text{-Si}^+$ ion product (reaction 3) at higher energy. Abstraction of one or two hydrogens, by the complexed Si^+ , via **3i** or **3k** produces the $\text{CH}_3\text{-SiH}_2^+$ and $\text{CH}_3\text{-SiH}^+$ ions, respectively (reactions 1 and 2).

Other possible channels to account for the products described above as well as other experimentally observed ones, involve more complex rearrangements on the Si_2CH_6^+ potential energy surface. Such rearrangement processes are most likely to begin with the insertion of Si^+ into Si-H (Figure 1a), C-Si (Figure 1b), and C-H (Figure 1c) bonds of methylsilane. Since the barriers for the Si-H and Si-C insertion reactions are calculated to be 18.8 and 6.0 kcal/mol below the separated reactants ($\text{Si}^+ + \text{CH}_3\text{-SiH}_3$), these insertions are predicted to occur at thermal energies. Our PUMP4/6-31G(d,p) barriers as well as their transition state structures are in good agreement with earlier results obtained by Raghavachari.⁷

For the Si-H insertion transition state (**4b**), the ROHF/6-31G(d) partially formed Si-Si bond distance of 2.75 Å, compares favorably with the 2.77 Å obtained with UHF/6-31G(d) in the previous study.⁷ Other structural parameters are in similar or better agreement. The partially formed Si-Si bond of 2.648 Å in the Si-C insertion transition state structure (**4c**: Figure 1b), is slightly shorter than the corresponding value in the Si-H

insertion transition state **4b** (Figure 1a). This is also consistent with the results obtained by Raghavachari.⁷

As expected, walking down the minimum energy path toward the products from transition states **4b** and **4c** leads to $\text{CH}_3\text{-SiH}_2\text{-SiH}^+$ (**3b**) and $\text{CH}_3\text{-Si-SiH}_3^+$ (**3a**), respectively. In the reverse direction these IRC's lead to the initially formed complex **3i**. With Si-Si and Si-C linkages, **3b** and **3a** are important intermediates for subsequent bond cleavage and elimination processes to produce products observed in reactions 1, 3, 5, 6 and 8. These reactions will be discussed in detail later. At the PUMP4/6-31G(d,p) level of theory, **3b** and **3a** lie 34.5 and 40.9 kcal/mol, respectively, below the reactants. These are essentially identical to values obtained by Raghavachari.⁷

Although the insertion of Si^+ into a C-H bond of methylsilane is exothermic by 14.0 kcal/mol, this insertion process must surmount a barrier that is 6.0 kcal/mol above the separated reactants, according to PUMP4/6-31G(d,p). This is not surprising, since a C-H bond is considerably stronger than either C-Si or Si-H bonds. The C-H insertion transition state structure (**4a**) is similar in nature to the Si-H insertion analog (Figure 1c). Tracing the IRC from this transition state leads to the isomer $\text{H}_3\text{Si-CH}_2\text{-SiH}^+$ (**3h**) in the forward direction and the ion-molecule complex **3i** in the reverse direction. At the ROHF/6-31G(d) level of theory, the minimum **3h** is distorted from C_s symmetry with an Si-C-Si-H dihedral angle of 81.2° . Calculated at the PUMP4/6-31G(d,p) level, **3h** lies 33.2 kcal/mol below the reactants. This is 4 kcal/mol lower than the C_s structure (with Si-C-Si-H dihedral angle of 0°) reported earlier by Raghavachari.⁷

Of the three insertion barriers, C-H insertion is the least favorable (+6.0 kcal/mol) followed by C-Si insertion (-6.0 kcal/mol) and Si-H insertion (-18.8 kcal/mol). However, the thermodynamic gains resulting from these three processes do not follow the same trends as the insertion activation barriers. The Si-C insertion product gains nearly 10 kcal/mol more

than do the Si-H and C-H insertion products. At thermal energies, Si-H and C-Si insertions would most likely be the dominant pathways. Insertion of Si^+ into a C-H bond of methylsilane is expected to be competitive at energies above 5-10 kcal/mol.

C. Isomerization reactions

As noted above, the intermediates resulting from the three insertion reactions (**3a**, **3b**, **3h**) can further isomerize. Presumably, such rearrangements may compete favorably with other processes, such as bond cleavage (i.e., SiH and SiH₃ elimination reactions) and H₂ eliminations. The complex patterns of isomerizations are summarized pictorially in Figure 2. In addition to the facile stepwise 1,2-hydrogen migration connecting minima **3a** ($\text{CH}_3\text{-Si-SiH}_3^+$) and **3b** ($\text{CH}_3\text{-SiH}_2\text{-SiH}^+$) reported by Raghavachari, 1,2-migration of a CH₃ group in **3b** followed by 1-2 hydrogen migration is also a low energy channel joining **3a** and **3b** (see Figure 2a). The PUMP4/6-31G(d) transition state for CH₃ migration (**5d**) is located at 25.1 kcal/mol below the reactants. This is 8.1 kcal/mol higher in energy than the 1-2 hydrogen migration transition state (**5a**) leading to **3d**. Structure **3d**, the lowest energy isomer on the Si₂CH₆⁺ potential energy surface, is 48.9 kcal/mol below the reactants. The second 1,2-hydrogen migration barrier (**5b**) connecting **3d** with **3a** is calculated to be 29.7 kcal/mol below the reactants. Both the PUMP4/6-31G(d,p) barriers and ROHF/6-31G(d) transition state structures (**5a** and **5b**) of 1,2-hydrogen migration from **3b** leading to **3a**, are essentially identical to those obtained earlier.⁷

As shown in Figure 2b, competing with the CH₃ and hydrogen migrations in the channels described above, is the isomerization of **3b** ($\text{CH}_3\text{-SiH}_2\text{-SiH}^+$) to **3h** ($\text{SiH}_3\text{-CH}_2\text{-SiH}^+$). The latter is the product of the insertion of Si^+ into the C-H bond of methylsilane (Recall that this channel is not open at thermal energies). This isomerization channel involves cyclic (**3e**) and bridged (**3c**) isomers connected to each other by a transition state lying at 36.4 kcal/mol below the reactants and 6-8 kcal/mol above the two isomers. At the

PUMP4/6-31G(d,p) level of theory, **3e** and **3c** are calculated to be 44.2 and 42.1 kcal/mol below the reactants, respectively. These two low energy isomers (**3e** and **3c**) are accessible by a stepwise hydrogen migration process, after the initial insertion of Si⁺ into either an Si-H (**3b**) or C-H (**3h**) bond of methylsilane (see Figure 1b). Starting from CH₃-SiH₂-SiH⁺ (**3b**), the first (**5c**) of three barriers leading to SiH₃-CH₂-SiH⁺ (**3h**) is a 1,3-hydrogen migration that lies 7.8 kcal/mol below the reactants (Figure 2b). Going down the IRC from **5c**, we obtain the cyclic **3e** with C-Si (1.872Å) and Si-Si (2.556Å) distances that are a little longer than that of the corresponding bonds of methylsilane and disilane, as predicted by ROHF/6-31G(d). Hydrogen migration from an SiH₂ group in **3e** leading to **3c** requires only 7.8 kcal/mol. The transition state structure (**5f**) involved in this process has a slightly lengthened Si-H bond (1.502Å) with a H-Si-C-Si dihedral angle approaching zero. The next step leading to **3h** is also a facile process. The barrier (**5i**) connecting **3c** to **3h** is calculated to be 34.1 kcal/mol below the reactants, at the MP4/6-31G(d,p) level of theory. This is about 1 kcal/mol *lower* than the product **3h**. This means that isomer **3h** may not be a true minimum on the potential energy surface, or that the MP4 transition state separating **3c** and **3h** is sufficiently shifted from the ROHF structure that a small barrier may still exist.

As shown in Figure 2c, isomer **3c** can undergo a 1,2-hydrogen shift from the CH₂ group to produce the C_{2v} hydrogen-bridged intermediate **3f**. This step has a net energy requirement of 10.6 kcal/mol and is therefore unlikely to occur at thermal energies. However, the product **3f** is 27.3 kcal/mol below the reactants [at the PUMP4/6-31G(d,p) level of theory]. A 1,3-hydrogen shift reaction from **3f** leads to another low energy isomer (**3j**), lying 26.0 kcal/mol below the reactants. Similar to other hydrogen shift reactions involving the breaking and forming of Si-H bonds, this process requires only 7.3 kcal/mol, starting from **3f**. A 1,2-hydrogen shift from **3j** leads to **3g**. This structure is 24 kcal/mol above the reactants. Isomerization barriers to other Si₂CH₆⁺ isomers were not considered.

It is worth noting that all reactions described above with net barriers higher than the separated reactants of Si^+ and $\text{CH}_3\text{-SiH}_3$ may not be observed under the experimental conditions in studies performed by Mandich et al.⁴ They are, however, accessible with external inputs of energy, such as in the experiments performed by Kickel et al. (0-10 eV) and by Mayer and Lampe (0-3 eV).⁶

2. Si_2CH_4^+ (Reaction 8)

Since the formation of Si_2CH_4^+ ionic products result from H_2 elimination reactions of Si_2CH_6^+ ionic intermediates, all Si_2CH_6^+ ions may be considered as potential intermediates for reaction 8. However, intermediates that are accessible in the fewest numbers of steps with the lowest activation energies present the most viable routes to the products. As the energy available to drive the reactions increases, high energy channels (e.g, C-H activation of methylsilane) with fewer steps become increasingly competitive with multistep low energy channels. In the following discussions, both single-step and two-step low and high energy channels are considered (Figure 3), starting with the former. This, however, does not encompass all possible paths for the H_2 elimination reactions. Channels that require more than two isomerization steps after the initial insertion reactions are not considered.

Since the initial low energy steps in the mechanism involve the insertions of Si^+ into a Si-H or a Si-C bond of methylsilane, $\text{CH}_3\text{-SiH}_2\text{-SiH}^+$ (**3b**) and $\text{SiH}_3\text{-Si-CH}_3^+$ (**3a**) are key viable intermediates for hydrogen elimination reactions (reaction 8). Both 1,1- (**6b**: Figure 3a) and 1,2- (**6c**: Figure 3b) H_2 elimination transition states connecting **3b** with Si_2CH_4^+ (verified in this work by following the IRC), had been considered earlier⁷ using the UHF/6-31G(d) wavefunctions for structure determinations. The calculated ROHF/6-31G(d) structures are essentially identical to those predicted by UHF. The PUMP4/6-31G(d,p) barriers corresponding to the **6b** and **6c** transition state structures lie 4.0 kcal/mol

above and 10.2 kcal/mol below the reactants, respectively. These barriers are in good agreement with the values (3.1 kcal/mol for **6b** and 10.8 kcal/mol for **6c**) obtained earlier.⁷ Thermodynamically, minima [CH₃-Si-SiH⁺ (**1e**) + H₂ and CH₃-SiH-Si⁺ (**1b**) + H₂] directly connected to **6b** and **6c** are exothermic by 6.0 and 15.9 kcal/mol, respectively. Note that transition state **6d** (Figure 3b) is also connected to **1b**. Since **6d** is 9.6 kcal/mol below the reactants, the elimination of H₂ from **3b** via **6d** is also energetically favorable at thermal energies.

The 1,3-elimination of H₂ from **3b** to yield [CH₂SiH₂Si⁺] is another potential route that has not been considered previously. As shown in figure **3a**, there is a net energy requirement of 3.4 kcal/mol to traverse this transition state (**6a**) to the product (**1a**), the thermodynamically most stable isomer (17.1 kcal/mol exothermic) on the Si₂CH₄⁺ potential energy surface. Structure **1a** has two C-Si bonds with lengths of 1.857 Å and 1.890 Å and a 2.646 Å bond joining the two silicon atoms. This suggests a cyclic ring, since typical C-Si and Si-Si single bond lengths are 1.89 and 2.34 Å, respectively. Similar to other H₂ elimination transition states, **6a** has a partially formed H₂ bond of 0.981 Å and a partially broken Si-H bond of 1.611 Å, as predicted by ROHF/6-31G(d).

Of the three elimination channels [1,1, 1,2 and 1,3-eliminations of H₂ from **3b** (CH₃-SiH₂-SiH⁺)] discussed above, only the 1,2-elimination channel has no overall barrier relative to initial reactants. The net barriers are 3.4 and 4.0 kcal/mol for the 1,3 and 1,1-elimination of H₂, respectively.

Since the CH₃-SiH-SiH₂⁺ intermediate (**3d**; Figure 2a) is accessible via many channels with no overall barriers, H₂ elimination barriers from this intermediate are potentially low in energy. Indeed, the 1,2 H₂ elimination transition state (**6e**) from **3d** to yield **1e** and H₂ was located slightly (-6.0 kcal/mol) below the reactants (Figure 3b), making

it a barrierless process. Despite a careful search, a transition state for 1,1 H₂ elimination from **3d** was not found.

Although reactions with overall barriers are unlikely to occur at thermal energies, they are expected to be competitive as the kinetic energy of the incoming ion increases. Such conditions exist in experiments performed by Mayer and Lampe⁶ and by Kickel, Fisher and Armentrout.⁵ At energies above 15 kcal/mol, activation of the C-H bonds of methylsilane becomes a facile process. The SiH₃-CH₂-SiH⁺ (**3h**) intermediate (Figure 2b) produced by the insertion of Si⁺ into the C-H bond of methylsilane may, therefore, be another alternative precursor for H₂ eliminations. This is considered in Figure 3c. The barrier (**6f**) for 1,1-H₂ elimination from the SiH₃ group of **3h** to yield H₂ and a cyclic Si₂CH₄⁺ minimum **1f**, is located 14.1 kcal/mol above the reactants. The isomer itself is predicted to lie 6.9 kcal/mol above the separated reactants, so this is a net endothermic process. The SCF/6-31G(d) transition structure (**6f**) of this H₂ elimination reaction has a partially formed H-H bond of 0.981 Å; its Si-Si bond of 2.337 Å is also approaching that (2.113 Å) of the connecting cyclic product **1f**.

Since a shift hydrogen from SiH₃-CH₂-SiH⁺ (**3h**) to the bridged intermediate (**3c**) is a very facile process, a channel involving a hydrogen shift after the initial insertion of Si⁺ into the C-H bond of methylsilane has also been considered. The H₂ elimination transition state (**6g**) from **3c** was located at 2.1 kcal/mol below the reactants (Figure 3c). The transition state **6g**, is predicted to yield the cyclic ion **1a** based on IRC calculations. Note that 1,3 H₂ elimination from **6a** (CH₃-SiH₂-SiH⁺) also produced the product **1a**, as discussed above.

So far six transition states leading to four possible structural products (**1a**, **1b**, **1e** and **1f**) have been identified for reaction 8. The formation of other Si₂CH₄⁺ isomers via isomerization of **1a**, **1b**, **1e** and **1f** is considered in the next section.

3. Isomerization of Si_2CH_4^+ and Si_2CH_2^+ formation (reaction 10).

At higher than thermal energy Si_2CH_4^+ ion products undergo hydrogen molecule elimination and isomerization into other high energy isomers. Isomerization and hydrogen elimination reactions of Si_2CH_4^+ ions are summarized in Figures 4a and 4b. Similar to the isomerization of Si_2CH_6^+ ions, Si_2CH_4^+ isomerization processes involve migrations of H and CH_3 . Methyl migration transition state (**8d**) connects **1e** ($\text{CH}_3\text{SiSiH}^+$) and **1b** ($\text{CH}_3\text{SiHSi}^+$) and is located at 0.3 kcal/mol above the reactants. The 3-center transition structure **8d** has C_s symmetry with partially formed or broken C-Si bond lengths of 2.056 Å and 2.343 Å. The barriers to hydrogen migrations from the CH_3 group of **1e** (Figure 4b: **8c**) and **1b** (Figure 4a: **8a**) leading to the cyclic structures **1a** and **1f**, are located at 18.8 and 21.2 kcal/mol above reactants, respectively. Similar to other hydrogen migration transitions described in Figure 2, **8c** and **8a** have slightly stretched Si-H and C-H bonds. Structure **1a** may also isomerize to another acyclic ion **1c** (Figure 4b) with a hydrogen migration barrier (**8b**) that is 35.7 kcal/mol above that reactants. Although the formation of **1c** is predicted to be 8.3 kcal/mol exothermic thermodynamically, H_2 elimination channels with barriers lower than **8b** (e.g. **7a** and **7b**) should render the hydrogen migration process less competitive.

Two hydrogen elimination channels leading to the formation of a high energy cyclic Si_2CH_2^+ (**11a**) were found to have net energy requirements of 22.5 (**7b**: Figure 4a) and 30.7 kcal/mol (**7a**: Figure 4b). IRC calculations connect transition state **7b** to **1f** (see Figure 4a) and transition state **7a** to **1e** (Figure 4b). Key structural parameters of these H_2 elimination transition states are similar in nature to the ones in reaction 8. The partially formed H-H distances are predicted to be near 1 Å at the transition states. Si-H and C-H distances in **7a** and **7b** are stretched to about 1.6 Å. As shown in Figure 4, thermodynamically, reaction 10 (formation cyclic Si_2CH_2^+ (**11a**) and 2H_2) is 10.5 kcal/mol endothermic. This is in good agreement with the endothermicity value of 8.8 ± 1.2

kcal/mol, reported by Kickel et al.⁵ The acyclic isomer Si-Si-CH₂⁺ (**11b**) is about 22 kcal/mol above the cyclic form (**11a**) (see Table Ia).

4. Si₂CH₅⁺ (Reaction 7)

Experimentally, mass overlap from Si₂CH₄⁺ prevents accurate thermodynamic measurements of the Si₂CH₅⁺ ion. An endothermicity of about 6.9 kcal/mol was estimated for reaction 7.⁵ Si₂CH₅⁺ ions formed in reaction 7 are probably the result of the loss of a hydrogen from Si₂CH₆⁺ intermediates. The Si₂CH₆⁺ PES (see Figures 1 and 2), therefore, provide insights for the formation of Si₂CH₅⁺ ions. For example, a loss of the SiH hydrogen from H₃Si-CH₂-SiH⁺ (**3h**; Figure 1c) may be one viable route leading to H₃Si-CH₂-Si⁺ (**2f**; Figure 5a), the lowest energy Si₂CH₅⁺ isomer. Structure **2f** lies only 5.0 kcal/mol above the initial reactants. Ion H₂Si-CH-SiH₂⁺ (**2a**) (Figure 5b) is another low energy isomer lying only 5.7 kcal/mol above the reactants; it is the only isomer found within 1 kcal/mol of **2f**. A loss of the bridging hydrogen from intermediate **3f** (Figure 2c) is one possible route to **2f**. Other alternatives may involve complex rearrangements of Si₂CH₅⁺ ions. Since isomerization of Si₂CH₅⁺ isomers are all quite high in energy (see Figure 5b), the most favorable route to **2a** and **2a** are probably simple bond cleavage. The predicted endothermicities (5.0 and 5.7 kcal/mol, respectively, for **2f** and **2a**) are in good agreement with the experimental value of 6.9 kcal/mol.⁵ Structures of other Si₂CH₅⁺ isomers and the corresponding interconnecting transition states are also displayed in Figures 5a, 5b and 5c.

Reaction enthalpies (reaction 7) and isomerization barriers (relative to reactants) are tabulated in Table Ib for all Si₂CH₅⁺ ions. Similar to Si₂CH₆⁺ and Si₂CH₄⁺ ions, methyl migration is a facile process. The methyl migration transition state (**9b**; Figure 5b) connecting **2b** and **2d** was located at 33.0 kcal/mol above the reactants using SCF/6-31G(d,p) (see Table Ib). However, electron correlation corrections lower the energy of **9b** below that of **2b** and **2d**. This appears to be a very flat region of the surface, and it is likely

that correlated wave functions are required to accurately determine minima in this region of the surface. In contrast to facile methyl migration, H migrations require larger activation barriers. The H migration transition states **9a** and **9c** are located at 36.0 and 66.0 kcal/mol above the reactants ($\text{Si}^+ + \text{CH}_3\text{SiH}_3$), corresponding to activation barriers of 60.3 and 11.1 kcal/mol going from **2a** to **2c** and **2c** to **2b**, respectively (see Figure 5b).

5. Si_2CH_3^+ formation (Reaction 9)

Si_2CH_5^+ ions can undergo H_2 elimination to form Si_2CH_3^+ ions. Structures of the calculated transition states and their relative energies are displayed in Figure 5c and Table Ib. This process has high activation barriers. The calculated H_2 -elimination transition state **10a** (Figure 5c) leading to the cyclic bridged structure (**14a**) is 76.1 kcal/mol above the reactants ($\text{Si}^+ + \text{CH}_3\text{-SiH}_3$). The IRC calculations connect transition state **10a** with the cyclic isomer **2c**. Structure **14a** plus the corresponding neutral products ($\text{H}_2 + \text{H}$) lie 37.0 kcal/mol above the reactants. A 1,1- H_2 elimination from **2a** (Figure 5b) leads to an isomer of **14a** (**14b**),²⁰ This isomer is 29.7 kcal/mol above the separated reactants. Kickel et al. estimate Si_2CH_3^+ to be 20.3 ± 0.9 kcal/mol above the reactants.⁵

The open form of Si_2CH_3^+ , structure **14c**, is 49.2 kcal/mol above the reactants. We have found two transition states (**10b** and **10c** in Figure 5c) that appear to lead to an open form of Si_2CH_3^+ , similar to **14c** in Figure 5c. These transition states lie 54.6 (**10b**) and 52.1 (**10c**) kcal/mol above the reactants. However, the ground state of **14c** appears to be a triplet that is 108.7 kcal/mol below the RHF closed shell singlet. It seems clear that **10b** and **10c** connect to singlet diradical, so the corresponding IRC's must be determined with multi-configurational wave functions.

6. SiH_4 (Reaction 6) and CH_4 elimination

From the Si_2CH_6^+ PES calculated earlier by Raghavachari,⁷ Kickel et al. speculated that the formation of SiH_4 may be the result of a reductive elimination from intermediate **3a**

(see Figure 1b). Since the formation of $\text{SiCH}_2^+ + \text{SiH}_4$ is endothermic, it can not compete with the exothermic production of $\text{SiCH}_3^+ + \text{SiH}_3$ via the same intermediate (**3a**, see Figure 2a). Our calculations predict the barrier and endothermicity of reaction 6 to be 7.4 and 2.0 kcal/mol, respectively. The predicted endothermicity of reaction 6 compares favorably with the observed value of 3.0–3.5 kcal/mol.⁵ Following the IRC from the transition state **12a** toward the products, a complex of SiCH_2^+ and SiH_4 (**3m**) was located at 11.4 kcal/mol below the reactants (see Figure 6). This complex (**3m**) has a bridging hydrogen with an apparently stretched Si-H distance of 1.567 Å. The product ion (SiCH_2^+) resulting from silane elimination from **3m** has C_{2v} symmetry (2B_2) with a Si-C distance of only 1.811 Å.

Although CH_4 elimination is thermodynamically more favorable (by nearly 15 kcal/mol) than silane elimination, this reaction was not observed experimentally. Unlike the endothermic process of silane elimination discussed above, the formation of CH_4 and SiSiH_2^+ is 12.8 kcal/mol exothermic. However, the barrier for CH_4 elimination is located at 19.1 kcal/mol, 8.4 kcal/mol higher than the corresponding SiH_4 elimination. The transition state for CH_4 elimination (**13a**) is connected to the $\text{CH}_3\text{-SiH-SiH}_2^+$ (**3d**) intermediate, as verified by IRC calculations following the direction toward the reactant. Following the IRC toward the products, a complex of CH_4 and SiSiH_2^+ with C_1 symmetry (**3n**) was located. This structure (**3n**) lies 17.3 kcal/mol below the reactants ($\text{Si}^+ + \text{CH}_3\text{-SiH}_3$).

7. Simple Bond Cleavage (Reaction 1, 2, 3, 5, 6, 7)

Despite a careful search, transition states for the elimination of SiH , SiH_2 , SiH_3 , SiH_3^+ , SiH^+ and H atom were not found. These reactions (1-3, 5-7) are, therefore, likely to proceed through simple bond cleavages. Based on the Si_2CH_6^+ potential energy surface, SiH^+ (reaction 6) and SiH (reaction 1) elimination reactions are likely to occur via intermediates **3i** (single bridge complex of Si^+ with methylsilane) and **3b** ($\text{CH}_3\text{-SiH}_2\text{-SiH}^+$) (Figure 1a). Thermodynamically, hydrogen atom abstraction by Si^+ to produce SiH^+ and

CH_3SiH_2 is less favorable than the simple Si-Si bond cleavage producing the corresponding $\text{CH}_3\text{SiH}_2^+$ ion and SiH neutral radical. At the MP4/6-31G(d,p) level of theory, the endothermicity of SiH elimination (reaction 1) is 8.1 kcal/mol, while SiH^+ elimination (reaction 6) is calculated to be 17.5 kcal/mol endothermic. The corresponding experimental endothermicities for reactions 1 and 6 are 10.8 ± 1.2 kcal/mol and 21.7 ± 1.4 kcal/mol, so experiment and theory are in good agreement.

Si-Si bond cleavage from intermediate **3d** (see Figure 1a) may lead to the formation of $\text{SiH}_2 + \text{CH}_3\text{SiH}^+$ or $\text{SiH}_2^{++} + \text{CH}_3\text{SiH}$. The former process corresponds to reaction 2 and is experimentally observed at energies above 1 eV.⁵ The experimental endothermicity of 24.4 ± 2.5 for reaction 2 is in good agreement with our calculated value of 23.6 kcal/mol. The reaction endothermicity for the formation of CH_3SiH and SiH_2^+ is calculated to be 36.4 kcal/mol. So, SiH_2 elimination from **3d** is nearly 13 kcal/mol more favorable (thermodynamically) than the SiH_2^+ elimination reaction. The structure of the CH_3SiH^+ ion and the corresponding neutral species are shown in Figure 7. The cation has shorter C-Si (1.853 Å) and Si-H (1.471 Å) bond distances than its neutral counterpart. This may account for the extra stability of CH_3SiH^+ over the neutral CH_3SiH .

Reactions 3 and 5 may be the result of Si-Si bond cleavage from intermediate **3a** ($\text{H}_3\text{Si-Si-CH}_3^+$). Experimentally, the former process produces SiCH_3^+ ion a dominant product at low energies. The latter process, reaction 5, was only observed at high energies with its cross section increasing at above 1 eV.⁵ Since at high energies little of intermediate **3a** can be formed, SiH_3^+ was speculated to be produced by other channels. The enthalpies of reactions 3 and 7 are essentially identical to those predicted by Raghavachari.⁷

Summary and Conclusion

The structures, energetics and reaction mechanisms of the $\text{Si}^+ + \text{CH}_3\text{-SiH}_3$ (1-10) have been investigated in detail. Reactions 3 and 8, elimination of SiH_3 and H_2 , were to

found to be exothermic, consistent with experiments⁴⁻⁶ and the previous theoretical study.⁷ These reactions proceed with an initial complex formation of Si^+ with methylsilane, followed by the insertion of Si^+ into either Si-H or Si-C bonds to form Si_2CH_6^+ intermediates that can undergo isomerizations, H_2 -elimination (reaction 8) and SiH_3 elimination (reaction 3) at thermal energy. The entire section of the potential energy surface that corresponds to the minimum energy path leading to the products of reaction 3 and 8 lies below the starting reactants. This explains why these are the observed products at thermal energies.

At higher energies, Si_2CH_6^+ can undergo H-elimination (reaction 7) as well as other bond cleavage processes (reactions 1, 2, 5, 6). The predicted endothermicities for reaction 7 (5.0 and 5.7 kcal/mol for the two Si_2CH_5^+ isomers **2f** and **2a**, respectively) are in good agreement with the experimental value of 6.9 kcal/mol. The calculated (observed) endothermicities of reactions 1, 2, 5, and 6 are 8.0 (10.8 1.2), 23.7 (24.4 2.5), 21.3 (25.5 6.9), 17.7 (21.7 1.4), respectively. The ionic products of reactions 8 (Si_2CH_4^+) and 7 (Si_2CH_5^+) are predicted to undergo H_2 -elimination at energies above 30 and 52 kcal/mol, respectively. The endothermicities of reactions 8 and 7 are predicted to be 10.5 and 37.0 kcal/mol, respectively. The barrier for the reductive elimination of SiH_4 (Reaction 4) and CH_4 is predicted to be about 7 and 19 kcal/mol, respectively. The latter process is not observed experimentally. Reaction 4 is predicted to be endothermic by 2 kcal/mol, in agreement with the experimental value of 3.0 3.5.

Acknowledgment

This research was supported in part by a grant (90-0052) from the Air Force Office of Scientific Research, and in part by a grant from the National Science Foundation (CHE-8911911). Calculations described in this work were performed on an IBM RS6000/530 (obtained through an AFOSR grant to MSG) at North Dakota State University, on an IBM

RS6000/350 generously provided Iowa State University, and on the Cray-2 at the National Center for Supercomputing Applications, Champaign, Illinois.

References

- (1) Mandich, M. L.; Reents, W. D.; Kolenbrander, K. D. *Pure & Appl. Chem.* **1990**, *62*, 1653.
- (2) (a) Wlodek, S.; Fox, A.; Bohme, D. K. *J. Am. Chem. Soc.* **1991**, *113*, 4461. (CH₄, C₂H₆, C₂H₄, C₂H₂, CH₂CCH₂, CH₃CCH, and C₄H₂). (b) Stewart, G. W.; Henis, J. M. S.; Gaspar, P. P. *J. Chem. Phys.* **1972**, *57*, 1990. (CH₄). (c) Boo, B. H.; Elkind, J. L.; Armentrout, P. B. *J. Am. Chem. Soc.* **1990**, *112*, 2083. (CH₄). (d) Boo, B. H.; Armentrout, P. B. *J. Am. Chem. Soc.* **1991**, *113*, 6401. (CH₃CH₃).
- (3) Mayer, T. M.; Lampe, F. W. *J. Phys. Chem.* **1988**, *92*, 6284.
- (4) Mandich, M. L.; Reents, W. D.; Bondybey, V. E. *J. Phys. Chem.* **1986**, *90*, 2315.
- (5) Kickel, B. L.; Fisher, E. R.; Armentrout, P. B. *J. Phys. Chem.* **1992**, *96*, 2603.
- (6) Mayer, T. M.; Lampe, F. W. *J. Chem. Phys.* **1992**, *96*, 2819.
- (7) Raghavachari, K. *J. Phys. Chem.* **1988**, *92*, 6284.
- (8) (a) Müller, C.; Plesset, M. S. *Phys. Rev.* **1934**, *46*, 618. (b) Krishnan, R.; Frisch, M. J.; Pople, J. A. *J. Chem. Phys.* **1980**, *72*, 4244. (c) Bartlett, R. J.; Sekino, H.; Purvis, G. D. *Chem. Phys. Lett.* **1983**, *98*, 66.
- (9) (a) Hariharan, P. C.; Pople, J. A. *Theor. Chim. Acta* **1973**, *28*, 213. (b) Francl, M. M.; Pietro, W. J.; Hehre, W. J.; Binkley, J. S.; Gordon, M. S.; DeFrees, J. D.; Pople, J. A. *J. Chem. Phys.* **1982**, *77*, 3654.
- (10) (a) Fukui, K. *Acc. Chem. Res.* **1981**, *14*, 363. (b) Fukui, K. *Pure Appl. Chem.* **1982**, *54*, 1825. (c) Fukui, K. *Int. J. Quantum Chem. Sym.* **1981**, *15*, 633.
- (11) (a) Ishida, K.; Morokuma, K.; Komornicki, A. *J. Chem. Phys.* **1977**, *66*, 2153. (b) Schmidt, M. W.; Gordon, M. S.; Dupuis, M. *J. Am. Chem. Soc.* **1985**, *107*, 2585. (c)

- Garrett, B. C.; Redmon, M. J.; Steckler, R.; Truhlar, D. G.; Baldrige, K. K.; Bartol, D.; Schmidt, M. W.; Gordon, M. S. *J. Chem. Phys.* **1988**, *92*, 1476. (d) Baldrige, K. K.; Gordon, M. S.; Steckler, R.; Truhlar, D. G. *J. Chem. Phys.* **1989**, *93*, 5107. (e) Gonzalez, C.; Schlegel, H. B. *J. Chem. Phys.* **1989**, *90*, 2154; *J. Phys. Chem.* **1990**, *94*, 2154; *J. Chem. Phys.* **1991**, *90*, 5853.
- (12) Guest, M. F.; Saunders, V. R. *Mol. Phys.* **1974**, *28*, 819.
- (13) Binkley, J. S.; Pople, J. A.; Hehre, W. J. *J. Am. Chem. Soc.* **1980**, *102*, 939.
- (14) (a) Gordon, M. S. *Chem. Phys. Lett.* **1980**, *76*, 163. (b) Hehre, W. J.; Ditchfield, R.; Pople, J. A. *J. Chem. Phys.* **1972**, *56*, 2257.
- (15) (a) GAMESS (General Atomic and Molecular Electronic Structure System): Schmidt, M. W.; Baldrige, K. K.; Boatz, J. A.; Jensen, J. H.; Koseki, S.; Gordon, M. S.; Nguyen, K. A.; Windus, T. L.; Elbert, S. T. *QCPE Bulletin*, **1990**, *10*, 52. (b) Schmidt, M. W.; Baldrige, K. K.; Boatz, J. A.; Elbert, S. T.; Gordon, M. S.; Jensen, J. H.; Koseki, S.; Matsunaga, N.; Nguyen, K. A.; Su, S. Windus, T. L. *J. Comp. Chem.* **1993**, *14*, 1347.
- (16) (a) Marcus, R. A.; *J. Chem. Phys.*, **1966**, *45*, 4493. (b) Marcus, R. A. *J. Chem. Phys.* **1968**, *49*, 2610. (c) Truhlar, D. G.; Kuperman, A. *J. Am. Chem. Soc.* **1971**, *93* 1840. (d) Schaefer, H. F. III. *Chem. Britain.* **1975**, *11*, 227.
- (17) Schlegel, H. B. *J. Chem. Phys.* **1986**, *84*, 4530.
- (18) GAUSSIAN88, Frisch, M. J.; Head-Gordon, M.; Schlegel, B. H.; Raghavachari, K.; Binkley, J. S.; Gonzalez, C.; Defrees, D. J.; Fox, D. J.; Whiteside, R. A.; Seeger, R.; Melius, C. F.; Baker, J. Martin, R.; Kahn, L. R.; Stewart, J. J. P.; Fluder, E. M.; Topiol, S. Pople, J. A. Gaussian, Inc., Pittsburgh, PA, **1988**.
- (19) GAUSSIAN92, Frisch, M. J.; Head-Gordon, M.; Schlegel, B. H.; Raghavachari, K.; Binkley, J. S.; Gonzalez, C.; Defrees, D. J.; Fox, D. J.; Whiteside, R. A.;

Seeger, R.; Melius, C. F.; Baker, J. Martin, R.; Kahn, L. R.; Stewart, J. J. P.;

Fluder, E. M.; Topiol, S. Pople, J. A. Gaussian, Inc., Pittsburgh, PA, 1992.

(20) $\text{H}_2\text{Si-CH-Si}^+$ (14b)

Table Ia. Relative Energies (in kcal mol⁻¹ with zero-point energy correction) Calculated with the 6-31G(d,p) Basis Set .

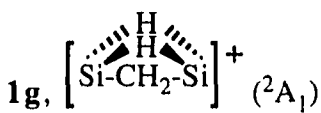
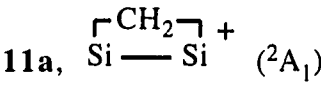
Structure	UHF	UMP2	UMP3	UMP4	PUMP4
Si ⁺ (² P) + H ₃ Si-CH ₃	0.0	0.0	0.0	0.0	0.0
Si ₂ CH ₄ ⁺ + H ₂					
1a , [H ₂ Si-CH ₂ -Si] ⁺ (² A')	-3.5	-16.9	-15.0	-16.8	-17.1
1b , H ₃ C-SiH-Si ⁺ (² A'')	-6.0	-13.3	-15.0	-14.7	-15.9
1c , H ₂ Si-CH-Si ⁺ (² A')	-0.2	-11.9	-9.1	-8.1	-8.3
1d , H ₃ Si-CH-Si ⁺ (² A')	38.0	18.9	21.4	18.7	17.8
1e , H ₃ C-Si-SiH ⁺ (² A)	2.9	-1.4	-0.9	-2.5	-6.0
1f , [HSi-CH ₂ -SiH] ⁺ (² B ₁)	24.7	5.4	8.1	6.9	6.9
1g ,  (² A ₁)	35.5	11.8	15.2	12.0	9.7
H ₂ Elimination Transition States					
7a (² A) + H ₂	61.1	34.0	36.6	32.5	30.7
7b (² A) + H ₂	49.5	27.7	29.5	25.7	22.5
Isomerization Transition States					
8a (² A) + H ₂	41.1	25.2	27.3	22.5	21.2
8b (² A) + H ₂	49.3	41.3	42.3	37.8	35.7
8c (² A) + H ₂	37.8	23.0	24.2	20.6	18.8
8d (² A) + H ₂	17.1	4.5	6.2	3.7	0.3
CH ₂ Si ₂ ⁺ + 2H ₂					
11a ,  (² A ₁)	28.9	13.4	13.4	10.5	10.2
11b , Si-Si-CH ₂ ⁺ (² A ₁)	55.5	37.2	38.3	32.5	32.3

Table Ib. Relative Energies (in kcal mol⁻¹ with zero-point energy correction)
 Calculated with the 6-31G(d,p) Basis Set .

Structure	RHF	MP2	MP3	MP4
Si ⁺ (² P) + H ₃ Si-CH ₃	0.0	0.0	0.0	0.0
Si ₂ CH ₅ ⁺ + H				
2a , H ₂ Si-CH-SiH ₂ ⁺	7.6	-0.3	7.3	5.7
2b , H ₃ C-SiH ₂ -Si ⁺	24.8	22.4	23.6	23.1
2c , $\overline{\text{H}_2\text{Si}-\text{CH}_2-\text{SiH}^+}$	29.9	20.9	25.9	24.9
2d , H ₃ C-Si-SiH ₂ ⁺	30.0	25.0	26.7	25.6
2e , H ₃ C-SiH-SiH ⁺	22.9	19.1	20.7	20.1
2f , H ₃ Si-CH ₂ -Si ⁺	8.6	2.9	6.1	5.0
2g , H ₂ CSiHSiH ₂ ⁺	38.7	26.0	31.4	27.4
Isomerization Transition States				
9a + H	50.6	36.2	39.9	36.0
9b + H	33.0	20.7	23.6	22.2
9c + H	67.7	65.8	68.4	66.0
H ₂ Elimination Transition States				
10a + H	100.1	74.5	79.6	76.1
10b + H	76.5	54.7	56.7	54.6
10c + H	79.1	58.2	55.1	52.1
CH ₃ Si ₂ ⁺ + H ₂ + H				
14a , $\overline{\text{Si}-\text{CH}_2-\text{Si}^+}$	51.4	37.6	39.6	37.0
14b , SiH ₂ -CH-Si ⁺	37.3	27.0	32.7	29.7
14c , CH ₃ Si-Si ⁺ (³ E)	52.9	49.4	51.2	49.2

Table Ic. Si_2CH_6^+ Relative Energies (in kcal mol⁻¹ with zero-point energy correction)
 Calculated with the 6-31G(d,p) Basis Set .

Structure	UHF	UMP2	UMP3	UMP4	PUMP4
$\text{Si}^+ (^2\text{P}) + \text{H}_3\text{Si}-\text{CH}_3$	0.0	0.0	0.0	0.0	0.0
3a , $\text{CH}_3-\text{Si}-\text{SiH}_3^+ (^2\text{A})$	-37.2	-42.8	-41.0	-41.0	-40.9
3b , $\text{HSi}-\text{SiH}_2-\text{CH}_3^+ (^2\text{A}')$	-31.7	-36.4	-34.8	-34.6	-34.5
3c , $\text{[SiH}_2-\text{CH}_2\text{SiH}]^+ (^2\text{A})$	-34.1	-45.6	-41.8	-42.2	-42.1
3d , $\text{CH}_3-\text{SiH}-\text{SiH}_2^+ (^2\text{A}'')$	-42.2	-51.1	-49.2	-49.0	-48.9
3e , $\text{[SiH}_2-\text{CH}_2-\text{SiH}_2]^+ (^2\text{A}_1)$	-35.3	-47.4	-43.8	-44.2	-44.2
3f , $\text{[SiH}_2-\text{CH}-\text{SiH}_2]^+ (^2\text{B}_1)$	-27.1	-28.5	-27.2	-27.0	-27.3
3g , $\text{H}_3\text{Si}-\text{C}-\text{SiH}_3^+ (^2\text{A}')$	10.3	28.7	25.3	24.9	24.6
3h , $\text{SiH}_3-\text{CH}_2-\text{SiH}^+ (^2\text{A})$	-29.8	-37.0	-32.9	-33.3	-33.2
3i , complex ($^2\text{A}'$)	-23.2	-28.2	-28.1	-28.3	-28.3
3j , $\text{SiH}_3-\text{CH}-\text{SiH}_2^+ (^2\text{A}'')$	-29.8	-27.5	-26.3	-26.0	-26.0
3k , complex ($^2\text{A}'$)	-23.2	-33.2	-32.8	-33.4	-33.3
3l , complex ($^2\text{A}'$)	-11.9	-19.2	-17.8	-18.6	-19.2
3m , complex ($^2\text{A}''$)	-10.7	-9.3	-11.2	-11.3	-11.4
3n , complex (^2A)	-7.6	-14.7	-16.5	-17.0	-17.3

Table Id. Relative energies (kcal mol⁻¹ with zero-point energy correction) calculated with the 6-31G(d,p) basis set.

Structure	UHF	UMP2	UMP3	UMP4	PUMP4
Si ⁺ (² P) + H ₃ Si-CH ₃	0.0	0.0	0.0	0.0	0.0
Si ⁺ insertion Transition States					
4a , C-H insertion (² A)	18.0	9.0	9.0	7.0	6.0
4b , Si-H insertion (² A)	-9.4	-17.9	-18.0	-18.6	-18.8
4c , Si-C insertion (² A)	3.1	-4.1	-3.1	-4.9	-6.0
Migration Transition States					
5a (² A)	-24.1	-34.9	-32.8	-33.1	-33.2
5b (² A)	-21.7	-31.3	-29.3	-29.6	-29.7
5c (² A)	1.5	-5.7	-4.7	-6.5	-7.8
5d (² A)	-13.7	-27.8	-24.4	-25.5	-25.1
5e (² A)	25.6	11.4	14.9	12.7	10.6
5f (² A)	-30.6	-40.0	-36.5	-36.5	-36.4
5g (² A)	-23.1	-21.2	-19.9	-19.7	-20.0
5h (² A)	-21.8	-28.8	-28.7	-29.1	-29.3
5i (² A)	-29.4	-37.7	-33.7	-34.2	-34.1
H ₂ eliminations Transition States					
6a (² A)	28.2	3.0	7.2	4.6	3.4
6b (² A)	25.5	5.2	7.5	5.7	4.0
6c (² A)	10.9	-9.9	-8.4	-9.5	-10.2
6d (² A)	11.7	-9.4	-7.8	-9.0	-9.6
6e (² A)	20.3	-1.0	1.1	-0.2	-0.3
6f (² A)	37.5	12.0	16.9	14.0	14.1
6g (² A)	19.2	0.5	2.5	0.2	-2.1

Table Ie. Relative Energies (in kcal mol⁻¹ with zero-point energy correction) Calculated with the 6-31G(d,p) Basis Set .

Structure	UHF	UMP2	UMP3	UMP4	PUMP4	EXP ^a
Si ⁺ (² P) + H ₃ Si-CH ₃	0.0	0.0	0.0	0.0	0.0	0.0
SiH ₃ (² A ₁) + CH ₃ -Si ⁺	-0.7	-3.2	-3.3	-3.6	-3.5	
SiH ₃ ⁺ + CH ₃ -Si (² A')	20.3	20.9	21.6	21.5	21.3	25.5 ± 6.9
SiH ₂ + CH ₃ -SiH ⁺ (² A')	22.3	23.4	23.8	23.6	23.7	24.4 ± 2.5
SiH ₂ ⁺ (² A ₁) + CH ₃ -SiH	35.1	35.8	36.6	36.4	36.6	
SiH + CH ₃ -SiH ₂ ⁺ (² A')	6.0	7.5	8.0	8.1	8.0	10.8 ± 1.2
SiH ⁺ (² A ₁) + CH ₃ -SiH ₂	18.9	18.1	17.9	17.5	17.7	21.7 ± 1.4
CH ₂ -Si ⁺ (² B ₂) + SiH ₄	-1.2	4.2	2.1	2.1	2.0	3.0 ± 3.5
H ₂ Si-Si ⁺ (² B ₂) + CH ₄	-5.8	-10.3	-12.3	-12.8	-12.8	

^areference 5.

Table IIa. Total Energies (Hartrees) Calculated with the 6-31G(d,p) Basis Set.

Structure	UHF	$\langle S^2 \rangle$	UMP2	UMP3	UMP4	PUMP4
$\text{Si}_2\text{CH}_4^+ + \text{H}_2$						
1a $[\text{H}_2\text{Si}-\text{CH}_2-\text{Si}]^+$ (${}^2\text{A}'$)	-618.82853	0.7721	-619.13625	-619.17652	-619.19413	-619.19526
1b , $\text{H}_3\text{C}-\text{SiH}-\text{Si}^+$ (${}^2\text{A}''$)	-618.83612	0.8778	-619.13442	-619.17769	-619.19445	-619.19690
1c , $\text{H}_2\text{Si}-\text{CH}-\text{SiH}^+$ (${}^2\text{A}'$)	-618.82164	0.7670	-619.12670	-619.16014	-619.17880	-619.17967
1d , $\text{H}_3\text{Si}-\text{CH}-\text{Si}^+$ (${}^2\text{A}'$)	-618.76034	0.7839	-619.07706	-619.11207	-619.13560	-619.13757
1e , $\text{H}_3\text{C}-\text{Si}-\text{SiH}^+$ (${}^2\text{A}$)	-618.81987	1.0346	-619.11315	-619.15562	-619.17293	-619.17918
1f , $[\text{HSi}-\text{CH}_2-\text{SiH}]^+$ (${}^2\text{B}_1$)	-619.78364	0.7601	-619.10115	-619.13803	-619.15639	-619.15699
1g , $\left[\begin{array}{c} \text{H} \\ \diagup \quad \diagdown \\ \text{Si}-\text{CH}_2-\text{Si} \end{array} \right]^+$ (${}^2\text{A}_1$)	-618.76793	0.8544	-619.09216	-619.12989	-619.14985	-619.15411
H_2 elimination Transition States						
7a (${}^2\text{A}$) + H_2	-618.72248	0.8447	-619.05203	-619.09123	-619.11264	-619.11600
7b (${}^2\text{A}$) + H_2	-618.73936	0.9414	-619.06037	-619.10075	-619.12176	-619.12734
Isomerization Transition States						
8a (${}^2\text{A}$) + H_2	-618.75630	0.8464	-619.06791	-619.10781	-619.13032	-619.13294
8b (${}^2\text{A}$) + H_2	-618.73932	0.8494	-619.03842	-619.08004	-619.10213	-619.10595
8c (${}^2\text{A}$) + H_2	-618.76157	0.8429	-619.07152	-619.11295	-619.13347	-619.13685
8d (${}^2\text{A}$) + H_2	-618.79767	1.0310	-619.10409	-619.14463	-619.16343	-619.16939
$\text{Si}_2\text{CH}_2^+ + \text{H}_2$						
11a , $\begin{array}{c} \text{CH}_2 \\ \diagup \quad \diagdown \\ \text{Si} - \text{Si} \end{array} +$ (${}^2\text{A}_1$)	-618.76793	0.7685	-619.07896	-619.12229	-619.14178	-619.14275
11b , $\text{Si}-\text{Si}-\text{CH}_2^+$ (${}^2\text{A}_1$)	-618.72587	0.7632	-619.04166	-619.08327	-619.10734	-619.10818

Table IIb. Total Energies (Hartrees) Calculated with the 6-31G(d,p) Basis Set.

Structure	UHF	MP2	MP3	MP4
Si₂CH₅⁺ + H				
2a , H ₂ Si-CH-SiH ₂ ⁺	-618.80823	-619.10715	-619.13844	-619.15581
2b , Si-SiH ₂ -CH ₃ ⁺	-618.78598	-619.07613	-619.11750	-619.13314
2c , H ₂ $\overline{\text{Si-CH}_2\text{-SiH}^+}$	-618.7735	-619.07420	-619.10963	-619.12593
2d , H ₃ C-Si-SiH ₂ ⁺	-618.77545	-619.06984	-619.11036	-619.12690
2e , H ₃ C-SiH-SiH ⁺	-618.78651	-619.07886	-619.11956	-619.13538
2f , H ₃ Si-CH ₂ -Si ⁺	-618.80808	-619.10354	-619.14175	-619.15827
2g , H ₂ CSiHSiH ₂	-618.75972	-619.06635	-619.10099	-619.12222
Migration Transition State				
9a + H	-618.74027	-619.04952	-619.08697	-619.10792
9b + H	-618.77126	-619.07773	-619.11590	-619.13296
9c + H	-618.70955	-618.99882	-619.03797	-619.05669
H₂ Elimination Transition State				
10a + H	-618.65941	-618.98661	-619.02178	-619.04223
10b + H	-618.69902	-619.02008	-619.06009	-619.07828
10c + H	-618.69390	-619.02302	-619.06179	-619.08144

Table IIc. Si₂CH₆⁺ Total Energies (Hartrees) Calculated with the 6-31G(d,p) Basis Set.

Structure	UHF	$\langle S^2 \rangle$	UMP2	UMP3	UMP4	PUMP4
3a , CH ₃ -Si-SiH ₃ ⁺ (² A)	-618.89219	0.7575	-619.18732	-619.22777	-619.24304	-619.24256
3b , HSi-SiH ₂ -CH ₃ ⁺ (² A')	-618.88329	0.7579	-619.17711	-619.21786	-619.23239	-619.23289
3c , $\begin{array}{c} \text{H} \\ \text{---} \\ \text{[SiH}_2\text{-CH}_2\text{-CH]}^+ \end{array}$ (² A)	-618.88646	0.7539	-619.19129	-619.22850	-619.24393	-619.24423
3d , CH ₃ -SiH-SiH ₂ ⁺ (² A'')	-618.90055	0.7579	-619.20105	-619.24129	-619.25583	-619.25630
3e , $\begin{array}{c} \text{---} \\ \text{[SiH}_2\text{-CH}_2\text{-SiH}_2]^+ \end{array}$ (² A ₁)	-618.88752	0.7580	-619.19318	-619.23073	-619.24621	-619.24671
3f , $\begin{array}{c} \text{H} \\ \text{---} \\ \text{[SiH}_2\text{-CH-SiH}_2]^+ \end{array}$ (² B ₁)	-618.87185	0.7611	-619.16039	-619.20172	-619.21617	-619.21722
3g , H ₃ Si-C-SiH ₃ ⁺ (² A')	-618.80743	0.7602	-619.06612	-619.11318	-619.12871	-619.12975
3h , SiH ₃ -CH ₂ -SiH ⁺ (² A)	-618.87845	0.7544	-619.17616	-619.21298	-619.22848	-619.22882
3i , complex (² A')	-618.87004	0.7626	-619.16434	-619.20735	-619.22261	-619.22347
3j , SiH ₃ -CH-SiH ₂ ⁺ (² A'')	-618.87569	0.7565	-619.15837	-619.19977	-619.21410	-619.21472
3k , complex (² A')	-618.87054	0.7684	-619.17293	-619.21561	-619.23129	-619.23246
3l , complex (² A')	-618.85213	0.7616	-619.15003	-619.19112	-619.20724	-619.20871
3m , complex (² A'')	-618.84443	0.7579	-619.12866	-619.17484	-619.18987	-619.19061
3n , complex (² A)	-618.84533	0.7652	-619.14295	-619.18905	-619.20477	-619.20566

Table II. Total energies (in Hartrees) calculated with the 6-31G(d,p) basis set.

Structure	UHF	$\langle S^2 \rangle$	UMP2	UMP3	UMP4	PUMP4
Si ⁺ insertion Transition States						
4a	-618.79804	0.7886	-619.09880	-619.14209	-619.16002	-619.16226
4b	-618.84563	0.7633	-619.14544	-619.18892	-619.20473	-619.20552
4c	-618.82701	0.7714	-619.12656	-619.16785	-619.18514	-619.18639
Isomerization Transition States						
5a	-618.87017	0.7606	-619.17369	-619.21366	-619.22889	-619.22958
5b	-618.86631	0.7609	-619.16792	-619.20801	-619.22329	-619.22399
5c	-618.82701	0.8072	-619.12477	-619.16644	-619.18414	-619.18681
5d	-618.85529	0.7583	-619.16420	-619.20208	-619.21798	-619.21854
5e	-618.78495	0.8207	-619.09393	-619.13174	-619.14998	-619.15387
5f	-618.87939	0.7648	-619.18071	-619.21769	-619.23329	-619.22508
5g	-618.86336	0.7606	-619.14676	-619.18798	-619.20242	-619.20344
5h	-618.86811	0.7648	-619.16562	-619.20865	-619.22408	-619.22508
5i	-618.87778	0.7545	-619.17727	-619.21434	-619.22990	-619.23024

Table IIe. Total energies (in Hartrees) calculated with the 6-31G(d,p) basis set.

Structure	UHF	$\langle S^2 \rangle$	UMP2	UMP3	UMP4	PUMP4
H ₂ elimination Transition States						
6a	-618.78394	0.7823	-619.11034	-619.14703	-619.16604	-619.16765
6b	-618.78916	0.8698	-619.10776	-619.14765	-619.16515	-619.16840
6c	-618.81220	0.7860	-619.13179	-619.17262	-619.18934	-619.19097
6d	-618.81105	0.7832	-619.13095	-619.17170	-619.18846	-619.19000
6e	-618.79736	0.7620	-619.11754	-619.15752	-619.17437	-619.17512
6f	-618.76925	0.7709	-619.09625	-619.13173	-619.15057	-619.15162
6g	-618.79583	0.8827	-619.11362	-619.15201	-619.17058	-619.17475
SiH ₄ and CH ₄ elimination Transition States						
12a (SiH₄)	-618.79075	0.9148	-619.09339	-619.13555	-619.15406	-619.16033
13a (CH₄)	-618.76215	0.7682	-619.08425	-619.12463	-619.14386	-619.14485

Table IIf. Total Energies (Hartrees) Calculated with the 6-31G(d,p) Basis Set.

Structure	UHF	$\langle S^2 \rangle$	UMP2	UMP3	UMP4	PUMP4
$\text{Si}^+ (^2\text{P}) + \text{H}_3\text{Si-CH}_3$	-618.83315	0.7599	-619.11950	-619.16279	-619.17762	-619.17816
$\text{SiH}_3 + \text{CH}_3\text{Si}^+ (^2\text{A}_1)$	-618.82855	0.7539	-619.11897	-619.16211	-619.17765	-619.17793
$\text{SiH}_4 + \text{CH}_2\text{Si}^+ (^2\text{B}_2)$	-618.82703	0.7572	-619.10476	-619.15144	-619.16635	-619.16703
$\text{CH}_4 + \text{H}_2\text{SiSi}^+ (^2\text{B}_2)$	-618.81498	0.7587	-619.09373	-619.13527	-619.14910	-619.19775
$\text{SiH} + \text{CH}_3\text{-SiH}^+ (^2\text{A}')$	-618.81864	0.7608	-619.10265	-619.14512	-619.15982	-619.16050
$\text{SiH}^+ (^2\text{A}_1) + \text{CH}_3\text{-SiH}_2$	-618.79811	0.7533	-619.08565	-619.12940	-619.14477	-619.14502
$\text{SiH}_2 + \text{CH}_3\text{-SiH}_2^+ (^2\text{A}')$	-618.79044	0.7544	-619.07510	-619.11762	-619.13284	-619.13317
$\text{SiH}_2^+ (^2\text{A}_1) + \text{CH}_3\text{-SiH}_2$	-618.76649	0.7534	-619.05170	-619.09376	-617.10893	-619.10920
$2\text{H}_2 + [\overline{\text{Si-CH}_2\text{-Si}}]^+ (^2\text{A}_1)$	-618.76793	0.7685	-619.07896	-619.12229	-619.14178	-619.14275

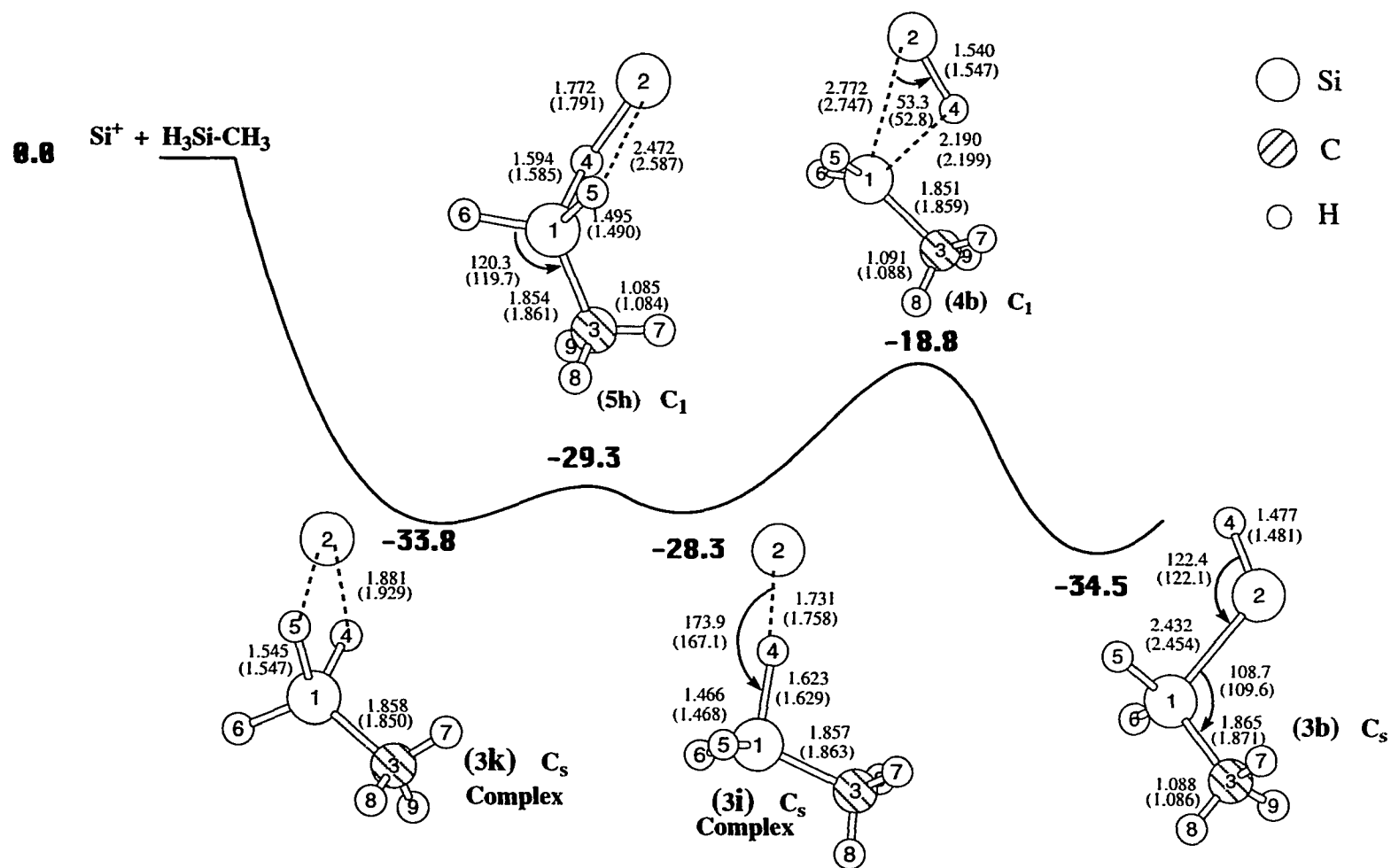


Figure 1a. PUMP4/6-31G(d) potential energy profile with relative energies (numbers in bold) in kcal/mol. The solid curve corresponds to the SCF/3-21G* level of theory. SCF/3-21G* and SCF/6-31G(d) (in parentheses) structures with bond distances in Å and bond angles in degrees.

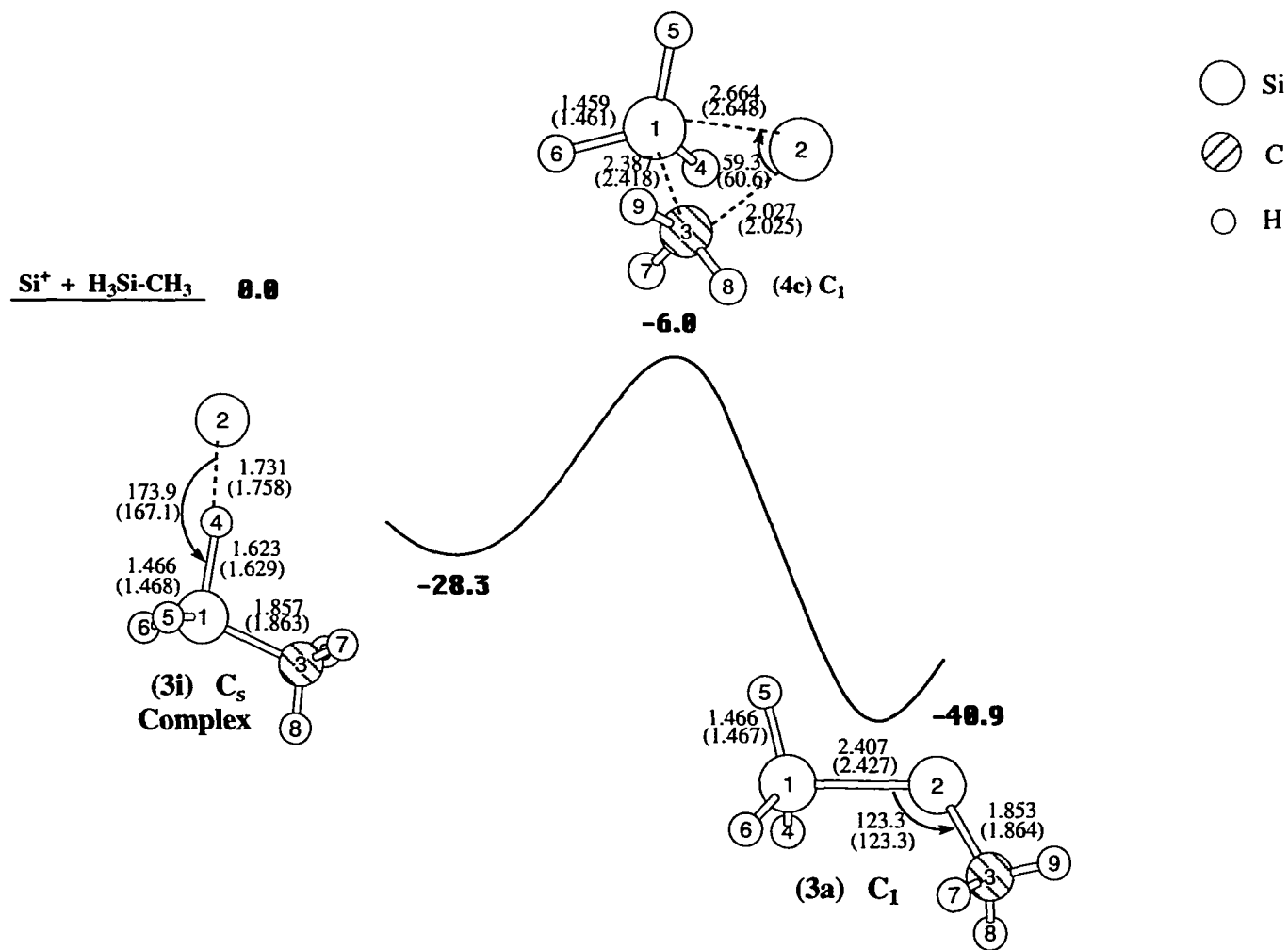


Figure 1b. PUMP4/6-31G(d) potential energy profile with relative energies (numbers in bold) in kcal/mol. The solid curve corresponds to the SCF/3-21G* level of theory. SCF/3-21G* and SCF/6-31G(d) (in parentheses) structures with bond distances in Å and bond angles in degrees.

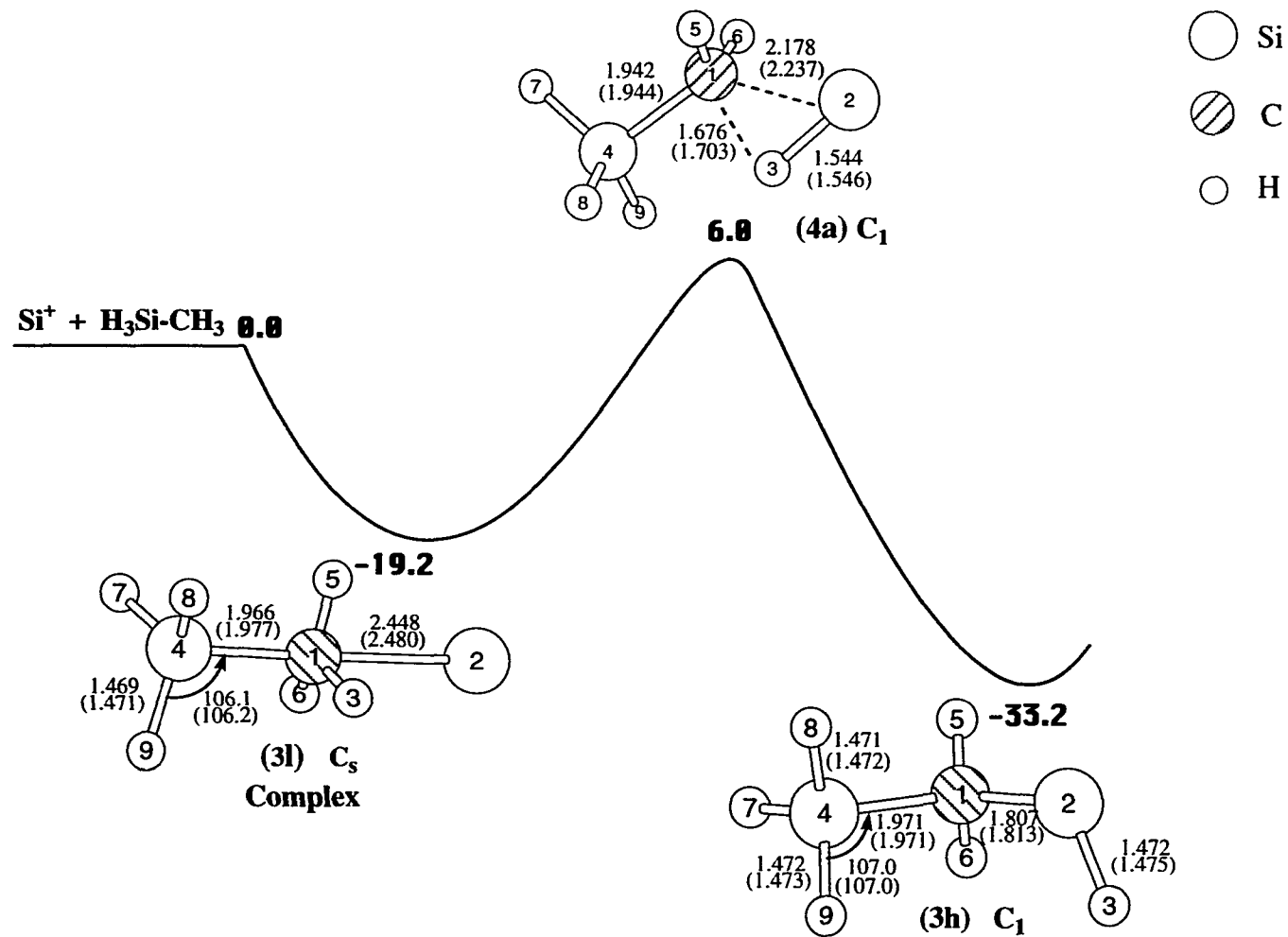


Figure 1c. PUMP4/6-31G(d) potential energy profile with relative energies (numbers in bold) in kcal/mol. The solid curve corresponds to the SCF/3-21G* level of theory. SCF/3-21G* and SCF/6-31G(d) (in parentheses) structures with bond distances in Å and bond angles in degrees.

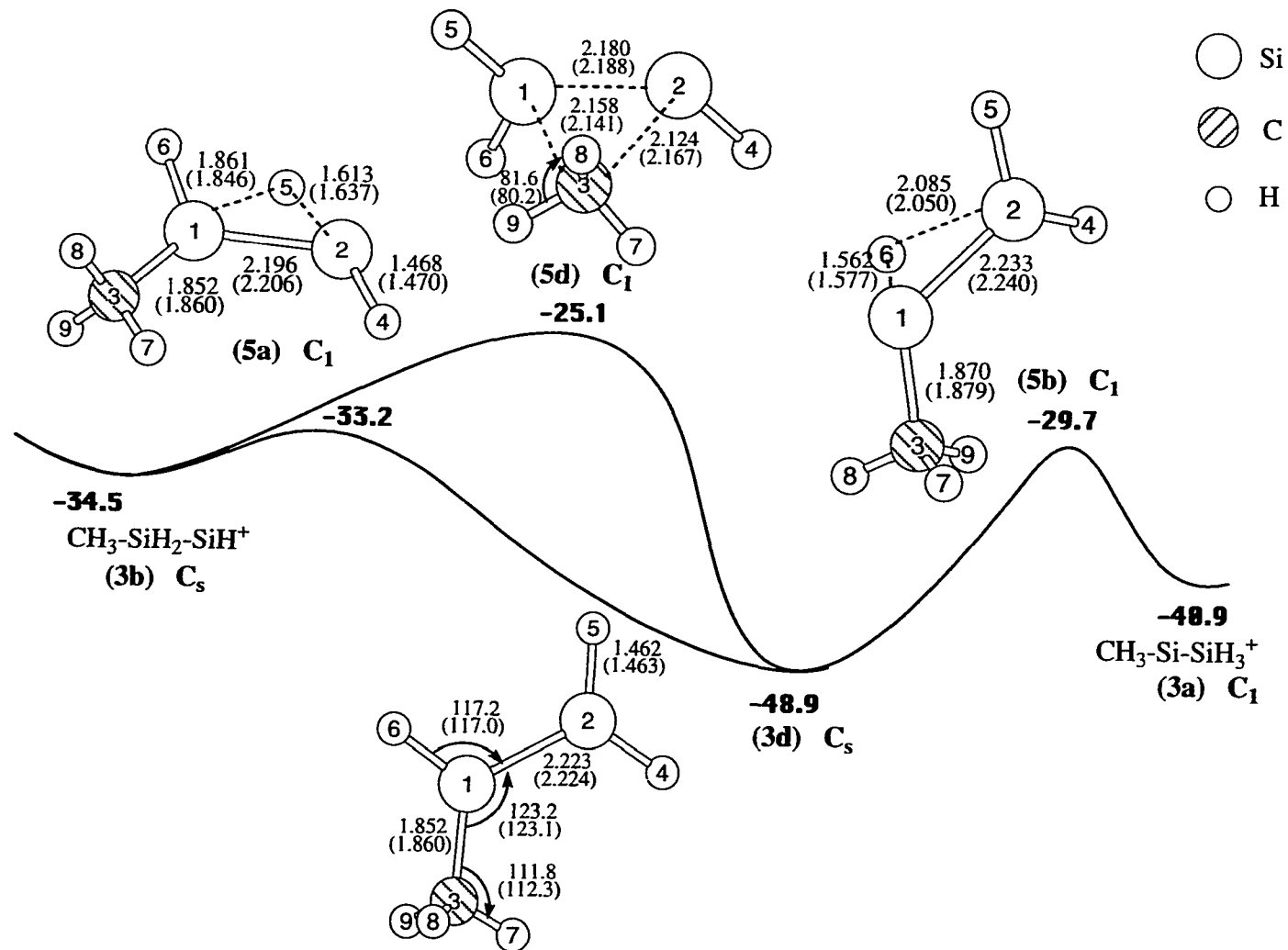


Figure 2a. PUMP4/6-31G(d) potential energy profile with relative energies (numbers in bold) in kcal/mol. The solid curves correspond to the SCF/3-21G* level of theory. SCF/3-21G* and SCF/6-31G(d) (in parentheses) structures with bond distances in Å and bond angles in degrees.

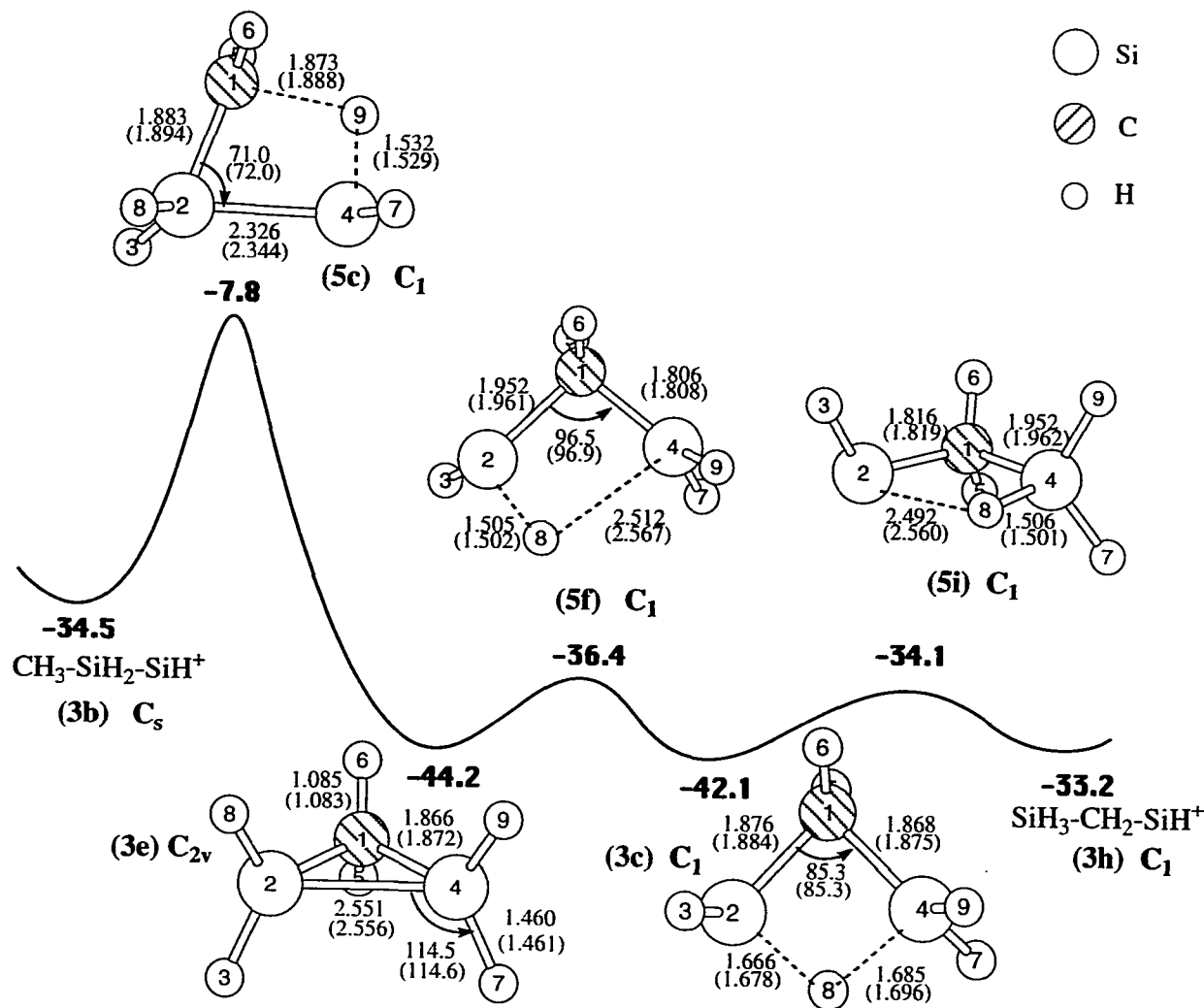


Figure 2b. PUMP4/6-31G(d) potential energy profile with relative energies (numbers in bold) in kcal/mol. The solid curve corresponds to the SCF/3-21G* level of theory. SCF/3-21G* and SCF/6-31G(d) (in parentheses) structures with bond distances in Å and bond angles in degrees.

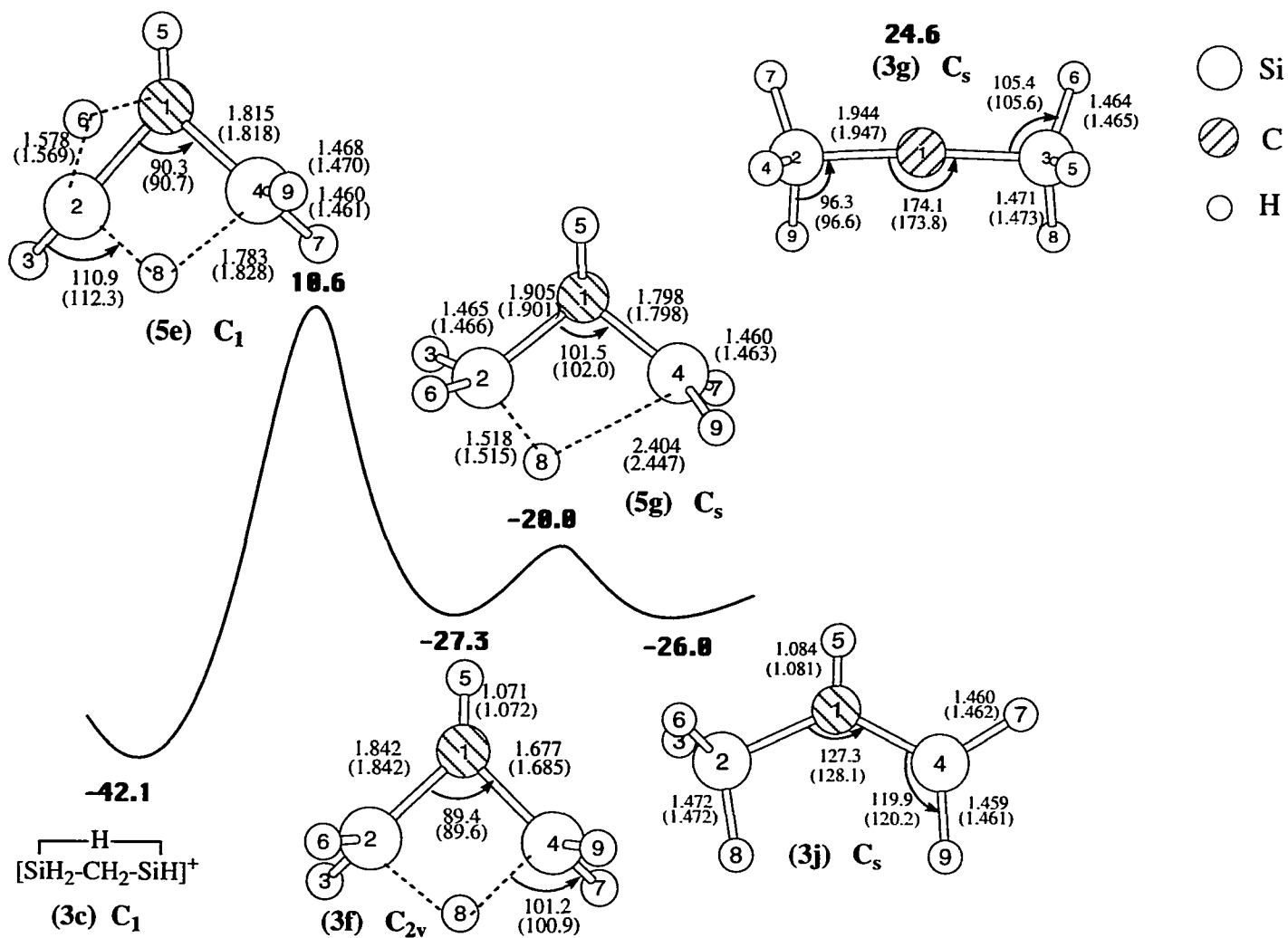


Figure 2c. PUMP4/6-31G(d) potential energy profile with relative energies (numbers in bold) in kcal/mol. The solid curve corresponds to the SCF/3-21G* level of theory. SCF/3-21G* and SCF/6-31G(d) (in parentheses) structures with bond distances in Å and bond angles in degrees.

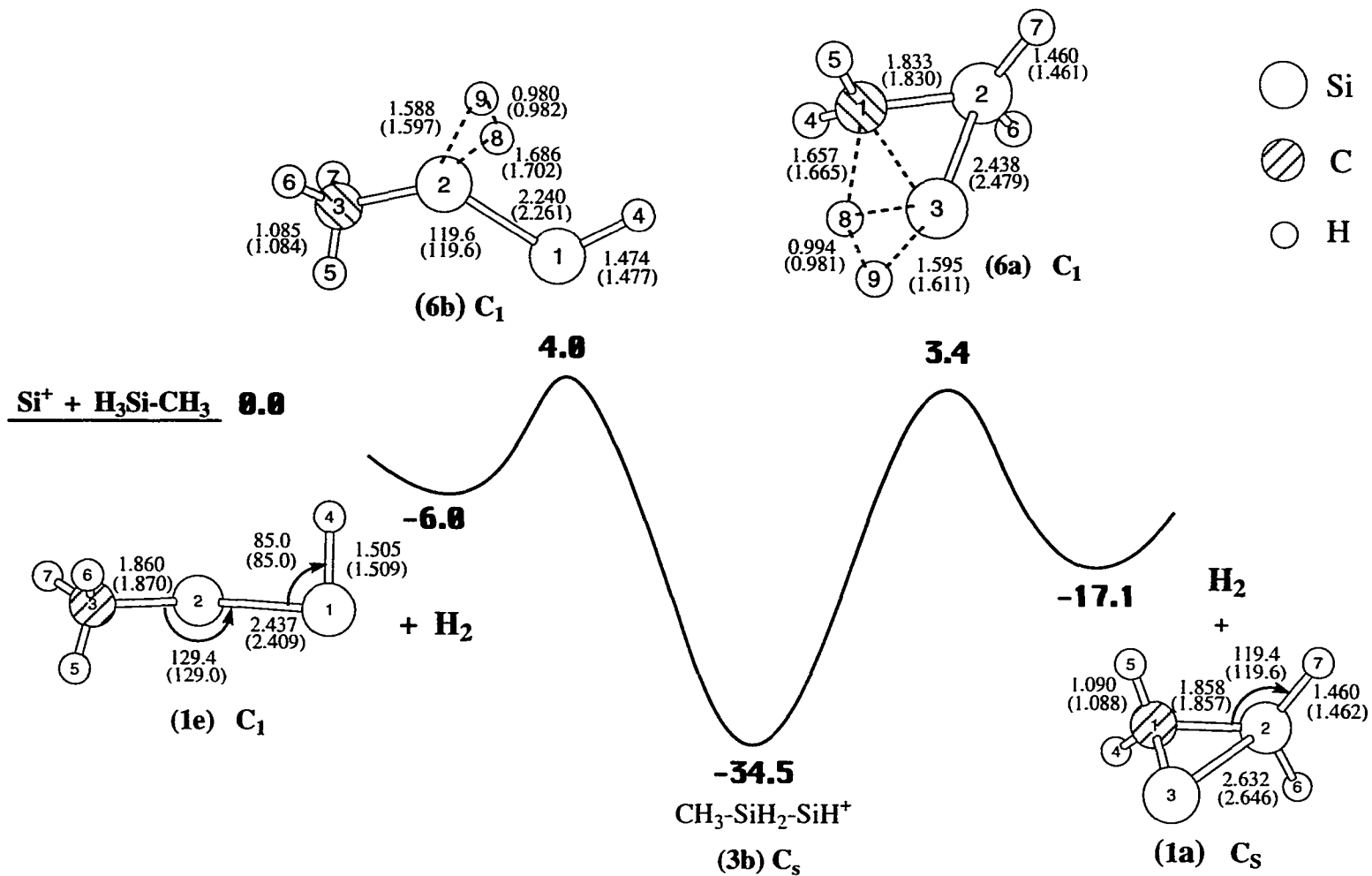


Figure 3a. PUMP4/6-31G(d) potential energy profile with relative energies (numbers in bold) in kcal/mol. The solid curve corresponds to the SCF/3-21G* level of theory. SCF/3-21G* and SCF/6-31G(d) (in parentheses) structures with bond distances in Å and bond angles in degrees.

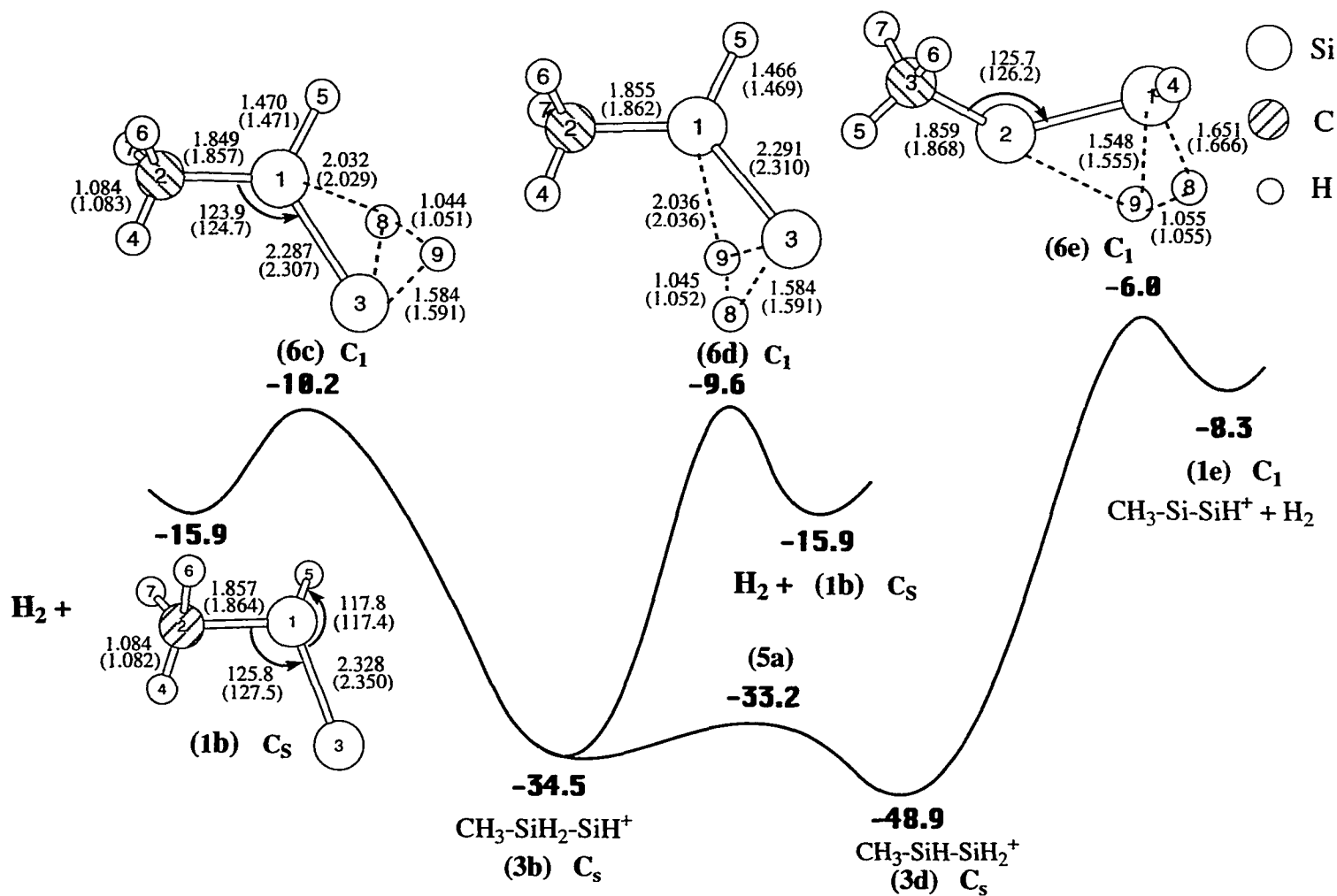


Figure 3b. PUMP4/6-31G(d) potential energy profile with relative energies (numbers in bold) in kcal/mol. The solid curve corresponds to the SCF/3-21G* level of theory. SCF/3-21G* and SCF/6-31G(d) (in parentheses) structures with bond distances in Å and bond angles in degrees.

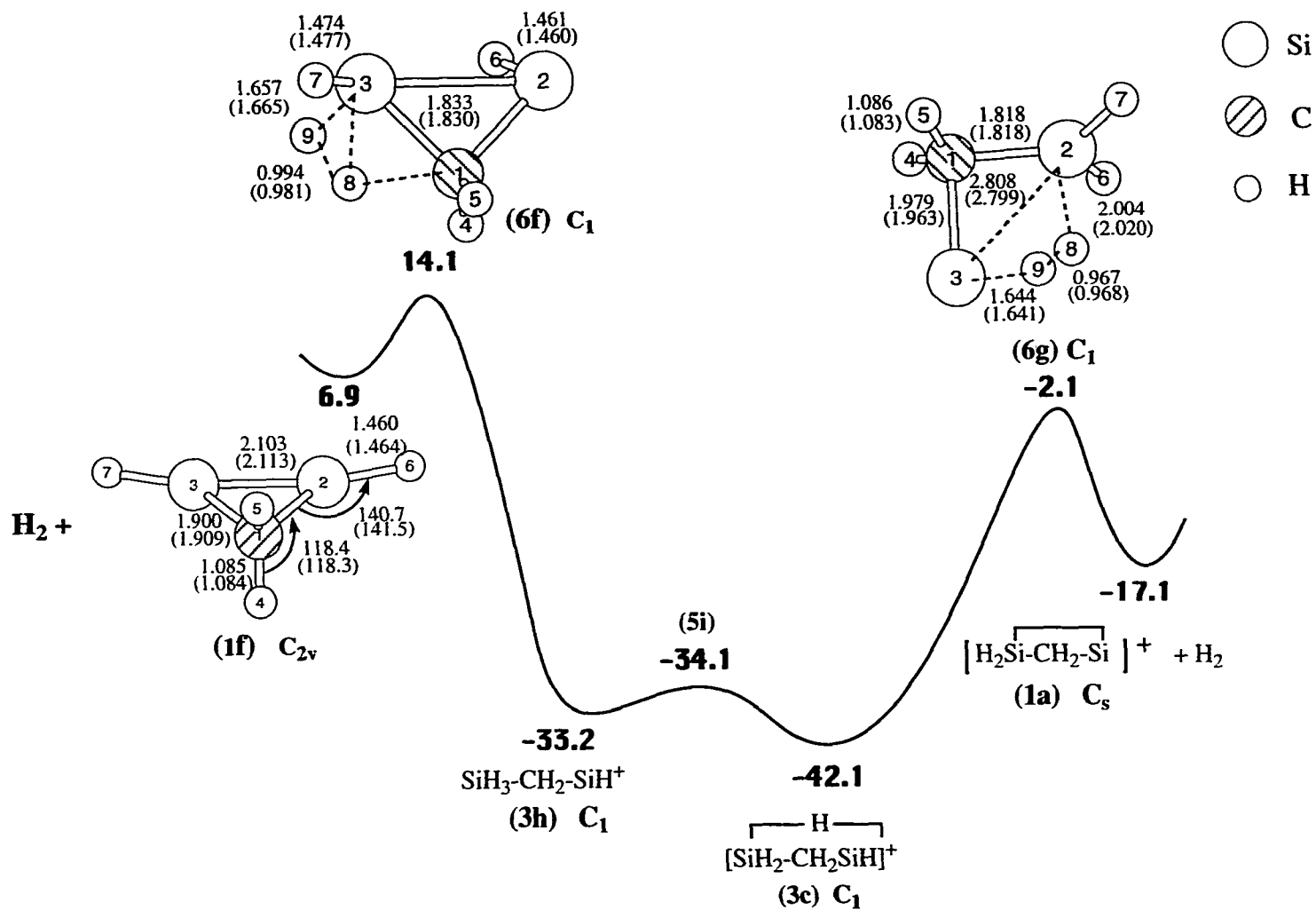


Figure 3c. PUMP4/6-31G(d) potential energy profile with relative energies (numbers in bold) in kcal/mol. The solid curve corresponds to the SCF/3-21G* level of theory. SCF/3-21G* and SCF/6-31G(d) (in parentheses) structures with bond distances in Å and bond angles in degrees.

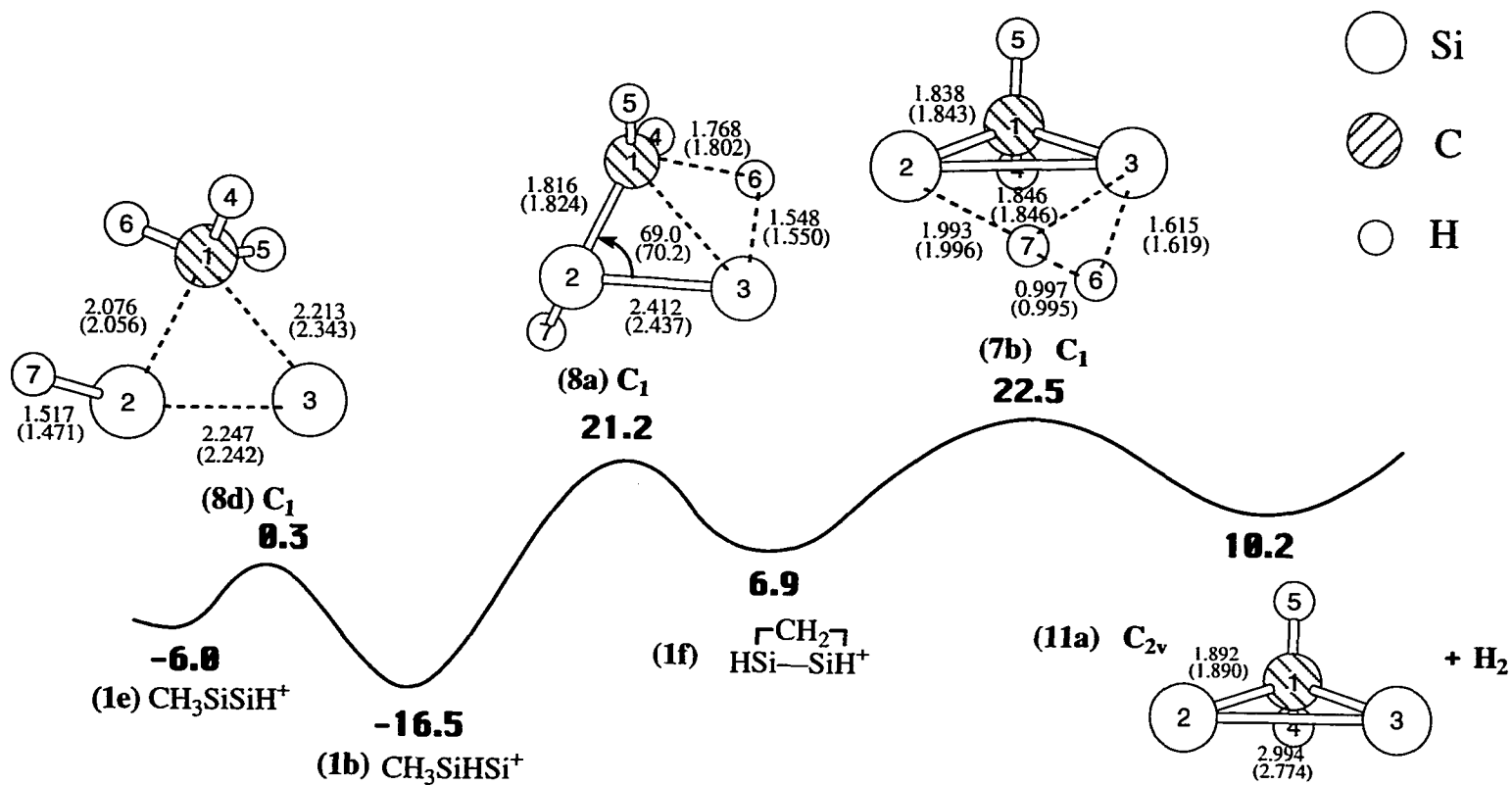


Figure 4a. PUMP4/6-31G(d) potential energy profile with relative energies (numbers in bold) in kcal/mol. The solid curve corresponds to the SCF/3-21G* level of theory. SCF/3-21G* and SCF/6-31G(d) (in parentheses) structures with bond distances in Å and bond angles in degrees.

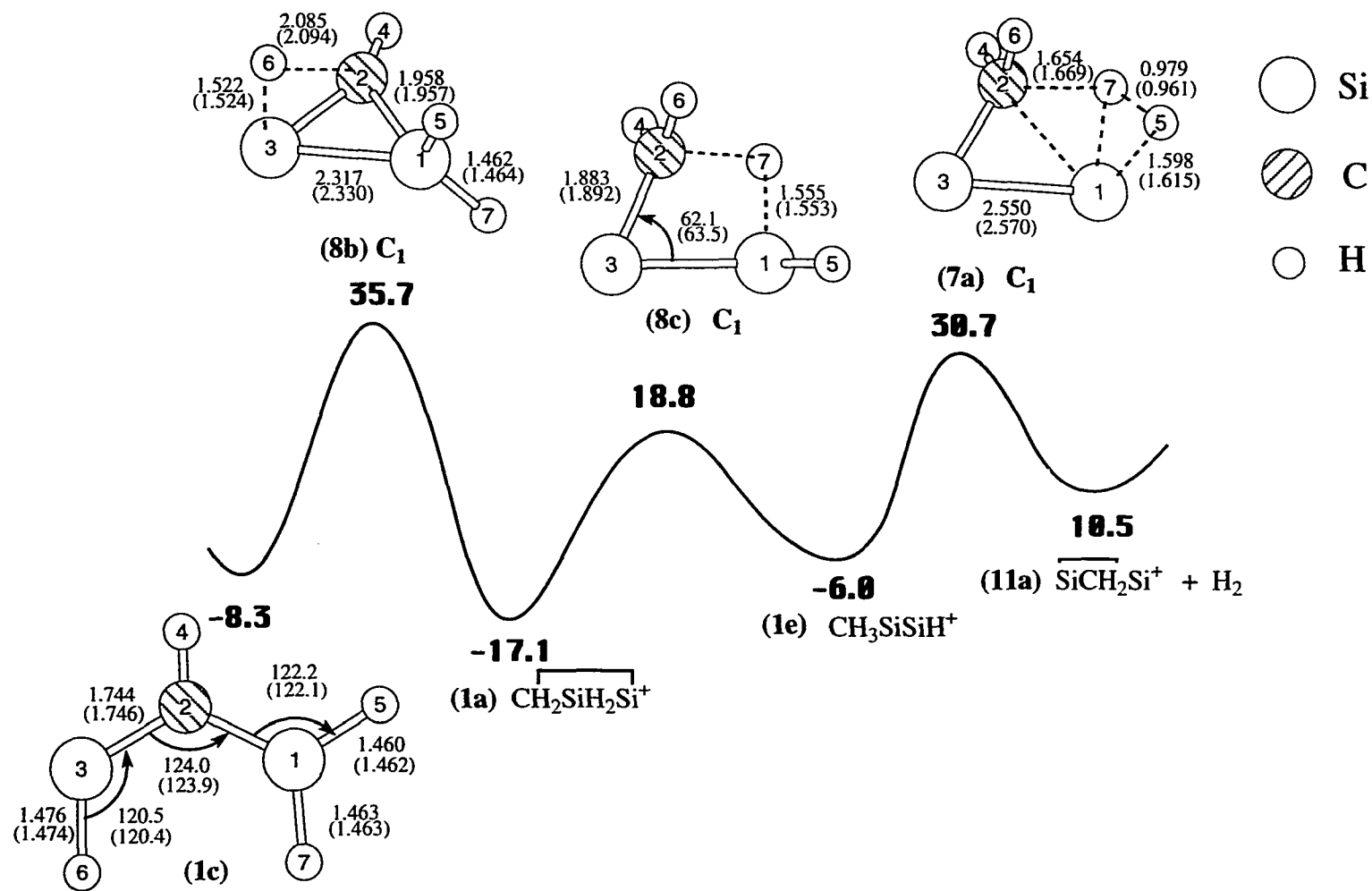


Figure 4b. PUMP4/6-31G(d) potential energy profile with relative energies (numbers in bold) in kcal/mol. The solid curve corresponds to the SCF/3-21G* level of theory. SCF/3-21G* and SCF/6-31G(d) (in parentheses) structures with bond distances in Å and bond angles in degrees.

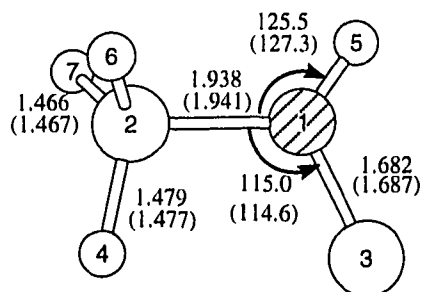
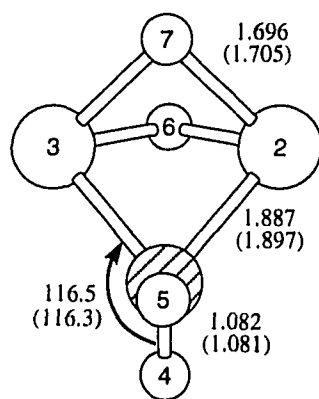
(1d) C_s (1g) C_{2v}

Figure 4c. SCF/3-21G* and SCF/6-31G(d) (in parentheses) structures with bond distances in Å and bond angles in degrees.

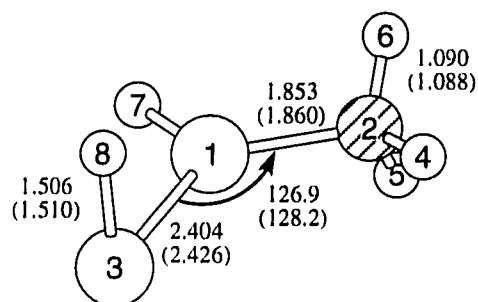
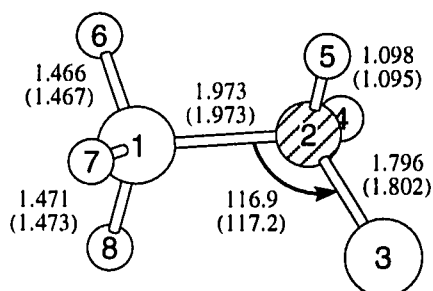
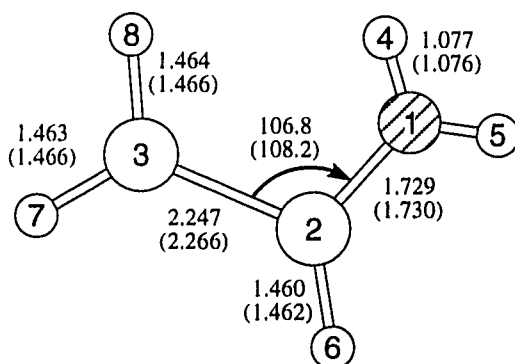
(2e) C_1 (2f) C_s (2g) C_s

Figure 5a. SCF/3-21G* and SCF/6-31G(d) (in parentheses) structures with bond distances in Å and bond angles in degrees.

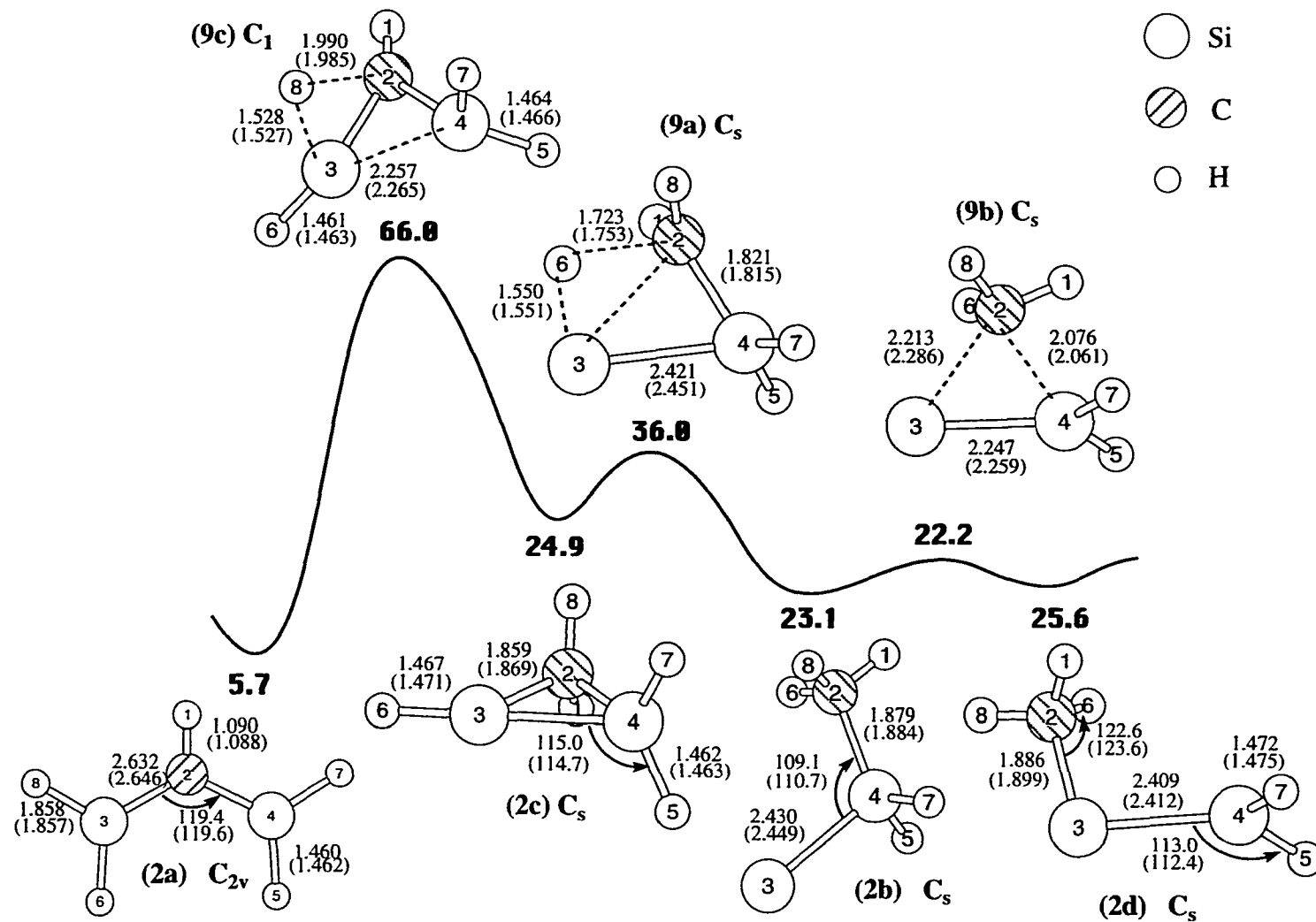


Figure 5b. PUMP4/6-31G(d) potential energy profile with relative energies (numbers in bold) in kcal/mol. The solid curve corresponds to the SCF/3-21G* level of theory. SCF/3-21G* and SCF/6-31G(d) (in parentheses) structures with bond distances in Å and bond angles in degrees.

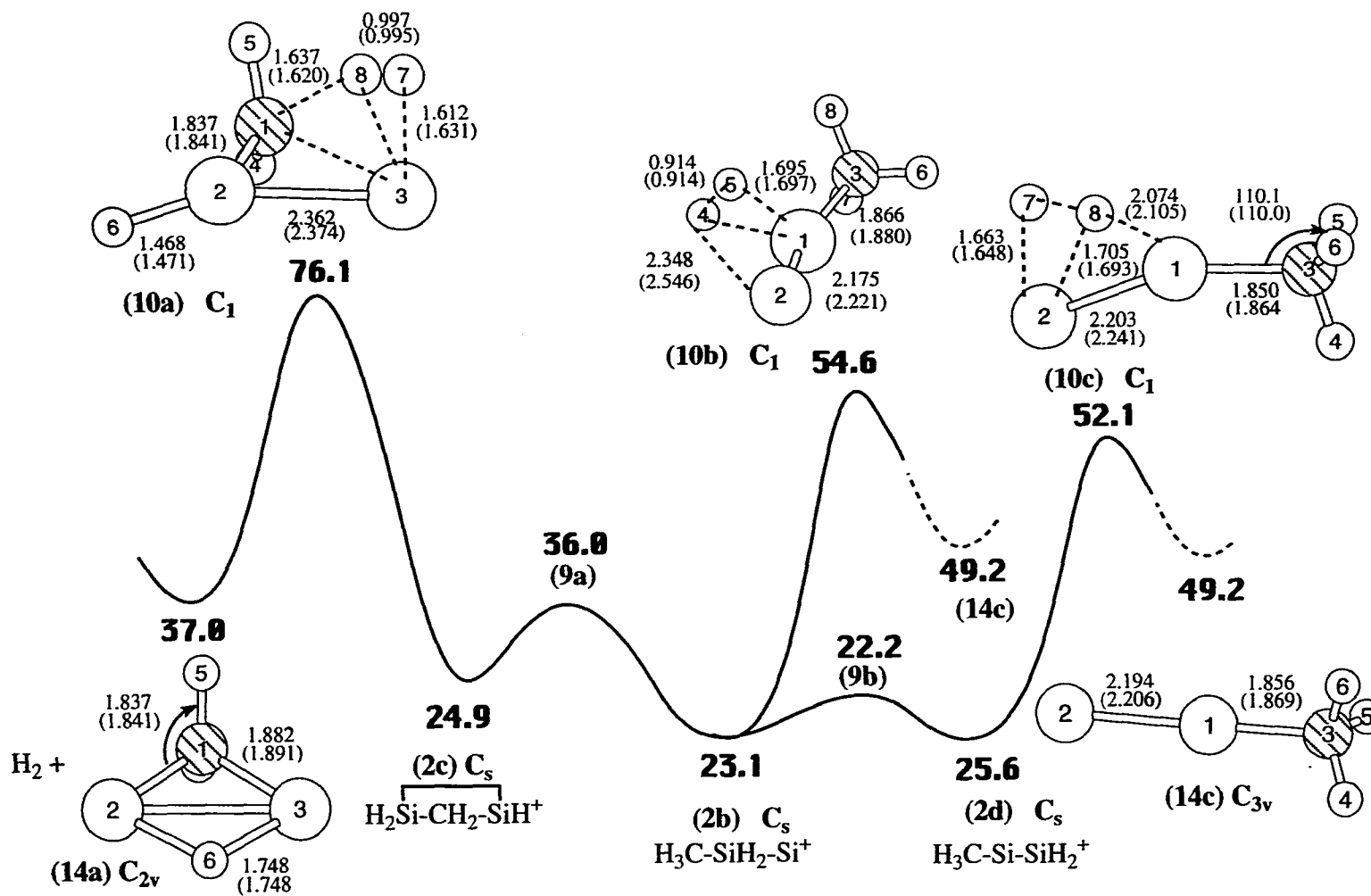


Figure 5c. PUMP4/6-31G(d) potential energy profile with relative energies (numbers in bold) in kcal/mol. The solid curves correspond to the SCF/3-21G* level of theory. SCF/3-21G* and SCF/6-31G(d) (in parentheses) structures with bond distances in Å and bond angles in degrees.

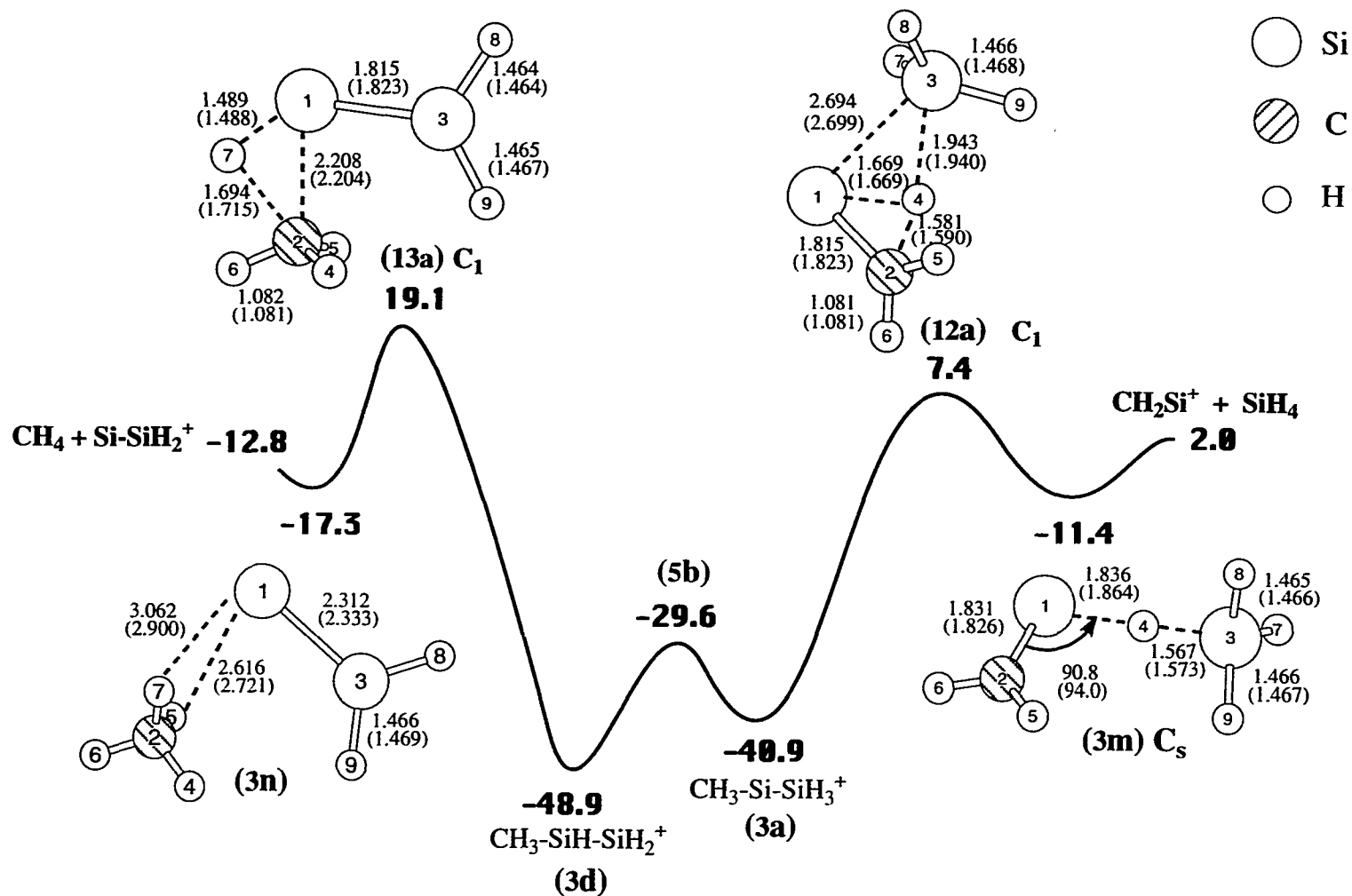


Figure 6. PUMP4/6-31G(d) potential energy profile with relative energies (numbers in bold) in kcal/mol. The solid curve corresponds to the SCF/3-21G* level of theory. SCF/3-21G* and SCF/6-31G(d) (in parentheses) structures with bond distances in Å and bond angles in degrees.

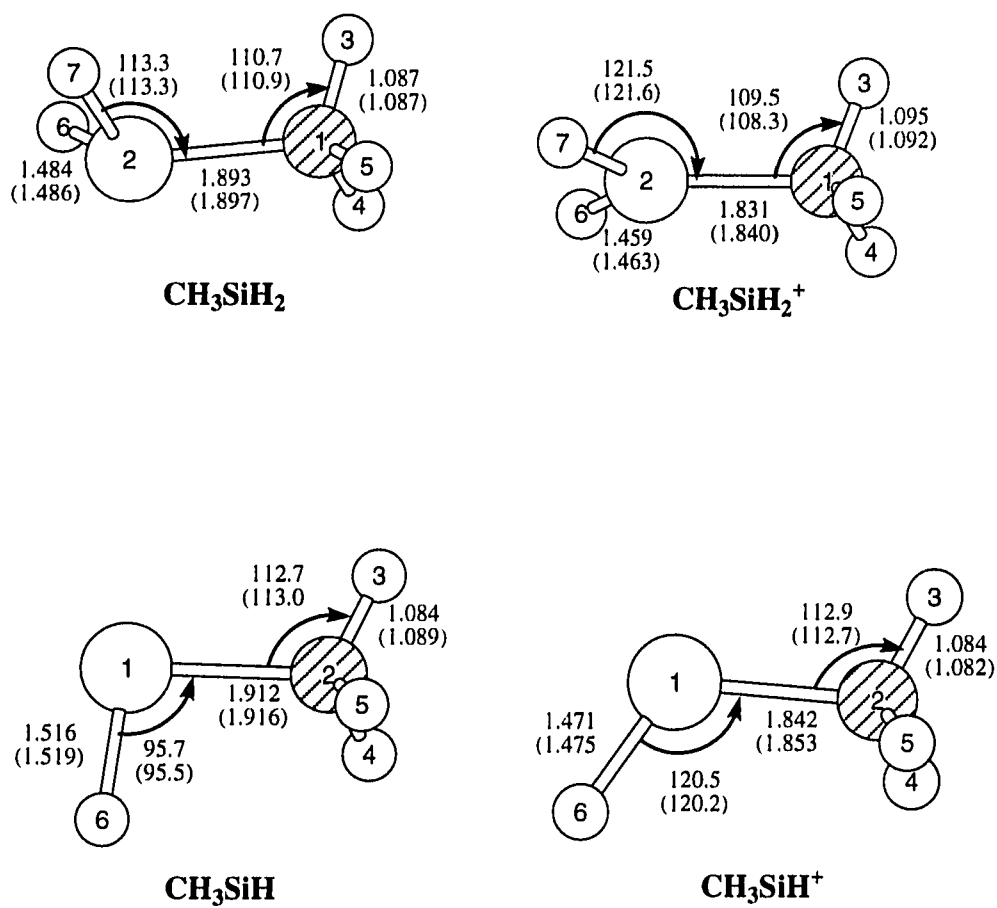


Figure 7. SCF/3-21G* and SCF/6-31G(d) (in parentheses) structures with bond distances in Å and bond angles in degrees.

CHAPTER 9. PARAMETERS FOR SCALING THE CORRELATION ENERGY OF THE BONDS Si-H, P-H, AND Cl-H AND APPLICATION TO THE REACTION OF SILYL RADICAL WITH SILANE

A paper published in and reprinted with permission from

J. Phys. Chem. **1989**, 93, 7356-7358

Copyright 1989 American Chemical Society

Mark S. Gordon, Kiet A. Nguyen, and Donald G. Truhlar

Abstract

Scale factors are determined for scaling all the correlation energy in Møller-Plesset perturbation theory calculations on third-period elements bonded to H. We consider 10 different basis sets and both second- and fourth-order perturbation theory for each bond type. We find p functions are needed on H for reliable scaling. The scale factors for Si-H bond are used for MP-SAC2 and MP-SAC4 calculations of the classical barrier height for the hydrogen-atom-transfer reaction of SiH₃ with SiH₄.

Introduction

A difficulty with using correlated electronic structure calculations employing basis-set expansions to estimate enthalpies of activation for chemical reactions is that the results may be very slowly convergent with respect to both the one-electron basis set and the treatment of higher order correlation effects.¹ These problems are in fact closely related since the basis set requirements are more severe for accurate calculations including electron correlation than for reaching the noncorrelated Hartree-Fock limit.^{2,3} A method that has been proposed to alleviate this problem, which is applicable when a single-determinant wave function provides a good zero-order description is the Møller-Plesset/scaling-all-correlation (MP-SAC)

approximation.⁴⁻⁶ Parameters have been proposed for this method for H-H, C-H, N-H, O-H, and F-H bonds,^{4,5} and for C-C, N-N, O-O, C-N, and C-O bonds⁵ as well. In this paper we extend the parametrization to include Si-H, P-H, S-H, and Cl-H bonds.

Theory

In the MP-SAC n method,⁴ the fraction \mathcal{F}_n of the valence correlation energy recovered by a particular order n of Møller-Plesset (MP) perturbation theory and on-electron basis set is assumed to be transferable for a given bond type. This transferability is assumed at least among different geometries for a given system, and it could also be assumed to hold among several systems if desired. Assuming transferability in a given system, since MP theory is size extensive, the value of \mathcal{F}_n can be obtained from a calculation on a dissociation energy. In particular we estimate \mathcal{F}_n using

$$\mathcal{F}_n = \frac{D(\text{MP}n) - D(\text{HF})}{D(\text{experiment}) - D(\text{HF})} \quad (1)$$

where D is the bond energy, and correlation energy is measured with respect to a single-determinant Hartree-Fock (HF) reference wave function for the one-electron basis set under consideration. The dissociation energies are referred to the classical equilibrium geometry; i.e., we calculate approximate values of D_e , not D_0 .

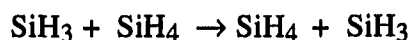
Having obtained \mathcal{F}_n values for a given bond type, one can adopt two strategies to proceed. First, one could adjust the basis set to make the \mathcal{F}_n values equal for all bond type exhibiting significant variation in internuclear distance for the problem under consideration. Alternatively, and this is the strategy considered in the rest of this paper, one can find average values of \mathcal{F}_n for a range of bond types.

Calculations

1. *Average Values of \mathcal{F}_n* . Table I gives calculated bond dissociative energies for third-period hydrides as obtained with several common and extended basis sets.⁷ The final row of the table gives experimental values.⁸ The notation for the basis sets is standard, e.g., (2d, p) means two sets of d functions on the heavy atoms and on set of p functions on the hydrogens; (,p) means no d sets on heavy and one p set on each hydrogen.

In Table II these dissociation energies are converted to \mathcal{F}_n values for a given bond type. These in turn are averaged—both including H₂, which yields an average value called A1, and excluding H₂, which yields the value denoted A2.

2. *Application to a chemical Reaction*. As an example of the use of this theory we calculate the barrier height for the reaction



The calculated classical barrier heights are given in Table III. The barrier heights in Table III were calculated assuming that the geometry of the saddle point need not to be reoptimized at each level of theory or value of \mathcal{F}_n . Thus all calculations were carried out with a geometry optimized at the HF/6-31G(d) level. This yields a structure with D_{3d} symmetry and bond lengths of 1.797 Å for the making and breaking Si-H bonds; the silyl Si-H bond lengths are 1.483 Å and the H-Si---H bond angles are 109.1°. The value labeled HF are from unrestricted Hartree-Fock calculations, those labeled MP n are from MP perturbation theory with $n = 2$ or 4, and those labeled MP-SAC n are calculated by

$$E(\text{MP} - \text{SAC}n) = E(\text{HF}) + \frac{E(\text{MP}n) - E(\text{HF})}{\mathcal{F}_n} \quad (2)$$

where E is the energy. Equation 2 is a straightforward consequence of the assumption that \mathcal{F}_n is constant over a given a given potential energy surface. Results are shown for two

values \mathcal{F}_n : the one determined from breaking the Si-H bond in silane and the A2 average value.

Discussion

Table II shows that the present calculations recover 30-98% of the correlation energy contribution to the dissociation energies. For a given order of perturbation theory and basis set the relative deviation of individual \mathcal{F}_n values from the average values is usually small. The best balanced basis set, i.e., those with least variation in \mathcal{F}_n , are 6-31G(d,p) and MC-311G(p) for $n = 2$ and 6-31G(d), MC-311G(d), and 6-31G(2d,p) for $n = 4$. We would recommend basis sets with $\mathcal{F}_n \geq 0.65$ for the most reliable results; this means polarization functions should be included on hydrogens.

Table III shows reasonably consistent barrier heights at the MP-SAC n level from all basis sets with polarization function on hydrogens. The results are not very sensitive to other details of the basis set or to which choice is made for \mathcal{F}_n . In addition there is much better agreement between the MP-SAC2 and MP-SAC4 barrier heights than between those calculated by MP2 and MP4 methods. The predicted barrier height is in the range 13.4 ± 0.6 kcal/mol for all these calculations. These calculations indicate good convergence both with respect to the level of perturbation theory and the number of polarization functions and also with respect to expanding the valence basis from double ζ and triple ζ . The results are very suggestive that the MP-SAC2 calculations are more reliable than MP4 calculations and equally as reliable as MP-SAC4 calculations with the same basis set, although the MP-SAC2 results are much less expensive. The barrier calculated by the MP-SAC2 method with the largest basis set calculated by the MP-SAC2 method with the largest basis set and the Si-H value of \mathcal{F}_2 is 13.0 kcal/mol.

The MP-SAC n option for energies, geometries, and frequencies⁶ has been added to the GAUSSIAN82⁹ program at North Dakota State University and at the Minnesota

Supercomputer Center,¹¹ and it should not be very difficult to implement to in other versions of the GAUSSIAN programs. We hope that the conclusions about basis set and \mathcal{F}_n values given in the present paper will be useful for studying a wide variety of reactions.

Acknowledgment

This work was supported by grants from the National Science Foundation (M.S.G., CHEM86-40771; D.G.T., CHEM86-17063) and by the Air Force Office of Scientific Research (M.S.G., 87-0049). We also acknowledge computer time and visitor grant made available by the Minnesota Supercomputer Institute and computer time made available the North Dakota State University Computer Center.

References

- (1) see, e.g.: Brown, F. B.; Truhlar, D. G. *Chem. Phys. Lett.* **1985**, 117, 307.
Bauschlicher, Jr., C. W.; Walch, S. P.; Langhoff, S. R.; Taylor, P. R.; Jaffe, R. L. *J. Chem. Phys.* **1988**, 88, 1743.
- (2) Ahlrichs, R.; Driessler, F.; Lischka, H.; Staemmler, V.; Kutzelnigg, W. *J. Chem. Phys.* **1975**, 62, 1235.
- (3) Almlöf, J.; Taylor, P. R. *J. Chem. Phys.* **1987**, 86, 4070.
- (4) Gordon, M. S.; Truhlar, D. G. *J. Am. Chem. Soc.* **1986**, 108, 5412.
- (5) Gordon, M. S.; Truhlar, D. G. *Int. J. Quantum Chem.* **1987**, 31, 81.
- (6) Truong, T. N.; Truhlar, D. G.; Baldrige, K. K.; Gordon, M. S.; Steckler, R. *J. Chem. Phys.* **1989**, 90, 7137.
- (7) (a) 6-31G, 6-31G(d), and 6-31G(d,p): Hariharan, P. C.; Pople, J. A. *Theor. Chim. Acta.* **1973**, 28, 213. Gordon, M. S. *Chem. Phys. Lett.* **1980**, 76, 163. (b) MC-311G, MC-311G(d), and MC-311G(d,p): McLean, A. D.; Chandler, G. S. *J. Chem. Phys.* **1980**, 72, 5639. Frisch, M. J.; Pople, J. A.; Binkley, J. S. *J. Chem. Phys.* **1984**, 80, 3265. (c) For a discussion of the remaining basis set, see ref 4 and 5. In

general, (2d) and (2p) refer to the polarization functions in GAUSSIAN86.

- (8) The experimental values of D_e are obtained from the heats of formation for the appropriate AH_n compounds [*J. Chem. Thermodyn.* **1975**, 10, 903. *JANAF Thermochemical Tables*, 2nd ed.; Stull, D. R.; Prophet, H., Eds.; National Bureau of Standards: Washington, DC, 1971, and supplements thereto] as outlined in ref 4.
- (9) Binkley, J. S.; Frisch, M. J.; DeFrees, D. J.; Krishnan, R.; Whiteside, R. A.; Schlegel, H. B.; Fleuder, E. M.; Pople, J. A. GAUSSIAN82; Carnegie-Mellon University: Pittsburgh, 1983.
- (10) Frisch, M. J.; Binkley, J. S.; Schlegel, H. B.; Raghavarchari, K.; Melius, C. F.; Martin, R. L.; Stewart, J. J. P.; Bobrowicz, F. W.; Rohlfing, C. M.; Kahn, L. R.; DeFrees, D. J.; Seeger, R.; Whiteside, R. A.; Fox, D. J.; Fleuder, E. M.; Topiol, S. Pople, J. A. GAUSSIAN86; Carnegie-Mellon Quantum Chemistry Publishing Unit: Pittsburgh, PA 15213.
- (11) The assistance of Kim Baldrige, Dennis Lienke, Rozeanne Steckler, Marty Storma, and Thanh Truong with SAC updates at NDSU, SDSC and MSC is gratefully acknowledged.

Table I: Energies (kcal/mol) for the Reaction $XH_m \rightarrow XH_{m-1} + H$

Basis	Si	P	S	Cl
6-31G				
SCF	68.2	54.6	55.6	59.9
MP2	76.3	64.8	68.1	74.0
MP4	78.6	67.3	70.7	76.5
6-31G(d)				
SCF	75.8	62.8	65.7	71.4
MP2	84.3	74.1	80.4	88.8
MP4	86.2	75.8	81.8	89.5
6-31G(d,p)				
SCF	76.6	63.9	67.9	75.3
MP2	89.4	79.6	87.2	97.1
MP4	91.8	87.2	88.7	97.8
MC-311G				
SCF	68.4	55.3	55.8	60.0
MP2	77.1	65.9	68.4	73.9
MP4	79.3	68.4	71.0	76.3
MC-311G(d)				
SCF	74.9	62.3	64.9	70.7
MP2	83.8	73.7	79.8	88.3
MP4	85.6	75.6	81.2	88.9
MC-311G(,p)				
SCF	73.4	61.2	64.6	71.7
MP2	88.1	78.3	84.9	92.6
MP4	91.2	81.4	87.9	95.5
MC-311G(d,p)				
SCF	76.1	63.8	67.9	75.6
MP2	90.4	81.0	88.7	99.0
MP4	93.3	83.3	90.4	99.8
6-31G(2d,p)				
SCF	76.6	64.2	68.7	76.7
MP2	89.6	80.6	88.8	100.0
MP4	91.9	82.2	89.7	99.9
MC-311G(2d,p)				
SCF	76.0	63.7	68.1	76.2
MP2	90.5	81.4	89.4	100.6
MP4	93.2	83.5	90.7	100.8
MC-311G(d,2p)				
SCF	76.1	63.8	68.3	76.2
MP2	91.3	82.7	91.9	102.0
MP4	94.4	85.1	93.6	102.9
experiment	94.8	88.5	94.7	106.1
<i>m</i>	4	3	2	1

Table II: Calculated \mathcal{F}_n values

Basis	H-H	Si-H	P-H	S-H	Cl-H	A2	A1
6-31G							
n = 2	0.39	0.30	0.30	0.32	0.31	0.31	0.32
n = 4	0.55	0.39	0.37	0.39	0.36	0.38	0.41
6-31G(d)							
n = 2	0.39	0.45	0.44	0.51	0.56	0.49	0.47
n = 4	0.55	0.55	0.51	0.56	0.52	0.54	0.54
6-31G(d,p)							
n = 2	0.67	0.70	0.64	0.72	0.71	0.69	0.69
n = 4	0.85	0.84	0.70	0.78	0.73	0.76	0.78
MC-311G							
n = 2	0.39	0.33	0.32	0.32	0.30	0.32	0.33
n = 4	0.54	0.41	0.39	0.39	0.35	0.39	0.42
MC-311G(d)							
n = 2	0.39	0.45	0.44	0.50	0.50	0.47	0.46
n = 4	0.54	0.54	0.51	0.55	0.51	0.53	0.53
MC-311G(p)							
n = 2	0.67	0.69	0.63	0.67	0.61	0.65	0.65
n = 4	0.85	0.83	0.74	0.77	0.69	0.76	0.78
MC-311G(d,p)							
n = 2	0.67	0.76	0.70	0.78	0.77	0.75	0.74
n = 4	0.85	0.92	0.79	0.84	0.79	0.84	0.84
6-31G(2d,p)							
n = 2	0.67	0.71	0.67	0.77	0.78	0.73	0.72
n = 4	0.85	0.84	0.74	0.81	0.79	0.80	0.81
MC-311G(2d,p)							
n = 2	0.67	0.77	0.71	0.80	0.82	0.78	0.75
n = 4	0.85	0.81	0.80	0.85	0.82	0.85	0.85
MC-311G(d,2p)							
n = 2	0.73	0.81	0.77	0.89	0.86	0.83	0.81
n = 4	0.91	0.98	0.86	0.96	0.89	0.92	0.92

Table III: Calculated Barrier Heights (kcal/mol) for $\text{SiH}_3 + \text{SiH}_4$

Basis	HF	MP2	MP4	MP2-SAC2		MP2-SAC4	
				SiH	A2	SiH	A2
6-31G(d)	22.0	16.4	15.2	9.6	10.6	9.6	9.4
6-31G(d,p)	21.5	16.0	15.2	13.6	13.5	14.0	13.2
6-31G(2d,p)	22.5	16.1	15.2	13.5	13.7	13.9	13.4
6-31G(d,2p)	21.2	14.6	13.6	13.0	a	13.4	a
MC-311G(d,p)	21.2	15.0	a	13.0	12.9	a	a

^aNot available

CHAPTER 10. EFFECT OF HYDRATION AND DIMERIZATION OF THE FORMAMIDINE REARRANGEMENT

A paper published in and reprinted with permission from

J. Am. Soc. Chem. **1991**, 113, 1596-1600

Copyright 1991 American Chemical Society

Kiet A. Nguyen, Mark S. Gordon, and Donald G. Truhlar

Abstract

Ab initio molecular orbital theory is used to predict the geometry of the transition state and the energy barrier for the double-proton transfer in formamidine dimer, using SCF/6-31G(d,p) and MP2/6-31G(d,p) wave functions, respectively. Intramolecular hydrogen transfer in the uncomplexed monomer (1) and double-proton transfer in the mixed dimer of formamidine and water (2) are also investigated at several levels of theory. All computational levels predict the barrier for the uncomplexed reaction (1) to be approximately twice that for the hydrated reaction (2). Isomerization by double-proton transfer in the dimer (3) is predicted to be the most favorable process. Indeed, for (3) the energy gained from the formation of the hydrogen-bonded complex is greater than the associated barrier for the double-proton transfer, thereby making this process very efficient.

I. Introduction

Amidine compounds are of interest because of their medical and biochemical importance.¹⁻⁵ They play a vital role in the biosynthesis of imidazole and purines and the catabolism of histidine. Biological activity studies have reported amidines to be antibiotic, antifungal, and anaesthetic.²⁻⁴ Formamidine (methanimidamine $\text{H}_2\text{N}-\text{CH}=\text{NH}$), a small amidine which also has established biological activity,^{6,7} has been the subject of both

experimental and theoretical investigations and is of particular interest as a prototype for this class of compounds.

Since biological activity depends greatly on the molecular conformation, theoretical^{1,8,9} studies of the *E* (trans) and *Z* (cis) configurations of formamidine have been performed. Calculations by Zielinski et al.,¹ using the 3-21G¹⁰ basis set at the Hartree-Fock¹¹ (HF) level of theory, predict the *E* and *Z* configurations of formamidine to be separated only 0.6 kcal/mol (the *E* configuration is more stable) with an “in-plane isomerization” barrier of 23.4 kcal/mol. A stabilization of 2.94 kcal/mol⁹ compared to the *Z* configuration is found for the *E* form of formamidine with the 4-31G¹² basis set at the same HF level of theory. A pseudopotential calculation⁸ predicts the *E* configuration to lie 1.6 kcal/mol below the *Z* configuration on the potential energy surface. Experimentally, the relative energies of the two isomers and the interconversion rotational barrier have not been determined. However, experimental observations¹³ of formamidine derivatives suggest the existence of two isomers. In additional experimental work, the kinetic isotope effects for double proton transfers have been studied in phenyl-substituted formamidines.^{13d,e}

In addition to serving as a simple model for hydrogen shift reactions¹⁴ and protonation and deprotonation¹ in bases of nucleic acids (e.g., adenine and cytosine), formamidine is a prime target for extensive theoretical investigations because of its hydrogen bonds with itself with and with water. The intramolecular hydrogen transfer in formamidine ([1,3] sigmatropic rearrangement, see Figure 1a) was first studied theoretically by Fukui and co-workers¹⁵ using the 4-31G basis set at the HF level. A more recent theoretical investigation¹⁴ of this system was performed at the HF level but with three larger basis sets [3-21G,¹⁰ 6-31G,¹⁶ and 6-31G(d,p)¹⁷], followed by CI calculations at the HF geometries. A very high barrier was reported for the intramolecular proton transfer at all levels of theory (52.6 kcal/mol at the highest level of theory¹⁴).

One mechanism for reducing the hydrogen-transfer barrier was considered by Fukui et al.,¹⁸ who found that assistance by a water molecule (see Figure 1b) reduces the barrier by one-third compared to the intramolecular rearrangement at the same level of theory. A barrier of 21.6 kcal/mol was reported for this water-assisted formamidine rearrangement, using the 4-31G basis set at the HF level without correlation correction. The reaction path was traced by using the minimum STO-3G¹⁹ basis set at the HF level of theory, and the isotope effect²⁰ and tunneling probability²¹ were also investigated. Another calculation² for the same mechanism, but with the 6-31G basis set, gave a 20.9 kcal/mol barrier.

The feasibility of double-proton transfer via the dimerization-assisted mechanism (Figure 1c) has been considered by Zielinski and Poirier.²² Quantitative investigations, however was performed using the 3-21G basis set which is known to favor planar structure for nitrogen-containing compound.^{23,24} Minima and transition states were not verified with force-field calculations in this investigation, and the importance of polarization functions and correlation corrections on the associated energetics was not considered. A recent theoretical investigation²⁵ on the dimerization-assisted double-proton transfer of formamidine was done with several basis sets at the HF level of theory. At the highest level of theory [SCF/6-31G(d)], double-proton-transfer transition states were not reported in this study. Furthermore, correlation corrections were not included at all the important points on the potential energy surface.

Proton-transfer mechanisms of formamidine may be considered as basic models for proton transfer in bases of nucleic acid^{2,26} and as a basic model for double for double-proton transfer.²⁶ They also provide a deeper understanding of hydrogen bonding, which is very important for biological activities of formamidine^{6,7} as well as the qualitative picture of chemical bonding in the large amidine families. Multiple-proton-transfer reactions are also

implicated in the charge-relay mechanism of hydrolyses catalyzed by enzymes and other enzyme-catalyzed and water-catalyzed tautomerizations.²⁷

In the present study, an investigation of the dimerization-assisted intermolecular hydrogen transfer in formamidine is carried out with a more extensive basis set than used previously and including electron correlation. Both concerted and nonconcerted mechanisms of the dimerization-assisted double-hydrogen transfer are examined. For comparison, calculations are also performed on the intermolecular water-assisted double-hydrogen transfer (Figure 1b) and the intramolecular hydrogen transfer (Figure 1a).

II. Computational Methods

Because the STO-3G basis set has only one contracted basis function for each component of a p orbital, one may expect it to underestimate the distance between the atoms in a hydrogen bond.¹⁸ It is also well-known that basis sets without d functions at N favor planar structure.^{23,24} Therefore, one needs a larger basis set, e.g., the 6-31G(d) basis, to obtain reasonable structures for the systems considered here.

All structures were optimized by using analytical energy gradients with the 6-31G(d) basis set^{17,18} at the SCF level of theory¹¹ [SCF/6-31G(d)]. For the dimer-assisted double-proton-transfer mechanism, the 6-31G(d,p) basis set¹⁷ was used to study the structural effects of polarization functions. Single-point correlation corrections were done with 6-31G(d,p) and the larger 6-311G(d,p)²⁹ basis sets with second-order (MP2) and fourth-order (MP4) many-body perturbation theory as formulated by Pople and co-worker³⁰ (only the valence electrons were correlated in all cases). All fourth-order calculations include the full set of single, double, triple, and quadruple (SDTQ) valence excitations. To obtain improved predictions for barrier heights, the MP-SAC extrapolation procedure³¹ has been used with the 6-31G(d,p) basis set, without reoptimization of structures. The scale factor of 0.815 [the average of NH and OH values for the 6-31G(d,p) basis set] was used for these calculations.

Minima and transition states were identified by diagonalizing the force constant matrices and verifying that they have zero and one negative eigenvalue, respectively.

All ab initio electronic structure calculations were performed by using the GAMESS³² and GAUSSIAN86³³ quantum chemistry programs. All SCF calculations are carried out in the restricted Hartree-Fock approximation. Except where indicated otherwise, zero-point vibrational energy corrections were included on the basis of the harmonic approximation. If ΔE^\ddagger is the electronic energy difference, including nuclear repulsions, between a transition state of a unimolecular process and the equilibrium structure of the reactant, the zero-point corrected barrier is

$$\Delta E_0^\ddagger = \Delta E^\ddagger + 1/2hc \left(\sum_{m=1}^{3n-7} \nu_m^\ddagger - \sum_{m=1}^{3n-6} \nu_m^R \right)$$

where ν_m^\ddagger and ν_m^R are transition-state and reactant frequencies, respectively, and n is the number of atoms. Zero-point corrections for thermodynamic reaction enthalpies are carried out similarly except that both sums, over product modes and over reactant modes, have $3n-6$ terms.

III. Results And Discussion

A. Intramolecular Proton Transfer.

The transition-state structure obtained by Fukui et al.,¹⁵ at the SCF/4-31G level, has C_{2v} symmetry, but the C_{2v} stationary point has two imaginary frequencies at the SCF/6-31G(d) level. Only one true nonplanar transition state is found, and it has C_s symmetry and a large imaginary frequency ($2440i \text{ cm}^{-1}$). This frequency indicates that the potential energy barrier is very narrow. The fully optimized transition state and the minimum-energy formamidine structures are shown in Figure 2. The calculated MP4/6-311G(d,p)//SCF/6-31G(d) barrier to intramolecular hydrogen transfer is 43.4 kcal/mol (see Table I; “//” means

“at the geometry of”), which is much lower than the SCF/4-31G value (59.1 kcal/mol) reported earlier.¹⁵ A significant difference is also found between the MP4(SDTQ)/6-31G(d,p)//SCF/6-31G(d) and CISD/6-31G(d,p)//SCF/6-31G calculations,¹⁴ as shown in Table I. Note also that at the MP4 level there is little difference between the barriers predicted with the 6-31G(d,p) and 6-311G(d,p) basis sets. These results illustrate that both polarization functions and correlation corrections are important for the description of the intramolecular hydrogen transfer, but expansion of the valence basis from double zeta to triple zeta is less important.

Finally, the intramolecular proton-transfer barriers calculated at the MP2/6-31G(d,p) level of theory were scaled by the MP-SAC2 method (SAC2), to estimate the remaining correlation energy contribution to the MP2 barrier energy. SAC2 predicts a barrier of 39.7 kcal/mol (see Table I) for the [1,3] sigmatropic rearrangement in formamidine.

B. Intermolecular Double-Proton Transfer in the Formamidine-Water System.

The SCF/6-31G(d) structures of the stationary points E and F (Figure 1b) on the potential energy surface are shown in Figure 3. As noted earlier,^{2,18} the equilibrium structure E is considered the starting point for this intermolecular hydrogen-transfer reaction. The hydrogen-bonded structure E is an intermediate on the reaction path in the reaction scheme shown in Figure 1b.

Energetically, the overall MP4/6-311G(d,p) energy barrier (the difference between the reactant D and the transition-state F in the reaction scheme of Figure 1b) for the intermolecular water-assisted proton transfer is 6.8 kcal/mol, as shown in Table II. This is significantly lower than the value, 21.6 kcal/mol, previously reported¹⁸ by Fukui and co-workers. The barrier is lowered almost to zero (0.7 kcal/mol) by extrapolating with SAC2/6-31G(d,p). As noted for the intramolecular hydrogen transfer, both polarization

functions and correlation corrections play a major role in determining the potential energy barrier for this process (see Table II). The results in Table II illustrate that the assistance of a water molecule lowers that barrier for the hydrogen transfer by 36.6 kcal/mol, relative to the intramolecular transfer, at the MP4/6-311G(d,p) level of theory, including zero-point corrections, and by a similar amount at the SAC2/6-31G(d,p) level. The net energy cost for the overall process (energy lowering due to hydrogen bond formation plus the barrier for water-assisted proton transfer) is 6.8 kcal/mol at the MP4(SDTQ)/6-311G(d,p) level of theory and 0.7 kcal/mol when SAC2/6-31G(d,p) is used.

C. Intermolecular Dimer-Assisted Double-Hydrogen Transfer.

Six stationary points were located on the dimer potential energy surface at several levels of theory. The following discussion will be focused mainly on the minima and transition-state structures. In view of the small differences seen in Tables I and II between relative energies predicted by the 6-31G(d,p) and 6-311G(d,p) basis sets and at the MP2 and MP4 levels of theory, the dimer energetics have been predicted at the MP2/6-31G(d,p)//SCF/6-31G(d) and MP2/6-31G(d,p)//SCF/6-31G(d,p) levels of theory.

The dimerization of formamidine (reaction $J \rightarrow K$ in Figure 1c) leads to two stable structures with C_i and C_2 symmetry. Both of these are verified minima on the SCF/6-31G(d) and SCF/6-31G(d,p) potential energy surfaces. These structures, K_a and K_b (shown in Figure 4), are presumably intermediates in the dimerization-assisted double-proton transfer (Figure 1c). The structure and energetics for these two species are virtually identical (see Table III and Figure 4). Dimerization enthalpies for both the C_i and C_2 structures are exothermic by 13.8 kcal/mol at the MP2/6-31G(d,p)//SCF/6-31G(d) level of theory. This may be compared with a stabilization energy of 15.8 kcal/mol for the formamidine-water dimer at the same level of theory. (Both values include zero-point

corrections.) Insignificant changes of both structures and relative energies of the two C_i and C_2 dimers are observed upon going from the 6-31G(d) to 6-31G(d,p) basis set.

Structure N with C_{2h} symmetry is fully optimized to a verified minimum on the potential energy surface by using both STO-3G and 3-21G basis sets. However, two imaginary frequencies, with the displacement vectors of the normal modes corresponding to out-of-plane bending motions, are obtained with the larger 6-31G(d) and 6-31G(d,p) basis sets for this planar structure.

The concerted double-hydrogen transfer transition state with D_{2h} symmetry, structure O in Figure 4, is not a true transition on either the 6-31G(d) and 6-31G(d,p) potential energy surface. This structure has two imaginary frequencies in both basis sets. One of these frequencies corresponds to the concerted double-proton transfer, where two hydrogens move simultaneously. Following the other mode leads to the structure M, which is a minimum with C_{2v} symmetry on the 6-31G(d) potential energy surface. However, one imaginary frequency is obtained for M with the 6-31G(d,p) basis. This structure (M) lies 4.2 and 2.3 kcal/mol below O (without zero-point correction) at the SCF/6-31G(d) and SCF/6-31G(d,p) levels, respectively. The order, however, is reversed at the MP2 level of theory. MP2/6-31G(d,p)//SCF/6-31G(d) and MP2/6-31G(d,p)//SCF/6-31G(d,p) predict O to lie 3.5 and 2.5 kcal/mol below M, respectively (without zero-point correction).

The nonsymmetric transition state L with C_s symmetry has one imaginary frequency ($328i\text{ cm}^{-1}$). This is apparently the lowest energy saddle point on the SCF/6-31G(d) potential energy surface for the nonconcerted double-proton transfer in the dimer. However, a SCF/6-31G(d,p) transition state search starting at the SCF/6-31G(d) structure L leads to structure O with C_{2v} symmetry. Energetically, the MP2/6-31G(d,p)//SCF/6-31G(d) calculation predicts structure O to be the one with the lowest overall barrier (see Table IIIC) for the dimerization-assisted double-proton transfer. This process is exothermic by 5.3

kcal/mol (without zero-point corrections) as predicted by the MP-SAC2/6-31G(d,p) method. The net energy cost for the dimer-assisted proton transfer (energy lowering due to dimer formation plus the barrier to proton transfer) is -5.3 kcal/mol.

IV. Summary and Conclusions

The present study has employed high levels of electronic structure theory to compare the [1,3] N-to-N sigmatropic rearrangement of formamidine for three mechanisms: (1) intramolecular proton transfer, (2) water-assisted double-proton transfer, and (3) dimerization-assisted double-proton transfer. All computational levels predict the barrier for (1) to be approximately twice that for (2). Energetically, the dimerization-assisted double-proton transfer appears to be the most favorable process with an enthalpy of activation of -5.8 kcal/mol followed by the water-assisted (3.5 kcal/mol) and the intramolecular (42.8 kcal/mol) processes, as predicted by MP2/6-31G(d,p). In all cases, MP-SAC2 calculations reduce the barriers, by 3-4 kcal/mol. The double-proton transfer is found to be rather low energy process, due in large part to the energy gained by the formation of hydrogen bonds.

The water-assisted and dimerization-assisted processes are extremely sensitive to basis sets used. To obtain reliable energetics, correlation corrections must be and were incorporated in the calculations. Polarization functions on hydrogen are also essential to locate the transition of the dimer double proton transfer.

We plan in future work to continue the present study by calculating rate coefficients using the present structural studies as starting point.

Acknowledgment

This research was supported in part by the National Science Foundation (Grants CHE86-17063, CHE-89-11911, and CHE89-22048) and by the Donors of the Petroleum Research Fund, administered by the American Chemical Society. These calculations were

performed in part on the CRAY1 at the Minnesota Supercomputer Institute and in part on the North Dakota State University IBM3090 (aided by a joint study agreement with IBM) and on the NDSU Quantum Chemistry VAX 8530 (funded by a grant from the Air Force Office of Scientific Research).

References

- (1) Zielinski, T. J.; Peterson, M. R.; Csizmadia, I. G.; Rein, R. *J. Comput. Chem.* **1982**, *3*, 62.
- (2) Zielinski, T. J.; Poirier, R. A.; Peterson, M. R.; Ciszmadia, I. G. *J. Comput. Chem.* **1983**, *4*, 419.
- (3) Steinman, U.; Estler, C. J.; Pann, O. *Drug. Dev. Res.* **1986**, *7*, 153.
- (4) Foussard-Blaupin, O; Quevauviller, A. *Ann. Pharm. Fr.* **1982**, *40*, 231.
- (5) Grant, R. J. In *The Chemistry of Amidines and Imidates*; Patai, S., Ed.; Wiley: New York, 1975; Chapter 6.
- (6) Johnson, T. L.; Knowles, C. O. *Gen. Pharmacol.* **1983**, *14*, 591.
- (7) Kaneda, M.; Oomura, Y.; Ishibashi, O.; Akaike, N. *Neurosci. Lett.* **1988**, *168*, 1.
- (8) Kinasiewicz, W.; Les, A.; Wawer, I. *J. Mol. Struct. (THEOCHEM)* **1988**, *168*, 1.
- (9) Radom, L.; Hehre, W. J.; Pople, J. A.; *J. Am. Chem. Soc.* **1971**, *93*, 289.
- (10) Binkley, J. S.; Pople, J. A.; Hehre, W. J. *J. Am. Chem. Soc.* **1980**, *102*, 939.
- (11) Roothan, C. C. *J. Rev. Mod. Phys.* **1951**, *23*, 69.
- (12) Hehre, W. J.; Binkley, J. S.; Ditchfield, R.; Pople, J. A. *J. Am. Chem. Soc.* **1971**, *54*, 724.
- (13) (a) Hegathy, A. F.; Chandler, A. *Tetrahedron Lett.* **1980**, 885. (b) Filleux, M. L.; Naulet, N.; Doric, J. P.; Pornet, J.; Miginiac, L. *Tetrahedron Lett.* **1974**, 1435. (c) Krajewski, J. W.; Urbanczyk-Lipkowska, Z.; Gluzinski, P.; Busko-Oszczapowicz, Z.; Bleidelis, J.; Kemme, A. *Pol. J. Chem.* **1981**, *55*, 1015. (d) Meschede, L.;

- Garritzen, D.; Limbach, H.-H. *Ber. Bunsenges. Phys. Chem.* **1988**, 92, 469. (e)
- Limbach, H.-H.; Meschede, L.; Scherer, G. *Z. Naturforsch.* **1989**, 44a, 459.
- (14) Poirier, R. A.; Majlessi, D.; Zielinski, T. J. *J. Comput. Chem.* **1986**, 7, 464.
- (15) Yamashita, K.; Kaminoyama, M.; Yamabe, T.; Fukui, K. *Theor. Chim. Acta* **1981**, 60, 303.
- (16) Hehre, W. J.; Ditchfield, R.; Pople, J. A.; *J. Chem. Phys.* **1972**, 56, 2257.
- (17) Hariharan, P. C.; Pople, J. A. *Theor. Chim. Acta* **1973**, 28, 213.
- (18) Yamabe, T.; Yamashita, K.; Kaminoyama, M.; Koizumi, M.; Tachibana, A.; Fukui, K. *J. Chem. Phys.* **1984**, 88, 1459.
- (19) (a) Hehre, W. J.; Stewart, R. F.; Pople, J. A.; *J. Chem. Phys.* **1969**, 51, 2657. (b) Hehre, W. J.; Ditchfield, R.; Stewart, R. F.; Pople, J. A.; *J. Chem. Phys.* **1970**, 52, 2769.
- (20) Kato, S.; Fukui, K. *J. Am. Chem. Soc.* **1976**, 98, 6395.
- (21) (a) Marcus, R. A.; Coltrin, M. E. *J. Chem. Phys.* **1977**, 67, 2609. (b) Marcus, R. A. *J. Chem. Phys.* **1979**, 83, 204.
- (22) Zielinski, T. J.; Poirier, R. A. *J. Comput. Chem.* **1984**, 5, 466.
- (23) Body, R. G.; McClure, D. S.; Clementi, E. *J. Chem. Phys.* **1968**, 49, 4916.
- (24) Rauk, A.; Allen, L. C.; Clementi, E. *J. Chem. Phys.* **1970**, 52, 4133.
- (25) Svensson, P.; Bergman, N.-Å; Ahlberg, P. *J. Chem. Soc. Commun.* **1990**, 82.
- (26) Scheiner, S.; Kern, C. W. *J. Am. Chem. Soc.* **1979**, 101, 4018.
- (27) Hibbert, F. *Adv. Phys. Org. Chem.* **1986**, 22, 113.
- (28) Francl, M. M.; Pietro, W. J. Hehre, W. J.; Binkley, J. S.; Gordon, M. S.; DeFrees, J. D.; Pople, J. A. *J. Chem. Phys.* **1982**, 77, 3654.
- (29) Krishnan, R.; Binkley, J. S.; Seeger, R.; Pople, J. A. *J. Chem. Phys.* **1980**, 72, 650.

- (30) (a) Møller, R.; Plesset, M. S. *Phys. Rev.* **1934**, 46, 618. (b) Pople, J. A., Binkley, J. S.; Seeger, R. *Int. J. Quantum Chem. Symp.* **1976**, 10, 1. (c) Pople, J. A.; Seeger, R.; Krishnan, R. *Int. J. Quantum Chem. Symp.* **1977**, 11, 149. (d) Krishnan, R.; Pople, J. A. *Int. J. Quantum Chem.* **1978**, 14, 91. (e) Krishnan, R.; Frisch, M. J.; Pople, J. A. *J. Chem. Phys.* **1980**, 72, 4244.
- (31) Gordon, M. S.; Truhlar, D. G. *J. Am. Chem. Soc.* **1986**, 108, 5412.
- (32) (a) Dupuis, M.; Spangler, D.; Wendoloski, J. J. *National Resource for Computational Chemistry Software Catalog*; University of California; Berkley, 1980; Prog. QG01. (b) Schmidt, M. W.; Boatz, J. A.; Baldrige, K. K.; Koseki, S.; Gordon, M. S.; Elbert, S. T. *QCPE Bulletin*, **1978**, 7, 115.
- (33) Frisch, M. J.; Binkley, J. S.; Schlegel, H. B.; Raghavachari, K.; Melius, C. F.; Kahn, L. R.; DeFrees, D. J.; Seeger, R.; Whiteside, R. A.; Rohlfing, C. M.; Fox, D. J.; Fleuder, E. M.; Pople, J. A. *GAUSSIAN86*; Carnegie-Mellon Quantum Chemistry Publishing Unit: Pittsburgh, PA, 1984.

Table I. Barriers (kcal/mol) for the Intramolecular Proton Transfer.

	6-31G(d,p)//SCF/6-31G		6-31G(d,p)//SCF/6-31G(d)			6-311G(d,p)//SCF/6-31G(d)			
	CISD	CISD-DQ	SCF	MP2	SAC2	MP4(SDTQ) SCF	MP2	MP4(SDTQ)	
$\Delta H_0^{\ddagger a}$			56.6	42.8	39.7	43.9	57.5	42.6	43.4
$\Delta E_0^{\ddagger b}$	54.5	52.6	60.6	46.9	43.8	48.0	61.6	47.7	47.5

^aCorrected for vibrational zero point energy (ZPE).

^bUncorrected for vibrational ZPE.

Table II
 (A) Zero-Point corrected Energy Differences (kcal/mol) and Barriers for the Water-Assisted Proton Transfer.

Reaction	6-311G(d,p)//SCF/6-31G(d)			6-31G(d,p)//SCF/6-31G(d)			
	SCF	MP2	MP4(SDTQ)	SCF	MP2	SAC2	MP4(SDTQ)
D \longrightarrow E ^a	-12.4	-12.8	15.1	-12.7	-15.8		-15.4
E \longrightarrow F	29.4	20.9	21.9	28.6	19.3	17.2	20.7
D \longrightarrow F	17.0	8.1	6.8	15.9	3.5	0.7	5.3

(B) Uncorrected Zero-Point Energy Differences (kcal/mol) and Barriers for the Water-Assisted Proton Transfer.

Reaction	6-311G(d,p)//SCF/6-31G(d)			6-31G(d,p)//SCF/6-31G(d)			
	SCF	MP2	MP4(SDTQ)	SCF	MP2	SAC2	MP4(SDTQ)
D \longrightarrow E ^a	-9.7	-12.8	-12.4	-10.0	-13.1		-12.7
E \longrightarrow F	32.1	23.6	24.6	31.4	22.1	20.0	23.5
D \longrightarrow F	22.4	10.8	12.2	11.4	9.0	8.5	10.8

^aThermodynamic energy difference; others are barriers.

Table III.

(A) Barriers (kcal/mol) for the Intermolecular Dimerization-Assisted proton transfer.

	6-31G(d)//SCF/6-31G(d)		SCF		6-31G(d,p)//SCF/6-31G(d)		SAC2	
	SCF ΔE^\ddagger	SCF ΔH_0^\ddagger	ΔE^\ddagger	ΔH_0^\ddagger	MP2 ΔE^\ddagger	MP2 ΔH_0^\ddagger	ΔE^\ddagger	ΔH_0^\ddagger
J \longrightarrow O (D_{2h})	18.4	13.8	14.7	10.1	-1.4	-6.0	-5.1	-9.7
K _a \longrightarrow L (C_s)	25.4	23.0	23.8	21.4	16.9	14.5	15.3	12.9
K _b \longrightarrow L (C_s)	25.3	23.1	23.7	21.5	16.8	14.6	15.2	13.0
K _a \longrightarrow O (D_{2h})	29.6	23.4	26.2	20.0	14.0	7.8	11.2	5.0

(B) Zero-point corrected Energy Differences (kcal/mol) for the intermolecular dimerization process.

	SCF/6-31G(d)//SCF/6-31G(d)		MP2/6-31G(d,p)//SCF/6-31G(d)	
	ΔE	ΔH_0	ΔE	ΔH_0
J \longrightarrow K _a (C_i)	-11.2	-9.6	-15.4	-13.8
J \longrightarrow K _b (C_2)	-11.1	-9.6	-15.2	-13.8
J \longrightarrow M (C_{2v})	14.2	14.2	2.1	2.1
J \longrightarrow N (C_{2h})	-11.0	-10.1	-15.2	14.3

Table III—continued

(C) Barriers (kcal/mol) for the Intermolecular Dimerization-Assisted Proton Transfer.

	SCF/6-31G(d,p)//SCF/6-31G(d,p)		6-31G(d,p)//SCF/6-31G(d,p)		SAC2	
	ΔE^\ddagger	ΔH_0^\ddagger	ΔE^\ddagger	ΔH_0^\ddagger	ΔE^\ddagger	ΔH_0^\ddagger
J \longrightarrow O (D_{2h})	14.7	10.5	-1.6	-5.8	-5.3	-9.5
J \longrightarrow M (C_{2v})	12.2	11.7	0.9	0.2	-1.7	-2.4
K _a \longrightarrow M (C_{2v})	23.8	21.6	16.3	14.1	14.6	12.4
K _b \longrightarrow M (C_{2v})	23.8	21.7	16.2	14.1	14.5	12.4
K _a \longrightarrow O (D_{2h})	26.1	20.4	13.8	8.1	11.0	5.3
K _b \longrightarrow O (D_{2h})	26.1	20.5	13.7	8.1	11.0	5.3

(D) Energy Differences (kcal/mol) for the Intermolecular Dimerization Process.

	SCF/6-31G(d)//SCF/6-31G(d)		MP2/6-31G(d,p)//SCF/6-31G(d)	
	ΔE	ΔH_0	ΔE	ΔH_0
J \longrightarrow K _a (C_i)	-11.4	-9.9	-15.4	-13.9
J \longrightarrow K _b (C_2)	-11.4	-10.0	-15.3	-13.9
J \longrightarrow N (C_{2h})	-11.4	-10.3	-15.3	-14.2

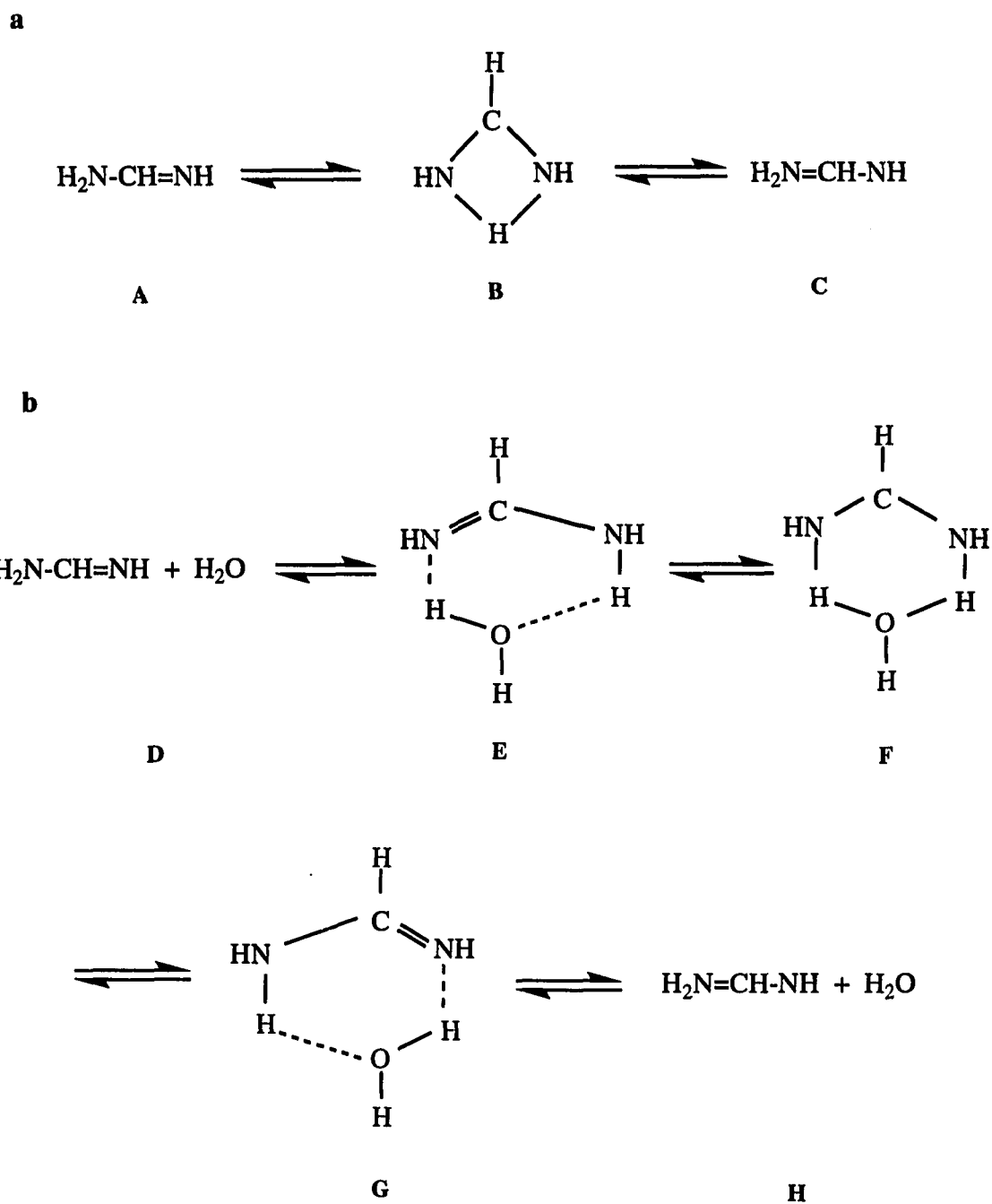


Figure 1. (a) Intramolecular hydrogen-transfer scheme. (b) Water-assisted intermolecular hydrogen-transfer scheme. (c) Dimerization-assisted intermolecular hydrogen-transfer scheme.

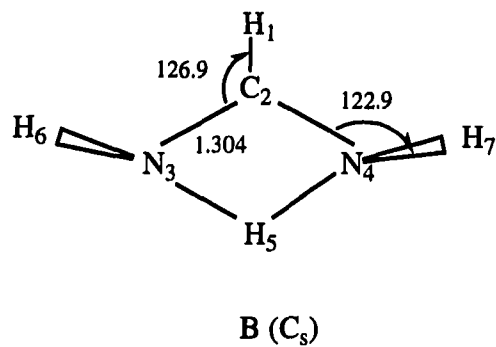
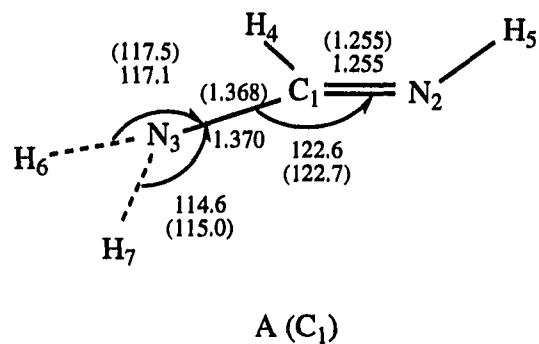


Figure 2. RHF/6-31G(d) structures, bond distances (R), and bond angles (A , ω -dihedral) with RHF/6-31G(d,p) bond distances and bond angles in parentheses. Bond lengths are in angstroms; angles are in degrees. (A) Formamidine: $R(1,4) = 1.084$ (1.085), $R(2,5) = 1.002$ (1.001), $R(3,6) = 0.996$ (0.994); $A(4,1,2) = 124.4$ (124.4), $A(5,2,1) = 111.1$ (111.1); $\omega(4,1,2,3) = 177.5$ (177.7), $\omega(5,2,1,3) = 183.8$ (183.6), $\omega(6,3,1,2) = -152.0$ (-153.6), $\omega(7,3,1,2) = -14.0$ (-12.9). (B) Intramolecular proton-transfer transition state; $R(1,2) = 1.079$, $R(5,2) = 1.632$, $R(6,3) = 0.998$; $\omega = 157.9$.

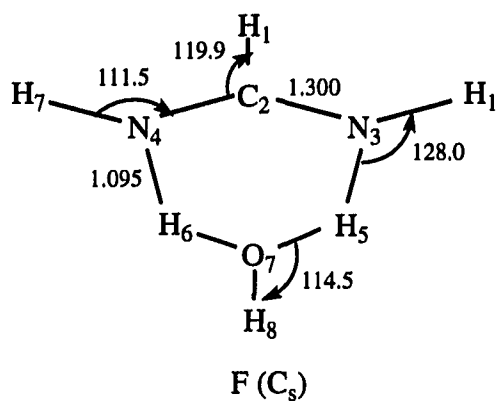
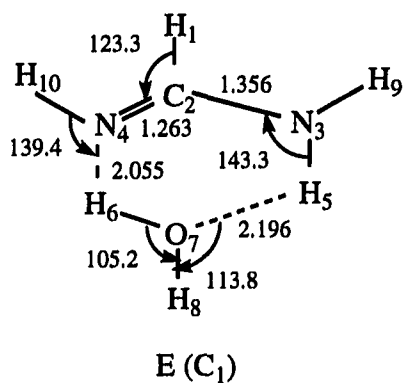


Figure 3. RHF/6-31G(d) structures. Bond lengths (R) are in angstroms; angles (A , ω -dihedral) are in degrees. (E) Formamidine-water complex: $R(1,2) = 1.084$, $R(5,3) = 1.001$, $R(7,6) = 0.958$, $R(9,3) = 0.994$, $R(8,7) = 0.974$, $R(10,4) = 1.001$; $A(1,2,3) = 113.5$, $A(5,3,2) = 116.6$, $A(5,3,9) = 116.5$, $A(6,4,2) = 108.2$; $\omega(4,2,3,1) = 178.0$, $\omega(5,3,2,1) = 190.9$, $\omega(6,3,1,2) = 170.6$, $\omega(7,5,3,2) = -9.1$, $\omega(9,3,5,7) = 203.6$, $\omega(10,3,6,7) = 180.7$. (F) Water-assisted double proton-transfer transition state: $R(2,1) = 1.078$, $R(2,7) = 2.860$, $R(3,9) = 0.994$, $R(7,8) = 0.948$; $\omega(4,2,3,9) = 179.8$, $\omega(10,4,2,1) = 181.9$, $\omega(10,4,6,7) = 186.6$.

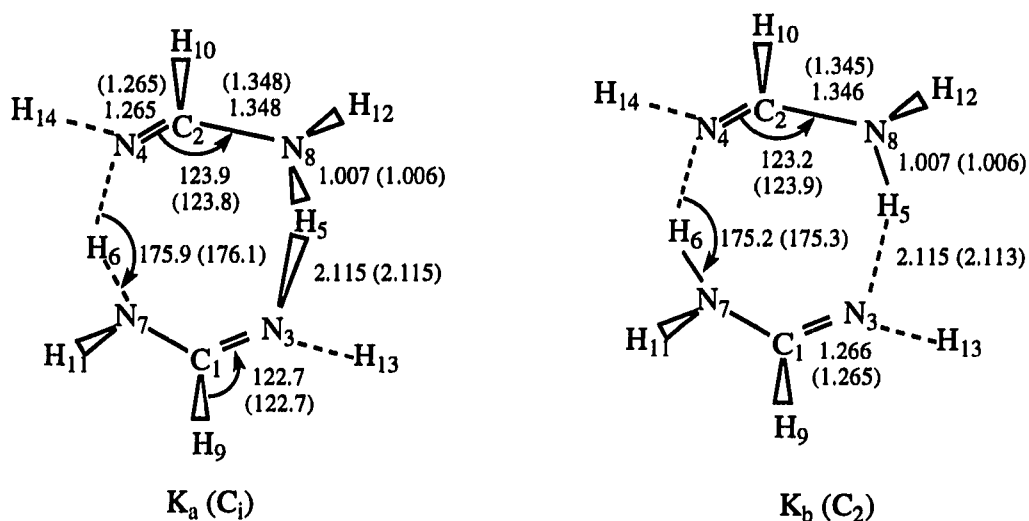


Figure 4. RHF/6-31G(d) structures, bond distances, and bond angles with RHF/6-31G(d,p) bond distances and bond angles in parentheses. Bond lengths (R) are in angstroms; angles (A , ω -dihedral) are in degrees. (K) Formamidine dimers. (K_a): $R(9,1) = 1.085$ (1.085), $R(11,7) = 0.993$ (0.992), $R(13,3) = 1.002$ (1.000); $A(10,2,4) = 122.7$ (122.7), $A(14,4,2) = 110.9$ (110.9), $A(5,3,1) = 120.0$ (120.0), $A(6,7,1) = 119.0$ (119.0), $A(11,7,1) = 118.3$ (118.2); $\omega(5,3,1,7) = 12.4$ (12.2), $\omega(10,2,4,8) = -178.1$ (-178.3), $\omega(11,7,1,3) = -164.0$ (-164.2), $\omega(14,4,2,8) = 177.4$ (177.7). (K_b): $R(9,1) = 1.084$ (1.086), $R(11,7) = 0.993$ (0.991), $R(13,3) = 1.002$ (1.001); $A(10,2,4) = 122.8$ (122.7), $A(14,4,2) = 110.9$ (110.9), $A(5,3,1) = 120.0$ (120.0), $A(6,7,1) = 119.8$ (119.7), $A(11,7,1) = 118.8$ (118.8); $\omega(5,3,1,7) = -2.8$ (-3.0), $\omega(10,2,4,8) = 178.4$ (178.6), $\omega(11,7,1,3) = -167.8$ (-168.3), $\omega(14,4,2,8) = -178.0$ (-178.2). (L) Nonconcerted dimer-assisted double-proton-transfer transition state: $R(9,1) = 1.091$, $R(10,2) = 1.079$, $R(11,7) = 0.999$, $R(12,8) = 0.994$, $R(13,3) = 1.000$, $R(14,4) = 0.996$; $A(2,4,6) = 122.1$, $A(2,8,5) = 121.3$, $A(1,7,6) = 121.1$, $A(1,3,5) = 118.9$, $A(9,1,3) = 117.2$, $A(10,2,4) = 117.2$, $A(11,7,5) = 118.8$, $A(12,8,2) = 117.6$, $A(13,3,1) = 112.2$, $A(11,7,1) = 111.3$. (M) Concerted dimer-assisted double-proton-transfer transition state: $R(10,2) = 1.008$ (1.008), $R(9,1) = 1.092$ (1.092), $R(12,8) = 0.995$ (0.993), $R(13,8) = 1.00$ (0.999); $A(10,2,8) = 117.8$ (117.8), $A(12,8,2) = 118.4$ (117.7), $A(9,1,3) = 117.7$ (117.8), $A(13,3,1) = 111.6$ (111.7), $A(2,8,2) = 121.7$ (121.5), $A(5,3,1) = 119.9$ (120.0). (N, O) Stationary points with two imaginary frequencies. (N): $R(10,2) = 1.084$ (1.086), $R(12,8) = 1.001$ (1.001), $R(13,3) = 0.991$ (0.990); $A(12,8,2) = 110.8$ (110.8), $A(13,3,1) = 120.0$ (120.0), $A(2,8,5) = 119.4$ (119.8), $A(5,3,1) = 121.3$ (120.8). (O): $R(10,2) = 1.086$ (1.084), $R(12,8) = 0.996$ (0.997); $A(12,8,2) = 123.9$ (124.2), $A(5,8,2) = 121.1$ (121.0).

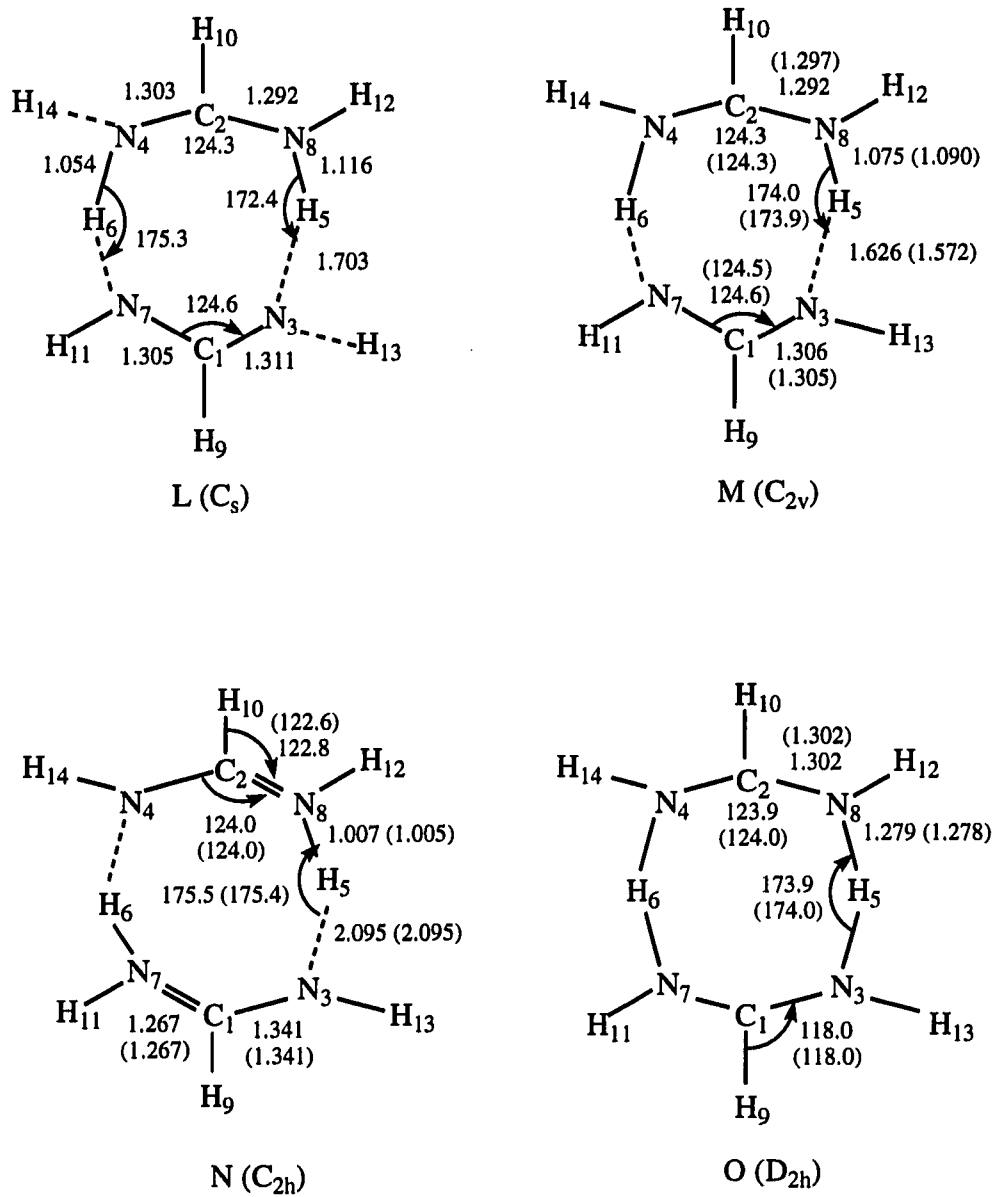


Figure 4.—continued

CHAPTER 11. CONCLUSIONS

In this chapter, the main findings of the *ab initio* electronic structure studies are summarized. We have found (Chapter 2) that the bonding interaction between the two bridgehead atoms (M_bM_b) of the [1.1.1]metallapropellanes decreases upon descending group IV. The study of group IV 2,4,5-trioxa[1.1.1]metallapropellanes and group IV 2,4,5-trithia[1.1.1]metallapropellanes (Chapter 3) has found that these species possess unusually short bridgehead distances for $M_b = \text{Si, Ge and Sn}$. However, this did not result in significant bonding interactions. Our calculations suggest substantial bridgehead bonding only in the 2,4,5-trithia[1.1.1]propellane system. We have found excellent agreement in structures and energetics between effective core potential (ECP) calculations and the 6-31G(d) all-electron calculations for all propellanes. Valence electron densities generated from ECP basis sets are similar to the corresponding densities generated from all electron basis sets. Therefore, the reactivity of large biochemical and transition metal systems not amenable to all electron calculations, may well be successfully determined by analyzing the charge density generated from ECP.

Several levels of *ab initio* electronic structure theory have been used to predict the structures, bonding and energetics of N_2O_2 isomers (Chapter 4). Four high energy isomers—bicyclodiazoxane, bond stretch bicyclodiazoxane, and 1,2-diaza-3,4-dioxocyclobutene, and asymmetric N-N-O-O(*a*- N_2O_2)—were located above 2NO. Of the four metastable (thermodynamically) species, *a*- N_2O_2 has been shown to dissociate via the spin-forbidden channel $a\text{-}N_2O_2(^1A') \rightarrow N_2O(X^1\Sigma^+) + O(^3P)$. Study of the kinetic stability of the other isomers with respect to spin-allowed and spin-forbidden processes is in progress.

The investigation of the inversion process of bicyclobutane and its isoelectronic analog bicyclodiazoxane is reported in Chapter 5. We have shown that the inversion of the latter system follows a two-step process via a D_{2h} bond stretch isomer, while the inversion of the former involves a transition region which contains three nearly isoenergetic stationary points. The isomerization process of bicyclobutane (Chapter 6) is predicted to proceed primarily via the concerted conrotatory mechanism. We have found that these reactions can not be treated in a consistent manner with single configuration-based methods.

In Chapter 7, an investigation of the β effect of group IV elements on the carbenium ion $H_3MCH_2CHR^+$ ($R = H$ and CH_3) has shown that the thermodynamics of this effect are consistent with the observed kinetics, although the trend is not as dramatic. This suggests that the nature of the transition state(s) for reaction 1 as a function of M also plays an important role. The magnitude of the β effect is predicted to increase steadily upon going from C to Sn in group IV. The structures, energetics and mechanisms of the $Si^+ + CH_3-SiH_3$ reactions have been investigated in detail (Chapter 8). These reactions are predicted to proceed with an initial complex formation of Si^+ with methylsilane, followed by the insertion of Si^+ into either Si-H or Si-C bonds to form $Si_2CH_6^+$ intermediates that can undergo: 1) isomerizations, H_2 -elimination and SiH_3 elimination at thermal energy; 2) hydrogen atom eliminations and bond cleavages at higher energy.

In Chapter 10, we apply high levels of electronic structure theory, including the MP-SAC2 method described in Chapter 9, to compare the [1,3] N-to-N sigmatropic rearrangement of formamidine for three mechanisms: (1) intramolecular proton transfer, (2) water-assisted double-proton transfer, and (3) dimerization-assisted double-proton transfer. All computational levels predict the barrier for (1) to be approximately twice that for (2). In all cases, MP-SAC2 calculations reduce the barriers, by 3-4 kcal/mol. The

double-proton transfer is found to be rather low energy process, due in large part to the energy gained by the formation of hydrogen bonds.